

JYU DISSERTATIONS 405

Andrecia Ramnath

Nonlinear Evolution in the Colour Glass Condensate



UNIVERSITY OF JYVÄSKYLÄ
FACULTY OF MATHEMATICS
AND SCIENCE

JYU DISSERTATIONS 405

Andrecia Ramnath

Nonlinear Evolution in the Colour Glass Condensate

Esitetään Jyväskylän yliopiston matemaattis-luonnontieteellisen tiedekunnan suostumuksella
julkisesti tarkastettavaksi kesäkuun 22. päivänä 2021 kello 12.

Academic dissertation to be publicly discussed, by permission of
the Faculty of Mathematics and Science of the University of Jyväskylä,
on June 22, 2021 at 12 o'clock.



JYVÄSKYLÄN YLIOPISTO
UNIVERSITY OF JYVÄSKYLÄ

JYVÄSKYLÄ 2021

Editors

Ilari Maasilta

Department of Physics, University of Jyväskylä

Päivi Vuorio

Open Science Centre, University of Jyväskylä

Copyright © 2021, by University of Jyväskylä

ISBN 978-951-39-8750-3 (PDF)

URN:ISBN:978-951-39-8750-3

ISSN 2489-9003

Permanent link to this publication: <http://urn.fi/URN:ISBN:978-951-39-8750-3>

Abstract

The Colour Glass Condensate is used as an effective theory to study Quantum Chromodynamics at high energies in various scattering processes. Several evolution equations are discussed, in particular the JIMWLK (Jalilian-Marian–Iancu–McLerran–Weigert–Leonidov–Kovner) equation. This is studied in two equivalent pictures, namely the Fokker–Planck formalism and the Langevin formalism. From the latter, we show how BFKL (Balitsky–Fadin–Kuraev–Lipatov) dynamics emerge in the dilute limit. This is discussed further in Paper [II]. From the Fokker–Planck formalism, we use the Gaussian Approximation scheme to study several different types of correlators of fundamental Wilson lines. The 6-point correlators that appear in the next-to-leading order BK (Balitsky–Kovchegov) equation are calculated – their numerical implementation is covered in Paper [III]. Finally, the Gaussian Approximation is extended as a means to derive an evolution equation for the so-called odderon. Simple correlators are also calculated to see how their parametric equations are modified. The extended approximation scheme and the numerical implementation of the odderon are studied further in Paper [I].

Abstract in Finnish

Kvanttiväridynamiikan ilmiöitä eri sirontaprosesseissa kuvataan värilasikondensaatioksi kutsutulla efektiivisellä kenttäteorialla. Tutkimuksen kohteena ovat erilaiset evoluutioyhtälöt, erityisesti JIMWLK (Jalilian-Marian-Iancu-McLerran-Weigert-Leonidov-Kovner) -yhtälö. JIMWLK-yhtälöä tutkitaan kahdesta eri lähestymistavasta, kirjoittaen se joko Fokker-Planck-muotoon tai Langevin-yhtälöksi. Lähtien yhtälön Langevin-muodosta osoitetaan, että heikon vuorovaikutuksen rajalla siitä voidaan johtaa BFKL (Balitsky-Fadin-Kuraev-Lipatov) -dynamiikka kuvaava yhtälö. Tätä käsitellään tarkasti artikkelissa [II]. Toisaalta Fokker-Planck-muotoa käytetään laskemaan fundamentaaliesityksen Wilson viivojen korrelaattoreita soveltaen Gaussista approksimaatiota. Väitöskirjassa lasketaan sellaiset 6-pistekorrelaattorit, joita tarvitaan BK (Balitsky-Kovchegov) -evoluutioyhtälön ratkaisemiseen alinta seuraavassa kertaluvussa. Analyytiset tulokset ja niiden numeerinen toteutus on raportoitu artikkelissa [III]. Gaussista approksimaatiota laajentaen johdetaan myös evoluutioyhtälö niin kutsutulle odderonille ja määritetään, miten odderon-kontribuutio vaikuttaa Wilsonin viivojen korrelaattoreiden lausekkeisiin. Näin johdetut korrelaattorit ja niiden numeerinen toteutus on esitetty artikkelissa [I].

– Translated from the English version by Heikki Mäntysaari

Author Andrecia Ramnath
Department of Physics
University of Jyväskylä
Finland

Supervisor Prof. Tuomas Lappi
Department of Physics
University of Jyväskylä
Finland

Reviewers Prof. Adrian Dumitru
Department of Natural Sciences
Baruch College, City University of New York
USA

Dr. Yoshitaka Hatta
Nuclear Theory Group
Brookhaven National Laboratory
USA

Opponent Prof. Stéphane Munier
Centre de Physique Théorique
École Polytechnique
France

Preface

There are several people and institutions I need to thank for making my doctoral studies possible. I am grateful for the financial support provided by the Finnish Center for International Mobility, the National Research Foundation of South Africa and the European Research Council under the European Union's Horizon 2020 research and innovation programme (grant agreement No. ERC-2015-CoG-681707). Travel to conferences to present this work has kindly been funded by the Academy of Finland (projects 273464 and 321840). The computational aspects of my work were made possible through the CSC-IT Center for Science in Espoo, Finland and from the Finnish Grid and Cloud Infrastructure (persistent identifier `urn:nbn:fi:research-infras-2016072533`).

My thanks go to Prof. Larry McLerran for the invitation to visit the Institute for Nuclear Theory, Washington, USA, and to Prof. Raju Venugopalan for the invitation to visit Brookhaven National Laboratory, New York, USA. I would also like to thank Prof. Kari Rummukainen from the University of Helsinki, Finland, and Prof. Heribert Weigert from the University of Cape Town, South Africa, for fruitful collaboration. Thanks also go to Prof. Weigert for encouraging me to pursue this degree in the first place. Thank you to my reviewers, Prof. Adrian Dumitru and Dr. Yoshitaka Hatta, for taking the time to read my lengthy thesis in detail and for the encouraging feedback. I am also thankful to Prof. Stéphane Munier, who has graciously agreed to act as my opponent.

The physics department at JYU has provided a nurturing and stimulating environment for my studies – thank you to the entire JYFL community for making this a happy place to work. I am grateful to the department's administrators, in particular Minttu Haapaniemi, Marjut Hilska and Eeva Partanen, for dealing with my many complicated bureaucratic issues. Thank you to the dynamic and ever-growing QCD theory group, as well as the ALICE team. I am thankful to Prof. Kari Eskola for leading us with great wisdom and a strong moral compass, and also for his personal advice to me over the years.

I would not have ended up in Finland if it was not for the vote of confidence and persuasion of my amazing supervisor, Prof. Tuomas Lappi. Thank you for your endless guidance and patience and for the opportunity to do physics all around the world. I cannot imagine someone more inspirational to have supervised me. Thank you to the other two “Lappi alumni”, Dr. Heikki Mäntysaari and Dr. Jarkko Peuron, for your friendship and guidance. You have been with me through thick and thin, from the very start of this journey in YFL 347. I would also like to thank Heikki for his assistance in writing this thesis and his collaboration with the research.

I have had many other great office mates, in particular, Wafa Almosly, Sami Demirci, Näel Soukouti, Linda Tenhu and Niyati Venkatesan. My fellow QCDists who have also contributed to many nights of revelry include Guillaume Beuf, Kirill Boguslavski, Bertrand Ducloué, Miguel Angel Escobedo and David Müller.

I have the fortune of having a very long list of other friends to thank. While I cannot thank you all by name, I hope that you know how grateful I am for your friendship. I would like to thank, in particular, Noora Aho, Maria Elena Kirk, Antti Koivurova, Tuomas Parsio, Tähti Pohjanmies, Pablo Guerrero Rodriguez, Jooa Sotejeff-Wilson, Kate Sotejeff-Wilson and Candice Townsend. Milano would like to thank Risto Paatelainen, Holly Tann and Johanna Wilson for taking such good care of him and allowing me to travel to further my career in physics. You have each become dear friends to me over the years.

I am so very grateful to have María Triviño De la Cal, Claire Cayol, Manoj Kumar and Anne Thonig in my life – I hold your supportive friendships dearly. To Topi Löytäinen, thank you for taking such good care of me and of our friendship, especially during the writing of this thesis. But mostly, thank you for just being you. To Elise Breissac, who has come to my rescue more times than I can count, thank you from the bottom of my heart for your selflessness. My life has truly changed due to your generosity and untamed spirit.

Finally, I have to thank my sister and the most important person in my life, Andrea “Mirchi” Ramnath. The gratitude I owe you would constitute a whole other thesis, and then you would have to proofread another endless document. You are my best friend and I would never have made it this far without you.

This thesis is dedicated to my parents, Maya Ramnath and Rajen Ramnath, for more than can ever be put into words. Thank you for my roots and my wings.

– Andrecia Ramnath, June 2021, Jyväskylä

Recipe,

*Those who want magic
must take precise measurements
as well as dreaming*

– haiku from *Journal of a New Man* (1986)
by Lionel Abrahams, South African poet

List of Publications

This document consists of an introduction, divided into nine chapters, as well as the following three publications:

[I] T. Lappi, A. Ramnath, K. Rummukainen and H. Weigert

JIMWLK evolution of the odderon

Phys. Rev. D. **94** (2016) 054014, [arXiv:1606.00551 \[hep-ph\]](#),

[II] T. Lappi and A. Ramnath

Unequal rapidity correlators in the dilute limit of the JIMWLK evolution

Phys. Rev. D. **100** (2019) 054003, [arXiv:1904.00782 \[hep-ph\]](#),

[III] T. Lappi, H. Mäntysaari and A. Ramnath

Next-to-leading order Balitsky-Kovchegov equation beyond large N_c

Phys. Rev. D. **102** (2020) 074027, [arXiv:2007.00751 \[hep-ph\]](#).

All research has been conducted at the University of Jyväskylä from 2014 to 2015 and from 2017 to 2020. Part of Paper [I] is based on work from the author's MSc at the University of Cape Town, conducted from 2012 to 2013. For Paper [I], the author has performed the theoretical calculations for Section V and the numerical implementation for Section VI using original code. For Paper [II], the author has performed all calculations and has participated in the writing and editing of the manuscript. For Paper [III], the author has performed all theoretical calculations, has produced Figures 1 to 5 and has written the first draft of the manuscript for publication. Figures 6 to 9 have been produced by the author using a modified code, originally written by collaborator H. Mäntysaari.

Contents

1	Introduction	1
2	The Colour Glass Condensate	5
2.1	Quantum chromodynamics	5
2.2	Light cone coordinates	7
2.3	Deep inelastic scattering	8
2.4	The parton model	9
2.5	Transverse structure of the target	11
2.6	Wilson lines	14
2.7	DIS cross section	17
3	Evolution Equations	21
3.1	DGLAP evolution	21
3.2	BFKL evolution	24
3.3	BK evolution	31
4	JIMWLK in the Fokker–Planck Formalism	39
4.1	How to derive the JIMWLK equation	40
4.2	The JIMWLK Hamiltonian	41
4.3	Lie derivatives	43
4.4	Operation of the JIMWLK Hamiltonian	45
4.5	The Balitsky hierarchy and BK evolution from JIMWLK	47
5	JIMWLK in the Langevin Formalism	51
5.1	The Langevin JIMWLK equation	51
5.2	Inclusive particle production	58
5.3	The Bilocal Langevin Equations	63
6	JIMWLK in the Dilute Limit	71
6.1	The Langevin equation in the dilute limit	72
6.2	Inclusive particle production in the dilute limit	80
7	The Gaussian Approximation	87
7.1	Parametrisation definition	88
7.2	Simple Correlators	89
7.3	4-point correlators	93
7.4	6-point correlators	100

8	Beyond the Gaussian Approximation	111
8.1	The extended GA operator	111
8.2	The 4-point correlator beyond the GA	117
8.3	The odderon contribution to simple correlators	123
9	Conclusion and Outlook	127
	Bibliography	129

1

Introduction

The understanding of matter at its most fundamental level has long been a pursuit of humankind. The current state of particle physics requires modern collider experiments to access unprecedented energy scales, well beyond those of everyday human experience. These experiments are able to collide various particles and nuclei at ultrarelativistic speeds, thereby probing the fundamental constituents of matter. Some examples of such facilities are the LHC (Large Hadron Collider) at CERN (European Organisation for Nuclear Research), RHIC (Relativistic Heavy Ion Collider) at BNL (Brookhaven National Laboratory) and HERA (Hadron-Electron Ring Accelerator) at DESY (German Electron-Synchrotron). In addition, the newly commissioned EIC (Electron-Ion Collider) at BNL is set to provide invaluable data for high energy physics, particularly within the scope of the work discussed in this thesis.

From the theoretical side, the current state of the field is encapsulated within *the Standard Model* of particle physics. *Quantum chromodynamics* (QCD) is the branch within this theory that deals with the strong nuclear force and is characterised by a large coupling. It is applicable to all fundamental particles that carry colour charge, namely quarks and gluons. QCD is of particular importance in understanding the structure of hadronic and nuclear matter. Prior to QCD, hadronic interactions at high energies were studied using *Regge theory* [4–6]. In this formalism, processes are dominated by the exchange of a so-called *Reggeon*. The *hard* scale (due to a large momentum transfer) in the problem allows for the application of perturbation theory. The nonperturbative part of the calculation can be factorised out into the quark and gluon distribution functions. Although we study QCD in this thesis, Regge theory is alluded to, particularly in Chapters 3 and 6.

Unlike a simpler Abelian theory such as quantum electrodynamics, the self-

interacting nature of gluons gives QCD the more complicated structure of a non-Abelian theory. This is one characteristic that makes QCD calculations far more complicated than analogous calculations in other branches of the Standard Model. In certain limiting cases, some technical difficulties may be circumvented by defining an effective field theory that encapsulates the main facets of QCD relevant to that specific limit. At the high energies obtained at colliders like the LHC and RHIC, the quarks and gluons constituting highly boosted hadronic and nuclear matter obtain a large enough momentum that processes are dominated by so-called *small-x* physics. Emission of *soft* (energetically low) gluons is enhanced, which leads to each nucleus effectively appearing as a dense medium of gluons from the perspective of the other nucleus.

An appropriate effective description at small x is the *Colour Glass Condensate* (CGC) [7, 8] field theory. This attempts to explain the fundamental interactions within a nuclear collision, starting from an effective description of the initial colliding nuclei as this dense gluonic medium. The QCD coupling is small enough in this context to allow for perturbation theory. Each boosted nucleus is modelled as a purely classical background colour field with which projectile particles from the other side of the collision can interact. Beyond understanding the CGC itself, initial-state effects are important for the study of later stages of a collision, such as the possible formation of a quark–gluon plasma.

A key tool within the CGC formalism is the *renormalisation group equation* (RGE), of which several are discussed in this thesis. In general, one starts by calculating the quantum corrections to a QCD process, which involve additional gluon emissions. These corrections contain an integral over the phase space of the emitted gluons, which generate a large logarithm. By absorbing the large logarithmic factors in a redefinition of some quantity, one derives an RGE that describes the evolution of this quantity on some typical scale within the calculation. The solution of the RGE then involves a resummation of the large logarithms.

One famous example of an RGE is the DGLAP (Dokshitzer–Gribov–Altarelli–Parisi) equations [9–12], which resum the large logarithms into quark and gluon distribution functions, thereby governing their evolution as a function of the energy Q^2 of the probe of the distributions. A more relevant type of RGE for the work discussed in this thesis is the class of equations that govern evolution in rapidity, or Bjorken- x . Some examples of such equations are the BFKL (Balitsky–Fadin–Kuraev–Lipatov) equation [13–17], the BK (Balitsky–Kovchegov) equation [18, 19] and the JIMWLK (Jalilian-Marian–Iancu–McLerran–Weigert–Leonidov–Kovner) equation [7, 8, 20–23]. The objects being evolved in such RGE equations are *Wilson line correlators*. These are expectation values of products of path-ordered exponentials that correspond to the QCD interaction between a projectile and a highly boosted

nucleus. It is important to study the behaviour of these correlators on different energy scales in order to understand the behaviour of cross sections of various processes.

This document is structured as follows. Some theoretical background is provided in Chapters 2 to 8 to explain the work contained in Papers [I], [II] and [III] that follow. In Chapter 2, the key concepts of the CGC are discussed, including the *Colour Dipole model* [24–28], in the context of *Deep Inelastic Scattering (DIS)*. In Chapter 3, we provide further explanation of the various RGEs mentioned above, particularly the DGLAP, BFKL and BK equations. The following two chapters are dedicated to the JIMWLK equation, first formulated as a Fokker–Planck equation in Chapter 4 and then as a mathematically equivalent Langevin equation in Chapter 5. Chapter 6 explores the the Langevin JIMWLK equation further, by going to the limiting case of a dilute nucleus – this is related directly to Paper [II]. Then, a truncation scheme called the Gaussian Approximation (GA) [49, 83, 96–101] is introduced in Chapter 7. We discuss the calculation of correlators of six Wilson lines, as studied in Paper [III]. Finally, Chapter 8 covers an extension to this approximation scheme. We show how this is used to derive an evolution equation for a parity-odd object called the *odderon*, as studied in Paper [I]. A brief conclusion and future prospects are provided in Chapter 9, before Papers [I], [II] and [III] are presented.

2

The Colour Glass Condensate

In this chapter, we introduce the Colour Glass Condensate (CGC) effective field theory that describes a highly boosted nucleus as a dense gluonic medium. The term *colour* in the CGC refers to the charge of QCD, which leads to critical non-Abelian effects. *Glass* refers to the dynamical behaviour of the medium on different time scales – this is explained further in Section 2.5. *Condensate*¹ refers to the saturation seen at very high energies, where high gluon occupation numbers dominate the medium. Several reviews of the CGC are available, which contain more details than provided here – for example, see [29–34].

We begin with an overview of the basic tools of QCD in Section 2.1 and physics on the light cone in Section 2.2. In Section 2.3, we introduce the process of deep inelastic scattering (DIS), which provides a simple concrete context for the ideas that follow in subsequent sections. Within the DIS framework, we explore the parton model in Section 2.4 and the transverse structure of the nucleus in Section 2.5. Section 2.6 deals with how exactly a probe interacts with this nucleus, as described by Wilson lines. Finally, we conclude the chapter with a discussion of the DIS cross section in Section 2.7.

2.1 Quantum chromodynamics

QCD is a non-Abelian Yang–Mills gauge theory with symmetry Lie group $SU(N_c)$. There are $N_c = 3$ colours in nature, but this parameter is left general throughout

¹Despite the more common use of the term “condensate” in reference to a phase transition, no such transition exists in the context of the CGC.

this thesis. The QCD Lagrangian density is

$$\mathcal{L}_{\text{QCD}} := \sum_{f=1}^{N_f} (\bar{\psi}_f)_i (i\gamma_\mu D_{ij}^\mu - m_f \delta_{ij}) (\psi_f)_j - \frac{1}{4} F_a^{\mu\nu} F_{\mu\nu}^a, \quad (2.1)$$

with fundamental indices $1 \leq i, j \leq N_c$ and adjoint indices $1 \leq a \leq N_c^2 - 1$. The summation is over all quark flavours f , of which there are $N_f = 6$ in nature. The fermionic and antifermionic fields are denoted by ψ_f and $\bar{\psi}_f := \psi_f^\dagger \gamma^0$, respectively. They have flavour f , spin $1/2$, mass m_f and transform under the fundamental representation of $\text{SU}(N_c)$. The γ 's are the Dirac matrices.

The covariant derivative in Eq. (2.1) is defined as

$$D_\mu := \partial_\mu - igA_\mu^a t^a, \quad (2.2)$$

where $\partial_\mu := \partial/\partial x^\mu$. The strong coupling in this definition is denoted by g and is often written as $\alpha_s = g^2/(4\pi)$. The group generators t^a are traceless Hermitian matrices in the Lie algebra $\mathfrak{su}(N_c)$. We use a lower case t^a for the fundamental representation and an upper case T^a for the adjoint representation. The gauge fields A_μ^a represent massless gluons with spin 1, which transform under the adjoint representation. For a fundamental $\text{SU}(N_c)$ matrix U , we write $\tilde{U}^{ab} = 2\text{tr}(t^a U t^b U^{-1})$ so that any such matrix with a tilde and two colour indices is understood henceforth to be in the adjoint representation. The field strength tensor in Eq. (2.1) is

$$F_{\mu\nu}^a := \partial_\mu \mathcal{A}_\nu^a - \partial_\nu \mathcal{A}_\mu^a + g f^{abc} \mathcal{A}_\mu^b \mathcal{A}_\nu^c, \quad (2.3)$$

where $f^{abc} = 2i\text{tr}(t^a [t^b, t^c])$ are the antisymmetric structure constants. The symmetric structure constants $d^{abc} = 2i\text{tr}(t^a \{t^b, t^c\})$ are also needed, particularly in Chapter 7 where colour multiplets are discussed.

Several colour factors appear throughout this thesis, which we define as follows. For any representation \mathcal{R} of dimension $d_{\mathcal{R}}$, we write

$$\text{tr}(t_{\mathcal{R}}^a t_{\mathcal{R}}^b)_{\mathcal{R}} = \alpha_{\mathcal{R}} \delta^{ab} \quad \text{and} \quad C_{\mathcal{R}} d_{\mathcal{R}} := \text{tr}(t_{\mathcal{R}}^a t_{\mathcal{R}}^a)_{\mathcal{R}} \quad (2.4)$$

$$\implies \alpha_{\mathcal{R}} d_{\mathcal{A}} = C_{\mathcal{R}} d_{\mathcal{R}}. \quad (2.5)$$

By convention, $\alpha_{\text{F}} = 1/2$ and $\alpha_{\text{A}} = N_c$ for the fundamental and adjoint representations, respectively. Using $d_{\text{F}} = N_c$ and $d_{\text{A}} = N_c^2 - 1$ leads to the Casimirs $C_{\text{F}} = (N_c^2 - 1)/(2N_c)$ and $C_{\text{A}} = N_c$. We also make use of the factor $C_{\text{d}} = (N_c^2 - 4)/N_c$, which follows from a contraction of the symmetric structure constants: $C_{\text{d}} \delta_{ab} := d^{acd} d^{bcd}$.

One defining feature of QCD is asymptotic freedom, which refers to the energy-dependent behaviour of the strong coupling

$$\alpha_s(|q^2|) = \frac{\alpha_s(\mu^2)}{1 + \frac{\alpha_s(\mu^2)}{12\pi} [11N_c - 2N_f] \ln \left[\frac{|q^2|}{\mu^2} \right]}, \quad |q^2| \gg \mu^2. \quad (2.6)$$

A probe defines the energy q – this is explained in the following section in the context of DIS. The fixed energy μ is a renormalisation scale used to define the QCD cutoff

$$\ln \Lambda_{\text{QCD}}(\mu^2) = \ln \mu^2 - \frac{12\pi}{(11N_c - 2N_f)\alpha_s(\mu^2)}. \quad (2.7)$$

For sufficiently high energies (which correspond to short length scales), α_s is small enough to act as an expansion parameter in perturbation theory. Beyond Λ_{QCD} , however, α_s becomes large and perturbation theory breaks down. In this case, quarks and gluons remain confined to colour-neutral bound states, whose internal structure is not accessible to the probe.

2.2 Light cone coordinates

Since the physics of a process is independent of the coordinate system chosen for a calculation, there is freedom to choose a convenient system based on the particular problem at hand. A natural choice for relativistic collisions is the light cone coordinate system, defined by the transformation

$$T := \begin{pmatrix} \frac{1}{\sqrt{2}} & 0 & 0 & \frac{1}{\sqrt{2}} \\ 0 & 1 & 0 & 0 \\ 0 & 0 & 1 & 0 \\ \frac{1}{\sqrt{2}} & 0 & 0 & -\frac{1}{\sqrt{2}} \end{pmatrix}. \quad (2.8)$$

The light cone metric is found using $g' = T^\top g T$. With the standard Minkowski metric $g = \text{diag}(1, -1, -1, -1)$, this gives

$$g' = \begin{pmatrix} 0 & 0 & 0 & 1 \\ 0 & -1 & 0 & 0 \\ 0 & 0 & -1 & 0 \\ 1 & 0 & 0 & 0 \end{pmatrix}. \quad (2.9)$$

The light cone components of a Minkowski 4-vector $x = (x^+, \mathbf{x}, x^-)$ are

$$x^\pm := \frac{1}{\sqrt{2}}(x^0 \pm x^3) \quad \text{and} \quad \mathbf{x} := (x^1, x^2), \quad (2.10)$$

so that the coordinate x^\pm -axes lie along the light cone, as shown in Fig. 2.2.

In the light cone system, a boost in the x^3 -direction is given by $x \rightarrow \Lambda' x$, where

$$\Lambda' := \text{diag}(e^Y, 1, 1, e^{-Y}). \quad (2.11)$$

This is written in terms of the rapidity $Y := \ln(1/\sqrt{1-v^2})$, where v is the relative speed between the two frames. The vectors along the two light cone axes are eigenvectors of the boost, i.e. $x^\pm \rightarrow e^{\pm Y} x^\pm$. This allows for an interpretation of a light cone “time”, despite the mixing of components $t = x^0$ and $z = x^3$ in the transformation. Since the x^+ -component increases by a factor e^Y when boosted, it can be interpreted as the light cone time that undergoes a Lorentz dilation. Similarly, the x^- -component decreases by a factor e^{-Y} and is therefore interpreted as a spatial component that undergoes a Lorentz contraction.

2.3 Deep inelastic scattering

In order to discuss the CGC in a concrete way, we now introduce the process of DIS. Generically, this is a collision between any leptonic projectile with a nuclear or hadronic target. In particular, we consider the interaction of an electron e with a proton p , as shown in Fig. 2.1. The electron projectile emits a virtual photon γ^* . Given sufficiently large momentum, the photon is able to probe the internal structure of the proton target. As mentioned in Section 2.2, the collision axis is taken as the boost direction x^3 . In the full relativistic limit, the photon’s trajectory is aligned with the x^+ -axis and the target’s trajectory with the x^- -axis, as shown in Fig. 2.2. The formalism developed here for DIS can be extended to many other photon-mediated processes in a relativist collision. In the case of a collision between two of the same nuclei, either may be taken as the projectile. If the colliding nuclei are different, the lighter of the two is typically considered in place of the leptonic projectile.

Due to the large boost in the ep collision considered, the target appears to be highly Lorentz contracted from the viewpoint of the probe. When $1/\alpha_s \gg 1$, the target field becomes perturbatively strong in the coupling and may be treated purely classically. The smallness in the coupling is what leads to the high gluon occupation numbers that form the “condensate” in the CGC acronym. To lowest order in perturbation theory, the strong interaction with the target occurs when the photon splits into a dipole consisting of a quark and an antiquark, as shown in Fig. 2.3. The typical lifetime of the dipole is much longer than the diameter of the target. The quark and antiquark may then interact with the target through an exchange of gluons. At high energies, the transverse separation between the

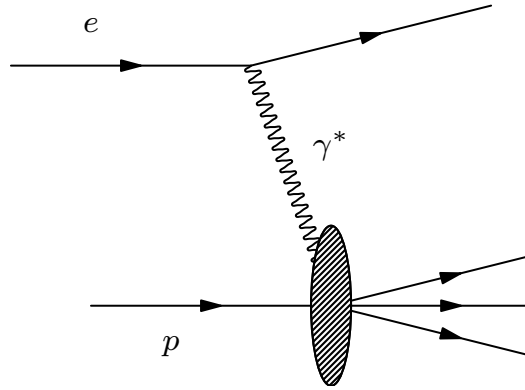


Figure 2.1. An example of a DIS process in which an electron e emits a virtual photon γ^* that interacts with a proton p .

quark and antiquark remains essentially fixed [35, 36]. This makes the transverse coordinate plane a convenient space for calculations in the dipole.

An elastic scattering (one in which the incoming and outgoing particles are the same) between the dipole and the target is shown in Fig. 2.3. In this case, the quark and the antiquark individually carry colour but together constitute a colour-neutral object. There is therefore no overall colour transfer between the target and the dipole. The same is true of other quantum numbers, such as spin and flavour – these are conserved within the dipole throughout the interaction. This fact is due to the incoming and outgoing photons being colour-neutral.

2.4 The parton model

The internal structure of the proton consists of an ever-changing number of quarks and gluons, called *partons*. This is due to continuous production and annihilation as the partons interact with each other. The time scales for these interactions, however, are much larger than the time scales relevant for DIS. This means that the target effectively appears to the dipole as a collection of noninteracting partons.

The appearance of the target from the viewpoint of the photon depends on two variables. The *virtuality* $Q^2 := -q^2$ is defined in terms of the square of the photon's spacelike momentum $q^2 < 0$. The second variable is the so-called *Bjorken- x*

$$x_{\text{Bj}} := \frac{-q^2}{2P \cdot q}, \quad (2.12)$$

where P is the target's momentum. In doing the full DIS calculation, x_{Bj} can be interpreted as the fraction of the interacting parton's momentum over the total

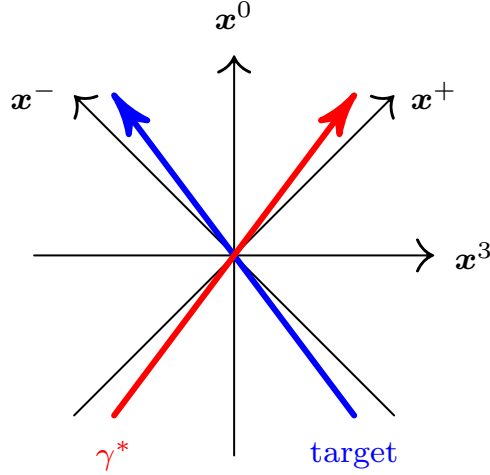


Figure 2.2. A two-dimensional coordinate plane showing the Minkowski axes x^0 and x^3 and the light cone axes x^+ and x^- . The photon's trajectory is aligned along the x^+ -axis and the target's trajectory is aligned along the x^- -axis. In the full relativistic limit, the two trajectories align exactly with the light cone axes.

target momentum. In processes other than DIS, an analogous x is used with the same interpretation. The two variables x_{Bj} and x are the same to leading order in the parton model, so we use them interchangeably. The Q^2 and x_{Bj} set the transverse and longitudinal scales, respectively, in the interaction.

The cross section for the ep collision can be calculated using standard QFT techniques – see [37–39], for example. The result in the proton's rest frame is

$$\frac{d\sigma}{d^3p'} = \frac{\alpha_{\text{EM}}^2}{EE'W^4} L_{\mu\nu} W^{\mu\nu}, \quad (2.13)$$

where α_{EM} is the electromagnetic coupling, E and E' are the energies of the incoming and outgoing electrons, respectively, and p' is the outgoing electron's 3-momentum. The contributions to the cross section from the electron and the proton factorise into the leptonic tensor $L_{\mu\nu}$ and hadronic tensor $W_{\mu\nu}$, respectively. The hadronic tensor is the part of the cross section that contains the physics of interest to us. It can be shown that $W^{\mu\nu}$ may be written in terms of two structure functions W_1 and W_2 as [29]

$$W^{\mu\nu} = -W_1(x, Q^2) \left(g^{\mu\nu} - \frac{q^\mu q^\nu}{q^2} \right) + \frac{W_2(x, Q^2)}{m^2} \left(P^\mu - \frac{P \cdot q}{q^2} q^\mu \right) \left(P^\nu - \frac{P \cdot q}{q^2} q^\nu \right). \quad (2.14)$$

At this stage, W_1 and W_2 are two unknown scalar functions that depend on both x and Q^2 and have the dimension of mass. They can be written in terms of

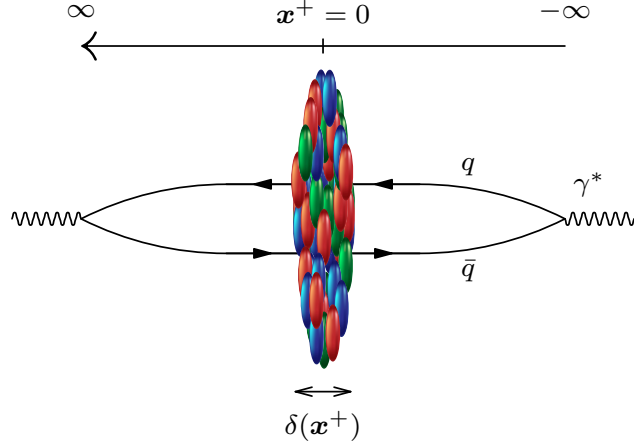


Figure 2.3. Elastic scattering between the virtual photon and the target in which the photon splits into a quark–antiquark pair, called a dipole. The dipole then interacts through gluon exchange with the target. Light cone time runs from right to left. Due to Lorentz contraction, the target is effectively localised where it is placed at $x^+ = 0$.

dimensionless functions F_1 and F_2 as

$$F_1(x, Q^2) := mW_1(x, Q^2), \quad (2.15)$$

$$F_2(x, Q^2) := \frac{Q^2}{2mx} W_2(x, Q^2), \quad (2.16)$$

where m is the mass of the proton. These dimensionless functions are typically calculated in the infinite momentum frame for convenience, i.e. a frame in which the proton is moving ultrarelativistically. For a full exposition using light cone perturbation theory, see [29]. After the full calculation, F_1 and F_2 actually turn out to be independent of Q^2 . This means that the hadronic part of the DIS cross section can be expressed entirely in terms of two dimensionless functions that depend solely on x – a fact known as *Bjorken scaling*. A famous experimental plot of this phenomenon is shown in Fig. 2.4. The function F_2 is plotted against Q^2 for various fixed values of x . The other structure function F_1 can be obtained from F_2 through the Callan–Gross relation $F_2(x) = 2xF_1(x)$ [40].

2.5 Transverse structure of the target

We now look more closely at the internal structure of the target. In the *Glauber model*, a nucleus is described as a large dilute homogeneous collection of $A \gg 1$ nucleons. Since correlations between nucleons are suppressed by powers of A , we assume that the nucleons do not interact with each other. In the setup shown in

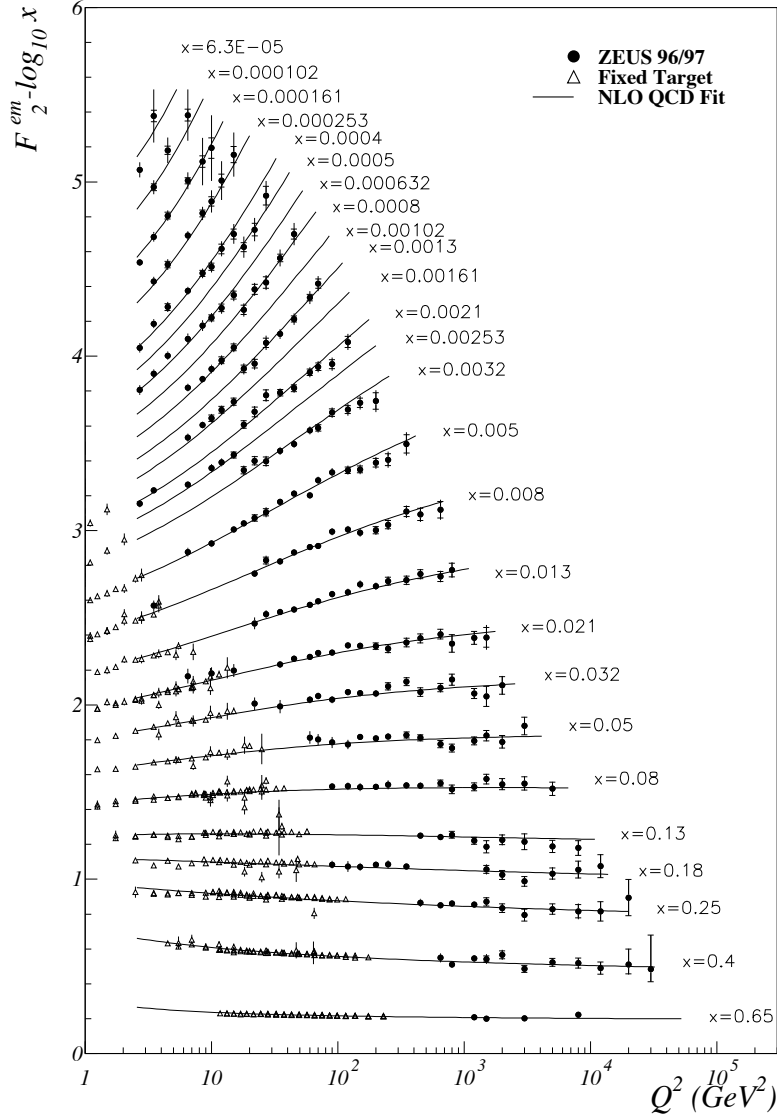


Figure 2.4. Data from the ZEUS collaboration at HERA for the F_2 structure function for neutral current positron–proton DIS, demonstrating Bjorken scaling [41]. The structure function F_2 is plotted against Q^2 for various fixed x . The triangular points are data from various fixed target experiments: the NMC and BCDMS experiments at CERN and the E665 experiment at Fermilab. The solid lines are from a ZEUS NLO QCD fit. The scaling at very small x is not as good as that at large x – this is a sign that higher-order corrections to the parton model become increasingly important with decreasing x . Reprinted by permission from Springer Nature Customer Service Centre GmbH: Springer Nature The European Physical Journal C – Particles and Fields, *Measurement of the neutral current cross section and F_2 structure function for deep inelastic e^+p scattering at HERA*, Chekanov, S. et al. © (2001).

Fig. 2.2, the target is highly Lorentz contracted in the x^+ -direction. In the full relativistic limit, it becomes entirely independent of x^+ . This is the behaviour to which the term “glass” in the CGC refers: at low x , the target evolves slowly enough that it is effectively independent of light cone time x^+ , whereas at high x , the time dependence cannot be neglected.

The phase diagram for the transverse structure of the target is shown in Fig. 2.5 in the Y - $\ln Q^2$ plane. The partons are point particles in reality, but their measured size depends on the resolution of the experimental probe. Since a photon with larger Q^2 and smaller wavelength has a better resolution, the apparent partonic size in the transverse plane is proportional to $1/Q^2$. This is seen along the horizontal axis in Fig. 2.5: as Q^2 decreases, the partons appear smaller. Along the vertical axis, larger rapidities correspond to smaller x and more available energy for gluon emission. For fixed small to moderate Q^2 , increasing Y therefore corresponds to more partons in the target.

In the top left of the phase diagram, the target becomes densely populated with apparently large partons. Their overlapping wave functions result in recombination effects that eventually lead to saturation. This is a direct consequence of QCD being a non-Abelian theory, since this means that gluons may self-interact. In this region of phase space, BFKL evolution is no longer able to accurately predict evolution in rapidity. Instead, evolution becomes nonlinear, as governed by the BK and JIMWLK equations. The various evolution equations along the Y and Q^2 axes in Fig. 2.5 are discussed in the next chapter.

From the experimental perspective, there are several observables that may provide signs of saturation within a collision. Two recent examples of the many instances where saturation is believed to be relevant include inclusive production (where only the produced particles are measured and the rest are summed over in the final state) of D mesons at forward rapidity [42] and exclusive production (no other particles produced) of J/Ψ and Υ mesons in ultra-peripheral collisions [43]. In [44], possible signs of saturation have been detected in di-hadron correlations in proton–lead collisions, after the subtraction of hydrodynamic effects. These are just a few examples of the many processes that potentially show signatures of saturation.

The effective colour charge density of the target in the transverse plane can be described by the *McLerran–Venugopalan (MV) model* [45–47]. In this model, typical colour charge density fluctuations are characterised by a hard momentum scale $\mu^2 \sim \Lambda_{\text{QCD}}^2 A^{1/3}$. This hard scale corresponds to small values of the coupling α_s , which suppress quantum corrections and allow for the target to be treated as a purely classical field governed by the Yang–Mills equations of motion.

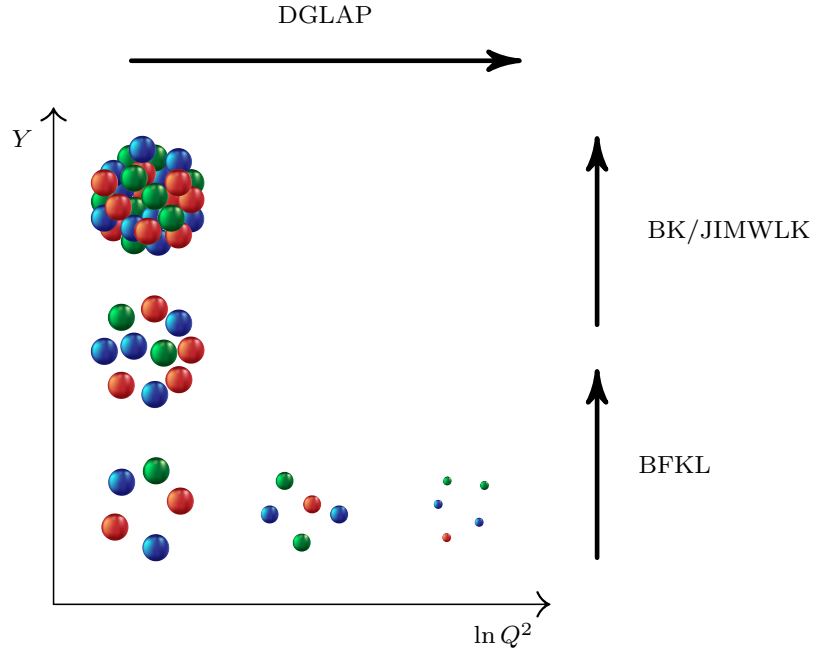


Figure 2.5. Phase diagram showing the transverse structure of the target as a function of rapidity Y and virtuality Q^2 . Also shown are the directions and regions of applicability of the DGLAP, BFKL and BK equations discussed in Chapter 3 and the JIMWLK equation discussed in Chapters 4 and 5.

2.6 Wilson lines

Now that we have an idea of the target structure, we explore the exact nature of its interaction with the photon probe. This section is a summary of the discussion provided in the review [30]. The optical theorem states that the total cross section is given by the difference between the interacting piece and the noninteracting piece of the imaginary part of the forward elastic scattering amplitude². In order to calculate the nontrivial part of the amplitude, we need to find expressions for the fermionic propagators (the dipole) in the presence of a background field (the target). Such propagators have been calculated in detail in [19, 48] and elsewhere. Here, we quote a result from [30] which encapsulates everything needed for the remainder of our discussion. The propagator for the simplified case of a massless scalar in a

²This can be deduced from the unitarity of the scattering matrix, which we write as $S = \mathbb{1} - iT$, so that unitarity implies $-i(T^\dagger - T) = T^\dagger T$.

background field A is given by

$$\frac{-i}{D^2[A]}(x, y) = \int_0^\infty ds \int_y^x [dz] \exp \left\{ - \int_0^s d\kappa \frac{\dot{z}^2(\kappa)}{4} \right\} \text{P exp} \left\{ -ig \int_y^x dz^\mu A_\mu(z) \right\}, \quad (2.17)$$

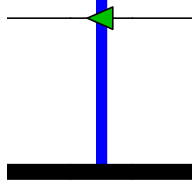
where the path integral is taken over trajectories z (parametrized by κ) that connect x (at $\kappa = 0$) to y (at $\kappa = s$).

In Section 2.2, it was noted that a boost in the x^3 -direction modifies the light cone vector components by $x^\pm \rightarrow e^{\pm Y} x^\pm$. This means that the corresponding components of the target field strength tensor get enhanced and suppressed accordingly. Additionally, the target is Lorentz contracted in the x^+ -direction and effectively independent of x^- due to time dilation. Working in the light cone gauge $A^+ = 0$, the gauge field is written as $A^\mu(z) = g^{\mu+} \delta(z^+) \beta(\mathbf{z})$, where $\beta(\mathbf{z})$ is a function that describes the transverse structure of the target. Due to the delta function at $x^+ = 0$, any projectile traversing the x^+ -axis propagates freely, except where it momentarily encounters the target. The momentum carried by the dipole is large enough that this localised interaction with the target at $x^+ = 0$ is insufficient to deflect the quark and the antiquark in the transverse plane. Instead, they propagate straight through the target field. They do, however, undergo a phase rotation in colour space and the interaction between the dipole and the target is said to *eikonalise*.

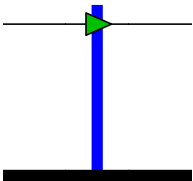
The eikonal approximation allows us to deform the path integral in Eq. (2.17) as

$$\text{P exp} \left\{ -ig \int_y^x dz^\mu A_\mu(z) \right\} \rightarrow \text{P exp} \left\{ -ig \int_{y^+}^{x^+} dz^+ A^-(z^+, \mathbf{x}, 0) \right\}. \quad (2.18)$$

Depending on the integration limits, we get the quark *Wilson line*

$$U_{\mathbf{x}} := \text{P exp} \left\{ -ig \int_{-\infty}^{\infty} dz^+ A^-(z^+, \mathbf{x}, 0) \right\} =: \quad \begin{array}{c} \text{---} \\ \uparrow \\ \text{---} \end{array}, \quad (2.19)$$


or the corresponding antiquark Wilson line

$$U_{\mathbf{x}}^\dagger := \text{P exp} \left\{ ig \int_{-\infty}^{\infty} dz^+ A^-(z^+, \mathbf{x}, 0) \right\} =: \quad \begin{array}{c} \text{---} \\ \downarrow \\ \text{---} \end{array}. \quad (2.20)$$


We have introduced a diagrammatic notation in the spirit of [49] that is used throughout this thesis. The notation for the Wilson lines is a shorthand for multiple gluon exchange between the projectile and the target:

$$U_{\mathbf{x}} = \begin{array}{c} \text{---} \\ | \\ \text{---} \end{array} \begin{array}{c} \blacktriangleleft \\ \bullet \\ \bullet \\ \bullet \end{array} \begin{array}{c} \text{---} \\ | \\ \text{---} \end{array} \dots \begin{array}{c} \text{---} \\ | \\ \text{---} \end{array} \quad (2.21)$$

The thin horizontal lines represent the projectile, the thick horizontal line at the bottom represents the target and the blue vertical line represents the background gauge field $A^-(z^+, \mathbf{x}, 0)$. An interaction between the target and the projectile is denoted by a green arrowhead along the projectile's line at the point where it meets the background field at $x^+ = 0$. Since the light cone time axis runs from right to left, as shown in Fig. 2.3, a Wilson line is represented by an arrowhead pointing left and the Hermitian conjugate Wilson line is represented by an arrowhead pointing right (since an antiquark is thought of as a quark propagating backwards in light cone time).

With this new diagrammatic notation, the interaction shown in Fig. 2.3 may be recast as Fig. 2.6. The $U_{\mathbf{x}}$ and $U_{\mathbf{y}}^\dagger$, respectively, replace the propagators of the eikonal quark and antiquark traversing the x^+ -axis. The quark and antiquark split from the virtual photon at $x^+ \rightarrow -\infty$, have transverse positions \mathbf{x} and \mathbf{y} , respectively, and then recombine into a photon at $x^+ \rightarrow \infty$. In reality, the dipole would form from the photon at some finite time before $x^- = 0$ and recombine into a photon at some finite time after $x^- = 0$. Both $U_{\mathbf{x}}$ and $U_{\mathbf{y}}^\dagger$ are elements of the $SU(N_c)$ Lie group; they transform under the fundamental and antifundamental representations, respectively. The non-Abelian nature of QCD manifests in the path ordering in Eqs. (2.19) and (2.20), since the order of interactions along the path of integration must be preserved to ensure that the noncommuting generators are kept ordered.

In subsequent chapters, we also consider gluon interactions with the target. The corresponding Wilson line is in the adjoint representation of $SU(N_c)$ and is denoted by a diamond instead of an arrowhead (since it is just a real number without direction):

$$\tilde{U}_z^{ab} = 2\text{tr} (t^a U_z t^b U_z^\dagger) =: \begin{array}{c} \text{---} \\ | \\ \text{---} \end{array} \begin{array}{c} \blacklozenge \\ \bullet \\ \bullet \\ \bullet \end{array} \begin{array}{c} \text{---} \\ | \\ \text{---} \end{array} \quad (2.22)$$

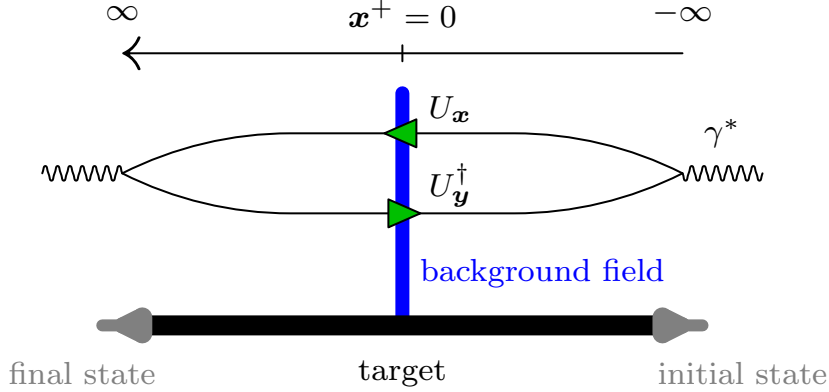


Figure 2.6. The interaction shown in Fig. 2.3 recast in the new diagrammatic notation for the Wilson lines, introduced in Eqs. (2.19) and (2.20). The vertical blue line represents the target background field. Following the notation of [49], the target’s initial and final states are denoted by grey endpoints on the target line at the bottom.

Note that $[\tilde{U}_z^\dagger]^{ab} = [\tilde{U}_z]_{ba} = [\tilde{U}_z^{-1}]_{ab}$.

2.7 DIS cross section

We now return to the subject of the DIS cross section from Section 2.3. One advantage of the dipole picture as shown in Fig. 2.6 is that the cross section factorises into two parts [50]:

$$\sigma^{\gamma^* A}(x, Q^2) = \int_{\mathbf{r}} \int_0^1 d\alpha |\psi^{\gamma^* \rightarrow q\bar{q}}(\alpha, \mathbf{r}^2, Q^2)|^2 \sigma^{q\bar{q}A}(\mathbf{r}, Y). \quad (2.23)$$

The photon wave function factor $|\psi^{\gamma^* \rightarrow q\bar{q}}|^2$ corresponds to the first part of the interaction, in which the photon splits into a dipole. It depends on three variables. The first of these is the longitudinal momentum fraction α of either the quark or the antiquark, which is integrated from 0 to 1. The second variable is the transverse dipole size $\mathbf{r} := |\mathbf{x} - \mathbf{y}|$; we use the shorthand $\int_{\mathbf{r}} := \int_0^\infty d^2r$. The third variable is the virtuality Q^2 defined in Section 2.4. The wave function contains the entire QED part of the photon–target interaction, and is not discussed further in this thesis. Some examples of how it is calculated may be found in [51–53].

Instead, we focus on the second factor $\sigma^{q\bar{q}A}$ in Eq. (2.23), which contains the QCD part of the photon–target interaction. This corresponds to the dipole interaction with the target, which depends on the transverse size \mathbf{r} of the dipole and the rapidity Y . Notice that neither factor in $\sigma^{\gamma^* A}$ depends on the exact coordinates

of the quark and the antiquark – only the transverse separation between the two appears. A pedagogical explanation of the calculation of $\sigma^{q\bar{q}A}$ may be found in [29]. One calculates the diagram in Fig. 2.6 using the fermionic propagator in a background field, which is similar to Eq. (2.17). This leads to the factor $U_{\mathbf{x}}$ for the quark and the factor $U_{\mathbf{y}}^\dagger$ for the antiquark, as noted in the diagram. The product of these two Wilson lines is traced over due to the contraction of colour indices at the photon–dipole vertex. This ensures that there is a zero net colour exchange between the dipole and the target. A normalisation N_c is included with the factor $\text{tr}(U_{\mathbf{x}}U_{\mathbf{y}}^\dagger)$, which can be calculated by setting both Wilson lines in the trace to $\mathbb{1}$.

This takes care of the interacting piece of the amplitude. For the noninteracting piece, we replace all the Wilson lines in the interacting piece by unit matrices (since there is no interaction with the target field in that case). Then the difference between the noninteracting and interacting pieces gives $N_{\mathbf{xy}} := \text{tr}(\mathbb{1} - U_{\mathbf{x}}U_{\mathbf{y}}^\dagger)/N_c$ and the dipole cross section becomes [30]

$$\sigma^{q\bar{q}A}(\mathbf{r}, Y) = \int_{\mathbf{b}} \langle N_{\mathbf{xy}} + N_{\mathbf{yx}} \rangle = 2 \int_{\mathbf{b}} \text{Re} \langle N_{\mathbf{xy}} \rangle. \quad (2.24)$$

The integral is over the impact parameter $\mathbf{b} := (\mathbf{x} + \mathbf{y})/2$, which ensures that $\sigma^{q\bar{q}A}$ scales with the transverse size of the target and vanishes outside of it. Notice that Eq. (2.24) contains no information about the intrinsic properties of the quark and the antiquark. This means that their quantum numbers are indeed preserved throughout the interaction with the target, as stated in Section 2.3.

The angle brackets in Eq. (2.24) denote an average over all configurations of the background field, thereby encapsulating all information about the target. An expectation value of a product of Wilson lines is called a *correlator*, since it signifies how well the Wilson lines are correlated with one another. In the ubiquitous McLerran–Venugopalan (MV) model [45, 46, 54], the target average for a Wilson line operator $F[U]$ is given by

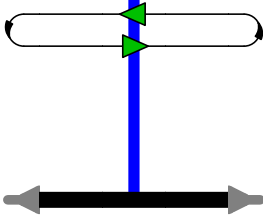
$$\langle F[U] \rangle = \frac{\int \mathcal{D}\rho F[U] W[\rho]}{\int \mathcal{D}\rho W[\rho]}, \quad (2.25)$$

where $\rho = \rho(x^+, \mathbf{x})$ is the light cone colour charge density in the target. The functional $W[\rho]$ is a weight such that

$$\int \mathcal{D}\rho W[\rho] := \int \mathcal{D}\rho \exp \left\{ - \int_{\mathbf{x}} \int_{-\infty}^{\infty} dx^+ \frac{\text{tr}(\rho^2)}{\mu^2} \right\}, \quad (2.26)$$

where $\mu^2 = \mu^2(x^+, \mathbf{x})$ is a measure of the colour charge fluctuations. More about these expectation values are discussed in the next chapter.

The operator N_{xy} is the interacting piece of the *dipole operator*³ $S_{xy}^{(2)} = 1 - N_{xy}$ and is represented diagrammatically as

$$\frac{1}{N_c} \text{tr} (U_x U_y^\dagger) = \frac{1}{N_c} \text{tr} \left(\text{Diagram} \right), \quad (2.27)$$


where the trace is denoted by the closed loop. Using the diagrammatic ingredients introduced up to this point, it is possible to consider more complicated correlators, such as those found in Chapter 3 onwards. For higher-point correlators, we use the general notation

$$S_{\mathbf{x}_1, \mathbf{x}_2, \dots, \mathbf{x}_{n-1}, \mathbf{x}_n}^{(n)} := \frac{1}{N_c} \text{tr} (U_{\mathbf{x}_1} U_{\mathbf{x}_2}^\dagger \dots U_{\mathbf{x}_{n-1}} U_{\mathbf{x}_n}^\dagger). \quad (2.28)$$

Since the fundamental Wilson lines are elements of $SU(N_c)$, the dipole correlator $\langle S_{xy}^{(2)} \rangle$ takes on values from zero to one. In the total absence of a target, there is no phase rotation in colour space and so $U_x = U_y^\dagger = \mathbb{1}$. This means $\langle S_{xy}^{(2)} \rangle = 1 \implies \langle N_{xy} \rangle = 0$ and the dipole cross section in Eq. (2.24) vanishes.

Chapter summary

In this chapter, we have discussed the main ingredients of QCD and the light cone needed in this thesis. The CGC effective field theory was introduced in the context of DIS. We have studied the structure of a nuclear target using the parton model and introduced Wilson lines to account for the interaction of a projectile with the target in the eikonal limit. Finally, we have given an expression for the DIS cross section in terms of the dipole correlator. The diagrammatic notation for Wilson lines used in subsequent chapters has also been introduced.

³Note that N_{xy} and $S_{xy}^{(2)}$ are sometimes defined to include the expectation value, whereas we exclude it.

3

Evolution Equations

Now that the main ingredients needed to understand the CGC have been introduced, we turn to the topic of the evolution equations for Wilson line correlators. The three equations discussed in this chapter are shown on the phase diagram in Fig. 2.5. The DGLAP equations govern evolution in Q^2 , along the horizontal axis. The BFKL equation is a linear equation that governs evolution in Y , along the vertical axis. For large Y , BFKL evolution breaks down and the BK equation is needed to more accurately describe evolution. The JIMWLK equation, which is also shown in Fig. 2.5, is deferred to Chapters 4 and 5.

We begin this chapter with DGLAP evolution in Section 3.1, including a discussion of parton distribution functions and an overview of how to derive the DGLAP equations. In section 3.2, we study BFKL evolution and the derivation of the evolution equation, after introducing the Low–Nussinov model for dipole–dipole scattering. We also discuss some of the problems with BFKL evolution, which lead to the consideration of nonlinear effects. This takes us to BK evolution in Section 3.3, where we begin with the Glauber–Gribov–Mueller model and Mueller’s dipole model. These are needed for the derivation of the BK equation at the end of the section.

3.1 DGLAP evolution

The DGLAP equations are a type of renormalisation group equation describing the evolution of the quark and gluon distribution functions in the nucleus as a function of (large) Q^2 . Their derivation may be found in several textbooks, for example [37–39, 55, 56]. Here, we outline the derivation provided in [29].

3.1.1 Parton distribution functions

Recall the structure functions F_1 and F_2 introduced in Section 2.4. With light cone perturbation theory, these can be used to obtain the quark distribution function

$$q^f(x, Q^2) = \sum_n \frac{1}{x} \int_{\mathbf{k}} \frac{1}{2(2\pi^3)} \frac{1}{S_n} \sum_{\sigma=\pm 1} \prod_{i=1}^n \int \frac{dx_i}{x_i} \int_{\mathbf{k}_i} \frac{1}{2(2\pi)^3} |\Psi_n^f(\{x_i, \mathbf{k}_i\}; x, \mathbf{k}, \sigma)|^2 \times (2\pi)^3 \delta^2 \left(\mathbf{k} + \sum_{j=1}^n \mathbf{k}_j \right) \delta \left(1 - x - \sum_{l=1}^n x_l \right) \quad (3.1)$$

and the gluon distribution function

$$g(x, Q^2) = \sum_n \frac{1}{x} \int_{\mathbf{k}} \frac{1}{2(2\pi^3)} \frac{1}{S_n} \sum_{\lambda=\pm 1} \prod_{i=1}^n \int \frac{dx_i}{x_i} \int_{\mathbf{k}_i} \frac{1}{2(2\pi)^3} |\Psi_n^f(\{x_i, \mathbf{k}_i\}; x, \mathbf{k}, \lambda)|^2 \times (2\pi)^3 \delta^2 \left(\mathbf{k} + \sum_{j=1}^n \mathbf{k}_j \right) \delta \left(1 - x - \sum_{l=1}^n x_l \right), \quad (3.2)$$

where λ is the measured gluon's polarisation. The quark distribution function is related to the structure functions through

$$F_1(x, Q^2) = \frac{1}{2} \sum_f Z_f^2 q^f(x, Q^2), \quad (3.3)$$

$$F_2(x, Q^2) = \sum_f Z_f^2 x q^f(x, Q^2), \quad (3.4)$$

where Z_f is the electric charge in units of the electron charge e of a quark of flavour f . In the function q^f , the proton is assumed to have n *spectator partons*, in addition to the one parton with which the photon interacts. The struck parton has momentum k (in the infinite momentum frame), longitudinal momentum fraction x and helicity σ . The spectator partons have momenta k_i and longitudinal momentum fractions x_i . The light cone wave function for the proton is then written in terms of the partonic wave functions Ψ_n^f . The symmetry factor S_n depends on the number of partons n , where $1 \leq n < \infty$.

The dependence of q^f on Q^2 enters through the renormalisation scale, so that all momentum integrals in Eq. (3.1) are bound from above by Q . The Bjorken scaling of the structure functions that was discussed in Section 2.4 follows from taking the limit $Q^2 \rightarrow \infty$ in the upper limit of the integrals when Q^2 is sufficiently large. This effectively renders the structure functions independent of Q^2 , as can be seen in Fig. 2.4 in the previous chapter.

3.1.2 How to derive the DGLAP equations

The derivation of the DGLAP equations from the quark and gluon distributions is now straightforward. In order to obtain the dependence of q^f on Q^2 , we first find the dependence of the proton wave function Ψ_n^f on the transverse momentum \mathbf{k} by calculating the QCD corrections to Ψ_n^f . For example, one type of leading-order correction to the diagram for q^f is any diagram with one added gluon line. By calculating these corrections, we may write Ψ_n^f in terms of Ψ_{n-1}^f , i.e. the same wave function but with $n - 1$ spectator partons (because one gluon has been removed from Ψ_n^f).

For large Q^2 , and assuming the transverse momenta are ordered as

$$Q^2 \gg \mathbf{k}^2 \gg \mathbf{k}_{n-1}^2 \gg \dots \gg \mathbf{k}_1^2 \sim \Lambda_{\text{QCD}}^2, \quad (3.5)$$

this procedure leads to a contribution to q^f that is proportional to $\alpha_s \ln(Q^2/\Lambda_{\text{QCD}}^2)$. For large Q^2 , $\alpha_s \ll 1$ and $\ln(Q^2/\Lambda_{\text{QCD}}^2) \gg 1$. Then the two factors together give $\alpha_s \ln(Q^2/\Lambda_{\text{QCD}}^2) \sim 1$, which can be used as a resummation parameter. The resummation of this parameter is called the *leading logarithmic approximation* (LLA). Diagrams that do not contain a factor $\alpha_s \ln(Q^2/\Lambda_{\text{QCD}}^2)$ – for example, those with an additional factor α_s – may be neglected to LLA accuracy in the calculation. By including all relevant one-gluon corrections to q^f in the LLA, and then differentiating by Q^2 , we obtain

$$Q^2 \frac{\partial q^f(x, Q^2)}{\partial Q^2} = \frac{\alpha_s(Q^2)}{2\pi} \int_x^1 \frac{dz}{z} P_{qq}(z) q^f\left(\frac{x}{z}, Q^2\right), \quad (3.6)$$

where $P_{qq}(z)$ is the quark–quark splitting function. The splitting function represents the probability that a quark splits from another, where the measured quark has a momentum fraction z of the original quark’s momentum. The calculation for the antiquark distribution function is similar, and the two results can be combined to give

$$Q^2 \frac{\partial \Delta^{f\bar{f}}(x, Q^2)}{\partial Q^2} = \frac{\alpha_s(Q^2)}{2\pi} \int_x^1 \frac{dz}{z} P_{qq}(z) \Delta^{f\bar{f}}\left(\frac{x}{z}, Q^2\right), \quad (3.7)$$

where $\Delta^{f\bar{f}} := q^f - q^{\bar{f}}$ is the so-called *flavour nonsinglet distribution function*.

In addition to quark–quark splitting in Eq. (3.7), quarks splitting from gluons within the gluon distribution given in Eq. (3.2) must be accounted for. Since this type of splitting also modifies the original gluon distribution, repeating the process for calculating Eq. (3.6) with all relevant splitting functions leads to a matrix differential equation

$$Q^2 \frac{\partial}{\partial Q^2} \begin{pmatrix} \Sigma(x, Q^2) \\ g(x, Q^2) \end{pmatrix} = \frac{\alpha_s(Q^2)}{2\pi} \int_x^1 \frac{dz}{z} \begin{pmatrix} P_{qq}(z) & P_{qg}(z) \\ P_{gq}(z) & P_{gg}(z) \end{pmatrix} \begin{pmatrix} \Sigma(x/z, Q^2) \\ g(x/z, Q^2) \end{pmatrix}. \quad (3.8)$$

Here, $\Sigma := \sum_f (q^f + q^{\bar{f}})$ is the so-called *flavour singlet distribution function*. Notice that the gluon distribution function does not affect Eq. (3.7), since gluon splitting necessarily results in equal numbers of quarks and antiquarks.

Eqs. (3.7) and (3.8) constitute the leading order DGLAP equations in the LLA. Higher orders may be derived by including the next-to-leading order corrections to the splitting functions; going past the LLA is possible by including contributions with additional logarithms in the resummation parameter. At small x , factors of $\ln(1/x)$ become important, so that a more appropriate resummation parameter is $\alpha_s \ln(1/x) \ln(Q^2/Q_0^2)$, where Q_0 is the virtuality at the initial condition. Resummation of this parameter is called the *double logarithmic approximation* (DLA).

In principle, the DGLAP equations are solvable analytically since they are linear differential equations. In practice, however, they are typically solved numerically. Although the evolution equations may be derived using standard perturbative methods, their initial conditions require nonperturbative input. As such, measurements over a range of Q^2 are required. DGLAP evolution has been successful in fitting data from experiments. Fig. 3.1 shows data from the ZEUS detector at HERA taken for the F_2 structure function for neutral current deep inelastic positron–proton scattering. The structure function is plotted against x for various values of fixed Q^2 in the range $22 - 150 \text{ GeV}^2$ (plots for other Q^2 values may be found in [41]).

3.2 BFKL evolution

Now we move on to evolution in rapidity, which is the main subject of this thesis. At fixed Q^2 , evolution in rapidity for small to moderate Y can be accounted for by the BFKL equation. Like the DGLAP equations, this is a type of renormalisation group equation, but with a different resummation parameter to that of DGLAP. In the previous section, it was mentioned that factors of $\alpha_s \ln(1/x) \ln(Q^2/Q_0^2)$ are resummed in the DLA. If Q^2 is now fixed at some (not necessarily large) value, the factor $\ln(Q^2/Q_0^2)$ in this can be neglected and we need only worry about factors of $\alpha_s \ln(1/x)$. Resummation of this parameter is called the LLA in $1/x$, as opposed to the LLA in Q^2 , which was discussed in reference to the DGLAP equations in the previous section. A derivation of the BFKL equation can be found in many textbooks, such as [55, 58, 59]. Here, we outline the calculation provided in [29].

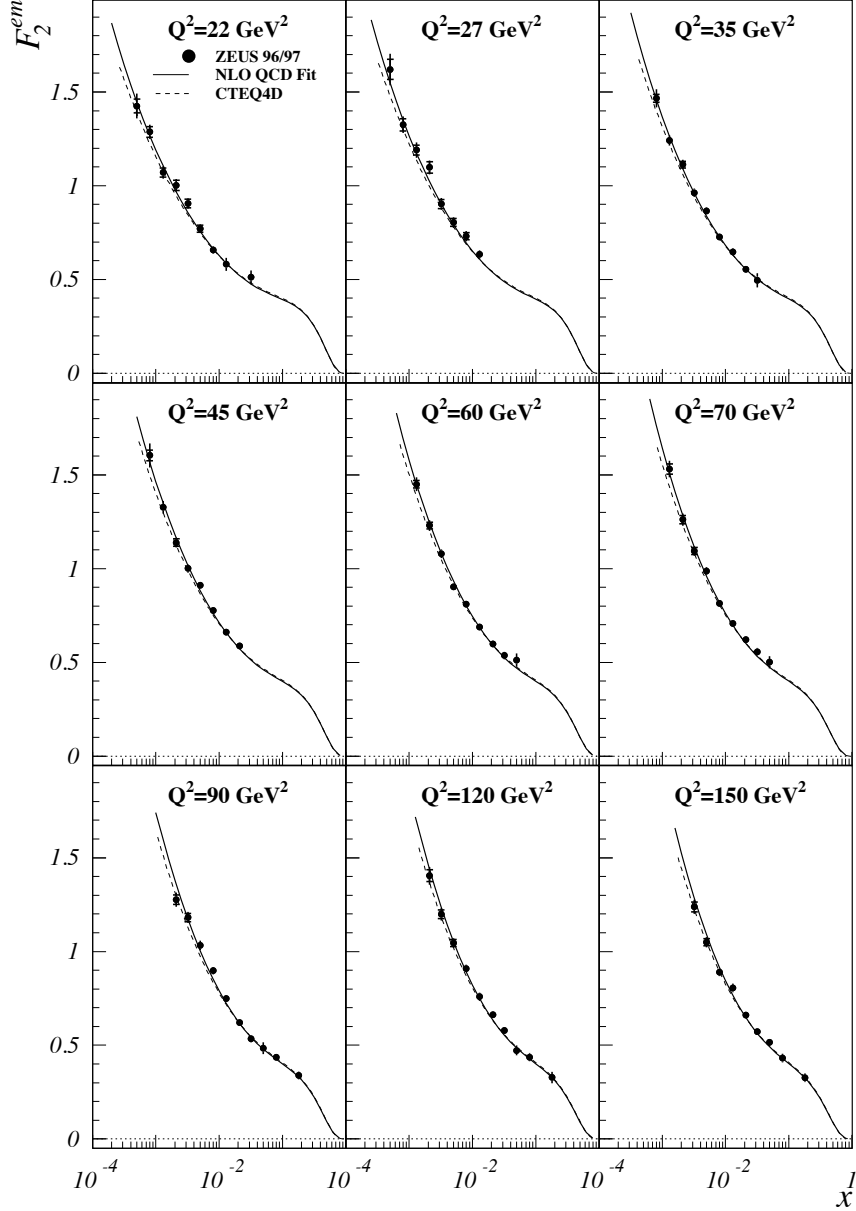


Figure 3.1. Data from the ZEUS collaboration at HERA for the F_2 structure function for neutral current positron–proton DIS [41]. The solid lines are a ZEUS NLO QCD fit that uses the DGLAP equations, demonstrating the success of the fit. The dashed lines are from the parton distribution and structure function program called CTEQ4D [57]. Reprinted by permission from Springer Nature Customer Service Centre GmbH: Springer Nature The European Physical Journal C – Particles and Fields, *Measurement of the neutral current cross section and F_2 structure function for deep inelastic e^+p scattering at HERA*, Chekanov, S. et al. © (2001).

3.2.1 The Low–Nussinov model

The BFKL equation has its origins in the Low–Nussinov model [60–62]. This is a theory that was proposed to explain the so-called *pomeron* in terms of QCD degrees of freedom. A pomeron is an exchanged Reggeon (see Chapter 1) with vacuum quantum numbers, that dominates process at high energies. It was introduced in Regge theory to account for the flatness of total cross sections in hadronic interactions around 10 - 20 GeV that was seen experimentally [59].

For concreteness, the scattering between two quark–antiquark bound states, called *quarkonia*, is considered. These interacting states may be partons within colliding nuclei or they may come from the splitting of a virtual photon into a quark–antiquark pair, as shown in Fig. 2.6. The simplest way to reproduce the vacuum quantum numbers of an exchanged pomeron between the two quarkonia is to model the exchanged object as two gluons. Then the relevant diagrams to calculate for the scattering amplitude at leading order in the LLA (for fixed α_s) are of the kind

$$(3.9)$$

where the transverse positions of the upper and lower quarkonia are \mathbf{x}_1 and \mathbf{x}_2 , respectively. We use the diagrammatic shorthand

$$(3.10)$$

so that any vertical grey line of this type signifies a sum over all possible gluon emissions or absorptions. This shorthand applies to both the upper and lower quarkonia in Eq. (3.9), giving four contributions.

Let us consider the diagram in which a gluon is exchanged between the two quarks. The quark from the upper quarkonium has momentum p_1 and the quark from the bottom quarkonium has momentum p_2 , as shown in Eq. (3.9). In the eikonal approximation, the only large momenta in the problem are p_1^- and p_2^+ . All other momenta are much smaller, including momentum l of the exchanged gluon. The scattering amplitude corresponding to the quark–quark scattering turns out to

be

$$M_{qq \rightarrow qq}^0(\mathbf{l}) = -2g^2 (t^a)_{i'i} (t^a)_{j'j} \delta_{\sigma_1 \sigma_1'} \delta_{\sigma_2 \sigma_2'} \frac{s}{\mathbf{l}^2}, \quad (3.11)$$

where the Kronecker deltas refer to the quark helicities. The cross section obtained from this is

$$\sigma_{qq \rightarrow qq} = \frac{2\alpha_s^2 C_F}{N_c} \int_{\mathbf{l}} \frac{1}{\mathbf{l}^4}, \quad (3.12)$$

which is an energy-independent expression. This is an example of a general rule that the t -channel exchange of a particle with spin j scales the total cross section by a factor s^{j-1} , where s is the square of the centre-of-mass energy [4, 63]. Setting $j = 1$ for gluons then makes this factor s^0 for our case of two-gluon exchange.

Taking into account all four diagrams that contribute to Eq. (3.9), the total cross section for quarkonium–quarkonium scattering is

$$\sigma = \int_{\mathbf{x}_1 \mathbf{x}_2} \int_0^1 dz_1 dz_2 |\Psi(\mathbf{x}_1, z_1)|^2 |\Psi(\mathbf{x}_2, z_2)|^2 \hat{\sigma}, \quad (3.13)$$

where

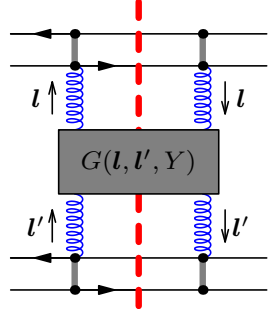
$$\hat{\sigma} := \frac{2\alpha_s^2 C_F}{N_c} \int_{\mathbf{l}} \frac{1}{\mathbf{l}^4} (2 - e^{-i\mathbf{l} \cdot \mathbf{x}_1} - e^{i\mathbf{l} \cdot \mathbf{x}_1}) (2 - e^{-i\mathbf{l} \cdot \mathbf{x}_2} - e^{i\mathbf{l} \cdot \mathbf{x}_2}). \quad (3.14)$$

Here, Ψ is the quarkonium light cone wave function and z_1 and z_2 are the interacting quarks' momentum fractions relative to their corresponding bound state momenta. The two-gluon exchange in this context is referred to as the *soft pomeron*, since it is governed by nonperturbative effects. Overall, the only differences between Eqs. (3.12) and (3.14) are so-called *impact factors* of the form $2 - e^{-i\mathbf{l} \cdot \mathbf{x}} - e^{i\mathbf{l} \cdot \mathbf{x}}$. It is therefore sufficient to calculate the corrections to quark–quark scattering and then extend the result to the full quarkonium–quarkonium case.

3.2.2 How to derive the BFKL equation

In order to derive the BFKL equation, we now calculate corrections to the quarkonium–quarkonium scattering cross section given in Eq. (3.14). A typical

contribution that needs to be calculated is of the kind



$$(3.15)$$

where the red dashed line separates the direct and complex conjugate amplitudes. The shaded rectangle labelled G represents all corrections to the total cross section to leading order in $\ln \alpha_s$. Other kinds of corrections, such as quark loops, are beyond LLA accuracy and may be neglected. The corrections G are a function of the gluon momenta \mathbf{l} and \mathbf{l}' , as well as rapidity $Y = \ln(s|\mathbf{x}_1||\mathbf{x}_2|)$. The generalisation of Eq. (3.14) is then

$$\hat{\sigma} = \frac{2\alpha_s^2 C_F}{N_c} \int_W \frac{1}{\mathbf{l}^2 \mathbf{l}'^2} (2 - e^{-i\mathbf{l}\cdot\mathbf{x}_1} - e^{i\mathbf{l}\cdot\mathbf{x}_1}) (2 - e^{-i\mathbf{l}'\cdot\mathbf{x}_2} - e^{i\mathbf{l}'\cdot\mathbf{x}_2}) G(\mathbf{l}, \mathbf{l}', Y). \quad (3.16)$$

The initial condition

$$G_0(\mathbf{l}, \mathbf{l}') := G(\mathbf{l}, \mathbf{l}', Y = 0) = \delta^2(\mathbf{l} - \mathbf{l}') \quad (3.17)$$

reproduces Eq. (3.14). Note that an *unintegrated gluon distribution* $\phi(x, \mathbf{l}^2)$ can be defined by including the corrections G in one of the quarkonium wave functions. Using Eqs. (3.13) and (3.16) to achieve this, gives

$$\phi(x, \mathbf{l}^2) := \frac{\alpha_s^2 C_F}{\pi} \int_{\mathbf{x}} \int_0^1 dz |\Psi(\mathbf{x}, z)|^2 \int_{\mathbf{l}'} \frac{1}{\mathbf{l}'^2} (2 - e^{-i\mathbf{l}'\cdot\mathbf{x}} - e^{i\mathbf{l}'\cdot\mathbf{x}}) G(\mathbf{l}, \mathbf{l}', \ln(1/x)), \quad (3.18)$$

which is the gluon distribution at a particular transverse momentum \mathbf{l} . In the LLA, this is related to the gluon distribution of Eq. (3.2) by

$$\phi(x, Q^2) = \frac{\partial x g(x, Q^2)}{\partial Q^2}. \quad (3.19)$$

G is calculated by first considering all corrections to the quark–quark scattering and then extending the result to the full case. There are two types of contributions that need to be considered, depending on whether the gluon is present in the final state (*real* emissions) or is not (*virtual* emissions). In the case of real emissions, five diagrams need to be calculated. These corrections sum to a total contribution

$$M_{qq \rightarrow qqg} = 2ig^2 (t^b)_{i'i} (t^c)_{j'j} \delta_{\sigma_1 \sigma'_1} \delta_{\sigma_2 \sigma'_2} \frac{s}{\mathbf{l}^2 (\mathbf{k} - \mathbf{l})^2} \epsilon^{\lambda*} \cdot \mathbf{\Gamma}^{abc} \quad (3.20)$$

to the quark–quark scattering amplitude, where k and ϵ^{λ^*} are the momentum and polarisation, respectively, of the added gluon. The factor

$$\Gamma^{abc} := 2gf^{abc} \left[\mathbf{k} - \mathbf{l} - \frac{(\mathbf{k} - \mathbf{l})^2}{\mathbf{k}^2} \mathbf{k} \right] \quad (3.21)$$

is the so-called *Lipatov vertex* [15, 64]. It provides a diagrammatic shorthand for the five gluon diagrams that constitute it. The cross section for real emission is then

$$\sigma_{qq \rightarrow qqg} = \frac{2\alpha_s^3 C_F}{\pi^2} \int_{kl} \frac{1}{\mathbf{k}^2 \mathbf{l}^2 (\mathbf{k} - \mathbf{l})^2} \int_0^Y dy, \quad (3.22)$$

where y is the added gluon’s rapidity, integrated over the whole rapidity range between the two interacting quarks. This result generalises to the quarkonium–quarkonium case, giving the same expression as Eq. (3.16), but with the replacement

$$G(\mathbf{l}, \mathbf{l}', Y) \rightarrow G_1^{\text{real}}(\mathbf{l}, \mathbf{l}', Y) := \frac{\alpha_s N_c}{\pi^2} Y \frac{1}{(\mathbf{l} - \mathbf{l}')^2}. \quad (3.23)$$

Next, we consider the virtual corrections to the quark–quark scattering, in which case there are several more diagrams to take into account. After a lengthy calculation, the total contribution to the scattering amplitude is

$$M_{qq \rightarrow qq}^1(\mathbf{l}) = M_{qq \rightarrow qq}^0(\mathbf{l}) \omega_g(\mathbf{l}) Y, \quad (3.24)$$

where

$$\omega_g(\mathbf{l}) = -\frac{\alpha_s N_c}{4\pi^2} \int_{\mathbf{q}} \frac{\mathbf{l}^2}{\mathbf{q}^2 (\mathbf{q} - \mathbf{l})^2} \quad (3.25)$$

defines the *gluon Regge trajectory*. The virtual emission diagrams lead to corrections that can be summed into an exponential, which effectively means that the gluon propagator may be replaced by the propagator of a *reggeised gluon*:

$$\frac{ig_{\mu\nu}}{\mathbf{l}^2} \rightarrow \frac{ig_{\mu\nu}}{\mathbf{l}^2} e^{\omega_g(\mathbf{l})Y}. \quad (3.26)$$

This represents an exchanged gluon with spin $j = 1 + \omega_g(\mathbf{l})$. A reggeised gluon is therefore a gluon plus all virtual corrections to leading order in $\ln(1/x)$. The virtual emissions result in a correction to the quarkonium–quarkonium cross section in Eq. (3.16) that equates to the replacement

$$G(\mathbf{l}, \mathbf{l}', Y) \rightarrow G_1^{\text{virtual}}(\mathbf{l}, \mathbf{l}', Y) := G_0(\mathbf{l}, \mathbf{l}') 2\omega_g(\mathbf{l}) Y. \quad (3.27)$$

Summing the real contributions from Eq. (3.23) and the virtual contributions from Eq. (3.27) gives a total correction factor

$$G(\mathbf{l}, \mathbf{l}', Y) = G_0(\mathbf{l}, \mathbf{l}') + \frac{\alpha_s N_c}{\pi^2} \int_0^Y dy \int_{\mathbf{q}} \frac{1}{(\mathbf{l} - \mathbf{q})^2} \left[G_0(\mathbf{q}, \mathbf{l}') - \frac{\mathbf{l}^2}{2\mathbf{q}^2} G_0(\mathbf{l}, \mathbf{l}') \right] + \mathcal{O}(\alpha_s^2) \quad (3.28)$$

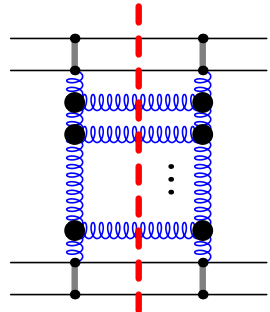
for the quarkonium–quarkonium scattering. To order α_s , this expression can be thought of as the solution to the BFKL equation

$$\partial_Y G(\mathbf{l}, \mathbf{l}', Y) = \frac{\alpha_s N_c}{\pi^2} \int_{\mathbf{q}} \frac{1}{(\mathbf{l} - \mathbf{q})^2} \left[G(\mathbf{q}, \mathbf{l}', Y) - \frac{\mathbf{l}^2}{2\mathbf{q}^2} G(\mathbf{l}, \mathbf{l}', Y) \right] \quad (3.29)$$

for the *BFKL Green's function* G . The initial condition is given in Eq. (3.17). A similar BFKL equation holds for the unintegrated gluon distribution:

$$\frac{\partial \phi(x, \mathbf{l}^2)}{\partial \ln(1/x)} = \frac{\alpha_s N_c}{\pi^2} \int_{\mathbf{q}} \frac{1}{(\mathbf{l} - \mathbf{q})^2} \left[\phi(x, \mathbf{q}^2) - \frac{\mathbf{l}^2}{2\mathbf{q}^2} \phi(x, \mathbf{l}^2) \right]. \quad (3.30)$$

At each iteration of Eq. (3.29), the Green's function gets corrected by one gluon. Several iterations therefore lead to a *BFKL ladder diagram*



$$, \quad (3.31)$$

where the big solid dots represent Lipatov vertices and the two vertical gluons are reggeised gluons. The horizontal gluons are ordered in increasing rapidity from top to bottom. This is a consequence of the constraints imposed on the gluons' plus and minus light cone momentum components in the derivation of Eq. (3.29). The BFKL ladder is referred to as the *hard pomeron*, since it is governed by perturbative effects.

3.2.3 Problems with BFKL evolution

Since Eqs. (3.29) and (3.30) are linear differential equations, they can be solved analytically – see, for example, [29]. Their solutions imply a cross section growth of

the form $\sigma \sim s^{\alpha_P-1}$, where α_P is the so-called *pomeron intercept* from Regge theory. In particular, this growth factor violates an important bound. The *Froissart–Martin theorem* states that the growth rate of the total cross section as a function of energy cannot be larger than $\ln^2 s$ [65, 66]. This is a direct consequence of the unitarity and analyticity of the scattering matrix. Since the cross section governed by BFKL evolution violates the Froissart–Martin bound, the BFKL equation clearly violates these important properties of the scattering matrix.

A second problem with BFKL evolution concerns its high energy limit. For very large rapidities, it is possible that the lower bound of the transverse momenta of the horizontal gluons in the ladder (the ladder “rungs”) approaches Λ_{QCD} . This calls into question the validity of perturbation theory in the high energy limit. These two serious problems with BFKL evolution may be cured by considering nonlinear effects at small x , as discussed in the next section. The point to which BFKL evolution is applicable is governed by a *saturation scale* Q_s . This is one of the defining features of the CGC, as it signals the onset of the nonlinear effects that lead to saturation. The associated *correlation length* $R_s := 1/Q_s$ defines the apparent size of the partons necessary for the overlaps in the partonic wave functions to be included in deriving the evolution equations.

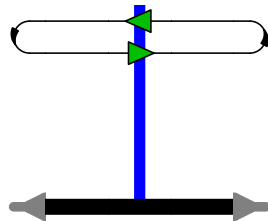
3.3 BK evolution

The two major problems with BFKL evolution discussed in the previous section may be cured by introducing nonlinear terms into the evolution equation. This is the role of the BK equation – a nonlinear renormalisation group equation that governs the evolution of the dipole correlator with increasing rapidity. A derivation of the BK equation is provided in [29]; we outline the procedure here.

3.3.1 The Glauber–Gribov–Mueller model

Consider the dipole operator

$$1 - N_{xy} = S_{xy}^{(2)} = \frac{1}{N_c} \text{tr} (U_x U_y^\dagger) = \frac{1}{N_c} \quad , \quad (3.32)$$



from Section 2.7, where the dipole–target cross section

$$\sigma^{q\bar{q}A}(\mathbf{r}, Y) = 2 \int_{\mathbf{b}} \text{Re} \langle N_{\mathbf{xy}} \rangle, \quad (3.33)$$

was discussed, as given in Eq. (2.24). In order to calculate $N_{\mathbf{xy}}$, the target is modelled using the Glauber model introduced in Section 2.5 and consider dipole–nucleon scattering in the *Glauber–Gribov–Mueller (GGM) model* [36, 67–71].

First, we consider the scattering between the dipole and a single nucleon from the target. This nucleon can be modelled as a dipole of size \mathbf{r}_2 , so that we may use Eq. (3.13). Both dipoles are considered small, so that $\mathbf{r} \sim \mathbf{r}_2 \ll 1/\Lambda_{\text{QCD}}$. For a large target, an angular average is taken to account for all possible orientations of the transverse vectors \mathbf{r} and \mathbf{r}_2 . This gives an approximate dipole–nucleon cross section

$$\sigma^{q\bar{q}N} \approx \frac{\alpha_s \pi^2}{N_c} \mathbf{r}^2 x g_N \left(x, \frac{1}{\mathbf{r}^2} \right), \quad (3.34)$$

where the gluon distribution xg_N refers to the single nucleon from the target. Averaging over all positions of the nucleon within the target and summing over a total of A nucleons gives the differential dipole–target cross section

$$\frac{d\sigma_{\text{LO}}^{q\bar{q}A}}{d^2b} = T(\mathbf{b}) \sigma^{q\bar{q}N}, \quad (3.35)$$

where

$$T(\mathbf{b}) := \int_{-\infty}^{\infty} db_3 \rho_A(\mathbf{b}, b_3) \quad (3.36)$$

is the *nuclear profile function* and ρ_A is the nucleon number density, typically given by the *Woods–Saxon model* [72].

Next, this result for a single nucleon scattering is extended to the dipole scattering with multiple nucleons. For simplicity, each of these nucleons is now modelled as a single quark instead of a dipole. In the covariant/Feynman gauge and still considering only two-gluon exchange, the dipole interacts with one nucleon at a time, ordered along the x^+ -axis. All other possible interactions are suppressed by a factor $A \gg 1$. By iterating Eq. (3.35) and summing over all the ways that the two exchanged gluons can attach to the quark and/or antiquark, we obtain

$$\frac{\partial s(\mathbf{r}, b^+)}{\partial b^+} = -\frac{1}{2} \rho_A(\mathbf{b}, b^+) \sigma^{q\bar{q}N} s(\mathbf{r}, b^+), \quad (3.37)$$

where $s(\mathbf{r}, L)$ corresponds to a dipole $S_{\mathbf{x}\mathbf{y}}^{(2)}$ that travels through the target up to point $b^+ \in (0, L)$ [36]. The dipole–nucleon cross section is given by

$$\sigma^{q\bar{q}N} = \int_l \frac{1}{(2\pi)^2} \frac{d\sigma_{qq \rightarrow qq}}{d^2l} (2 - e^{i\mathbf{l}\cdot\mathbf{r}} - e^{-i\mathbf{l}\cdot\mathbf{r}}), \quad (3.38)$$

where $\sigma_{qq \rightarrow qq}$ is determined from Eq. (3.12). At the initial condition, this can be used with the leading-order single-quark gluon distribution

$$xg_{\text{LO}}^{\text{quark}}(x, Q^2) = \frac{\alpha_s C_F}{\pi} \ln \frac{Q^2}{\Lambda_{\text{QCD}}^2}, \quad (3.39)$$

to write the *GGM multiple-rescattering formula*

$$\langle N(\mathbf{r}, \mathbf{b}, Y = 0) \rangle = 1 - \exp \left\{ -\frac{\mathbf{r}^2 Q_s^2(\mathbf{b})}{4} \ln \frac{1}{|\mathbf{r}| \Lambda_{\text{QCD}}} \right\}. \quad (3.40)$$

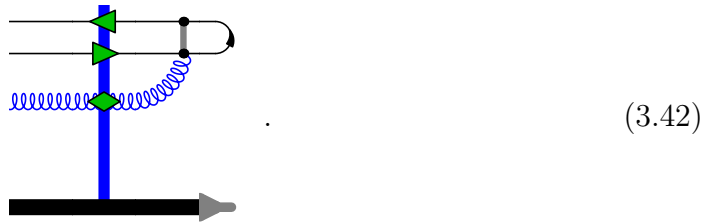
The saturation scale that was discussed in Section 3.2.3 is defined here as

$$Q_s^2(\mathbf{b}) := \frac{4\pi\alpha_s^2 C_F}{N_c} T(\mathbf{b}), \quad (3.41)$$

in terms of the nuclear profile function $T(\mathbf{b})$ given in Eq. (3.36).

3.3.2 Mueller’s dipole model

The task is now to calculate and resum all corrections to Eq. (3.40) in the LLA in $\ln(1/x)$. The diagrams that give the appropriate factor $\alpha_s \ln(1/x)$ are those in which the dipole emits an s -channel gluon that interacts with the target, i.e. contributions of the form



After the interaction, the emitted gluon is reabsorbed by the dipole. Other types of corrections, such as additional t -channel gluons of the kind shown in Eq. (3.9), do not contribute the required resummation factor and may be neglected. During the interaction with the target, scattering occurs off nucleons ordered in x^+ within the target. Gluon emission from the dipole during this time is suppressed by $1/s$ and can be neglected in the eikonal approximation. We assume that the light cone

3. Evolution Equations

plus component of the emitted gluon's momentum is much smaller than that of the quark or the antiquark. On the other hand, all the other transverse momenta in the problem remain unconstrained and unordered.

The dipole is written in terms of the quarkonium wave function first introduced in Eq. (3.13). Using standard techniques to calculate the required diagrams of the form shown in Eq. (3.42) gives a modification

$$\int_{z_0}^{\min\{z_1, 1-z_1\}} \frac{dz_2}{z_2} \int_{\mathbf{x}_2} \frac{1}{4\pi} \sum_{\sigma, \sigma', \lambda, a} \left| \Psi_{\sigma\sigma'}^{(1)} \right|^2 = \int_{z_0}^{\min\{z_1, 1-z_1\}} \frac{dz_2}{z_2} \int_w \frac{\alpha_s C_F}{\pi^2} \tilde{\mathcal{K}}_{\mathbf{x}\mathbf{z}\mathbf{y}} \sum_{\sigma, \sigma'} \left| \Psi_{\sigma\sigma'}^{(0)} \right|^2 \quad (3.43)$$

from the real corrections to the original quarkonium wave function $\Psi^{(0)}$ [27]. The *conformal kernel* that appears here is given by

$$\tilde{\mathcal{K}}_{\mathbf{x}\mathbf{w}\mathbf{y}} := 2\mathcal{K}_{\mathbf{x}\mathbf{w}\mathbf{y}} - \mathcal{K}_{\mathbf{x}\mathbf{w}\mathbf{x}} - \mathcal{K}_{\mathbf{y}\mathbf{w}\mathbf{y}} = \frac{(\mathbf{x} - \mathbf{y})^2}{(\mathbf{x} - \mathbf{w})^2 (\mathbf{w} - \mathbf{y})^2}, \quad (3.44)$$

where

$$\mathcal{K}_{\mathbf{x}\mathbf{w}\mathbf{y}} := \mathcal{K}_{\mathbf{x}\mathbf{w}}^i \mathcal{K}_{\mathbf{w}\mathbf{y}}^i \quad (3.45)$$

and

$$\mathcal{K}_{\mathbf{x}\mathbf{w}}^i := \frac{(x - w)^i}{(\mathbf{x} - \mathbf{w})^2} \quad (3.46)$$

is the *Weizsäcker-Williams emission kernel*. The kernel $\mathcal{K}_{\mathbf{x}\mathbf{w}}^i$ denotes the quark \rightarrow quark + gluon splitting wave function. Notice that the bare wave function $\Psi_{\sigma\sigma'}^{(0)}$ factorises out in Eq. (3.43). The virtual corrections require the calculation of several more diagrams, which are not included here. The total contribution from the virtual corrections modifies the bare quarkonium wave function by

$$\Psi_{\sigma\sigma'}^{(0)}(\mathbf{r}, z_1) \Big|_{\mathcal{O}(\alpha_s)} = -\frac{2\alpha_s C_F}{\pi} \ln \frac{|\mathbf{r}|}{\rho} \int_{z_0}^{\min\{z_1, 1-z_1\}} \frac{dz_2}{z_2} \Psi_{\sigma\sigma'}^{(0)}(\mathbf{r}, z_1) \Big|_{\mathcal{O}(\alpha_s^0)}, \quad (3.47)$$

where ρ is an ultraviolet cutoff that regulates the divergences from the factors $\mathbf{x} - \mathbf{w}$ and $\mathbf{y} - \mathbf{w}$ in the denominator of Eq. (3.43) [27].

Now that we have considered both the real and the virtual corrections to the dipole, some remarks are in order. Both Eqs. (3.43) and (3.47) contain a factor α_s and an integral $\int dz_2/z_2$, which confirm that they are LLA contributions. The resummation procedure to derive a renormalisation group equation in this case is complicated, but simplifies significantly in the large- N_c limit. In this limit, we

set $N_c \rightarrow \infty$ while simultaneously keeping $\alpha_s N_c$ constant. Each gluon line in the diagrams is replaced by a pair of lines denoting a quark–antiquark pair. These are in a colour octet state, called a daughter dipole.

In the case of a diagram with several gluons emitted from the original parent dipole, these daughter dipoles need only be considered as noninteracting. Those diagrams in which they do interact with each other are N_c -suppressed, although they may act as sources of further gluon emission. An additional simplification is that the gluon emissions need only be considered ordered in momentum as $z_1 \gg z_2 \gg z_3 \gg \dots \gg z_0$, where the gluon with longitudinal momentum fraction z_2 is emitted before the gluon with z_3 , etc. Diagrams in which the emitted gluons are not ordered in this way are beyond the LLA.

The most concise way to write all the corrections to the quarkonium wave function is through the dipole generating functional

$$\begin{aligned} Z(\mathbf{r}, \mathbf{b}, Y; u) &= \sum_{\sigma\sigma'} \left| \Psi_{\sigma\sigma'}^{(0)} \right|^2 \Big|_{\mathcal{O}(\alpha_s^0)} \\ &:= \sum_{n=1}^{\infty} \frac{1}{n!} \int_{\mathbf{r}_1 \mathbf{b}_1 \dots \mathbf{r}_n \mathbf{b}_n} \left| \Psi^{[n]}(\mathbf{r}_1, \mathbf{b}_1, \dots, \mathbf{r}_n, \mathbf{b}_n) \right|^2 u(\mathbf{r}_1, \mathbf{b}_1) \dots u(\mathbf{r}_n, \mathbf{b}_n). \end{aligned} \quad (3.48)$$

The wave function $\Psi^{[n]}$ denotes a quarkonium state with n dipoles, as opposed to a state $\Psi^{(n)}$ with n gluons. Each dipole i is of size \mathbf{r}_i and has impact parameter \mathbf{b}_i . The dummy functions $u(\mathbf{r}_i, \mathbf{b}_i)$ allow us to take derivatives $\delta Z / \delta u$ in Eq. (3.48) to generate a wave function with any required number of emitted dipoles.

Taking into account the real and virtual corrections given in Eqs. (3.43) and (3.47), respectively, an evolution equation

$$\begin{aligned} \partial_Y Z(\mathbf{r}, \mathbf{b}, Y; u) &= \frac{\alpha_s N_c}{2\pi^2} \int_{\mathbf{w}} \tilde{\mathcal{K}}_{\mathbf{x}\mathbf{w}\mathbf{y}} \left[Z\left(\mathbf{y} - \mathbf{w}, \mathbf{b} + \frac{1}{2}(\mathbf{w} - \mathbf{x}), Y; u\right) \right. \\ &\quad \left. \times Z\left(\mathbf{w} - \mathbf{x}, \mathbf{b} + \frac{1}{2}(\mathbf{w} - \mathbf{y}), Y; u\right) - Z(\mathbf{y} - \mathbf{x}, \mathbf{b}, Y; u) \right], \end{aligned} \quad (3.49)$$

can be obtained, with the initial condition $Z(\mathbf{y} - \mathbf{x}, \mathbf{b}, Y = 0; u) = u(\mathbf{y} - \mathbf{x}, \mathbf{b})$. We have defined $\partial_Y := \partial / \partial Y$ and taken $C_F \rightarrow N_c / 2$ in the large- N_c limit. The transverse coordinate structure of Eq. (3.49) is as follows. The original parent dipole has size $\mathbf{r} = \mathbf{x} - \mathbf{y}$ and centre-of-mass $\mathbf{b} = (\mathbf{x} + \mathbf{y}) / 2$. The gluon emission kernel $\tilde{\mathcal{K}}_{\mathbf{x}\mathbf{w}\mathbf{y}}$ on the right side of the equation corresponds to a gluon emitted at transverse coordinate \mathbf{w} . The kernel is proportional to \mathbf{r} , since a dipole of zero size cannot emit gluons. The first term under the integral corresponds to the emitted gluon

forming two new daughter dipoles, one with size $\mathbf{y} - \mathbf{w}$ and centre of mass

$$\frac{1}{2}(\mathbf{y} + \mathbf{w}) = \frac{1}{2}(\mathbf{y} + \mathbf{x} - \mathbf{x} + \mathbf{w}) = \mathbf{b} + \frac{1}{2}(\mathbf{w} - \mathbf{x}), \quad (3.50)$$

and the other with size $\mathbf{w} - \mathbf{x}$ and centre-of-mass

$$\frac{1}{2}(\mathbf{w} + \mathbf{x}) = \frac{1}{2}(\mathbf{w} - \mathbf{y} + \mathbf{y} + \mathbf{x}) = \mathbf{b} + \frac{1}{2}(\mathbf{w} - \mathbf{y}). \quad (3.51)$$

Since both of the new daughter dipoles have to interact with the target, they appear as a product of generating functionals in the integrand. The second term in Eq. (3.49) is a virtual term, which accounts for probability conservation; it therefore has the same coordinate structure as the original parent dipole. As a consistency check, it is possible to derive an equation that is equivalent to the BFKL equation by taking one derivative of Eq. (3.49) with respect to u [26–28, 73–75].

3.3.3 How to derive the BK equation

Given the dipole generating functional obtained above, it is now straightforward to derive the BK equation. It has already been noted that the cascade of gluons emitted from the parent dipole before the interaction with the target can be modelled as a cascade of daughter dipoles in the large- N_c limit. The interaction of the parent and daughter dipoles with the target is dominated by cases in which each dipole interacts with a single and different nucleon to the other dipoles. It can be shown that any other scenarios, such as two dipoles interacting with the same nucleon, are N_c -suppressed to leading order in A [18]. So we only need to consider independent dipole–nucleon interactions, instead of all the possible ways in which the dipole cascade may interact with the target.

The scattering amplitude is therefore a convolution of two parts: the dipole cascade developed from the parent dipole before the interaction and the multiple rescattering with the target. For the first part, we take k derivatives of the dipole generating functional given in Eq. (3.48):

$$\frac{\delta^k}{\delta u(\mathbf{r}_1, \mathbf{b}_1) \dots \delta u(\mathbf{r}_k, \mathbf{b}_k)} Z(\mathbf{r}, \mathbf{b}, Y; u) \Big|_{u=0}. \quad (3.52)$$

This gives the probability of finding k daughter dipoles in the wave function of the parent dipole. For the dipole amplitude, the sum over all k values gives

$$\begin{aligned} \langle S^{(2)}(\mathbf{r}, \mathbf{b}, Y) \rangle &= \sum_{k=1}^{\infty} \frac{1}{k!} \int_{\mathbf{r}_1 \mathbf{b}_1 \dots \mathbf{r}_k \mathbf{b}_k} \frac{\delta^k}{\delta u(\mathbf{r}_1, \mathbf{b}_1) \dots \delta u(\mathbf{r}_k, \mathbf{b}_k)} Z(\mathbf{r}, \mathbf{b}, Y; u) \Big|_{u=0} \\ &\quad \times \langle S^{(2)}(\mathbf{r}_1, \mathbf{b}_1, Y=0) \rangle \dots \langle S^{(2)}(\mathbf{r}_k, \mathbf{b}_k, Y=0) \rangle, \end{aligned} \quad (3.53)$$

with the initial condition given in Eq. (3.40) [18]. This summation leads to the result

$$\langle S^{(2)}(\mathbf{r}, \mathbf{b}, Y) \rangle = Z(\mathbf{r}, \mathbf{b}, Y; u = \langle S^{(2)}(\mathbf{r}, \mathbf{b}, Y=0) \rangle), \quad (3.54)$$

from which we can deduce that the dipole correlator $\langle S^{(2)} \rangle$ and the generating functional Z obey the same evolution equation. Using Eq. (3.49) to write this common evolution equation in terms of $N_{\mathbf{x}\mathbf{y}}$, we get the BK equation [18, 19]

$$\partial_Y \langle N_{\mathbf{x}\mathbf{y}} \rangle = \frac{\alpha_s N_c}{2\pi^2} \int_{\mathbf{w}} \tilde{\mathcal{K}}_{\mathbf{x}\mathbf{w}\mathbf{y}} [\langle N_{\mathbf{x}\mathbf{w}} \rangle + \langle N_{\mathbf{w}\mathbf{y}} \rangle - \langle N_{\mathbf{x}\mathbf{y}} \rangle - \langle N_{\mathbf{x}\mathbf{w}} \rangle \langle N_{\mathbf{w}\mathbf{y}} \rangle]. \quad (3.55)$$

The initial condition is given by Eq. (3.40) and the saturation scale $Q_s^2(\mathbf{b}) \rightarrow Q_{s0}^2(\mathbf{b})$ is taken at $Y = 0$.

In writing Eq. (3.55), it has already been assumed that $\langle N_{\mathbf{x}\mathbf{y}} \rangle$ is independent of the impact parameter \mathbf{b} . This assumption holds for large nuclei, far from its edges. The nucleus can also be assumed to be isotropic, in which case each factor $\langle N_{\mathbf{x}\mathbf{y}} \rangle$ simply becomes a function of the transverse length $|\mathbf{x} - \mathbf{y}|$. Each iteration of the BK equation leads to one soft s -channel gluon being emitted by the parent dipole corresponding to $N_{\mathbf{x}\mathbf{y}}$ on the left of Eq. (3.55). The only difference between the BFKL equation and BK equation is the inclusion of the nonlinear term $\langle N_{\mathbf{x}\mathbf{w}} \rangle \langle N_{\mathbf{w}\mathbf{y}} \rangle$ within the integrand on the right side of Eq. (3.55). At large rapidities, this nonlinear term becomes important, leading to saturation and the slowing down of energy growth. It is this nonlinearity of the BK equation that allows it to cure the problems with BFKL evolution discussed in Section 3.2.3.

In Paper [III], we study the BK equation at next-to-leading order. This may be derived in the same way as the LO equation but keeping terms of order α_s^2 at every stage of the calculation. The resulting evolution equation is of the form [76]

$$\partial_Y \langle S_{\mathbf{x},\mathbf{y}}^{(2)} \rangle = \frac{\alpha_s N_c}{2\pi^2} \int_{\mathbf{z}} K_1^{\text{BC}} \langle D_1 \rangle + \frac{\alpha_s^2 N_c^2}{16\pi^4} \int_{\mathbf{z},\mathbf{z}'} (K_{2,1} \langle D_{2,1} \rangle + K_{2,2} \langle D_{2,2} \rangle + K_f \langle D_f \rangle). \quad (3.56)$$

The full expressions for the kernels are provided in Paper [III]. In this thesis, we focus on the correlators

$$\langle D_1 \rangle = \langle S_{\mathbf{x},\mathbf{z}}^{(2)} S_{\mathbf{z},\mathbf{y}}^{(2)} - S_{\mathbf{x},\mathbf{y}}^{(2)} \rangle, \quad (3.57)$$

$$\langle D_{2,1} \rangle = \left\langle S_{\mathbf{x},\mathbf{z}}^{(2)} S_{\mathbf{z},\mathbf{z}'}^{(2)} S_{\mathbf{z}',\mathbf{y}}^{(2)} \right\rangle - \left\langle \frac{1}{N_c^2} S_{\mathbf{x},\mathbf{z},\mathbf{z}',\mathbf{y},\mathbf{z},\mathbf{z}'}^{(6)} \right\rangle - (\mathbf{z}' \rightarrow \mathbf{z}), \quad (3.58)$$

$$\langle D_{2,2} \rangle = \left\langle S_{\mathbf{x},\mathbf{z}}^{(2)} S_{\mathbf{z},\mathbf{z}'}^{(2)} S_{\mathbf{z}',\mathbf{y}}^{(2)} \right\rangle, \quad (3.59)$$

$$\langle D_f \rangle = \left\langle \frac{1}{N_c^2} \text{tr} (t^a U_{\mathbf{x}} t^b U_{\mathbf{y}}^\dagger) \left[\text{tr} (t^a U_{\mathbf{z}} t^b U_{\mathbf{z}'}^\dagger) - (\mathbf{z}' \rightarrow \mathbf{z}) \right] \right\rangle. \quad (3.60)$$

The calculation of these correlators in the Gaussian approximation is discussed in Chapter 7.

Chapter summary

In this chapter, we have discussed three types of evolution equations. The DGLAP equations govern the evolution of the parton distribution functions as functions of virtuality Q^2 . For evolution in rapidity Y , we first considered the BFKL equation. This linear equation was shown to have some problems, particularly at large rapidities. Finally, the BK equation was discussed. Its nonlinear terms are able to cure the problems with the BFKL equation by taking into account multiple gluon self-interactions.

4

JIMWLK in the Fokker–Planck Formalism

In the previous chapter, we discussed three types of evolution equations: DGLAP, BFKL and BK. These are all labelled on the phase diagram provided in Fig. 2.5. In this chapter, we discuss the last of the evolution equations labelled there, namely the JIMWLK equation. This is a nonlinear renormalisation group equation that applies in the saturation regime at low to moderate Q^2 and large rapidity Y . JIMWLK evolution describes the change in the target field as a function of rapidity by incorporating the soft gluons emitted at small x into the target wave function, as opposed to incorporating them into the projectile wave function. In this chapter, we introduce JIMWLK evolution in the form of a Fokker-Planck equation. In Chapter 5, an equivalent formulation is given in terms of a Langevin equation. While we only discuss the leading-order equations here, much work has been done towards understanding the next-to-leading order JIMWLK equation [76–78]. The JIMWLK equation is not solvable analytically, but it has been implemented on the lattice, for example, in [79]. It also has applications in other areas, such as in the calculation of nonglobal jet observables [30].

We begin in Section 4.1 with a discussion on the derivation of the JIMWLK equation. The Hamiltonian that appears in this equation is obtained in Section 4.2. The Lie derivatives contained in the Hamiltonian are studied in Section 4.3. In Section 4.4, we use the diagrammatic notation introduced in Chapter 2 to further study the operation of the JIMWLK Hamiltonian on Wilson line operators. Finally, in Section 4.5, we relate the JIMWLK equation to the BK equation of the previous chapter.

4.1 How to derive the JIMWLK equation

In order to derive the JIMWLK equation, we consider quantum corrections to the MV model that was mentioned in Section 2.5. For more detailed derivations, see [29, 30, 80], for example. As with the MV model, it is necessary to consider the small- x and large- x gluons in the target separately. Since larger- x gluons have a much longer lifetime, they appear as “frozen” sources to the shorter-lived smaller- x gluons, and constitute a classical background field. As rapidity increases, this field can act as a source of emission, creating more small- x gluons. At the next rapidity step, the emitted gluons become large- x gluons and get incorporated into the classical field, thus continuing the process of emitting more small- x gluons and so on.

In the context of the MV model, an expression was introduced for the expectation value of any functional $F[U]$ of Wilson lines, as given in Eq. (2.25). In that case, the correlators did not have a rapidity dependence. Since we are now interested in evolution in rapidity, these correlators need to be considered as rapidity-dependent objects. In place of Eq. (2.25), we now have

$$\langle F[U] \rangle_Y = \frac{\int \mathcal{D}\rho F[U] W_Y[\rho]}{\int \mathcal{D}\rho W_Y[\rho]}, \quad (4.1)$$

where the correlator $\langle F[U] \rangle_Y$ and the weight functional $W_Y[\rho]$ have gained rapidity labels to denote their rapidity dependence. The weight functional $W_Y[\rho]$ is not known directly, but its variation can be computed by considering the freezing of partons within an infinitesimal rapidity interval [81]. Eq. (4.1) can be written more compactly as

$$\langle F[U] \rangle_Y = \int \bar{D}[U] F[U] W_Y[U], \quad (4.2)$$

where the weight functional is normalised as $\int D[U] W_Y[U] = 1$. The two group theoretical constraints on the Wilson lines have been absorbed into the definition of the functional De Haar measure such that $\bar{D}[U] := D[U] \delta(UU^\dagger - \mathbb{1}) \delta(\det U - 1)$.

The goal is now to find an expression for $\partial_Y W_Y[U]$. Differentiating both sides of Eq. (4.2) gives

$$\partial_Y \langle F[U] \rangle_Y = \int \tilde{D}[U] F[U] \partial_Y W_Y[U]. \quad (4.3)$$

Since $\partial_Y \langle F[U] \rangle_Y$ is the energy evolution of a correlator, it can be written in terms of the governing Hamiltonian of the theory, labelled $H_{\text{JIMWLK}}[U]$. Then

$$\partial_Y \langle F[U] \rangle_Y = \langle -H_{\text{JIMWLK}}[U] F[U] \rangle_Y. \quad (4.4)$$

Replacing the expectation value on the right side by the definition given in Eq. (4.2) gives

$$\partial_Y \langle F[U] \rangle_Y = \int \bar{D}[U] (-H_{\text{JIMWLK}}[U] F[U]) W_Y[U]. \quad (4.5)$$

Assuming H_{JIMWLK} is Hermitian, this can be partially integrated to get

$$\langle F[U] \rangle_Y = \int \bar{D}[U] F[U] (-H_{\text{JIMWLK}}[U] W_Y[U]). \quad (4.6)$$

Finally, equating this equation with Eq. (4.3) gives

$$\int \bar{D}[U] F[U] \partial_Y W_Y[U] = \int \bar{D}[U] F[U] (-H_{\text{JIMWLK}}[U] W_Y[U]), \quad (4.7)$$

from which the JIMWLK equation

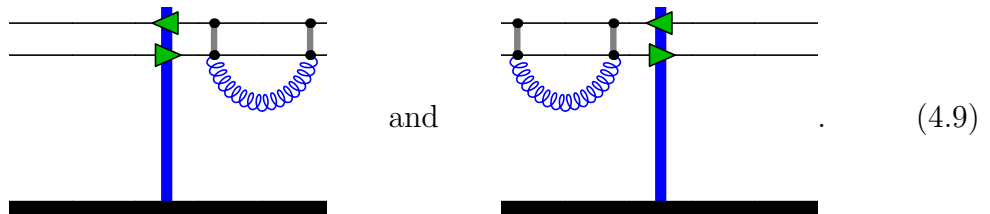
$$\partial_Y W_Y[U] = -H_{\text{JIMWLK}}[U] W_Y[U] \quad (4.8)$$

follows. The Hermiticity of the Hamiltonian is verified in the next section, after an explicit expression is found.

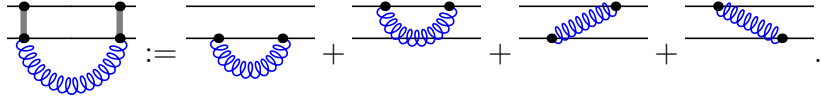
4.2 The JIMWLK Hamiltonian

In order to find the JIMWLK Hamiltonian H_{JIMWLK} that appears in the evolution equation for the weight functional in Eq. (4.8), we go back to Eq. (4.4) where it is first introduced. As a simple test operator, we may choose $F[U] \rightarrow (U_{\mathbf{x}})_{ij} (U_{\mathbf{y}}^\dagger)_{kl}$, with the definitions of the Wilson lines in the fundamental and antifundamental representations given in Eqs. (2.19) and (2.20), respectively. Now we find an evolution equation for this test function. As with BK evolution in Section 3.3, one step of JIMWLK evolution in the LLA in $\ln(1/x)$ should generate all possible diagrams with a single gluon added.

There are eight self-energy contributions, four from each of the diagrams

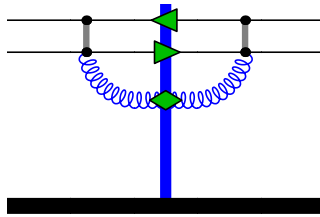


Recall that the vertical grey lines denote a sum over all possible gluon insertions so that, for example,



$$:= \text{[diagram]} + \text{[diagram]} + \text{[diagram]} + \text{[diagram]}. \quad (4.10)$$

In addition to the self-energy diagrams, there are four real contributions which come from the diagrams in which the gluon interacts with the target field:



$$. \quad (4.11)$$

All twelve diagrams can be calculated using standard techniques – see [29] for a detailed calculation using light cone perturbation theory. The six diagrams in which the gluon attaches to both the quark and the antiquark sum to

$$(\bar{\chi}_{\mathbf{x}\mathbf{y}}^{q\bar{q}})_{ijkl} := -\frac{\alpha_s}{\pi^2} \int dY \int_w \mathcal{K}_{\mathbf{x}\mathbf{w}\mathbf{y}} [(\mathbb{1} - U_{\mathbf{x}} U_{\mathbf{w}}^\dagger) (\mathbb{1} - U_{\mathbf{w}} U_{\mathbf{y}}^\dagger)]^{ab} (t^a U_{\mathbf{x}})_{ij} \otimes (U_{\mathbf{y}}^\dagger t^b)_{kl}, \quad (4.12)$$

where the convolution notation $U_{\mathbf{x}} \otimes U_{\mathbf{y}}^\dagger$ ensures that matrix elements (as opposed to whole matrices) are multiplied. The gluon emission kernel $\mathcal{K}_{\mathbf{x}\mathbf{w}\mathbf{y}}$ has been defined in Eq. (3.45). The three diagrams in which the gluon attaches only to the quark line sum to

$$(\bar{\chi}_{\mathbf{x}\mathbf{y}}^{qq})_{ijkl} := \frac{\alpha_s}{\pi^2} \int dY \int_w \mathcal{K}_{\mathbf{x}\mathbf{w}\mathbf{x}} [\mathbb{1} - U_{\mathbf{x}} U_{\mathbf{w}}^\dagger]^{ab} (t^b t^a U_{\mathbf{x}})_{ij} \otimes (U_{\mathbf{y}}^\dagger)_{kl}. \quad (4.13)$$

The three diagrams in which the gluon attaches only to the antiquark line sum to

$$(\bar{\chi}_{\mathbf{x}\mathbf{y}}^{\bar{q}\bar{q}})_{ijkl} := \frac{\alpha_s}{\pi^2} \int dY \int_w \mathcal{K}_{\mathbf{y}\mathbf{w}\mathbf{y}} [\mathbb{1} - U_{\mathbf{w}} U_{\mathbf{y}}^\dagger]^{ab} (U_{\mathbf{x}})_{ij} \otimes (U_{\mathbf{y}}^\dagger t^b t^a)_{kl}. \quad (4.14)$$

After some manipulations, the sum of all twelve diagrams (namely the sum of Eqs. (4.12), (4.13) and (4.14)) can be written compactly as an evolution equation for $\langle U_{\mathbf{x}} \otimes U_{\mathbf{y}}^\dagger \rangle_Y$:

$$\partial_Y \langle U_{\mathbf{x}} \otimes U_{\mathbf{y}}^\dagger \rangle_Y = \frac{1}{2} \langle \chi_{\mathbf{u}\mathbf{v}}^{ab} L_{\mathbf{u}}^a L_{\mathbf{v}}^b (U_{\mathbf{x}} \otimes U_{\mathbf{y}}^\dagger) \rangle_Y + \langle \sigma_{\mathbf{v}}^a L_{\mathbf{v}}^a (U_{\mathbf{x}} \otimes U_{\mathbf{y}}^\dagger) \rangle_Y, \quad (4.15)$$

where

$$\chi_{\mathbf{uv}}^{ab} := \frac{1}{4\pi^3} \int_{\mathbf{z}} \mathcal{K}_{\mathbf{uzv}} [(\mathbb{1} - U_{\mathbf{u}}^\dagger U_{\mathbf{z}}) (\mathbb{1} - U_{\mathbf{z}}^\dagger U_{\mathbf{v}})]^{ab} \quad (4.16)$$

and

$$\sigma_{\mathbf{v}}^a = \frac{i}{8\pi^3} \int_{\mathbf{z}} \mathcal{K}_{\mathbf{vzv}} \text{tr} \left(T^a \tilde{U}_{\mathbf{v}}^\dagger \tilde{U}_{\mathbf{z}} \right). \quad (4.17)$$

The operator $L_{\mathbf{u}}^a$ that appears in Eq. (4.15) is a “left” Lie derivative, which is discussed further in the next section.

The procedure to find an evolution equation for the test operator $U_{\mathbf{x}} \otimes U_{\mathbf{y}}^\dagger$ can be repeated for any Wilson line operator. By comparing Eqs. (4.4) and (4.15), an expression can be read off for the JIMWLK Hamiltonian from Eq. (4.15). After partial integration, this gives

$$H_{\text{JIMWLK}} := \frac{1}{2} L_{\mathbf{u}}^a L_{\mathbf{v}}^b \chi_{\mathbf{uv}}^{ab} - L_{\mathbf{v}}^a \sigma_{\mathbf{v}}^a. \quad (4.18)$$

With this, Eq. (4.8) is now complete and the JIMWLK equation

$$\partial_Y W_Y[U] = -\frac{1}{2} L_{\mathbf{u}}^a L_{\mathbf{v}}^b \chi_{\mathbf{uv}}^{ab} W_Y[U] + L_{\mathbf{v}}^a \sigma_{\mathbf{v}}^a W_Y[U] \quad (4.19)$$

follows. Since the weight functional W_Y represents the probability distribution within the target, the JIMWLK equation is a partial differential equation for this object. We can see from Eq. (4.19) that it is a first-order equation in “time”, which in this context is rapidity. The two Lie derivatives introduce two transverse coordinates \mathbf{u} and \mathbf{v} , which makes it a second-order equation in space. Eq. (2.26) may be used as the initial condition for Eq. (4.19).

4.3 Lie derivatives

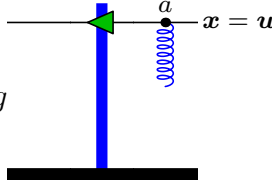
The Lie derivatives that appear in the JIMWLK equation are used throughout this thesis. The “left” and “right” Lie derivatives, respectively, are defined as

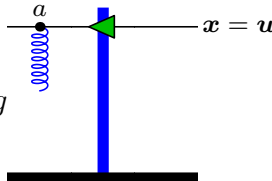
$$L_{\mathbf{u}}^a := -ig[U_{\mathbf{u}} t^a]_{\alpha\beta} \frac{\delta}{\delta[U_{\mathbf{u}}]_{\alpha\beta}} \quad \text{and} \quad R_{\mathbf{u}}^a := -ig[t^a U_{\mathbf{u}}]_{\alpha\beta} \frac{\delta}{\delta[U_{\mathbf{u}}]_{\alpha\beta}}, \quad (4.20)$$

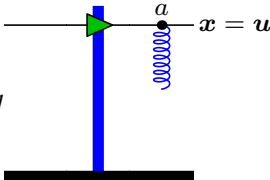
where α and β are matrix indices and $\delta/\delta U_{\mathbf{u}}$ acts as an ordinary functional derivative, i.e. as

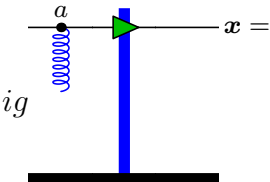
$$\frac{\delta}{\delta[U_{\mathbf{u}}]_{\alpha\beta}} [U_{\mathbf{x}}]_{\gamma\rho} = \delta_{\alpha\gamma} \delta_{\beta\rho} \delta_{\mathbf{ux}}. \quad (4.21)$$

The shorthand $\delta_{xy} := \delta^{(2)}(\mathbf{x} - \mathbf{y})$ is used henceforth for the transverse coordinate plane. The Lie derivatives operate on Wilson lines according to

$$L_{\mathbf{u}}^a U_x = -ig\delta_{\mathbf{u}x} U_x t^a = -ig \quad , \quad (4.22)$$


$$R_{\mathbf{u}}^a U_x = -ig\delta_{\mathbf{u}x} t^a U_x = -ig \quad , \quad (4.23)$$


$$L_{\mathbf{u}}^a U_x^\dagger = ig\delta_{\mathbf{u}x} t^a U_x^\dagger = ig \quad , \quad (4.24)$$


$$R_{\mathbf{u}}^a U_x^\dagger = ig\delta_{\mathbf{u}x} U_x^\dagger t^a = -ig \quad . \quad (4.25)$$


In this way, they colour-rotate the Wilson lines on the left or right of the target field. “Left” and “right” are swapped in these diagrams, since the light cone time axis runs from right to left, as shown in Fig. 2.6, for example. Notice that

$$(R_{\mathbf{u}}^a U_x)^\dagger = U_x^\dagger R_{\mathbf{u}}^{a\dagger} = ig\delta_{\mathbf{u}x} U_x^\dagger t^a = R_{\mathbf{u}}^a U_x^\dagger \quad , \quad (4.26)$$

where $R_{\mathbf{u}}^{a\dagger}$ acts to the left. In the same way, $U_x R_{\mathbf{u}}^{a\dagger} = R_{\mathbf{u}}^a U_x$ and similar expressions hold for the left Lie derivative.

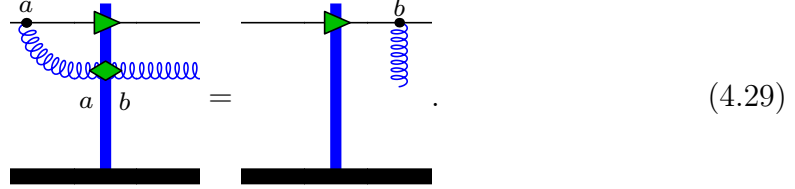
The Lie derivatives obey the commutation relations

$$[L_{\mathbf{u}}^a, L_{\mathbf{v}}^b] = g\delta_{\mathbf{u}\mathbf{v}} f^{abc} L_{\mathbf{v}}^c, \quad [R_{\mathbf{u}}^a, R_{\mathbf{v}}^b] = -g\delta_{\mathbf{u}\mathbf{v}} f^{abc} R_{\mathbf{v}}^c, \quad [L_{\mathbf{u}}^a, R_{\mathbf{v}}^b] = 0. \quad (4.27)$$

They are related to each other through the adjoint Wilson line according to

$$\tilde{U}_{\mathbf{u}}^{\dagger ba} R_{\mathbf{u}}^a = L_{\mathbf{u}}^b \quad , \quad (4.28)$$

which can be drawn acting on a Wilson line as



This relation follows from multiplying Eq. (4.24) by $\tilde{U}_u^{\dagger ba}$, and then using the group identity

$$\tilde{U}_u^{\dagger ba} t^a = U_u t^b U_u^\dagger. \quad (4.30)$$

4.4 Operation of the JIMWLK Hamiltonian

Now that we have properly defined the Lie derivatives that appear in Eq. (4.15), we return to our discussion of the JIMWLK Hamiltonian as given in Eq. (4.18). By noticing the relation

$$\sigma_v^b = -\frac{1}{2g} L_u^a \chi_{uv}^{ab}, \quad (4.31)$$

Eq. (4.18) can be recast as

$$H_{\text{JIMWLK}} = \frac{1}{2} L_u^a \chi_{uv}^{ab} L_v^b. \quad (4.32)$$

This is now in the form of a Fokker–Planck equation [50], as proposed at the beginning of this chapter. The Hamiltonian written in the form of Eq. (4.32) is helpful in showing its Hermiticity, which was assumed in writing Eq. (5.1). Note that the Fokker–Planck form applies only to the leading-order JIMWLK equation, as is the subject of this chapter. At higher orders, the presence of more Lie derivatives does not allow for the Hamiltonian to take the simple form of Eq. (4.37).

In order to see an explicit diagrammatic interpretation of the JIMWLK Hamiltonian, we carry out the following manipulations. The integrand factor from the definition of χ_{uv}^{ab} given in Eq. (4.16) can be combined with the Lie derivatives in Eq. (4.32) to give

$$\begin{aligned} & L_u^a [(\mathbb{1} - U_u U_z^\dagger) (\mathbb{1} - U_z U_v^\dagger)]^{ab} L_v^b \\ &= L_u^a \delta^{ab} L_v^b - L_u^a (U_u U_z^\dagger)^{ab} L_v^b - L_u^a (U_z U_v^\dagger)^{ab} L_v^b + L_u^a (U_u U_z^\dagger U_z U_v^\dagger)^{ab} L_v^b. \end{aligned} \quad (4.33)$$

The unitarity condition for Wilson lines, combined with Eq. (4.28), allows us to simplify the last term to

$$L_u^a (U_u U_z^\dagger U_z U_v^\dagger)^{ab} L_v^b = R_u^a \delta^{ab} R_v^b. \quad (4.34)$$

Eq. (4.28) can also be used to simplify the second and third terms in Eq. (4.33); the sum of these then becomes

$$L_u^a (U_u U_z^\dagger)^{ab} L_v^b + L_u^a (U_z U_v^\dagger)^{ab} L_v^b = R_u^a \tilde{U}_z^{ab} L_v^b + L_u^a \tilde{U}_z^{\dagger ab} R_v^b \quad (4.35)$$

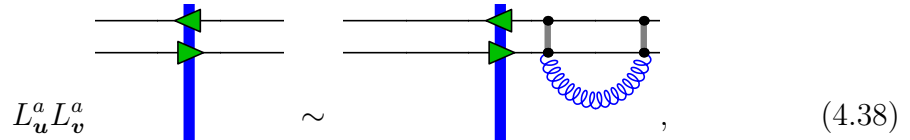
and Eq. (4.33) is simply

$$L_u^a [(\mathbb{1} - U_u U_z^\dagger) (\mathbb{1} - U_z U_v^\dagger)]^{ab} L_v^b = L_u^a L_v^a + \tilde{U}_z^{ab} (R_u^a L_v^b + L_u^a R_v^b) + R_u^a R_v^a. \quad (4.36)$$

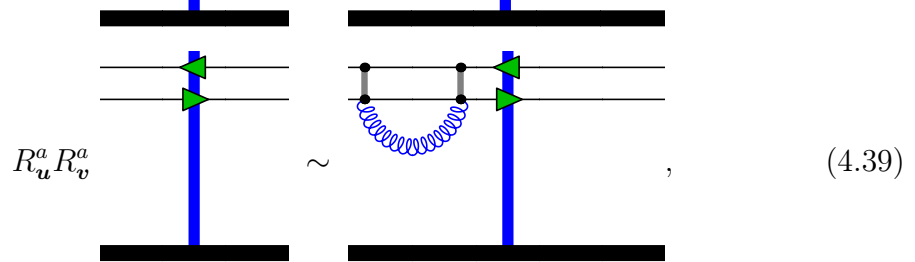
Using this result in Eq. (4.32) gives

$$H_{\text{JIMWLK}} = -\frac{1}{8\pi^3} \int_z \mathcal{K}_{uzv} \left[L_u^a L_v^a + \tilde{U}_z^{ab} (R_u^a L_v^b + L_u^a R_v^b) + R_u^a R_v^a \right]. \quad (4.37)$$

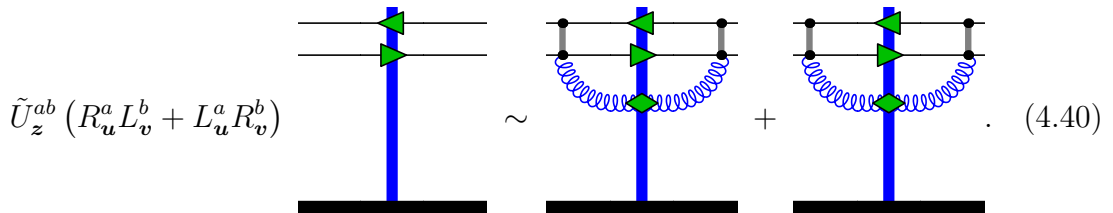
The Hamiltonian in this form can be used to find a diagrammatic interpretation for its operation on any functional of Wilson lines. As a test operator, we once again consider $U_x \otimes U_y^\dagger$. Then each of the terms in Eq. (4.37) acts as



$$L_u^a L_v^a \sim \text{diagram with wavy line to the right}, \quad (4.38)$$



$$R_u^a R_v^a \sim \text{diagram with wavy line to the left}, \quad (4.39)$$



$$\tilde{U}_z^{ab} (R_u^a L_v^b + L_u^a R_v^b) \sim \text{diagram with wavy line to the left} + \text{diagram with wavy line to the right}. \quad (4.40)$$

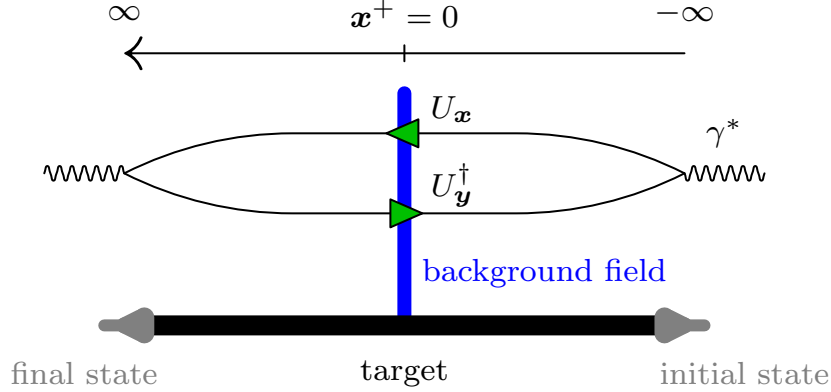


Figure 4.1. Figure from Chapter 2 showing the interaction of a dipole with the target.

From this, we see that each time the JIMWLK Hamiltonian acts on an operator, it adds one gluon to the operator in all possible ways. By construction, this is indeed what it should do: each successive rapidity step adds an s -channel gluon to the correlator to account for its small- x evolution. The same physics holds for the evolution of any other Wilson line correlator.

Another feature of JIMWLK evolution is the longitudinal growth of the projectile with increasing rapidity. In order to illustrate this, let us consider the dipole interaction with the target as shown in Fig. 2.6. An increase in energy corresponds to a lengthening of the distance along the x^+ -axis between the photon–dipole vertex (where the virtual photon probe splits into the quark–antiquark pair) and the target background field (effectively localised at $x^+ = 0$). This means that there is more phase space for multiple gluon emissions at higher rapidities, so that the probability for gluon emission increases.

4.5 The Balitsky hierarchy and BK evolution from JIMWLK

To conclude our discussion of JIMWLK evolution formulated as a Fokker–Planck equation, we now relate it back to the BK equation studied in Section 3.3. The JIMWLK equation is equivalent to an infinite set of coupled differential equations, called the *Balitsky hierarchy*. Each equation in the hierarchy governs the evolution of an n -point correlator. The set of equations is open in the sense that the n -order equation needs input from $n + 1$ -order correlators. In order to demonstrate the relation between the JIMWLK equation and the Balitsky hierarchy, we derive the first equation in the hierarchy from the JIMWLK equation. Since all correlators

henceforth are of the form $\langle \rangle_Y$, the rapidity label is omitted for clarity.

The first equation in the Balitsky hierarchy is the evolution equation for the dipole correlator $\langle S_{xy}^{(2)} \rangle$. In order to derive this in the JIMWLK formalism, Eq. (4.4) is applied (with the JIMWLK Hamiltonian in the form given in Eq. (4.37)) to the dipole correlator. This results in

$$\begin{aligned} \partial_Y \left\langle \frac{1}{N_c} \text{tr} (U_x U_y^\dagger) \right\rangle &= \left\langle -H_{\text{JIMWLK}} \frac{1}{N_c} \text{tr} (U_x U_y^\dagger) \right\rangle \\ &= \frac{1}{8\pi^3} \int_z \mathcal{K}_{uzv} \left\langle \left[L_u^a L_v^a + \tilde{U}_z^{ab} (R_u^a L_v^b + L_u^a R_v^b) + R_u^a R_v^a \right] \frac{1}{N_c} \text{tr} (U_x U_y^\dagger) \right\rangle. \end{aligned} \quad (4.41)$$

Each of the four terms in the integrand on the right side can be simplified individually. After evaluating the two left Lie derivatives in the first term, it becomes

$$\mathcal{K}_{uzv} L_u^a L_v^a \frac{1}{N_c} \text{tr} (U_x U_y^\dagger) = -g^2 \mathcal{K}_{uzv} (-\delta_{ux} + \delta_{uy}) (-\delta_{vx} + \delta_{vy}) \frac{1}{N_c} \text{tr} (U_x t^a t^a U_y^\dagger) \quad (4.42)$$

$$= -g^2 C_F \tilde{\mathcal{K}}_{xzy} \frac{1}{N_c} \text{tr} (U_x U_y^\dagger), \quad (4.43)$$

with the conformal kernel as defined in Eq. (3.44). Similarly, the term in Eq. (4.41) with two right Lie derivatives becomes the same:

$$\mathcal{K}_{uzv} R_u^a R_v^a \frac{1}{N_c} \text{tr} (U_x U_y^\dagger) = -g^2 C_F \tilde{\mathcal{K}}_{xzy} \frac{1}{N_c} \text{tr} (U_x U_y^\dagger). \quad (4.44)$$

The first mixed term in Eq. (4.41) simplifies to

$$\begin{aligned} &\mathcal{K}_{uzv} \tilde{U}_z^{ab} R_u^a L_v^a \frac{1}{N_c} \text{tr} (U_x U_y^\dagger) \\ &= -g^2 \mathcal{K}_{uzv} \tilde{U}_z^{ab} (-\delta_{ux} + \delta_{uy}) (-\delta_{vx} + \delta_{vy}) \frac{1}{N_c} \text{tr} (t^a U_x t^b U_y^\dagger) \end{aligned} \quad (4.45)$$

$$= -g^2 \tilde{\mathcal{K}}_{xzy} \tilde{U}_z^{ab} \frac{1}{N_c} \text{tr} (t^a U_x t^b U_y^\dagger) \quad (4.46)$$

and the second mixed term is the same:

$$\mathcal{K}_{uzv} \tilde{U}_z^{ab} L_u^a R_v^a \frac{1}{N_c} \text{tr} (U_x U_y^\dagger) = -g^2 \tilde{\mathcal{K}}_{xzy} \tilde{U}_z^{ab} \frac{1}{N_c} \text{tr} (t^a U_x t^b U_y^\dagger). \quad (4.47)$$

Putting the four simplified terms together, Eq. (4.41) becomes

$$\partial_Y \left\langle \frac{1}{N_c} \text{tr} (U_x U_y^\dagger) \right\rangle = \frac{g^2}{4\pi^3} \int_z \tilde{\mathcal{K}}_{xzy} \left\langle -\frac{C_F}{N_c} \text{tr} (U_x U_y^\dagger) + \frac{1}{N_c} \tilde{U}_z^{ab} \text{tr} (t^a U_x t^b U_y^\dagger) \right\rangle. \quad (4.48)$$

This is the evolution equation for the dipole correlator in the Balitsky hierarchy. By considering higher-point correlators in the JIMWLK equation, the higher-order equations in the hierarchy may be derived in a similar way.

The evolution equation for the dipole correlator as given in Eq. (4.48) can also be used to show the relation between the leading-order JIMWLK and BK equations. One way to close Eq. (4.48) is to use the large- N_c approximation to write the 3-point correlator that appears on the right side of the equation in terms of the dipole. First, the Fierz identity

$$2\tilde{U}_z^a \text{tr}(t^a U_x t^b U_y^\dagger) = \text{tr}(U_x U_z^\dagger) \text{tr}(U_z U_y^\dagger) - \frac{1}{N_c} \text{tr}(U_x U_y^\dagger) \quad (4.49)$$

is used to write

$$\begin{aligned} & \partial_Y \left\langle \frac{1}{N_c} \text{tr}(U_x U_y^\dagger) \right\rangle \\ &= \frac{\alpha_s}{\pi^2} \int_z \tilde{\mathcal{K}}_{xyz} \left\langle \frac{1}{2N_c} \text{tr}(U_x U_z^\dagger) \text{tr}(U_z U_y^\dagger) - \frac{1}{2N_c^2} \text{tr}(U_x U_y^\dagger) - C_F \frac{1}{N_c} \text{tr}(U_x U_y^\dagger) \right\rangle \end{aligned} \quad (4.50)$$

$$= \frac{N_c \alpha_s}{2 \pi^2} \int_z \tilde{\mathcal{K}}_{xyz} \left\langle \frac{1}{N_c^2} \text{tr}(U_x U_z^\dagger) \text{tr}(U_z U_y^\dagger) - \frac{1}{N_c} \text{tr}(U_x U_y^\dagger) \right\rangle. \quad (4.51)$$

In the large- N_c limit, the expectation value of a product of two traces factorises into the product of expectation values:

$$\left\langle \frac{1}{N_c^2} \text{tr}(U_x U_z^\dagger) \text{tr}(U_z U_y^\dagger) \right\rangle \xrightarrow{N_c \rightarrow \infty} \left\langle \frac{1}{N_c} \text{tr}(U_x U_z^\dagger) \right\rangle \left\langle \frac{1}{N_c} \text{tr}(U_z U_y^\dagger) \right\rangle. \quad (4.52)$$

Cross-talk between dipoles (traces) has been shown to be N_c -suppressed [50, 82]. With this approximation, Eq. (4.51) becomes the BK equation

$$\begin{aligned} & \partial_Y \left\langle \frac{1}{N_c} \text{tr}(U_x U_y^\dagger) \right\rangle \\ &= \frac{N_c \alpha_s}{2 \pi^2} \int_z \tilde{\mathcal{K}}_{xyz} \left(\left\langle \frac{1}{N_c} \text{tr}(U_x U_z^\dagger) \right\rangle \left\langle \frac{1}{N_c} \text{tr}(U_z U_y^\dagger) \right\rangle - \left\langle \frac{1}{N_c} \text{tr}(U_x U_y^\dagger) \right\rangle \right) \end{aligned} \quad (4.53)$$

(cf. Eq. (3.55)). In Section 3.3.3, we saw that the only difference between the BK equation and the BFKL equation is the nonlinear term present in the former. Since we have shown how the BK equation arises from the JIMWLK equation, we can make the statement that linearising the JIMWLK equation results in the BFKL equation. This is important in Chapter 6, where the dilute limit of the JIMWLK equation from the Langevin formalism is studied.

Chapter summary

This concludes the chapter on JIMWLK evolution and the JIMWLK equation written as a Fokker-Planck equation. In this chapter, we have outlined the derivation of the evolution equation and discussed some important properties of the JIMWLK Hamiltonian. This required the introduction of Lie derivatives, which we use to write gluon emissions in a Wilson line operator in a convenient way. We have also shown the relation between JIMWLK evolution and the Balitsky hierarchy, which are two equivalent formulations of the same kind of evolution. We have seen that the BK equation is the JIMWLK equation for the dipole correlator, taken in the large- N_c limit.

5

JIMWLK in the Langevin Formalism

We have thus far discussed JIMWLK evolution in the form of a Fokker–Planck equation. In Chapter 4, the physical picture was of a target field configuration evolving in rapidity by inclusion of a soft gluon emitted from the projectile at each evolution step. Generically, any stochastic process governed by a Fokker–Planck equation can be described by an equivalent Langevin equation. For the JIMWLK equation, the latter formalism is particularly of interest for two reasons. Firstly, it allows for a numerical implementation of JIMWLK evolution that is computationally cost effective. Secondly, it gives an alternative physical picture of evolution as a random walk in the functional space of Wilson lines. This stochastic interpretation proves particularly useful in the study of multi-particle correlations for particles that are separated from each other by rapidity intervals larger than $\Delta Y \gtrsim 1/\alpha_s$.

In this chapter, we give a theoretical background of the Langevin JIMWLK equation that was studied in Paper [II]. In Section 5.1, the evolution equation for Wilson lines is derived. In Section 5.2, we consider inclusive particle production, first at equal rapidity and then at unequal rapidity. This leads to the bilocal Langevin equations, which we discuss in Section 5.3. The equations derived in this chapter are necessary for Chapter 6, where they are expanded in the dilute limit.

5.1 The Langevin JIMWLK equation

The Langevin picture of JIMWLK evolution was first described formally in [81] and implemented numerically in [79, 83–85]. In [81], standard methods were used to derive a Langevin equation from a Fokker–Planck equation by considering changes in the system under consideration during an infinitesimal time interval. In the case

of JIMWLK evolution, the equivalence between the two descriptions follows from an alternative formulation of the expectation value given in Eq. (4.2),

$$\langle F[U] \rangle = \int \bar{D}[U] F[U] W_Y[U]. \quad (5.1)$$

Now the system is considered to be an ensemble of Wilson lines randomly distributed at rapidity Y according to the weight functional $W_Y[U]$. The expectation value of some operator is a sum, taken separately at each Y , over all N configurations in this ensemble:

$$\langle F[U] \rangle \approx \frac{1}{N} \sum F[U]. \quad (5.2)$$

Rapidity acts as “time” and evolution is considered over some interval $\Delta Y \gtrsim 1/\alpha_s$. This interval is discretised into N pieces of size ϵ , i.e. $\Delta Y = Y_{\text{fin}} - Y_{\text{in}} = \epsilon N$ with $\mathbb{Z} \ni N \rightarrow \infty, \epsilon \rightarrow 0$. Quantities at each evolution step are labelled by index $0 \leq n \leq N$.

An appropriate degree of freedom to consider in the Langevin picture is the classical field $\alpha_Y(x^+, \mathbf{x}) := A^-(x^+, \mathbf{x}, 0)$. Recall that this field appears directly in the definition of the Wilson line given in Eq. (2.20),

$$U_{\mathbf{x}}^\dagger := \text{P exp} \left\{ ig \int_{-\infty}^{\infty} dx^+ A^-(x^+, \mathbf{x}, 0) \right\}. \quad (5.3)$$

As already mentioned in Chapter 4, the weight functional $W_Y[\alpha]$ that appears in Eq. (5.1) is not known, but its variation within an infinitesimal rapidity interval $(Y, Y + \epsilon)$ can be calculated. The partons that freeze out in this rapidity interval have longitudinal momenta $e^{-\epsilon}\Lambda < k^- < \Lambda$ [81]. Random fluctuations $\alpha_Y(\mathbf{x})\epsilon$ over the field $\alpha_Y(x^+, \mathbf{x})$ are induced by the freezing out of these degrees of freedom. The fluctuations are calculated as

$$\alpha_Y^a(\mathbf{x})\epsilon := \int dx^+ \delta\alpha_Y(x^+, \mathbf{x}), \quad (5.4)$$

where [7]

$$\delta\alpha_Y(x^+, \mathbf{x}) \propto \theta(x^+) \frac{1}{x^+} [\exp\{-ie^{-\epsilon}\Lambda x^+\} - \exp\{-i\Lambda x^+\}]. \quad (5.5)$$

The x^+ dependence in the field can be shown to be integrated out in Eq. (5.4), leaving a factor ϵ . Then the field at some intermediate rapidity Y_n and transverse position \mathbf{x} can be written as $\alpha_{\mathbf{x},n} = \alpha_{\mathbf{x},n}^a t^a$, that is, with no x^+ -dependence. The components $\alpha_{\mathbf{x},n}^a$ are now treated as a random variable with a Gaussian distribution and obeying [81]

$$\langle \alpha_{\mathbf{x},n+1}^a \rangle = \sigma_{\mathbf{x},n}^a, \quad \text{and} \quad \langle \alpha_{\mathbf{x},n+1}^a \alpha_{\mathbf{y},n+1}^b \rangle = \frac{1}{\epsilon} \chi_{\mathbf{x}\mathbf{y},n}^{ab}. \quad (5.6)$$

The definitions of $\chi_{\mathbf{x}\mathbf{y},n}^{ab}$ and $\sigma_{\mathbf{x},n}^a$ follow from Eqs. (4.16) and (4.17), respectively, with the Wilson lines from there taken at step n .

An equivalent formulation of the constraints in Eq. (5.6) is the Langevin equation [81]

$$\alpha_{\mathbf{x},n+1}^a = \sigma_{\mathbf{x},n}^a + \int_{\mathbf{z}} \varepsilon_{\mathbf{x}\mathbf{z},n}^{ab,i} \nu_{\mathbf{z},n+1}^{b,i}, \quad (5.7)$$

where $\varepsilon_{\mathbf{x}\mathbf{z},n}^{ab}$ is the square root of $\chi_{\mathbf{x}\mathbf{y},n}^{ab} = \varepsilon_{\mathbf{x}\mathbf{z},n}^{ac} \varepsilon_{\mathbf{z}\mathbf{y},n}^{cb}$, so that

$$\varepsilon_{\mathbf{x}\mathbf{z},n}^{ab,i} := \frac{1}{2\pi^{3/2}} \mathcal{K}_{\mathbf{x}\mathbf{z}}^i \left[\mathbb{1} - \tilde{U}_{\mathbf{x},n}^\dagger \tilde{U}_{\mathbf{z},n} \right]^{ab}. \quad (5.8)$$

(The Weizsäcker-Williams kernel $\mathcal{K}_{\mathbf{x}\mathbf{y}}^i$ was defined in Eq. (3.46)). The $\nu_{\mathbf{z},n+1}^{b,i}$ appearing in Eq. (5.7) is a real-numbered auxiliary Gaussian white noise, satisfying

$$\langle f[\nu] \rangle = \int \mathcal{D}[\nu] f[\nu] e^{-\frac{1}{2}\nu\nu}, \quad (5.9)$$

for any functional $f[\nu]$. In particular,

$$\langle \nu_{\mathbf{x},n}^{a,i} \rangle = 0 \quad \text{and} \quad \langle \nu_{\mathbf{x},m}^{a,i} \nu_{\mathbf{y},n}^{b,j} \rangle = \frac{1}{\epsilon} \delta_{mn} \delta^{ab} \delta^{ij} \delta_{\mathbf{x}\mathbf{y}}, \quad (5.10)$$

where the factor $1/\epsilon$ comes from the continuous version of the localisation of rapidity $\delta(Y_m - Y_n) \rightarrow \delta_{mn}/\epsilon$. The localisation of the noise in this way is useful in that it greatly reduces the computational cost involved in numerical simulations.

In terms of Wilson lines, the continuous version of Eq. (5.7) is

$$\partial_Y U_{\mathbf{x}} = U_{\mathbf{x}} i t^a \left(\int_{\mathbf{y}} \varepsilon_{\mathbf{x}\mathbf{y}}^{ab,i} \nu_{\mathbf{y}}^{b,i} + g \sigma_{\mathbf{x}}^a \right). \quad (5.11)$$

This expression allows for a direct interpretation of evolution as an infinitesimal step in $\text{SU}(N_c)$ space. The factor enclosed in round brackets acts as the ‘‘angle’’ parametrising a local gauge transformation in transverse space and the $\sigma_{\mathbf{x}}^a$ term represents a deterministic ‘‘drift’’ [30]. Eq. (5.11) can be recast as a discretised evolution equation for the Wilson lines:

$$U_{\mathbf{x},n+1} = U_{\mathbf{x},n} \exp \left\{ -i g \epsilon t^a \left(\int_{\mathbf{y}} \varepsilon_{\mathbf{x}\mathbf{y}}^{ab,i} \nu_{\mathbf{y}}^{b,i} + g \sigma_{\mathbf{x}}^a \right) \right\}. \quad (5.12)$$

It is this form of the evolution equation that we explore further.

5.1.1 Expansion in rapidity step size

Since the rapidity step size ϵ is infinitesimal, it can be used to expand the exponential in Eq. (5.12). An expansion in ϵ is useful in order to better show the physical meaning of the evolution equation. It also allows us to use Eq. (5.10) to simplify linear and quadratic terms in the noise. Terms of order ϵ and higher can be neglected because these vanish in the limit $\epsilon \rightarrow 0$. The power counting in ϵ needs to be done carefully, bearing in mind that Eq. (5.10) effectively makes each ν of order $\epsilon^{-1/2}$.

The first term in the expansion of Eq. (5.12) is simply $U_{x,n} \times \mathbb{1}$. The second term in the series is

$$U_{x,n} \times \left\{ -ig\epsilon t^a \left(\int_{\mathbf{y}} \varepsilon_{\mathbf{x}\mathbf{y}}^{ab,i} \nu_{\mathbf{y}}^{b,i} + g\sigma_{\mathbf{x}}^a \right) \right\} = -\frac{ig\epsilon}{2\pi^{3/2}} \int_{\mathbf{y}} \mathcal{K}_{\mathbf{x}\mathbf{y}}^i \nu_{\mathbf{y}}^{a,i} U_{x,n} \left(t^a - \tilde{U}_{\mathbf{y},n}^{\dagger ab} t^b \right) - \frac{\epsilon g^2}{8\pi^3} \int_{\mathbf{z}} \mathcal{K}_{\mathbf{x}\mathbf{z}\mathbf{x}} U_{x,n} t^a t^b \left(\tilde{U}_{\mathbf{x},n}^{\dagger bc} \tilde{U}_{\mathbf{z},n}^{ca} - \tilde{U}_{\mathbf{x},n}^{\dagger ac} \tilde{U}_{\mathbf{z},n}^{cb} \right). \quad (5.13)$$

To simplify this expression, the definitions of χ and σ have been used, as well as some basic $SU(N_c)$ identities. Similarly, the third term in the ϵ expansion is

$$U_{x,n} \times \left\{ -g^2 \epsilon^2 t^a \left(\int_{\mathbf{y}} \varepsilon_{\mathbf{x}\mathbf{y}}^{ab,i} \nu_{\mathbf{y}}^{b,i} + g\sigma_{\mathbf{x}}^a \right) t^c \left(\int_{\mathbf{z}} \varepsilon_{\mathbf{x}\mathbf{z}}^{cd,j} \nu_{\mathbf{z}}^{d,j} + g\sigma_{\mathbf{x}}^c \right) \right\} = -U_{x,n} \frac{\epsilon g^2}{4\pi^3} \int_{\mathbf{y}} \mathcal{K}_{\mathbf{x}\mathbf{y}\mathbf{x}} \left(2t^a t^a - t^a t^b \tilde{U}_{\mathbf{x},n}^{\dagger bc} \tilde{U}_{\mathbf{y},n}^{ca} - t^a t^b \tilde{U}_{\mathbf{x},n}^{\dagger ac} \tilde{U}_{\mathbf{y},n}^{cb} \right) + \mathcal{O}(\nu\epsilon^2). \quad (5.14)$$

The second and third terms of Eq. (5.14) cancel and double, respectively, when combined with the last two terms of Eq. (5.13). Altogether, the expansion of Eq. (5.12) becomes

$$U_{x,n+1} = U_{x,n} + \int_{\mathbf{z}} \left(U_{x,n} t^a - \tilde{U}_{\mathbf{z},n}^{\dagger ab} t^b U_{x,n} \right) \left(-\frac{ig}{\sqrt{4\pi^3}} \mathcal{K}_{\mathbf{x}\mathbf{z}}^i \nu_{\mathbf{z},n}^{a,i} - \frac{\epsilon g^2}{4\pi^3} \mathcal{K}_{\mathbf{x}\mathbf{z}\mathbf{x}} t^a \right) + \mathcal{O}(\nu\epsilon^2). \quad (5.15)$$

There is a subtlety that must be mentioned in using Eq. (5.10) to obtain Eq. (5.15). An expectation value expression is used to simplify an operator expression that does not contain expectation values. However, this can be justified as follows. Ultimately, Wilson lines need to be calculated within cross sections, in which they always appear in pairs. The DIS cross section discussed in Section 2.7, for example, contains the dipole correlator $\langle \text{tr} (U_{\mathbf{x}} U_{\mathbf{y}}^{\dagger}) / N_c \rangle$. In that case, the expansion of

Eq. (5.12) leads to terms that go like

$$\begin{aligned} & \left\langle \frac{1}{N_c} \text{tr} \left(U_{\mathbf{x},n+1}^\dagger U_{\mathbf{y},n+1} \right) \right\rangle \\ & \sim \left\langle \left(\sum_{k=0}^{\infty} \frac{1}{k!} [\mathcal{O}(\nu\epsilon) + \mathcal{O}(\epsilon)]^k \right) \times \left(\sum_{l=0}^{\infty} \frac{1}{l!} [\mathcal{O}(\nu\epsilon) + \mathcal{O}(\epsilon)]^l \right) \right\rangle \quad (5.16) \\ & \sim \langle \mathcal{O}(1) + \mathcal{O}(\nu\epsilon) + \mathcal{O}(\epsilon) + \mathcal{O}(\nu^2\epsilon^2) + \mathcal{O}(\nu\epsilon^2) + \text{higher orders} \rangle. \quad (5.17) \end{aligned}$$

If we wish to work to order ϵ accuracy, we therefore only need to keep terms up to second order in ν in the expansion of each Wilson line. Then the expectation values from Eq. (5.10) can be used safely for each term in Eq. (5.17). Since this procedure applies at the end of any cross section calculation, we may use Eq. (5.10) to simplify factors of ν from the start, even in operator expressions that do not contain any expectation values.

In order to reconcile Eq. (5.15) with the notion of evolution discussed in Chapter 4, it is expressed in terms of Wilson line diagrams. If the Wilson line of a quark projectile at the initial condition is represented as

$$U_{x,0} = \begin{array}{c} \text{---} \leftarrow \text{---} \\ | \\ \text{---} \end{array}, \quad (5.18)$$

then one step in evolution according to Eq. (5.15) gives

$$\begin{aligned} U_{x,1} = & \begin{array}{c} \text{---} \leftarrow \text{---} \quad x \\ | \\ \text{---} \end{array} - \frac{i\epsilon g}{\sqrt{4\pi^3}} \int_z \mathcal{K}_{xz}^i \nu_{z,0}^{a,i} \left(\begin{array}{c} a \\ \text{---} \leftarrow \text{---} \quad x \\ | \\ \text{---} \end{array} - \begin{array}{c} \text{---} \leftarrow \text{---} \quad x \\ | \\ \text{---} \end{array} \begin{array}{c} b \\ \text{---} \leftarrow \text{---} \quad x \\ | \\ \text{---} \end{array} \right) \\ & - \frac{\epsilon g^2}{4\pi^3} \int_z \mathcal{K}_{xzx} \left(\begin{array}{c} a \quad a \\ \text{---} \leftarrow \text{---} \quad x \\ | \\ \text{---} \end{array} - \begin{array}{c} a \quad b \\ \text{---} \leftarrow \text{---} \quad x \\ | \\ \text{---} \end{array} \right) + \mathcal{O}(\nu\epsilon^2). \quad (5.19) \end{aligned}$$

This takes into account all possible diagrams with a single gluon added to the initial condition $U_{x,0}$. The first term is simply the original Wilson line. The second and third terms contain the gluon emitted either before or after the quark interaction

with the target. The gluon remains unabsorbed by the quark, with an open colour index that contracts with the colour index of the noise factor. The fourth and fifth terms in Eq. (5.19) contain the gluon emitted either before or after the target line, but now the gluon is reabsorbed by the quark after the interaction with the target field. Both kernels that appear in Eq. (5.19) correspond to the vertical separation in the diagrams between transverse coordinates \mathbf{x} (the quark) and \mathbf{z} (the emitted gluon). We can see from these diagrams that evolution in the Langevin picture does indeed agree with that of the Fokker–Planck formalism in that a single soft s -channel gluon gets added to the diagrams at each step in evolution.

As a cross check, it is possible to derive the BK equation from Eq. (5.15). For each Wilson line in the dipole $\text{tr}(U_{\mathbf{x},n+1}^\dagger U_{\mathbf{y},n+1})/N_c$, the expansion is used up to order $\nu\epsilon$ to write an expression in terms of Wilson lines and noise factors at step n . Using Eq. (5.10) and the Fierz identity gives

$$\begin{aligned} \frac{1}{\epsilon N_c} \text{tr} \left(U_{\mathbf{x},n+1}^\dagger U_{\mathbf{y},n+1} - U_{\mathbf{x},n}^\dagger U_{\mathbf{y},n} \right) &= \frac{\alpha_s N_c}{\pi^2} \frac{1}{2} \int_{\mathbf{z}} \tilde{\mathcal{K}}_{\mathbf{x}\mathbf{y}\mathbf{z}} \\ &\times \left[\frac{1}{N_c^2} \text{tr} (U_{\mathbf{y},n} U_{\mathbf{z},n}^\dagger) \text{tr} (U_{\mathbf{z},n} U_{\mathbf{x},n}^\dagger) - \frac{1}{N_c} \text{tr} (U_{\mathbf{x},n}^\dagger U_{\mathbf{y},n}) \right] + \mathcal{O}(\nu\epsilon^2). \end{aligned} \quad (5.20)$$

After identifying the left side with $\partial_Y \text{tr}(U_{\mathbf{x}}^\dagger U_{\mathbf{y}})/N_c$ and taking the expectation value on both sides, this expression becomes the BK equation given in Eq. (3.55), written in terms of $S_{\mathbf{x}\mathbf{y}}^{(2)}$ instead of $N_{\mathbf{x}\mathbf{y}}$.

5.1.2 Alternative form

The expanded form of the Langevin equation for the Wilson lines has another important use. It allows us to write Eq. (5.12) in a more useful form, as was first shown in [86]. An alternative form of Eq. (5.12) that would lead to the same expanded expression up to order $\nu\epsilon^2$ is

$$U_{\mathbf{x},n+1} = e^{i\epsilon g \alpha_{\mathbf{x},n}^L} U_{\mathbf{x},n} e^{-i\epsilon g \alpha_{\mathbf{x},n}^R}, \quad (5.21)$$

where “right” and “left” traceless Hermitian colour fields¹

$$\alpha_{\mathbf{x},n}^R := \frac{1}{\sqrt{4\pi^3}} \int_{\mathbf{z}} \mathcal{K}_{\mathbf{x}\mathbf{z}}^i \nu_{\mathbf{z},n}^{a,i} t^a =: \frac{1}{\sqrt{4\pi^3}} \int_{\mathbf{z}} \mathcal{K}_{\mathbf{x}\mathbf{z}}^i \nu_{\mathbf{z},n}^i, \quad (5.22)$$

$$\alpha_{\mathbf{x},n}^L := \frac{1}{\sqrt{4\pi^3}} \int_{\mathbf{z}} \mathcal{K}_{\mathbf{x}\mathbf{z}}^i \nu_{\mathbf{z},n}^{a,i} \tilde{U}_{\mathbf{z},n}^{\dagger ab} t^b =: \frac{1}{\sqrt{4\pi^3}} \int_{\mathbf{z}} \mathcal{K}_{\mathbf{x}\mathbf{z}}^i U_{\mathbf{z},n} \nu_{\mathbf{z},n}^i U_{\mathbf{z},n}^\dagger, \quad (5.23)$$

¹Note that the choice of left and right in the definitions of the colour fields is opposite to that of Paper [III]. They have been redefined here to remain consistent with the labelling of the Lie derivatives in Chapter 4.

have been introduced, respectively. The shorthand $\nu_{z,n}^i := \nu_{z,n}^{a,i} t^a$ is used and the group identity $\tilde{U}_{z,n}^{\dagger ab} t^b = U_{z,n} t^a U_{z,n}^\dagger$ is used in the definition of $\alpha_{x,n}^L$.

In keeping with the stochastic interpretation of evolution in the context of the Langevin picture, the two matrix exponentials in Eq. (5.21) act as infinitesimal colour rotations to the left and to the right of the target field. This causes the random walk of the evolving Wilson line in colour space. To see this diagrammatically, the colour fields are applied at the initial condition to the Wilson line initial condition given in Eq. (5.18). This gives

$$\begin{aligned}
 U_{x,0} \alpha_{x,0}^R &= \frac{1}{\sqrt{4\pi^3}} \int_z \mathcal{K}_{xz}^i \nu_{z,0}^{a,i} , \\
 \alpha_{x,0}^L U_{x,0} &= \frac{1}{\sqrt{4\pi^3}} \int_z \mathcal{K}_{xz}^i \nu_{z,0}^{a,i} .
 \end{aligned}$$

The definitions of the right and left fields can be interchanged by defining a rotated noise

$$\tilde{\nu}_{x,n}^i := \tilde{\nu}_{x,n}^{a,i} t^a := \nu_{x,n}^{a,i} \tilde{U}_{x,n}^{\dagger ab} t^b , \quad (5.24)$$

as discussed in Paper [II]. It can be shown that $\tilde{\nu}$ satisfies the same constraints as Eq. (5.10), namely

$$\langle \tilde{\nu}_{x,n}^{a,i} \rangle = 0 \quad \text{and} \quad \langle \tilde{\nu}_{x,m}^{a,i} \tilde{\nu}_{y,n}^{b,j} \rangle = \frac{1}{\epsilon} \delta_{mn} \delta^{ab} \delta^{ij} \delta_{xy} . \quad (5.25)$$

This means that the definitions of α^R and α^L in terms of $\tilde{\nu}$ may just as well be used in Eq. (5.21), without changing the meaning of the evolution equation. The choice of ν or $\tilde{\nu}$ is a matter of convention – we consistently use the former. Indeed, the expansion of Eq. (5.21) in ϵ can be shown to give the same expression as Eq. (5.15) up to order $\nu\epsilon^2$. One advantage of Eq. (5.21) over Eq. (5.12) is that the new form explicitly shows the left–right symmetry inherent in JIMWLK evolution. A second advantage is that the numerically costly drift term in Eq. (5.12) has been removed. This makes Eq. (5.21) a computationally preferable form of the Langevin JIMWLK equation [86].

If we now want to consider quark–gluon production, we can “produce” a gluon with transverse momentum \mathbf{k} by acting on the dipole $S_{\mathbf{x}\bar{\mathbf{x}}}^{(2)}$ with the so-called production Hamiltonian [89–91]

$$H_{\text{prod}}(\mathbf{k}) := \frac{1}{4\pi^3} \int_{\mathbf{y}\bar{\mathbf{y}}} e^{-i\mathbf{k}\cdot(\mathbf{y}-\bar{\mathbf{y}})} \int_{\mathbf{u}\bar{\mathbf{u}}} \mathcal{K}_{\mathbf{y}\mathbf{u}}^i \mathcal{K}_{\bar{\mathbf{y}}\bar{\mathbf{u}}}^i \left(L_{\mathbf{u}}^a - \tilde{U}_{\mathbf{y}}^{\dagger ab} R_{\mathbf{u}}^b \right) \left(\bar{L}_{\bar{\mathbf{u}}}^a - \bar{\tilde{U}}_{\bar{\mathbf{y}}}^{\dagger ac} \bar{R}_{\bar{\mathbf{u}}}^c \right). \quad (5.28)$$

Barred Lie derivatives only operate on barred Wilson lines and unbarred Lie derivatives only operate on unbarred Wilson lines. Notice that Eq. (5.28) is effectively the JIMWLK Hamiltonian from Eq. (4.37), which was shown in Section 4.4 to add a gluon in all possible ways to the operator on which it acts. A key difference between H_{prod} and H_{JIMWLK} is that, unlike in H_{JIMWLK} , the two adjoint Wilson lines in H_{prod} are at distinctly different transverse coordinates \mathbf{y} and $\bar{\mathbf{y}}$. This is a consequence of the separation of the DA and the CCA in the calculation.

The cross section for inclusive quark–gluon production is then [89–91]

$$\frac{d\sigma_{\text{qg}}}{d\eta_p d^2p d\eta_k d^2k} = \frac{1}{16\pi^4} \int_{\mathbf{x}\bar{\mathbf{x}}} e^{-i\mathbf{p}\cdot(\mathbf{x}-\bar{\mathbf{x}})} \left\langle H_{\text{prod}}(\mathbf{k}) S_{\mathbf{x}\bar{\mathbf{x}}}^{(2)} \Big|_{\bar{U}=U} \right\rangle_Y, \quad (5.29)$$

where \mathbf{k} and η_k refer to the transverse momentum and pseudo-rapidity, respectively, of the produced gluon. Eq. (5.29) can be simplified using the definitions of the Lie derivatives given in Eq. (4.20). After the production Hamiltonian acts on the dipole operator, it is safe to set $\bar{U} = U$. Evaluating the integrals over \mathbf{u} and $\bar{\mathbf{u}}$ gives

$$\begin{aligned} \frac{d\sigma_{\text{qg}}}{d\eta_p d^2p d\eta_k d^2k} &= \frac{C_F}{16\pi^4} \frac{\alpha_s}{\pi^2} \int_{\mathbf{x}\bar{\mathbf{x}}\mathbf{y}\bar{\mathbf{y}}} e^{-i\mathbf{p}\cdot(\mathbf{x}-\bar{\mathbf{x}})-i\mathbf{k}\cdot(\mathbf{y}-\bar{\mathbf{y}})} \mathcal{K}_{\mathbf{y}\mathbf{x}}^i \mathcal{K}_{\bar{\mathbf{y}}\bar{\mathbf{x}}}^i \left\langle \frac{1}{N_c} \text{tr} \left(U_{\mathbf{x}} U_{\bar{\mathbf{x}}}^\dagger \right) \right. \\ &\quad \left. - \frac{1}{N_c C_F} \left(\tilde{U}_{\mathbf{y}}^\dagger + \tilde{U}_{\bar{\mathbf{y}}}^\dagger \right)^{ab} \text{tr} \left(t^b U_{\mathbf{x}} t^a U_{\bar{\mathbf{x}}}^\dagger \right) + \frac{1}{N_c C_F} \left(U_{\mathbf{y}} U_{\bar{\mathbf{y}}}^\dagger \right)^{ab} \text{tr} \left(t^a U_{\mathbf{x}} U_{\bar{\mathbf{x}}}^\dagger t^b \right) \right\rangle_Y. \end{aligned} \quad (5.30)$$

This is the final expression for the cross section for inclusive quark–gluon production in the case that the produced quark and gluon are separated by a small rapidity $\Delta Y \lesssim 1/\alpha_s$. Eq. (5.30) is in agreement with the two-gluon analogue obtained in [92] in the soft gluon limit.

5.2.2 Extension to unequal rapidities

We now try to calculate the cross section in Eq. (5.30) for the case that the produced quark and gluon are separated by a large rapidity $\Delta Y \gtrsim 1/\alpha_s$. We follow the formalism developed in [93] for the case of double inclusive two-gluon production in proton–nucleus collisions. We present the main points of the discussion from

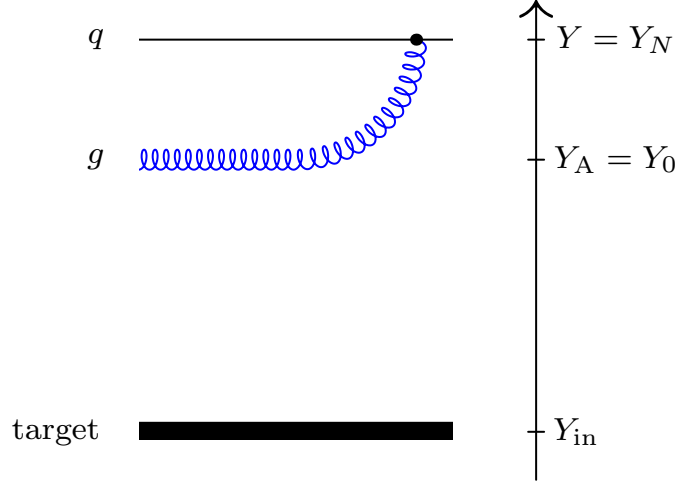


Figure 5.1. A physical picture of the inclusive quark–gluon production cross section considered, showing the rapidities of the produced quark and gluon and of the target. In particular, the quark and gluon are now separated by a large rapidity, as opposed to the case studied in Section 5.2.1.

there for the slightly different case of quark–gluon production. A similar scenario has also been studied in [94]. The physical picture considered is shown in Fig. 5.1. A quark is produced at rapidity Y relative to the target’s rapidity Y_{in} . A gluon is produced at some earlier rapidity Y_A , where $Y - Y_A \gtrsim 1/\alpha_s$. Following the notation of [93], the “A” label pertains to all quantities at the intermediate rapidity Y_A . This labelling system can then be extended to include additional produced gluons at other rapidities Y_B, Y_C , etc. as needed.

The large rapidity separation between the quark and the gluon means that the whole rapidity interval from Y_{in} to Y needs to be considered in two separate parts – one for the interval Y_{in} to Y_A and another for the interval Y_A to Y . Working backwards in rapidity, we have the following steps to calculate the cross section:

1. The quark alone evolves from the intermediate rapidity Y_A up to the final rapidity Y . This is represented in the cross section by the same fundamental dipole expectation value as was considered in Section 5.2.1, namely $\langle S_{x\bar{x}}^{(2)} \rangle_{Y-Y_A}$. The expectation value is traded for an average over the noise ν at the end of the stochastic process, so that now $\langle S_{x\bar{x},N}^{(2)} \rangle_\nu$.
2. A gluon with transverse momentum \mathbf{k}_A is produced at Y_A from the quark dipole. We act with the production Hamiltonian given in Eq. (5.28) on the dipole, i.e. we calculate $H_{\text{prod}}(\mathbf{k}_A) \langle S_{x\bar{x},N}^{(2)} \rangle_\nu$. All quantities for H_{prod} given

in Eq. (5.28) pertain to rapidity Y_A , which corresponds to the rapidity step index $n = 0$.

- Both the quark and the gluon evolve from the target rapidity Y_{in} up to Y_A . This is represented by a second expectation value as

$$\left\langle H_{\text{prod}}(\mathbf{k}_A) \left\langle S_{\mathbf{x}\bar{\mathbf{x}},N}^{(2)} \right\rangle_{\nu} \Big|_{\bar{U}_A=U_A} \right\rangle_{Y_A}.$$

The two expectation values here are not calculated in the same way. The outer expectation value $\langle \rangle_{Y_A}$ is calculated in the standard way using Eq. (4.2). The inner expectation value $\langle \rangle_{Y-Y_A}$, however, now involves a conditional expression, since it needs to have knowledge of the partially evolved Wilson lines at the intermediate rapidity Y_A . Instead of Eq. (4.2), the inner expectation value is calculated according to

$$\left\langle S_{\mathbf{x}\bar{\mathbf{x}}}^{(2)} \right\rangle_{Y-Y_A} := \int [\bar{D}U\bar{D}\bar{U}] W_{Y-Y_A} [U, \bar{U} | U_A, \bar{U}_A] S_{\mathbf{x}\bar{\mathbf{x}}}^{(2)}. \quad (5.31)$$

The weight functional is now a conditional one, obeying the evolution equation [89]

$$\partial_Y W_{Y-Y_A} [U, \bar{U} | U_A, \bar{U}_A] = -H_{\text{evol}} W_{Y-Y_A} [U, \bar{U} | U_A, \bar{U}_A] \quad (5.32)$$

by analogy with Eq. (4.8). The initial condition at Y_A for this differential equation corresponds to the fundamental dipole evolved up to Y_A :

$$W_{Y_A} [U, \bar{U} | U_A, \bar{U}_A] = \delta [U - U_A] \delta [\bar{U} - \bar{U}_A]. \quad (5.33)$$

At any other rapidity Y_B , the condition

$$W_{Y_B} [U, \bar{U} | U_A, \bar{U}_A] = \delta [U - \bar{U}] W_{Y_B} [U | U_A], \quad (5.34)$$

holds, where $W_{Y_B} [U | U_A]$ evolves according to Eq. (4.8), with the initial condition

$$W_{Y_A} [U | U_A] = \delta [U - U_A]. \quad (5.35)$$

Instead of the JIMWLK Hamiltonian that appears in Eq. (4.8), the so-called evolution Hamiltonian in Eq. (5.32) is

$$H_{\text{evol}} := H_{11} + 2H_{12} + H_{22}, \quad (5.36)$$

where

$$H_{11} := -\frac{1}{8\pi^3} \int_{\mathbf{u}\mathbf{v}\mathbf{z}} \mathcal{K}_{\mathbf{u}\mathbf{z}\mathbf{v}} \left(L_{\mathbf{u},n}^a - \tilde{U}_{\mathbf{z},n}^{\dagger ab} R_{\mathbf{u},n}^b \right) \left(L_{\mathbf{v},n}^a - \tilde{U}_{\mathbf{z},n}^{\dagger ac} R_{\mathbf{v},n}^c \right), \quad (5.37)$$

$$H_{12} := -\frac{1}{8\pi^3} \int_{\mathbf{u}\bar{\mathbf{v}}\bar{\mathbf{z}}} \mathcal{K}_{\mathbf{u}\bar{\mathbf{z}}\bar{\mathbf{v}}} \left(L_{\mathbf{u},n}^a - \tilde{U}_{\mathbf{z},n}^{\dagger ab} R_{\mathbf{u},n}^b \right) \left(\bar{L}_{\bar{\mathbf{v}},n}^a - \tilde{U}_{\bar{\mathbf{z}},n}^{\dagger ac} \bar{R}_{\bar{\mathbf{v}},n}^c \right), \quad (5.38)$$

$$H_{22} := -\frac{1}{8\pi^3} \int_{\bar{\mathbf{u}}\bar{\mathbf{v}}\bar{\mathbf{z}}} \mathcal{K}_{\bar{\mathbf{u}}\bar{\mathbf{z}}\bar{\mathbf{v}}} \left(\bar{L}_{\bar{\mathbf{u}},n}^a - \tilde{U}_{\bar{\mathbf{z}},n}^{\dagger ac} \bar{R}_{\bar{\mathbf{u}},n}^b \right) \left(\bar{L}_{\bar{\mathbf{v}},n}^a - \tilde{U}_{\bar{\mathbf{z}},n}^{\dagger ac} \bar{R}_{\bar{\mathbf{v}},n}^c \right). \quad (5.39)$$

Each of these three terms is essentially the JIMWLK Hamiltonian from Eq. (4.37). The only reason for the added complication of having three distinct terms H_{11} , H_{12} and H_{22} in this case is the separation of the DA and the CCA in our current calculation.

Instead of Eq. (5.29), the cross section is now

$$\frac{d\sigma_{qg}}{dY d^2p dY_A d^2k_A} = \frac{1}{16\pi^4} \int_{\mathbf{x}\bar{\mathbf{x}}} e^{-i\mathbf{p}\cdot(\mathbf{x}-\bar{\mathbf{x}})} \left\langle H_{\text{prod}}(\mathbf{k}_A) \left\langle S_{\mathbf{x}\bar{\mathbf{x}},N}^{(2)} \right\rangle_{\nu} \Big|_{\bar{U}_A=U_A} \right\rangle_{Y_A}, \quad (5.40)$$

which differs from Eq. (5.29) in that it contains two averaging procedures [93]. The integrand can be recast in a more enlightening form by using the relevant definitions for the two expectation values. The definition for the inner expectation value given in Eq. (5.31) gives

$$H_{\text{prod}}(\mathbf{k}_A) \left\langle S_{\mathbf{x}\bar{\mathbf{x}},N}^{(2)} \right\rangle_{\nu} \Big|_{\bar{U}_A=U_A} = \int [\bar{D}\bar{U}_A] \delta[\bar{U}_A - U_A] \int [\bar{D}U\bar{D}\bar{U}] \times W_{Y-Y_A}[U, \bar{U} | U_A, \bar{U}_A] H_{\text{prod}}(\mathbf{k}_A) S_{\mathbf{x}\bar{\mathbf{x}},N}^{(2)}, \quad (5.41)$$

where a delta function has been introduced that sets $\bar{U}_A = U_A$. This can be used in place of the test operator $F[U]$ in Eq. (4.2) to do the outer averaging, giving

$$\left\langle H_{\text{prod}}(\mathbf{k}_A) \left\langle S_{\mathbf{x}\bar{\mathbf{x}},N}^{(2)} \right\rangle_{\nu} \Big|_{\bar{U}_A=U_A} \right\rangle_{Y_A} = \int [\bar{D}U_A] W_{Y_A}[U_A] \int [\bar{D}\bar{U}_A] \delta[\bar{U}_A - U_A] \times \int [\bar{D}U\bar{D}\bar{U}] W_{Y-Y_A}[U, \bar{U} | U_A, \bar{U}_A] H_{\text{prod}}(\mathbf{k}_A) S_{\mathbf{x}\bar{\mathbf{x}},N}^{(2)}. \quad (5.42)$$

Just as was done for the equal rapidity case in Section 5.2.1, we act with the production Hamiltonian on the dipole operator. Using Eq. (5.28), this gives

$$H_{\text{prod}}(\mathbf{k}_A) S_{\mathbf{x}\bar{\mathbf{x}},N}^{(2)} = \frac{1}{4\pi^3} \int_{\mathbf{y}\bar{\mathbf{y}}} e^{-i\mathbf{k}_A\cdot(\mathbf{y}-\bar{\mathbf{y}})} \int_{\mathbf{u}\bar{\mathbf{u}}} \mathcal{K}_{\mathbf{y}\mathbf{u}}^i \mathcal{K}_{\bar{\mathbf{y}}\bar{\mathbf{u}}}^i \times \left(L_{\mathbf{u},0}^a - \tilde{U}_{\mathbf{y},0}^{\dagger ab} R_{\mathbf{u},0}^b \right) \left(\bar{L}_{\bar{\mathbf{u}},0}^a - \tilde{\bar{U}}_{\bar{\mathbf{y}},0}^{\dagger ac} \bar{R}_{\bar{\mathbf{u}},0}^c \right) \frac{1}{N_c} \text{tr} \left(U_{\mathbf{x},N} \bar{U}_{\bar{\mathbf{x}},N}^{\dagger} \right) \quad (5.43)$$

$$= \frac{1}{4\pi^3} \int_{\mathbf{y}\bar{\mathbf{y}}} e^{-i\mathbf{k}_A\cdot(\mathbf{y}-\bar{\mathbf{y}})} \int_{\mathbf{u}\bar{\mathbf{u}}} \mathcal{K}_{\mathbf{y}\mathbf{u}}^i \mathcal{K}_{\bar{\mathbf{y}}\bar{\mathbf{u}}}^i \frac{1}{N_c} \mathcal{I}_N, \quad (5.44)$$

where

$$\mathcal{I}_n := \text{tr} \left(L_{\mathbf{u},0}^a U_{\mathbf{x},n} \bar{L}_{\bar{\mathbf{u}},0}^a \bar{U}_{\bar{\mathbf{x}},n}^{\dagger} - \tilde{U}_{\mathbf{y},0}^{\dagger ab} R_{\mathbf{u},0}^b U_{\mathbf{x},n} \bar{L}_{\bar{\mathbf{u}},n}^a \bar{U}_{\bar{\mathbf{x}},n}^{\dagger} - \tilde{\bar{U}}_{\bar{\mathbf{y}},0}^{\dagger ac} L_{\mathbf{u},0}^a U_{\mathbf{x},n} \bar{R}_{\bar{\mathbf{u}},0}^c \bar{U}_{\bar{\mathbf{x}},n}^{\dagger} + \tilde{U}_{\mathbf{y},0}^{\dagger ab} \tilde{\bar{U}}_{\bar{\mathbf{y}},0}^{\dagger ac} R_{\mathbf{u},0}^b U_{\mathbf{x},n} \bar{R}_{\bar{\mathbf{u}},0}^c \bar{U}_{\bar{\mathbf{x}},n}^{\dagger} \right). \quad (5.45)$$

We emphasise that fundamental and antifundamental Wilson lines in \mathcal{I}_n are taken at step n , since these originate from the dipole. On the other hand, the adjoint Wilson lines and all the Lie derivatives in \mathcal{I}_n are taken at the initial condition $n = 0$, since these originate from the production Hamiltonian.

Substituting Eq. (5.44) into Eq. (5.41) allows us to write the final expression for the cross section from Eq. (5.40) as

$$\begin{aligned} \frac{d\sigma_{qg}}{dY d^2p dY_A d^2k_A} &= \frac{1}{4\pi^3} \frac{1}{16\pi^4} \int_{x\bar{x}y\bar{y}u\bar{u}} \mathcal{K}_{y\mathbf{u}}^i \mathcal{K}_{\bar{y}\bar{u}}^i e^{-i\mathbf{p}\cdot(\mathbf{x}-\bar{\mathbf{x}})-i\mathbf{k}_A\cdot(\mathbf{y}-\bar{\mathbf{y}})} \int [\bar{D}U_A] W_{Y_A}[U_A] \\ &\times \int [\bar{D}\bar{U}_A] \delta[\bar{U}_A - U_A] \int [\bar{D}U\bar{D}\bar{U}] W_{Y-Y_A}[U, \bar{U}|U_A, \bar{U}_A] \frac{1}{N_c} \mathcal{I}_N, \end{aligned} \quad (5.46)$$

or more compactly as

$$\frac{d\sigma_{qg}}{dY d^2p dY_A d^2k_A} = \frac{1}{4\pi^3} \frac{1}{16\pi^4} \int_{x\bar{x}y\bar{y}u\bar{u}} \mathcal{K}_{y\mathbf{u}}^i \mathcal{K}_{\bar{y}\bar{u}}^i e^{-i\mathbf{p}\cdot(\mathbf{x}-\bar{\mathbf{x}})-i\mathbf{k}_A\cdot(\mathbf{y}-\bar{\mathbf{y}})} \left\langle \left\langle \frac{1}{N_c} \mathcal{I}_N \right\rangle \right\rangle_{\nu, Y_A}. \quad (5.47)$$

This is the final expression for the double inclusive quark–gluon cross section studied in Paper [II]. All that is left to evaluate is the trace \mathcal{I} at the final rapidity step N . From its definition in Eq. (5.45), we see that each of the four terms in \mathcal{I} contains a product of two factors, each of which is a Lie differentiated Wilson line. The first term in Eq. (5.45), for example, consists of a factor $\bar{L}\bar{U}$ pertaining to the CCA and a second factor LU^\dagger pertaining to the DA. Terms containing a right Lie derivative are accompanied by the relevant adjoint Wilson line, since these terms involve a gluon crossing the target field. In the next section, the Lie differentiated Wilson lines are studied further, since these hold the physics of interest in Eq. (5.47).

5.3 The Bilocal Langevin Equations

The definition of \mathcal{I}_n in Eq. (5.45) contains four factors that need to be evaluated: RU^\dagger , RU , LU^\dagger and LU . Each of these quantities is bilocal in the sense that the Lie derivative and Wilson line of each term are always at different transverse coordinates. By acting with the Lie derivatives on the Langevin equation for the Wilson line as given in Eq. (5.21), it is possible to derive a Langevin equation for the bilocal quantities. This procedure was first outlined in [93], leading to the bilocal Langevin equation for RU^\dagger . From this, the equation for RU follows by taking the Hermitian conjugate of RU^\dagger ; the equations for LU^\dagger and LU follow after using the relation $L_{\mathbf{u},n}^a = \tilde{U}_{\mathbf{u},n}^{\dagger ab} R_{\mathbf{u},n}^b$. Instead of evolving all four factors from $n = 0$ to $n = N$, it is therefore only necessary to evolve one of them and then obtain the other three evolved factors from it.

5.3.1 The RU^\dagger Langevin equation

The bilocal Langevin equation for RU^\dagger was derived in [93] by acting with a right Lie derivative on the Hermitian conjugate of the Langevin equation in Eq. (5.21). By the product rule, this gives three terms

$$R_{\mathbf{u},0}^a U_{\mathbf{x},n+1}^\dagger = \left(R_{\mathbf{u},0}^a e^{i\epsilon g \alpha_{\mathbf{x},n}^R} \right) U_{\mathbf{x},n}^\dagger e^{-i\epsilon g \alpha_{\mathbf{x},n}^L} + e^{i\epsilon g \alpha_{\mathbf{x},n}^R} \left(R_{\mathbf{u},0}^a U_{\mathbf{x},n}^\dagger \right) e^{-i\epsilon g \alpha_{\mathbf{x},n}^L} + e^{i\epsilon g \alpha_{\mathbf{x},n}^R} U_{\mathbf{x},n}^\dagger \left(R_{\mathbf{u},0}^a e^{-i\epsilon g \alpha_{\mathbf{x},n}^L} \right). \quad (5.48)$$

The first term is zero because there is no Wilson line in α^R on which to act with R . The third term can be calculated by expanding the exponential in ϵ , giving

$$R_{\mathbf{u},0}^a e^{-i\epsilon g \alpha_{\mathbf{x},n}^L} = R_{\mathbf{u},0}^a \left[\mathbb{1} - i\epsilon g \alpha_{\mathbf{x},n}^L - \frac{1}{2} \epsilon^2 g^2 (\alpha_{\mathbf{x},n}^L)^2 + \mathcal{O}(\nu \epsilon^2) \right] \quad (5.49)$$

$$= -\frac{i\epsilon g}{\sqrt{4\pi^3}} \int_{\mathbf{z}} \mathcal{K}_{\mathbf{xz}}^i R_{\mathbf{u},0}^a (U_{\mathbf{z},n} \nu_{\mathbf{z},n}^i U_{\mathbf{z},n}^\dagger) + \mathcal{O}(\nu \epsilon^2). \quad (5.50)$$

The order $(\alpha^L)^2$ term has been neglected because

$$\langle (\alpha_{\mathbf{x},n}^L)^2 \rangle = \frac{1}{4\pi^3} \int_{\mathbf{zw}} \langle \left(\mathcal{K}_{\mathbf{xz}}^i \nu_{\mathbf{z},n}^{a,i} \tilde{U}_{\mathbf{z},n}^{\dagger ab} \right) \left(\mathcal{K}_{\mathbf{xw}}^j \nu_{\mathbf{z},n}^{c,j} \tilde{U}_{\mathbf{z},n}^{\dagger cd} \right) \rangle = \frac{C_F}{4\pi^3 \epsilon} \int_{\mathbf{z}} \mathcal{K}_{\mathbf{xz}\mathbf{x}} \quad (5.51)$$

after using Eq. (5.10). Doing the differentiation in Eq. (5.50) gives two terms which can be written as

$$R_{\mathbf{u},0}^a e^{-i\epsilon g \alpha_{\mathbf{x},n}^L} = -\frac{i\epsilon g}{\sqrt{4\pi^3}} \int_{\mathbf{z}} \mathcal{K}_{\mathbf{xz}}^i [U_{\mathbf{z},n} \nu_{\mathbf{z},n}^i U_{\mathbf{z},n}^\dagger, U_{\mathbf{z},n} R_{\mathbf{u},0}^a U_{\mathbf{z},n}^\dagger] + \mathcal{O}(\nu \epsilon^2). \quad (5.52)$$

We have used the trick

$$0 = R_{\mathbf{u},0}^a (\mathbb{1}) = R_{\mathbf{u},0}^a (U_{\mathbf{x},n} U_{\mathbf{x},n}^\dagger) = (R_{\mathbf{u},0}^a U_{\mathbf{x},n}) U_{\mathbf{x},n}^\dagger + U_{\mathbf{x},n} (R_{\mathbf{u},0}^a U_{\mathbf{x},n}^\dagger) \quad (5.53)$$

$$\implies R_{\mathbf{u},0}^a U_{\mathbf{x},n} = -U_{\mathbf{x},n} (R_{\mathbf{u},0}^a U_{\mathbf{x},n}^\dagger) U_{\mathbf{x},n} \quad (5.54)$$

to write the two terms from the differentiation in Eq. (5.50) as a commutator.

Putting all the pieces together, the bilocal Langevin equation that follows from Eq. (5.48) is

$$R_{\mathbf{u},0}^a U_{\mathbf{x},n+1}^\dagger = e^{i\epsilon g \alpha_{\mathbf{x},n}^R} R_{\mathbf{u},0}^a U_{\mathbf{x},n}^\dagger e^{-i\epsilon g \alpha_{\mathbf{x},n}^L} - \frac{i\epsilon g}{\sqrt{4\pi^3}} e^{i\epsilon g \alpha_{\mathbf{x},n}^R} U_{\mathbf{x},n}^\dagger \int_{\mathbf{z}} \mathcal{K}_{\mathbf{xz}}^i [U_{\mathbf{z},n} \nu_{\mathbf{z},n}^i U_{\mathbf{z},n}^\dagger, U_{\mathbf{z},n} R_{\mathbf{u},0}^a U_{\mathbf{z},n}^\dagger] + \mathcal{O}(\nu \epsilon^2). \quad (5.55)$$

For consistency, the remaining three exponentials in this expression can be expanded in ϵ to give

$$R_{\mathbf{u},0}^a U_{x,n+1}^\dagger = R_{\mathbf{u},0}^a U_{x,n}^\dagger + \int_z \left(\frac{i\epsilon g}{\sqrt{4\pi^3}} \mathcal{K}_{xz}^i \nu_{z,n}^{i,b} - \frac{\epsilon g^2}{4\pi^3} \mathcal{K}_{xzx} t^b \right) [t^b R_{\mathbf{u},0}^a U_{x,n}^\dagger - R_{\mathbf{u},0}^a U_{x,n}^\dagger \tilde{U}_{z,n}^{\dagger bc} t^c - U_{x,n}^\dagger U_{z,n} (t^b R_{\mathbf{u},0}^a U_{z,n}^\dagger - R_{\mathbf{u},0}^a U_{z,n}^\dagger \tilde{U}_{z,n}^{\dagger bc} t^c)] + \mathcal{O}(\nu\epsilon^2). \quad (5.56)$$

The initial condition

$$R_{\mathbf{u},0}^a U_{x,0}^\dagger = ig\delta_{ux} U_{x,0}^\dagger t^a \quad (5.57)$$

can be read off from Eq. (4.25).

In order to understand the physical meaning of Eq. (5.56), it is useful to express it in terms of diagrams. If the initial condition is represented as

$$U_{x,0}^\dagger = \begin{array}{c} \text{---} \xrightarrow{\text{green arrow}} \text{---} \\ | \\ \text{---} \end{array}, \quad (5.58)$$

then one step in rapidity gives

$$R_{\mathbf{u},0}^a U_{x,1}^\dagger = ig \begin{array}{c} \text{---} \xrightarrow{\text{green arrow}} \text{---} \\ | \\ \text{---} \end{array} + ig \frac{i\epsilon g}{\sqrt{4\pi^3}} \int_z \mathcal{K}_{xz}^i \nu_{z,0}^{i,b} \{I\} - ig \frac{\epsilon g^2}{4\pi^3} \int_z \mathcal{K}_{xzx} \{II\} + \mathcal{O}(\nu\epsilon^2), \quad (5.59)$$

where

$$\{I\} := \begin{array}{c} \text{---} \xrightarrow{\text{green arrow}} \text{---} \\ | \\ \text{---} \end{array} - \begin{array}{c} \text{---} \xrightarrow{\text{green arrow}} \text{---} \\ | \\ \text{---} \end{array} + \begin{array}{c} \text{---} \xrightarrow{\text{green arrow}} \text{---} \\ | \\ \text{---} \end{array}, \quad (5.60)$$

$$\{II\} := \text{[Diagram 1]} - \text{[Diagram 2]} + \text{[Diagram 3]} \quad (5.61)$$

When compared to Eq. (5.19), we can see that Eq. (5.59) is just the evolution equation for the Wilson line, but with an additional gluon added in all possible ways after the target interaction. The Lie derivative $R_{\mathbf{u},0}^a$ assigns transverse coordinate \mathbf{u} to either \mathbf{x} or \mathbf{z} and colour index a to the additional gluon.

The evolution equations for RU , LU and LU^\dagger contain similar diagrams, with the additional gluon on the relevant side of the target interaction and the relevant direction arrowhead representing the Wilson line. In particular, notice that the third diagram in Eq. (5.60) already begins to resemble part of one half of a BFKL ladder diagram of the kind

$$\text{[Diagram 5.62]} \quad (5.62)$$

that was discussed in Section 3.2.2. In order to see this more clearly, however, it is necessary to go to the dilute limit, as is done in Chapter 6.

5.3.2 Alternative form

One addition that Paper [II] makes to the work of [93] is that the bilocal Langevin equations are written in a way that is more conducive to numerical computations. We define a new bilocal quantity $R_{\mathbf{u}\mathbf{x},n}^a := U_{\mathbf{x},n} (R_{\mathbf{u},0}^a U_{\mathbf{x},n}^\dagger)$, which is conveniently a member of the Lie algebra $\mathfrak{su}(N_c)$. Its Langevin equation can be obtained from Eq. (5.55), with Eq. (5.21) multiplied from the left. This results in the cancellation

of the right-field exponentials α^R , giving

$$R_{\mathbf{u}\mathbf{x},n+1}^a = e^{i\epsilon g \alpha_{\mathbf{x},n}^L} R_{\mathbf{u}\mathbf{x},n}^a e^{-i\epsilon g \alpha_{\mathbf{x},n}^L} - \frac{i\epsilon g}{\sqrt{4\pi^3}} e^{i\epsilon g \alpha_{\mathbf{x},n}^L} \int_{\mathbf{z}} \mathcal{K}_{\mathbf{x}\mathbf{z}}^i [\tilde{\nu}_{\mathbf{z},n}^i, R_{\mathbf{u}\mathbf{z},n}^a], \quad (5.63)$$

with the rotated noise $\tilde{\nu}$ defined in Eq. (5.24). The advantage of this expression over Eq. (5.55) is that it is a linear evolution equation for a single quantity $R_{\mathbf{u}\mathbf{x},n}^a$ that contains no explicit Wilson lines and only one type of colour field α^L . Expanded in ϵ , Eq. (5.63) becomes

$$R_{\mathbf{u}\mathbf{x},n+1}^a = R_{\mathbf{u}\mathbf{x},n}^a + \int_{\mathbf{z}} \frac{i\epsilon g}{\sqrt{4\pi^3}} \mathcal{K}_{\mathbf{x}\mathbf{z}}^i [\tilde{\nu}_{\mathbf{z},n}^i, R_{\mathbf{u}\mathbf{x},n}^a - R_{\mathbf{u}\mathbf{z},n}^a] - \frac{N_c}{2} \frac{\epsilon g^2}{4\pi^3} \int_{\mathbf{z}} \mathcal{K}_{\mathbf{x}\mathbf{z}\mathbf{x}} (R_{\mathbf{u}\mathbf{x},n}^a - R_{\mathbf{u}\mathbf{z},n}^a) + \mathcal{O}(\nu\epsilon^2). \quad (5.64)$$

Its initial condition follows from Eq. (5.57), namely $R_{\mathbf{u}\mathbf{x},0}^a = ig\delta_{\mathbf{u}\mathbf{x}}t^a$. Note that it is not possible to simplify Eq. (5.64) further by pulling out an overall R because of the commutator in the second term on the right.

Similarly to $R_{\mathbf{u}\mathbf{x},n}^a$, it is possible to define three other quantities

$$R_{\mathbf{u},0}^a U_{\mathbf{x},n} \rightarrow \tilde{R}_{\mathbf{u}\mathbf{x},n}^a := (R_{\mathbf{u},0}^a U_{\mathbf{x},n}) U_{\mathbf{x},n}^\dagger, \quad (5.65)$$

$$L_{\mathbf{u},0}^a U_{\mathbf{x},n}^\dagger \rightarrow L_{\mathbf{u}\mathbf{x},n}^a := U_{\mathbf{x},n} (L_{\mathbf{u},0}^a U_{\mathbf{x},n}^\dagger), \quad (5.66)$$

$$L_{\mathbf{u},0}^a U_{\mathbf{x},n} \rightarrow \tilde{L}_{\mathbf{u}\mathbf{x},n}^a := (L_{\mathbf{u},0}^a U_{\mathbf{x},n}) U_{\mathbf{x},n}^\dagger. \quad (5.67)$$

Their evolution equations can be derived in a similar manner to Eq. (5.63) or they can be obtained directly from Eq. (5.63). They are

$$\tilde{R}_{\mathbf{u}\mathbf{x},n+1}^a = e^{i\epsilon g \alpha_{\mathbf{x},n}^L} \tilde{R}_{\mathbf{u}\mathbf{x},n}^a e^{-i\epsilon g \alpha_{\mathbf{x},n}^L} - \frac{i\epsilon g}{\sqrt{4\pi^3}} \int_{\mathbf{z}} \mathcal{K}_{\mathbf{x}\mathbf{z}}^i [\tilde{\nu}_{\mathbf{z},n}^i, \tilde{R}_{\mathbf{u}\mathbf{z},n}^a] e^{-i\epsilon g \alpha_{\mathbf{x},n}^L}, \quad (5.68)$$

$$L_{\mathbf{u}\mathbf{x},n+1}^a = e^{i\epsilon g \alpha_{\mathbf{x},n}^L} L_{\mathbf{u}\mathbf{x},n}^a e^{-i\epsilon g \alpha_{\mathbf{x},n}^L} - \frac{i\epsilon g}{\sqrt{4\pi^3}} e^{i\epsilon g \alpha_{\mathbf{x},n}^L} \int_{\mathbf{z}} \mathcal{K}_{\mathbf{x}\mathbf{z}}^i [\tilde{\nu}_{\mathbf{z},n}^i, L_{\mathbf{u}\mathbf{z},n}^a], \quad (5.69)$$

$$\tilde{L}_{\mathbf{u}\mathbf{x},n+1}^a = e^{i\epsilon g \alpha_{\mathbf{x},n}^L} \tilde{L}_{\mathbf{u}\mathbf{x},n}^a e^{-i\epsilon g \alpha_{\mathbf{x},n}^L} - \frac{i\epsilon g}{\sqrt{4\pi^3}} \int_{\mathbf{z}} \mathcal{K}_{\mathbf{x}\mathbf{z}}^i [\tilde{\nu}_{\mathbf{z},n}^i, \tilde{L}_{\mathbf{u}\mathbf{z},n}^a] e^{-i\epsilon g \alpha_{\mathbf{x},n}^L}. \quad (5.70)$$

When expanded in ϵ , these reduce to the same form as Eq. (5.64):

$$\tilde{R}_{\mathbf{u}\mathbf{x},n+1}^a = \tilde{R}_{\mathbf{u}\mathbf{x},n}^a + \int_{\mathbf{z}} \frac{i\epsilon g}{\sqrt{4\pi^3}} \mathcal{K}_{\mathbf{x}\mathbf{z}}^i [\tilde{\nu}_{\mathbf{z},n}^i, \tilde{R}_{\mathbf{u}\mathbf{x},n}^a - \tilde{R}_{\mathbf{u}\mathbf{z},n}^a] - \frac{N_c}{2} \frac{\epsilon g^2}{4\pi^3} \int_{\mathbf{z}} \mathcal{K}_{\mathbf{x}\mathbf{z}\mathbf{x}} (\tilde{R}_{\mathbf{u}\mathbf{x},n}^a - \tilde{R}_{\mathbf{u}\mathbf{z},n}^a) + \mathcal{O}(\nu\epsilon^2), \quad (5.71)$$

$$L_{\mathbf{u}\mathbf{x},n+1}^a = L_{\mathbf{u}\mathbf{x},n}^a + \frac{i\epsilon g}{\sqrt{4\pi^3}} \int_{\mathbf{z}} \mathcal{K}_{\mathbf{xz}}^i [\tilde{\nu}_{\mathbf{z},n}^i, L_{\mathbf{u}\mathbf{x},n}^a - L_{\mathbf{u}\mathbf{z},n}^a] - \frac{N_c}{2} \frac{\epsilon g^2}{4\pi^3} \int_{\mathbf{z}} \mathcal{K}_{\mathbf{xz}\mathbf{x}} (L_{\mathbf{u}\mathbf{x},n}^a - L_{\mathbf{u}\mathbf{z},n}^a) + \mathcal{O}(\nu\epsilon^2), \quad (5.72)$$

$$\tilde{L}_{\mathbf{u}\mathbf{x},n+1}^a = \tilde{L}_{\mathbf{u}\mathbf{x},n}^a + \frac{i\epsilon g}{\sqrt{4\pi^3}} \int_{\mathbf{z}} \mathcal{K}_{\mathbf{xz}}^i [\tilde{\nu}_{\mathbf{z},n}^i, \tilde{L}_{\mathbf{u}\mathbf{x},n}^a - \tilde{L}_{\mathbf{u}\mathbf{z},n}^a] - \frac{N_c}{2} \frac{\epsilon g^2}{4\pi^3} \int_{\mathbf{z}} \mathcal{K}_{\mathbf{xz}\mathbf{x}} (\tilde{L}_{\mathbf{u}\mathbf{x},n}^a - \tilde{L}_{\mathbf{u}\mathbf{z},n}^a) + \mathcal{O}(\nu\epsilon^2). \quad (5.73)$$

The initial conditions follow from Eqs. (4.22), (4.23) and (4.24):

$$\tilde{R}_{\mathbf{u}\mathbf{x},0}^a = ig\delta_{\mathbf{u}\mathbf{x}} t^a, \quad (5.74)$$

$$L_{\mathbf{u}\mathbf{x},0}^a = ig\delta_{\mathbf{u}\mathbf{x}} \tilde{U}_{\mathbf{x},0}^{\dagger ab} t^b, \quad (5.75)$$

$$\tilde{L}_{\mathbf{u}\mathbf{x},0}^a = ig\delta_{\mathbf{u}\mathbf{x}} \tilde{U}_{\mathbf{x},0}^{\dagger ab} t^b. \quad (5.76)$$

The trace that enters the cross section in Eq. (5.47) can be rewritten in terms of the newly defined bilocal quantities. By inserting $\mathbb{1} = U_{\mathbf{x},n}^\dagger U_{\mathbf{x},n} \bar{U}_{\bar{\mathbf{x}},n}^\dagger \bar{U}_{\bar{\mathbf{x}},n}$ into each term in Eq. (5.45), we get

$$R_{\mathbf{u},0}^a U_{\mathbf{x},n} \rightarrow \tilde{R}_{\mathbf{u}\mathbf{x},n}^a := (R_{\mathbf{u},0}^a U_{\mathbf{x},n}) U_{\mathbf{x},n}^\dagger, \quad (5.77)$$

$$L_{\mathbf{u},0}^a U_{\mathbf{x},n}^\dagger \rightarrow L_{\mathbf{u}\mathbf{x},n}^a := U_{\mathbf{x},n} (L_{\mathbf{u},0}^a U_{\mathbf{x},n}^\dagger), \quad (5.78)$$

$$L_{\mathbf{u},0}^a U_{\mathbf{x},n} \rightarrow \tilde{L}_{\mathbf{u}\mathbf{x},n}^a := (L_{\mathbf{u},0}^a U_{\mathbf{x},n}) U_{\mathbf{x},n}^\dagger. \quad (5.79)$$

and \mathcal{I}_n becomes

$$\mathcal{I}_n := \text{tr} \left(\tilde{L}_{\mathbf{u}\mathbf{x},n}^a U_{\mathbf{x},n} \bar{U}_{\bar{\mathbf{x}},n}^\dagger \bar{L}_{\bar{\mathbf{u}}\bar{\mathbf{x}},n}^a - \tilde{U}_{\mathbf{y},0}^{\dagger ab} \tilde{R}_{\mathbf{u}\mathbf{x},n}^b U_{\mathbf{x},n} \bar{U}_{\bar{\mathbf{x}},n}^\dagger \bar{L}_{\bar{\mathbf{u}}\bar{\mathbf{x}},n}^a - \tilde{U}_{\bar{\mathbf{y}},0}^{\dagger ac} \tilde{L}_{\mathbf{u}\mathbf{x},n}^a U_{\mathbf{x},n} \bar{U}_{\bar{\mathbf{x}},n}^\dagger \bar{R}_{\bar{\mathbf{u}}\bar{\mathbf{x}},n}^c + \tilde{U}_{\mathbf{y},0}^{\dagger ab} \tilde{U}_{\bar{\mathbf{y}},0}^{\dagger ac} \tilde{R}_{\mathbf{u}\mathbf{x},n}^b U_{\mathbf{x},n} \bar{U}_{\bar{\mathbf{x}},n}^\dagger \bar{R}_{\bar{\mathbf{u}}\bar{\mathbf{x}},n}^c \right). \quad (5.80)$$

From this, we see that two evolution equations need to be solved numerically in order to completely determine \mathcal{I}_N . One is for the Wilson lines $\bar{U}_{\bar{\mathbf{x}},n}$ and $U_{\mathbf{x},n}^\dagger$ and the other is for the bilocal quantities $\tilde{L}_{\mathbf{u}\mathbf{x},n}^a$, etc. This information is sufficient to obtain everything else that appears in \mathcal{I}_N and therefore the cross section in Eq. (5.47).

Chapter summary

In this chapter, we have studied the JIMWLK equation in Langevin form. Inclusive particle production has been considered as a concrete context. We have seen that it is necessary to keep the DA and the CCA separate up until the end of evolution. In the specific case of quark–gluon production, Lie derivatives of Wilson lines enter the cross section. Starting from the Langevin equation for Wilson lines, we have shown how to derive a bilocal Langevin equation; that is, an evolution equation for a Lie differentiated Wilson line. We have recast this bilocal evolution equation in a form that makes it simpler to solve numerically. Both the Langevin equation for the Wilson line and the bilocal Langevin equation have been expressed in diagrams, making their physical interpretation easier. This becomes particularly useful in the dilute limit in the next chapter, when we wish to extract BFKL ladder diagrams from within the stochastic picture of evolution.

6

JIMWLK in the Dilute Limit

In Chapter 4, the JIMWLK equation was discussed in the Fokker–Planck formalism. In Chapter 5, an alternative formalism was discussed in which evolution was interpreted as a stochastic dissipation through colour space. The purpose of this chapter is to link those two pictures by expanding the Langevin equations from Chapter 5 in the dilute limit. Physically, it is expected that the dilute limit reduces JIMWLK evolution to BFKL evolution. In a dilute target field, the overlapping partonic wave functions that lead to saturation are not present. The nonlinearity of the BK and JIMWLK equations is then removed and what remains is the BFKL equation. In Section 4.5, we already saw how the BFKL equation arises from the JIMWLK equation in the Fokker–Planck picture. By rederiving the BFKL equation in the Langevin picture, we can better understand how the two formalisms are related.

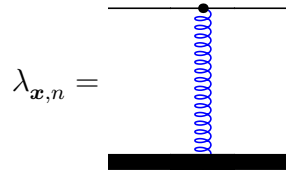
The chapter is divided into two sections. In Section 6.1, the Langevin equation for the Wilson line from Section 5.1 is studied in the dilute limit. We discuss some properties of the dilute equation, including a formal solution and its Reggeisation. The BFKL equation for the unintegrated gluon distribution is also derived. In Section 6.2, we study the cross section for double inclusive quark–gluon production at unequal rapidities from Section 5.2.2. We also expand the bilocal Langevin equations from Section 5.3 in the dilute limit and see how BFKL ladder diagrams emerge. Paper [II] covers much of the same material, but we provide some additional explanations here that were omitted there.

6.1 The Langevin equation in the dilute limit

In the dilute limit, the target is considered as a dilute field, as opposed to the highly dense gluonic medium of the previous chapters. Instead of the Wilson lines that have appeared thus far, we use expanded versions in terms of elements of the Lie algebra $\mathfrak{su}(N_c)$. For the antifundamental Wilson line, we write

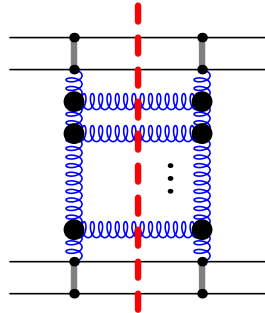
$$U_{\mathbf{x},n}^\dagger =: e^{i\lambda_{\mathbf{x},n}} = \mathbb{1} + i\lambda_{\mathbf{x},n} + \mathcal{O}(\lambda^2), \quad (6.1)$$

where $\lambda \in \mathfrak{su}(N_c)$ is a real matrix that can be expanded in the group generators as $\lambda_{\mathbf{x},n} = \lambda_{\mathbf{x},n}^a t^a$. (Recall from the previous chapter that rapidity has been discretised into N pieces of size ϵ and that n is the rapidity step index). Physically, λ corresponds to a single t -channel gluon exchanged between the target and projectile:



The diagram shows a vertical blue wavy line representing a gluon exchange between a horizontal black line at the top (target) and a horizontal black line at the bottom (projectile). The label $\lambda_{\mathbf{x},n} =$ is to the left of the wavy line, and the equation number (6.2) is to the right.

Since we wish to ultimately reproduce a BFKL ladder diagram of the form



The diagram shows a vertical red dashed line representing a target, and a vertical blue wavy line representing a projectile. They are connected by a ladder of horizontal black lines representing Wilson lines. The ladder consists of four horizontal lines, with a vertical ellipsis in the middle indicating more lines. The label (6.3) is to the right of the diagram.

from Section 3.2.2, it is sufficient to work to order λ at each step n and for each distinct transverse coordinate.

By the unitarity of the Wilson lines, the transpose $\lambda_{\mathbf{x},n}^\top = \lambda_{\mathbf{x},n}$, so that the Hermitian conjugate of Eq. (6.1) is

$$U_{\mathbf{x},n} = e^{-i\lambda_{\mathbf{x},n}} = \mathbb{1} - i\lambda_{\mathbf{x},n} + \mathcal{O}(\lambda^2). \quad (6.4)$$

For the adjoint representation, the expansion of the group identity $\tilde{U}_{\mathbf{x},n}^{\dagger ab} t^b = U_{\mathbf{x},n} t^a U_{\mathbf{x},n}^\dagger$ leads to

$$\tilde{U}_{\mathbf{x},n}^{\dagger ab} = \delta^{ab} + f^{abc} \lambda_{\mathbf{x},n}^c + \mathcal{O}(\lambda^2), \quad (6.5)$$

after multiplying from the right by t^a and taking the trace. Alternatively, we can expand $\tilde{U}_{x,n}^{\dagger ab} = 2\text{tr}(t^a U_{x,n}^\dagger t^b U_{x,n})$ to get the same expression. Diagrammatically, the expansion of an adjoint Wilson line at the initial condition looks similar to the expansion of a fundamental or antifundamental Wilson line:

$$U_{x,0} = \begin{array}{c} \text{---} \\ | \text{---} \\ \text{---} \end{array} = \begin{array}{c} \text{---} \\ | \text{---} \\ \text{---} \end{array} - i \begin{array}{c} \text{---} \\ | \text{---} \\ \text{---} \end{array} + \mathcal{O}(\lambda^2), \quad (6.6)$$

$$\tilde{U}_{x,0}^{\dagger ab} = \begin{array}{c} \text{---} \\ | \text{---} \\ \text{---} \end{array} = \begin{array}{c} \text{---} \\ | \text{---} \\ \text{---} \end{array} + \begin{array}{c} \text{---} \\ | \text{---} \\ \text{---} \end{array} + \mathcal{O}(\lambda^2). \quad (6.7)$$

Equipped with Eqs. (6.1), (6.4) and (6.5), it is possible to find the dilute limit of any expression from Chapter 5. The Langevin equation for the Wilson line expanded in rapidity step size ϵ was given in Eq. (5.15), namely

$$U_{x,n+1} = U_{x,n} + \int_{\mathbf{z}} \left(U_{x,n} t^a - \tilde{U}_{z,n}^{\dagger ab} t^b U_{x,n} \right) \left(-\frac{i\epsilon g}{\sqrt{4\pi^3}} \mathcal{K}_{\mathbf{xz}}^i \nu_{z,n}^{a,i} - \frac{\epsilon g^2}{4\pi^3} \mathcal{K}_{\mathbf{xz}} t^a \right) + \mathcal{O}(\nu\epsilon^2). \quad (6.8)$$

The expansion to first order in λ of each Wilson line in this expression leads to the Langevin equation for λ :

$$\lambda_{x,n+1} = \lambda_{x,n} + \int_{\mathbf{z}} \left(\frac{i\epsilon g}{\sqrt{4\pi^3}} \mathcal{K}_{\mathbf{xz}}^i \nu_{z,n}^{i,a} - \frac{\epsilon g^2}{4\pi^3} \mathcal{K}_{\mathbf{xz}} t^a \right) i f^{abc} t^c (\lambda_{x,n}^b - \lambda_{z,n}^b) + \mathcal{O}(\nu\epsilon^2, \lambda^2). \quad (6.9)$$

After one evolution step, the diagrams that appear in this expression are

$$\begin{aligned}
 \lambda_{x,1} = & \text{Diagram } x + \frac{i\epsilon g}{\sqrt{4\pi^3}} \int_z \mathcal{K}_{xz}^i \nu_{z,0}^{i,a} i \left(\text{Diagram } x - \text{Diagram } z \right) \\
 & - \frac{\epsilon g^2}{4\pi^3} \int_z \mathcal{K}_{xzx} \left(\text{Diagram } x - \text{Diagram } z \right) + \mathcal{O}(\nu\epsilon^2, \lambda^2). \quad (6.10)
 \end{aligned}$$

In the terms containing $\nu_{z,0}^{i,a}$, the three-gluon vertices can also be drawn as separate gluons by writing

$$i f^{abc} t^c \lambda_0^b = [t^a, \lambda_0] \quad (6.11)$$

$$\begin{aligned}
 i \text{Diagram } x & = \text{Diagram } x_1 - \text{Diagram } x_2. \quad (6.12)
 \end{aligned}$$

Similarly, the terms proportional to the kernel \mathcal{K}_{xzx} can be written separately as

$$t^a i f^{abc} t^c \lambda_0^b = C_F \lambda_0 - t^a \lambda_0 t^a \quad (6.13)$$

$$\begin{aligned}
 i \text{Diagram } x & = \text{Diagram } x_1 - \text{Diagram } x_2. \quad (6.14)
 \end{aligned}$$

Eq. (6.9) is the main topic of Section IV in Paper [II], which goes on to discuss its analytical solution, the so-called Reggeisation of λ and how to obtain the BFKL equation by effectively squaring Eq. (6.9). Each of these points is addressed next.

6.1.1 Analytical solution

Formally, the evolution equation for λ can be solved analytically, since it is a linear iterative equation. By writing Eq. (6.9) as

$$\begin{aligned} & \lambda_{\mathbf{x},n+1}^a t^a \\ &= \int_{\mathbf{w}} \left[\delta_{\mathbf{w}\mathbf{x}} t^d \delta^{de} + \int_{\mathbf{z}} \left(\frac{i\epsilon g}{\sqrt{4\pi^3}} \mathcal{K}_{\mathbf{xz}}^i \nu_{\mathbf{z},n}^{i,a} - \frac{\epsilon g^2}{4\pi^3} \mathcal{K}_{\mathbf{xz}\mathbf{x}} t^a \right) i f^{abc} t^c (\delta_{\mathbf{w}\mathbf{x}} - \delta_{\mathbf{w}\mathbf{z}}) \delta^{be} \right] \lambda_{\mathbf{w},n}^e \\ & \quad + \mathcal{O}(\nu\epsilon^2, \lambda^2), \end{aligned} \quad (6.15)$$

multiplying from the right by t^g and taking the trace gives

$$\lambda_{\mathbf{x},n+1}^a = \int_{\mathbf{w}} \mathcal{M}_{\mathbf{xw},n}^{ab} \lambda_{\mathbf{w},n}^b + \mathcal{O}(\nu\epsilon^2, \lambda^2), \quad (6.16)$$

where the evolution matrix

$$\mathcal{M}_{\mathbf{xw},n}^{ab} := \delta_{\mathbf{xw}} \delta^{ab} + \int_{\mathbf{z}} \left(\frac{\epsilon g}{\sqrt{4\pi^3}} \mathcal{K}_{\mathbf{xz}}^i \nu_{\mathbf{z},n}^{i,c} f^{abc} - \frac{\epsilon g^2}{4\pi^3} \frac{N_c}{2} \mathcal{K}_{\mathbf{xz}\mathbf{x}} \delta^{ab} \right) (\delta_{\mathbf{xw}} - \delta_{\mathbf{zw}}) \quad (6.17)$$

has been defined. By writing the first few terms of Eq. (6.16) explicitly, it is straightforward to obtain the formal solution

$$\lambda_{\mathbf{w}_{n+1},n+1}^{b_{n+1}} = \left(\prod_{j=0}^n \int_{\mathbf{w}_j} \mathcal{M}_{\mathbf{w}_{j+1}\mathbf{w}_j,j}^{b_{j+1}b_j} \right) \lambda_{\mathbf{w}_0,0}^{b_0}. \quad (6.18)$$

The product of evolution matrices can be simplified further if necessary, using the constraints on the noise given in Eq. (5.25). For example, after two evolution steps this is

$$\lambda_{\mathbf{x},2}^a = \int_{\mathbf{w}_1} \mathcal{M}_{\mathbf{xw}_1,1}^{ab_1} \int_{\mathbf{w}_0} \mathcal{M}_{\mathbf{w}_1\mathbf{w}_0,0}^{b_1b_0} \lambda_{\mathbf{w}_0,0}^{b_0}. \quad (6.19)$$

This contains a factor ν from each \mathcal{M} , which leads to something of the form $\langle \nu_{\mathbf{z}_1,1}^{i_1,c_1} \nu_{\mathbf{z}_0,1}^{i_0,c_0} \rangle = \delta^{i_1 i_0} \delta^{c_1 c_0} \delta_{\mathbf{z}_1 \mathbf{z}_0} / \epsilon$ after taking the expectation value.

6.1.2 Reggeisation of λ

An interesting property of λ relates to the old formalism of Regge theory that was mentioned in Section 3.2.1. After taking the expectation value of the Langevin equation for λ given in Eq. (6.9) and using

$$\frac{1}{\epsilon} \langle \lambda_{\mathbf{x},n+1} - \lambda_{\mathbf{x},n} \rangle \xrightarrow{\epsilon \rightarrow \infty} \partial_Y \lambda_{\mathbf{x}}, \quad (6.20)$$

we get

$$\langle \partial_Y \lambda_{\mathbf{x}} \rangle = \frac{N_c \alpha_s}{2 \pi^2} \int_{\mathbf{z}} \mathcal{K}_{\mathbf{xz}\mathbf{x}} \langle \lambda_{\mathbf{z}} - \lambda_{\mathbf{x}} \rangle + \mathcal{O}(\epsilon^2, \lambda^2). \quad (6.21)$$

The term linear in ν has already been set to zero according to Eq. (5.25). After Fourier transforming the components using

$$\lambda^a(\mathbf{p}) = \int_{\mathbf{z}} e^{i\mathbf{p}\cdot\mathbf{z}} \lambda_{\mathbf{z}}^a, \quad (6.22)$$

this becomes

$$\langle \partial_Y \lambda^a(\mathbf{p}) \rangle = \langle \alpha_g(\mathbf{p}) \lambda^a(\mathbf{p}) \rangle + \mathcal{O}(\epsilon^2, \lambda^2), \quad (6.23)$$

where

$$\alpha_g(\mathbf{p}) := \frac{N_c \alpha_s}{2 \pi^2} \int_{\mathbf{z}} \frac{1}{z^2} (e^{i\mathbf{p}\cdot\mathbf{z}} - 1) \quad (6.24)$$

is related to the gluon Regge trajectory ω_g defined in Section 3.2.2. The significance of α_g is that it governs the power-law behaviour of the scattering amplitude in terms of the centre-of-mass energy s , i.e. the scattering amplitude is proportional to s^{α_g} . The gluon corresponding to λ is said to have reggeised. This means that its propagator may be replaced by a gluon propagator dressed with all virtual corrections to leading order in $\ln(1/x)$, as discussed in Section 3.2.2. The reader is referred to [95] for more about reggeised gluons in the context of JIMWLK and related evolution equations.

6.1.3 The BFKL equation for the unintegrated gluon distribution

One of the goals of studying the Langevin evolution of Wilson lines in the dilute limit is to relate it to the BFKL physics that emerges from the Fokker–Planck description of JIMWLK evolution. In Section 3.2.2, we discussed the formation of BFKL ladder diagrams. Motivated by the dipole operator

$$S_{\mathbf{x}\bar{\mathbf{x}}}^{(2)} := \frac{1}{N_c} \text{tr} \left(U_{\mathbf{x}} \bar{U}_{\bar{\mathbf{x}}}^\dagger \right) = \frac{1}{N_c} \text{tr} \left(\begin{array}{c} \left(\bar{\mathbf{x}} \text{---} \leftarrow \text{---} \rightarrow \mathbf{x} \right) \\ \left| \begin{array}{c} \text{blue bar} \\ \text{red dashed bar} \\ \text{blue bar} \end{array} \right. \\ \text{---} \end{array} \right), \quad (6.25)$$

for the transverse momentum integrals. In writing Eq. (6.30), it is not necessary to transform \mathbf{x} and $\bar{\mathbf{x}}$ separately because $\phi_{\mathbf{x}\bar{\mathbf{x}}}$ is a function of the relative length $|\mathbf{x} - \bar{\mathbf{x}}|$. In order to Fourier transform the kernels present in Eq. (6.29), we first transform each Weizsäcker-Williams kernel as

$$\mathcal{K}^i(\mathbf{p}) = \int_{\mathbf{u}-\mathbf{v}} e^{i\mathbf{p}\cdot(\mathbf{u}-\mathbf{v})} \frac{(u-v)^i}{(\mathbf{u}-\mathbf{v})^2}. \quad (6.32)$$

(Recall that $\mathcal{K}_{uvv} := \mathcal{K}_{uw}^i \mathcal{K}_{wv}^i$ - cf. Eqs. (3.45) and (3.46)). Then

$$\mathcal{K}^i(\mathbf{p}) = 2\pi i \frac{p^i}{\mathbf{p}^2} \quad \Longrightarrow \quad \mathcal{K}_{uv}^i = 2\pi i \int_{\mathbf{p}} e^{-i\mathbf{p}\cdot(\mathbf{u}-\mathbf{v})} \frac{p^i}{\mathbf{p}^2}. \quad (6.33)$$

After some algebra, Eqs. (6.30) and (6.33) in Eq. (6.29) gives

$$\begin{aligned} & \frac{1}{\epsilon} [\phi^{n+1}(\mathbf{q}) - \phi^n(\mathbf{q})] \\ &= 4N_c \alpha_s \int_{\mathbf{p}} \left[\frac{\mathbf{p}^2}{(\mathbf{q}-\mathbf{p})^2 \mathbf{q}^2} \phi^n(\mathbf{p}) - \frac{(\mathbf{q}-\mathbf{p}) \cdot \mathbf{q}}{\mathbf{p}^2 (\mathbf{q}-\mathbf{p})^2} \phi^n(\mathbf{q}) \right] + \mathcal{O}(\nu\epsilon^2, \phi^{3/2}). \end{aligned} \quad (6.34)$$

In order to get this into the standard textbook form, the left side is written as $\partial_Y \phi(\mathbf{q})$ when $\epsilon \rightarrow 0$, we define $\tilde{\phi}(\mathbf{q}) := \mathbf{q}^2 \phi(\mathbf{q})$ and manipulate the second term by writing

$$\int_{\mathbf{p}} \frac{(\mathbf{q}-\mathbf{p}) \cdot \mathbf{q}}{\mathbf{p}^2 (\mathbf{q}-\mathbf{p})^2} = \int_{\mathbf{p}} \frac{(\mathbf{q}-\mathbf{p}) \cdot (\mathbf{q}-\mathbf{p}+\mathbf{q})}{\mathbf{p}^2 (\mathbf{q}-\mathbf{p})^2} = \frac{1}{2} \int_{\mathbf{p}} \frac{\mathbf{q}^2}{(\mathbf{q}-\mathbf{p})^2 \mathbf{p}^2}. \quad (6.35)$$

Eq. (6.34) then becomes

$$\partial_Y \tilde{\phi}(\mathbf{q}) = 4N_c \alpha_s \int_{\mathbf{p}} \frac{1}{(\mathbf{q}-\mathbf{p})^2} \left[\tilde{\phi}(\mathbf{p}) - \frac{1}{2} \frac{\mathbf{q}^2}{\mathbf{p}^2} \tilde{\phi}(\mathbf{q}) \right] + \mathcal{O}(\nu\epsilon^2, \phi^{3/2}). \quad (6.36)$$

This is the colour singlet, zero momentum transfer BFKL equation (cf. Eq. (3.30)) as it appears, for example, in [58]. With this, we have shown how the well-known BFKL equation emerges from the Langevin JIMWLK equation in the dilute limit.

6.1.4 Mueller's form of the BFKL equation

At the end of Section 3.3.3, it was remarked that the BFKL equation can also be written in the form of the BK equation given in Eq. (3.55), without the nonlinear term:

$$\partial_Y \langle N_{\mathbf{y}\mathbf{x}} \rangle = \frac{\alpha_s N_c}{2\pi^2} \int_{\mathbf{w}} \tilde{\mathcal{K}}_{\mathbf{x}\mathbf{w}\mathbf{y}} (\langle N_{\mathbf{y}\mathbf{w}} \rangle + \langle N_{\mathbf{w}\mathbf{x}} \rangle - \langle N_{\mathbf{y}\mathbf{x}} \rangle). \quad (6.37)$$

In order to write an evolution equation for φ , Eq. (6.29) is used for each of the three terms in this expression, giving

$$\frac{1}{\epsilon} (\varphi_{\mathbf{x}\mathbf{y}}^{n+1} - \varphi_{\mathbf{x}\mathbf{y}}^n) = -\frac{N_c \alpha_s}{2 \pi^2} \int_{\mathbf{z}} \tilde{\mathcal{K}}_{\mathbf{x}\mathbf{z}\mathbf{y}} (\varphi_{\mathbf{x}\mathbf{y}}^n - \varphi_{\mathbf{x}\mathbf{z}}^n - \varphi_{\mathbf{y}\mathbf{z}}^n) + \mathcal{O}(\varphi^{3/2}). \quad (6.43)$$

Eq. (6.43) is exactly Eq. (6.37), written in terms of the operator $N_{\mathbf{x}\mathbf{y}}$ in the dilute limit. Note that ϕ is typically written in momentum space, since it usually appears in diagrams that are more easily calculated in momentum space. On the other hand, φ is typically written in coordinate space, since it is usually discussed in the context of the dipole picture.

6.2 Inclusive particle production in the dilute limit

We now return to the subject of inclusive particle production that was introduced in Section 5.2. We recap some of the main expressions from there that are expanded in the dilute limit in this section. The main points of this discussion may be found in Section VI of Paper [II].

The cross section for double inclusive quark–gluon production was given in Eq. (5.40):

$$\frac{d\sigma_{qg}}{dY d^2p dY_A d^2k_A} = \frac{1}{16\pi^4} \int_{\mathbf{x}\bar{\mathbf{x}}} e^{-i\mathbf{p}\cdot(\mathbf{x}-\bar{\mathbf{x}})} \left\langle H_{\text{prod}}(\mathbf{k}_A) \left\langle S_{\mathbf{x}\bar{\mathbf{x}},N}^{(2)} \right\rangle_{\nu} \Big|_{\bar{U}_A=U_A} \right\rangle_{Y_A} \quad (6.44)$$

$$= \frac{1}{4\pi^3} \frac{1}{16\pi^4} \int_{\mathbf{x}\bar{\mathbf{x}}\mathbf{y}\bar{\mathbf{y}}\mathbf{u}\bar{\mathbf{u}}} \mathcal{K}_{\mathbf{y}\mathbf{u}}^i \mathcal{K}_{\bar{\mathbf{y}}\bar{\mathbf{u}}}^i e^{-i\mathbf{p}\cdot(\mathbf{x}-\bar{\mathbf{x}})-i\mathbf{k}_A\cdot(\mathbf{y}-\bar{\mathbf{y}})} \left\langle \left\langle \frac{1}{N_c} \mathcal{I}_N \right\rangle_{\nu} \right\rangle_{Y_A}. \quad (6.45)$$

The production Hamiltonian was defined as

$$H_{\text{prod}}(\mathbf{k}) := \frac{1}{4\pi^3} \int_{\mathbf{y}\bar{\mathbf{y}}} e^{-i\mathbf{k}\cdot(\mathbf{y}-\bar{\mathbf{y}})} \int_{\mathbf{u}\bar{\mathbf{u}}} \mathcal{K}_{\mathbf{y}\mathbf{u}}^i \mathcal{K}_{\bar{\mathbf{y}}\bar{\mathbf{u}}}^i \left(L_{\mathbf{u}}^a - \tilde{U}_{\mathbf{y}}^{\dagger ab} R_{\mathbf{u}}^b \right) \left(\bar{L}_{\bar{\mathbf{u}}}^a - \tilde{\bar{U}}_{\bar{\mathbf{y}}}^{\dagger ac} \bar{R}_{\bar{\mathbf{u}}}^c \right) \quad (6.46)$$

in Eq. (5.28) and we defined

$$\mathcal{I}_n := \text{tr} \left(L_{\mathbf{u},0}^a U_{\mathbf{x},n} \bar{L}_{\bar{\mathbf{u}},0}^a \bar{U}_{\bar{\mathbf{x}},n}^{\dagger} - \tilde{U}_{\mathbf{y},0}^{\dagger ab} R_{\mathbf{u},0}^b U_{\mathbf{x},n} \bar{L}_{\bar{\mathbf{u}},n}^a \bar{U}_{\bar{\mathbf{x}},n}^{\dagger} - \tilde{\bar{U}}_{\bar{\mathbf{y}},0}^{\dagger ac} L_{\mathbf{u},0}^a U_{\mathbf{x},n} \bar{R}_{\bar{\mathbf{u}},0}^c \bar{U}_{\bar{\mathbf{x}},n}^{\dagger} \right. \\ \left. + \tilde{U}_{\mathbf{y},0}^{\dagger ab} \tilde{\bar{U}}_{\bar{\mathbf{y}},0}^{\dagger ac} R_{\mathbf{u},0}^b U_{\mathbf{x},n} \bar{R}_{\bar{\mathbf{u}},0}^c \bar{U}_{\bar{\mathbf{x}},n}^{\dagger} \right) \quad (6.47)$$

in Eq. (5.45). The evolution equation for RU^\dagger was given in Eq. (5.56) as

$$R_{\mathbf{u},0}^a U_{\mathbf{x},n+1}^\dagger = R_{\mathbf{u},0}^a U_{\mathbf{x},n}^\dagger + \int_{\mathbf{z}} \left(\frac{i\epsilon g}{\sqrt{4\pi^3}} \mathcal{K}_{\mathbf{xz}}^i \nu_{\mathbf{z},n}^{i,b} - \frac{\epsilon g^2}{4\pi^3} \mathcal{K}_{\mathbf{xzx}} t^b \right) [t^b R_{\mathbf{u},0}^a U_{\mathbf{x},n}^\dagger - R_{\mathbf{u},0}^a U_{\mathbf{x},n}^\dagger \tilde{U}_{\mathbf{z},n}^{\dagger bc} t^c - U_{\mathbf{x},n}^\dagger U_{\mathbf{z},n} (t^b R_{\mathbf{u},0}^a U_{\mathbf{z},n}^\dagger - R_{\mathbf{u},0}^a U_{\mathbf{z},n}^\dagger \tilde{U}_{\mathbf{z},n}^{\dagger bc} t^c)] + \mathcal{O}(\nu\epsilon^2). \quad (6.48)$$

6.2.1 The bilocal Langevin equations in the dilute limit

In order to expand Eq. (6.48) in the dilute limit, Eq. (6.1) is used to expand each of the Wilson lines. This leads to

$$R_{\mathbf{u},0}^a \lambda_{\mathbf{x},n+1} = R_{\mathbf{u},0}^a \lambda_{\mathbf{x},n} + \int_{\mathbf{z}} \left(\frac{i\epsilon g}{\sqrt{4\pi^3}} \mathcal{K}_{\mathbf{xz}}^i \nu_{\mathbf{z},n}^{i,d} - \frac{\epsilon g^2}{4\pi^3} \mathcal{K}_{\mathbf{xzx}} t^d \right) i f^{dbc} t^c R_{\mathbf{u},0}^a (\lambda_{\mathbf{x},n}^b - \lambda_{\mathbf{z},n}^b) + \mathcal{O}(\nu\epsilon^2, \lambda^2), \quad (6.49)$$

which is the same as $R_{\mathbf{u},0}^a$ acting on Eq. (6.9). The initial condition for this evolution equation follows from the expansion of the initial condition for Eq. (6.48), as given in Eq. (5.57):

$$R_{\mathbf{u},0}^a U_{\mathbf{x},0}^\dagger = ig \delta_{\mathbf{u}\mathbf{x}} U_{\mathbf{x},0}^\dagger t^a \quad \implies \quad R_{\mathbf{u},0}^a \lambda_{\mathbf{x},0} = g \delta_{\mathbf{u}\mathbf{x}} t^a + \mathcal{O}(\lambda). \quad (6.50)$$

Eq. (6.49) is a linear iterative equation for the quantity $R\lambda$ in the same way that Eq. (6.16) was an equation for λ . A formal analytical solution can therefore be written for Eq. (6.49) in a similar way as was done in Section 6.1.1 for Eq. (6.16). The equation for $L\lambda$ and its initial condition are the same as Eqs. (6.49) and (6.50), respectively, with $R \rightarrow L$.

In order to make sense of the Lie derivatives operating on elements of the group algebra, we start with their definitions given in Eq. (4.20),

$$L_{\mathbf{u}}^a := -ig [U_{\mathbf{u}} t^a]_{\alpha\beta} \frac{\delta}{\delta [U_{\mathbf{u}}]_{\alpha\beta}} \quad \text{and} \quad R_{\mathbf{u}}^a := -ig [t^a U_{\mathbf{u}}]_{\alpha\beta} \frac{\delta}{\delta [U_{\mathbf{u}}]_{\alpha\beta}}, \quad (6.51)$$

and make a change of variables by expanding each Wilson line in powers of λ . This results in [95]

$$L_{\mathbf{u},0}^a = g \left[\delta^{ac} - \frac{1}{2} f^{abc} \lambda_{\mathbf{u},0}^b + \mathcal{O}(\lambda^2) \right] \frac{\delta}{\delta \lambda_{\mathbf{u},0}^c}, \quad (6.52)$$

$$R_{\mathbf{u},0}^a = g \left[\delta^{ac} + \frac{1}{2} f^{abc} \lambda_{\mathbf{u},0}^b + \mathcal{O}(\lambda^2) \right] \frac{\delta}{\delta \lambda_{\mathbf{u},0}^c}. \quad (6.53)$$

Recall from Eq. (6.46) that the Lie derivatives are only required at the initial rapidity $Y_0 = Y_A$. This means that the $\lambda_{\mathbf{u},0}^b$ present in Eqs. (6.52) and (6.53) remain unevolved.

The physical significance of Eq. (6.49) is clearer in diagrams. After one evolution step, and using Eq. (6.50) for the initial condition, Eq. (6.49) gives

$$\begin{aligned}
 R_{\mathbf{u},0}^a \lambda_{x,1} = g \delta_{\mathbf{u}x} &+ \frac{i\epsilon g}{\sqrt{4\pi^3}} \int_z \mathcal{K}_{xz}^i \nu_{z,0}^{i,b} i g (\delta_{\mathbf{u}x} - \delta_{\mathbf{u}z}) \\
 &- \frac{\epsilon g^2}{4\pi^3} \int_z \mathcal{K}_{xzx} i g (\delta_{\mathbf{u}x} - \delta_{\mathbf{u}z}) + \mathcal{O}(\nu\epsilon^2, \lambda). \quad (6.54)
 \end{aligned}$$

This is effectively Eq. (6.10), with $R_{\mathbf{u},0}^a$ acting to sever the connection between the t -channel gluon and the target as it “differentiates away” one factor of λ . These diagrams already start to resemble one half of a BFKL ladder.

6.2.2 The cross section in the dilute limit

Now that the bilocal Langevin equations are known in the dilute limit, it is possible to use them to find the cross section in Eq. (6.45) in the dilute limit. One way to proceed would be to use Eq. (6.53) and the corresponding equation for $L\lambda$ to calculate each of the terms in the Eq. (6.47) in the dilute limit. It is then reasonable to see how BFKL ladders might arise from the square of Eq. (6.54).

An alternative way to calculate the cross section is to use Eq. (6.44) after expanding both the dipole operator and the production Hamiltonian in the dilute limit. The former has already been calculated in Eq. (6.55), from which we can read off

$$S_{x\bar{x},n}^{(2)} = 1 - \frac{1}{4N_c} (\lambda_{x,n}^a - \bar{\lambda}_{\bar{x},n}^a)^2 + \mathcal{O}(\lambda^3). \quad (6.55)$$

For the production Hamiltonian, Eq. (6.5) is used to expand the adjoint Wilson lines and Eqs. (6.52) and (6.53) are used to expand the Lie derivatives. This gives

$$L_{\mathbf{u},0}^a - \tilde{U}_{\mathbf{y},0}^{\dagger ab} R_{\mathbf{u},0}^b = g f^{abc} [\lambda_{\mathbf{u},0}^c - \lambda_{\mathbf{y},0}^c + \mathcal{O}(\lambda^2)] \frac{\delta}{\delta \lambda_{\mathbf{u},0}^b}. \quad (6.56)$$

Acting on the initial condition $\lambda_{x,0}$, this looks like

$$\left(L_{\mathbf{u},0}^a - \tilde{U}_{\mathbf{y},0}^{\dagger ab} R_{\mathbf{u},0}^b \right) \begin{array}{c} \text{---} \\ | \\ \bullet \\ | \\ \text{---} \\ x \end{array} = g\delta_{\mathbf{u}\mathbf{x}} \left(\begin{array}{c} b \\ | \\ \bullet \\ | \\ b \\ | \\ \bullet \\ | \\ c \\ | \\ a \\ | \\ \text{---} \\ u \end{array} - \begin{array}{c} b \\ | \\ \bullet \\ | \\ b \\ | \\ \bullet \\ | \\ c \\ | \\ a \\ | \\ \text{---} \\ y \end{array} \right) + \mathcal{O}(\lambda^2). \quad (6.57)$$

The full operator in H_{prod} is the square of Eq. (6.56):

$$\begin{aligned} & \left(L_{\mathbf{u},0}^a - \tilde{U}_{\mathbf{y},0}^{\dagger ab} R_{\mathbf{u},0}^b \right) \left(\bar{L}_{\bar{\mathbf{u}},0}^a - \tilde{U}_{\bar{\mathbf{y}},0}^{\dagger ac} \bar{R}_{\bar{\mathbf{u}},0}^c \right) \\ &= g^2 f^{abc} f^{ade} [(\lambda_{\mathbf{u},0}^c - \lambda_{\mathbf{y},0}^c) (\bar{\lambda}_{\bar{\mathbf{u}},0}^e - \bar{\lambda}_{\bar{\mathbf{y}},0}^e) + \mathcal{O}(\lambda^3)] \frac{\delta}{\delta \lambda_{\mathbf{u},0}^b} \frac{\delta}{\delta \bar{\lambda}_{\bar{\mathbf{u}},0}^d}. \end{aligned} \quad (6.58)$$

Since this contains both a λ derivative and a $\bar{\lambda}$ derivative, the only term from the expanded dipole operator in Eq. (6.55) that survives the operation of H_{prod} is the $\lambda\bar{\lambda}$ term. Then

$$\begin{aligned} & \left(L_{\mathbf{u},0}^a - \tilde{U}_{\mathbf{y},0}^{\dagger ab} R_{\mathbf{u},0}^b \right) \left(\bar{L}_{\bar{\mathbf{u}},0}^a - \tilde{U}_{\bar{\mathbf{y}},0}^{\dagger ac} \bar{R}_{\bar{\mathbf{u}},0}^c \right) S_{\mathbf{x}\bar{\mathbf{x}},n}^{(2)} = \frac{1}{N_c} \mathcal{I}_n \\ &= \frac{g^2}{2N_c} f^{abc} f^{ade} [(\lambda_{\mathbf{u},0}^c - \lambda_{\mathbf{y},0}^c) (\bar{\lambda}_{\bar{\mathbf{u}},0}^e - \bar{\lambda}_{\bar{\mathbf{y}},0}^e) + \mathcal{O}(\lambda^3)] \frac{\delta \lambda_{\mathbf{x},n}^f}{\delta \lambda_{\mathbf{u},0}^b} \frac{\delta \bar{\lambda}_{\bar{\mathbf{x}},n}^f}{\delta \bar{\lambda}_{\bar{\mathbf{u}},0}^d}. \end{aligned} \quad (6.59)$$

It is straightforward to keep track of which λ 's originate from which factor in the full dense expression by following the transverse coordinate assignments.

The colour algebra simplifies when the initial condition of the dipole operator is taken into account. According to Eq. (6.55), λ and $\bar{\lambda}$ have the same colour index at $n = 0$. This means that $c = e$ in Eq. (6.59) and

$$\begin{aligned} & \left(L_{\mathbf{u},0}^a - \tilde{U}_{\mathbf{y},0}^{\dagger ab} R_{\mathbf{u},0}^b \right) \left(\bar{L}_{\bar{\mathbf{u}},0}^a - \tilde{U}_{\bar{\mathbf{y}},0}^{\dagger ac} \bar{R}_{\bar{\mathbf{u}},0}^c \right) S_{\mathbf{x}\bar{\mathbf{x}},n}^{(2)} \\ &= \frac{g^2}{2} [(\lambda_{\mathbf{u},0}^c - \lambda_{\mathbf{y},0}^c) (\bar{\lambda}_{\bar{\mathbf{u}},0}^c - \bar{\lambda}_{\bar{\mathbf{y}},0}^c) + \mathcal{O}(\lambda^3)] \frac{\delta \lambda_{\mathbf{x},n}^a}{\delta \lambda_{\mathbf{u},0}^b} \frac{\delta \bar{\lambda}_{\bar{\mathbf{x}},n}^a}{\delta \bar{\lambda}_{\bar{\mathbf{u}},0}^b}. \end{aligned} \quad (6.60)$$

which are more physically intuitive. Together with the BFKL Green's function, this makes Eq. (6.60)

$$\left\langle \frac{1}{N_c} \mathcal{I}_n \right\rangle = \frac{g^2}{2} (\phi_{u\bar{u}}^0 - \phi_{u\bar{y}}^0 - \phi_{y\bar{u}}^0 + \phi_{y\bar{y}}^0) \mathcal{F}_{x,\bar{x},u,\bar{u}}^n + \mathcal{O}(\phi^{3/2}). \quad (6.66)$$

This can be equally well written in terms of φ instead of ϕ if needed.

In order to calculate the cross section at the end of evolution, the only quantity that requires evolving in 6.66 is \mathcal{F} . Since the derivatives in \mathcal{F} are taken at $n = 0$, the only evolution that we need to keep track of is that of the dipole term $\lambda_{x,n}^a \bar{\lambda}_{\bar{x},n}^a$ in the definition of \mathcal{F} . Fortunately, the evolution equation for this quantity has already been found in Eq. (6.28), which we now differentiate by $\lambda_{u,0}^b$ and $\bar{\lambda}_{\bar{u},0}^b$ to write everything in terms of \mathcal{F} . The resulting expression is the evolution equation for the BFKL Green's function

$$\begin{aligned} & \frac{1}{\epsilon} (\mathcal{F}_{x,\bar{x},u,\bar{u}}^{n+1} - \mathcal{F}_{x,\bar{x},u,\bar{u}}^n) \\ &= -\frac{N_c \alpha_s}{2 \pi^2} \int_z \left[\mathcal{K}_{xz\bar{x}} (\mathcal{F}_{x,\bar{x},u,\bar{u}}^n - \mathcal{F}_{z,\bar{x},u,\bar{u}}^n) + \mathcal{K}_{\bar{x}z\bar{x}} (\mathcal{F}_{x,\bar{x},u,\bar{u}}^n - \mathcal{F}_{x,z,u,\bar{u}}^n) \right. \\ & \quad \left. - 2\mathcal{K}_{xz\bar{x}} (\mathcal{F}_{x,\bar{x},u,\bar{u}}^n - \mathcal{F}_{x,z,u,\bar{u}}^n - \mathcal{F}_{z,\bar{x},u,\bar{u}}^n + \mathcal{F}_{z,z,u,\bar{u}}^n) \right] + \mathcal{O}(\nu\epsilon^2, \mathcal{F}^{3/2}), \end{aligned} \quad (6.67)$$

which can be read off from Eq. (6.29), with the replacement $\phi_{x\bar{x}}^n \rightarrow \mathcal{F}_{x,\bar{x},u,\bar{u}}^n$. The initial condition has already been calculated in writing Eq. (6.61):

$$\mathcal{F}_{x,\bar{x},u,\bar{u}}^0 = \frac{\delta\lambda_{x,0}^a \delta\bar{\lambda}_{\bar{x},0}^a}{\delta\lambda_{u,0}^b \delta\bar{\lambda}_{\bar{u},0}^b} = (N_c^2 - 1) \delta_{ux} \delta_{\bar{u}\bar{x}}. \quad (6.68)$$

In Paper [II], the BFKL Green's function is Fourier transformed to write a momentum space version of Eq. (6.67) and subsequently, the cross section in momentum space:

$$\begin{aligned} & \frac{d\sigma_{qg}}{dY d^2p dY_A d^2k_A} \\ &= -\frac{\alpha_s}{N_c} \int_{\mathbf{q}} \frac{\mathbf{q}^2}{(\mathbf{q} - \mathbf{k}_A)^2 \mathbf{k}_A^2} \varphi^0(-\mathbf{q}) \mathcal{F}^n(-\mathbf{p}, \mathbf{p}, \mathbf{q} - \mathbf{k}_A, -\mathbf{q} + \mathbf{k}_A) + \mathcal{O}(\varphi^{3/2}). \end{aligned} \quad (6.69)$$

This does indeed have the BFKL ladder structure

that was seen in Section 3.2.2 in quarkonium–quarkonium scattering. In place of G , we now have \mathcal{F}^n ; in place of the quarkonia, we have a quark projectile and nuclear target. The transverse momentum structure of 6.69 is covered in detail in Paper [II], so we omit further discussion here.

Chapter summary

In this chapter, we have studied the Langevin formulation of JIMWLK evolution in the dilute limit. First, the Langevin equation for the Wilson line was expanded. This was used to derive the BFKL equation for two quantities, the unintegrated gluon distribution ϕ and the BFKL pomeron φ . Next, the bilocal Langevin equations were expanded in the dilute limit. These were used in the cross section for inclusive quark–gluon production. In expanding the relevant equations from Chapter 5, we have seen how BFKL ladder diagrams emerge from a stochastic picture of evolution.

7

The Gaussian Approximation

In Section 2.7, we saw how the dipole correlator enters the cross section for DIS. More complicated processes may require the calculation of higher-order correlators. In Chapter 4.5, the evolution for such correlators was discussed in terms of the Balitsky hierarchy and the JIMWLK equation. In practice, it may not be possible to use such equations to calculate the evolution of a particular correlator, due to the required input from even higher-order correlators. For example, the evolution equation for the dipole correlator

$$\partial_Y \left\langle \frac{1}{N_c} \text{tr} (U_{\mathbf{x}} U_{\mathbf{y}}^\dagger) \right\rangle = -C_F \frac{\alpha_s}{\pi^2} \int_z \tilde{\mathcal{K}}_{\mathbf{xzy}} \left\langle \frac{1}{N_c} \text{tr} (U_{\mathbf{x}} U_{\mathbf{y}}^\dagger) - \frac{1}{N_c C_F} \tilde{U}_z^{ab} \text{tr} (t^a U_{\mathbf{x}} t^b U_{\mathbf{y}}^\dagger) \right\rangle \quad (7.1)$$

was provided in Eq. (4.48). In Section 4.5, the large N_c approximation was used to write the 3-point correlator that appears on the right side of this equation in terms of the dipole, thus closing the equation and giving us the BK equation.

In order to go beyond the equation for the dipole correlator in a systematic way, a self-consistent truncation scheme is needed to close the infinite hierarchy of evolution equations. One possibility which has proven successful, is the Gaussian Approximation (GA). In this chapter, we use the GA to calculate the previously known 2-, 3- and 4-point correlators. With the method established from these, we move on to the 6-point correlators, which are of particular interest due to their presence in the NLO BK equation, as shown in Section 3.3.3.

Since the notation for correlators of several Wilson lines becomes tedious, we extend the definition

$$S_{\mathbf{xy}}^{(2)} := \frac{1}{N_c} \text{tr} (U_{\mathbf{x}} U_{\mathbf{y}}^\dagger) \quad (7.2)$$

introduced at the end of Section 2.7 to include any number of Wilson lines:

$$S_{\mathbf{x}_1, \mathbf{x}_2, \dots, \mathbf{x}_{n-1}, \mathbf{x}_n}^{(n)} := \frac{1}{N_c} \text{tr} (U_{\mathbf{x}_1} U_{\mathbf{x}_2}^\dagger \cdots U_{\mathbf{x}_{n-1}} U_{\mathbf{x}_n}^\dagger). \quad (7.3)$$

This is also the notation used in Paper [III]. In the case of 4- and 6-point correlators, the target line at the bottom of the diagrams is henceforth left out the sake of clarity.

We begin this chapter with an introduction to the GA in Section 7.1. In Section 7.2, parametric equations are calculated for the 2- and 3-point correlators in order to demonstrate the use of the GA. In Section 7.3, this method is extended to 4-point correlators, which prove to be a much more involved calculation due to the matrix structure of expressions. Finally, we discuss the calculation of the 6-point correlators in Section 7.4. Since this is covered in detail in Paper [III], we only give a brief outline of the main points here.

7.1 Parametrisation definition

In the GA, a correlator is parametrised in terms of a rapidity-dependent two-point function, which is labelled G_{uv} . The parametrisation allows us to express any higher-order correlator in terms of the dipole correlator. The GA is so named due to its equivalence with a nonlocal Gaussian approximation for the weight functional $W_Y[\rho]$ (see Section 2.7). These weights are written as

$$\tilde{W}_\eta[\rho] = \exp \left\{ - \int^\eta d\tilde{\eta} \int_{uv} \frac{\rho_c(\tilde{\eta}, \mathbf{u}) \rho_c(\tilde{\eta}, \mathbf{v})}{2\mu^2(\tilde{\eta}, \mathbf{u}, \mathbf{v})} \right\}, \quad (7.4)$$

where ρ_c is a colour source with variance μ^2 and $\tilde{W}_\eta[\rho]$ is an equivalent weight to $W_Y[\rho]$ [49]. The rapidity η is specifically a *parametrisation rapidity* – it is not necessarily the same as the evolution rapidity Y . The reader is referred to Paper [I] and to [99] for further discussion about this small distinction.

Generically, the truncation of an infinite hierarchy requires certain constraints to be imposed to ensure that the approximation remains legitimate. For the Schwinger–Dyson equations, for example, the Ward identities must be satisfied when the hierarchy is truncated at some specific order. The group theoretical constraints in the local limits of transverse coordinates, which are called *coincidence limits* following [49], are the appropriate analogue to the Ward identities in the context of the GA. One crucial advantage of the GA is that it automatically satisfies these group theoretical constraints, as we show explicitly for some of the correlators discussed in this chapter.

The starting point of the GA is the parametrisation of a generic correlator of any Wilson line operator $\mathcal{O}[U]$ as

$$\langle \mathcal{O}[U] \rangle (\eta) = \left\langle \exp \left\{ -\frac{1}{2} \int^\eta d\tilde{\eta} \int_{\mathbf{uv}} G_{\mathbf{uv}}(\tilde{\eta}) L_{\mathbf{u}}^a L_{\mathbf{v}}^a \right\} \mathcal{O}[U] \right\rangle (\eta_0). \quad (7.5)$$

A more practical form of this equation is

$$\partial_\eta \langle \mathcal{O}[U] \rangle (\eta) = \left\langle -\frac{1}{2} \int_{\mathbf{uv}} G_{\mathbf{uv}}(\tilde{\eta}) L_{\mathbf{u}}^a L_{\mathbf{v}}^a \mathcal{O}[U] \right\rangle (\eta), \quad (7.6)$$

which is used to calculate various correlators in this chapter by simply operating with two Lie derivatives on the relevant $\mathcal{O}[U]$ and inserting the result on the right side. The overall operator that acts on $\mathcal{O}[U]$ in this expression is denoted by the shorthand \mathcal{M} and is referred to as the *transition matrix*. Since the Lie derivatives in Eq. (7.6) are symmetric under exchange of \mathbf{u} and \mathbf{v} , we have $G_{\mathbf{uv}} = G_{\mathbf{vu}}$.

7.2 Simple Correlators

7.2.1 The 2-point correlator

We begin by demonstrating the use of Eq. (7.6) on the simplest operator, the dipole $\text{tr}(U_{\mathbf{x}} U_{\mathbf{y}}^\dagger) / N_c$. Diagrammatically, we need to solve

$$\partial_\eta \left\langle \frac{1}{N_c} \text{Dipole} \right\rangle = \left\langle -\frac{1}{2} \frac{1}{N_c} \text{Transition} \times \int_{\mathbf{uv}} G_{\mathbf{uv}}(\tilde{\eta}) L_{\mathbf{u}}^a L_{\mathbf{v}}^a \times \text{Dipole} \right\rangle \quad (7.7)$$

$$\sim \left\langle \text{Dipole with Gluon Insertion} \right\rangle, \quad (7.8)$$

where the red line in the rightmost diagram represents the parametrisation of a gluon insertion in the dipole diagram. This is not to be confused with the gluon diagram

$$\text{Dipole with Blue Gluon} \neq \text{Dipole with Red Gluon}. \quad (7.9)$$

7. The Gaussian Approximation

Operating with $L_u^a L_v^a$ as described in Section 4.3 on the dipole operator, we get all the ways that a gluon can be added to the right of the target line:

$$L_u^a L_v^a \sim \text{[Diagram 1]} + \text{[Diagram 2]} + \text{[Diagram 3]} + \text{[Diagram 4]} + \text{[Diagram 5]} \quad (7.10)$$

$$=: \text{[Diagram 6]} \quad (7.11)$$

Eq. (7.7) then gives

$$\partial_\eta \left\langle \frac{1}{N_c} \text{tr} (U_x U_y^\dagger) \right\rangle = \left\langle -\frac{C_F}{2} [G_{xx}(\eta) + G_{yy}(\eta) - 2G_{xy}(\eta)] \frac{1}{N_c} \text{tr} (U_x U_y^\dagger) \right\rangle. \quad (7.12)$$

By defining

$$\mathcal{G}_{xy}(\eta) := \int^\eta d\bar{\eta} \left[G_{xy}(\bar{\eta}) - \frac{1}{2} [G_{xx}(\bar{\eta}) + G_{yy}(\bar{\eta})] \right], \quad (7.13)$$

such that $\mathcal{G}_{xy} = \mathcal{G}_{yx}$ and $\mathcal{G}_{xx} = 0$, and taking the derivative $\mathcal{G}'_{xy}(\eta) := \partial_\eta \mathcal{G}_{xy}(\eta)$, Eq. (7.12) can be written more compactly as

$$\partial_\eta \left\langle \frac{1}{N_c} \text{tr} (U_x U_y^\dagger) \right\rangle = \left\langle -C_F \mathcal{G}'_{xy}(\eta) \frac{1}{N_c} \text{tr} (U_x U_y^\dagger) \right\rangle. \quad (7.14)$$

This has a simple exponential solution

$$\left\langle \frac{1}{N_c} \text{tr} \left(\text{[Diagram 7]} \right) \right\rangle = \exp \{ -C_F \mathcal{G}_{xy}(\eta) \}, \quad (7.15)$$

which is the well-known result for the dipole correlator in the GA [49]. The calculation can be repeated in any representation. In the adjoint representation, for example, the result is the same with a different colour factor $C_F \rightarrow C_A = N_c$ and a different normalisation $d_F = N_c \rightarrow d_A = N_c^2 - 1$. The explicit η -dependence labelled in \mathcal{G} is dropped henceforth for clarity.

7.2.2 The 3-point correlator

Another simple correlator to calculate in the GA is $\langle \tilde{U}_z^{ab} \text{tr} (t^a U_x t^b U_y^\dagger) / (N_c C_F) \rangle$, which appears, for example, in Eq. (7.1). Using Eq. (7.6), we need to solve

$$\partial_\eta \left\langle \frac{1}{N_c C_F} \text{Diagram} \right\rangle = \left\langle -\frac{1}{2} \frac{1}{N_c C_F} \text{Diagram} \times \int_{uv} G_{uv} L_u^a L_v^a \times \text{Diagram} \right\rangle. \quad (7.16)$$

The operation of the Lie derivatives can be carried out using the product rule, giving

$$\begin{aligned} & L_u^c L_v^c \left[\frac{1}{N_c C_F} \tilde{U}_z^{ab} \text{tr} (t^a U_x t^b U_y^\dagger) \right] \\ &= \frac{1}{N_c C_F} \left[L_u^c L_v^c \tilde{U}_z^{ab} \right] \text{tr} (t^a U_x t^b U_y^\dagger) + \frac{1}{N_c C_F} \left[L_v^c \tilde{U}_z^{ab} \right] \left[L_u^c \text{tr} (t^a U_x t^b U_y^\dagger) \right] \\ &+ \frac{1}{N_c C_F} \left[L_u^c \tilde{U}_z^{ab} \right] \left[L_v^c \text{tr} (t^a U_x t^b U_y^\dagger) \right] + \frac{1}{N_c C_F} \tilde{U}_z^{ab} \left[L_u^c L_v^c \text{tr} (t^a U_x t^b U_y^\dagger) \right]. \end{aligned} \quad (7.17)$$

In order to act with the Lie derivatives on adjoint Wilson lines, they are written as $\tilde{U}_z^{ab} = 2 \text{tr} (t^a U_z t^b U_z^\dagger)$. Then

$$L_v^c \tilde{U}_z^{ab} = i f^{acd} \tilde{U}_z^{db} \delta_{vz}, \quad (7.18)$$

$$L_u^c L_v^c \tilde{U}_z^{ab} = C_A \tilde{U}_z^{ab} \delta_{uz} \delta_{vz}. \quad (7.19)$$

Using these expressions, each of the four terms in Eq. (7.17) can be calculated separately. After using the delta functions to perform the transverse integrals, the first term becomes

$$\int_{uv} G_{uv} \frac{1}{N_c C_F} \left[L_u^c L_v^c \tilde{U}_z^{ab} \right] \text{tr} (t^a U_x t^b U_y^\dagger) = C_A G_{zz} \frac{1}{N_c C_F} \tilde{U}_z^{ab} \text{tr} (t^a U_x t^b U_y^\dagger). \quad (7.20)$$

The second and third terms simplify after some colour algebra to give

$$\begin{aligned} & \int_{uv} G_{uv} \frac{1}{N_c C_F} \left[L_v^c \tilde{U}_z^{ab} \right] \left[L_u^c \text{tr} (t^a U_x t^b U_y^\dagger) \right] \\ &= \int_{uv} G_{uv} \frac{1}{N_c C_F} \left[L_u^c \tilde{U}_z^{ab} \right] \left[L_v^c \text{tr} (t^a U_x t^b U_y^\dagger) \right] \end{aligned} \quad (7.21)$$

$$= -\frac{C_A}{2} (G_{xz} + G_{yz}) \tilde{U}_z^{db} \frac{1}{N_c C_F} \text{tr} (t^d U_x t^b U_y^\dagger). \quad (7.22)$$

Similarly, some basic colour algebra reduces the fourth term to

$$\begin{aligned} & \int_{uv} G_{uv} \frac{1}{N_c C_F} \tilde{U}_z^{ab} \left[L_u^c L_v^c \text{tr} (t^a U_x t^b U_y^\dagger) \right] \\ &= (-2C_F \mathcal{G}'_{xy} + C_A G_{xy}) \frac{1}{N_c C_F} \tilde{U}_z^{ab} \text{tr} (t^a U_x t^b U_y^\dagger). \end{aligned} \quad (7.23)$$

7. The Gaussian Approximation

Putting all four results together and using Eq. (7.13) to express all G 's as \mathcal{G} 's, Eq. (7.17) simplifies to

$$\begin{aligned} \partial_\eta \left\langle \frac{1}{N_c C_F} \tilde{U}_z^{ab} \text{tr} (t^a U_x t^b U_y^\dagger) \right\rangle \\ = \left\langle - \left[\frac{C_A}{2} (\mathcal{G}'_{xz} + \mathcal{G}'_{yz} - \mathcal{G}'_{xy}) + C_F \mathcal{G}'_{xy} \right] \frac{1}{N_c C_F} \tilde{U}_z^{ab} \text{tr} (t^a U_x t^b U_y^\dagger) \right\rangle. \end{aligned} \quad (7.24)$$

Like the dipole correlator, this has an exponential solution

$$\left\langle \frac{1}{N_c C_F} \tilde{U}_z^{ab} \text{tr} (t^a U_x t^b U_y^\dagger) \right\rangle = \exp \left\{ - \frac{C_A}{2} (\mathcal{G}_{xz} + \mathcal{G}_{yz} - \mathcal{G}_{xy}) - C_F \mathcal{G}_{xy} \right\}, \quad (7.25)$$

which is the well-known result for the 3-point correlator in the GA [49].

A self-consistency check can be performed on the parametric equation of any correlator by taking certain coincidence limits. For the 3-point correlator, we see that Eq. (7.25) in the particular limit

$$\lim_{y \rightarrow x} \frac{1}{N_c C_F} \tilde{U}_z^{ab} \text{tr} (t^a U_x t^b U_y^\dagger) = \frac{1}{d_A} \tilde{U}_z^{ab} \tilde{U}_x^{ab}, \quad (7.26)$$

results in two adjoint Wilson lines. This is expected, since the quark and antiquark are placed on top of each other at the same coordinate and become equivalent to a gluon at that coordinate. In diagrams,



$$(7.27)$$

Another scenario to consider is one in which the gluon is placed on top of either the quark or antiquark. Then

$$\lim_{z \rightarrow y} \frac{1}{N_c C_F} \tilde{U}_z^{ab} \text{tr} (t^a U_x t^b U_y^\dagger) = \lim_{z \rightarrow x} \frac{1}{N_c C_F} \tilde{U}_z^{ab} \text{tr} (t^a U_x t^b U_y^\dagger) = \frac{1}{N_c} \text{tr} (U_x U_y^\dagger). \quad (7.28)$$

This is also an expected result, since all that remains after taking the limit is the fundamental dipole. The last limiting case that may be considered is

$$\lim_{\substack{z \rightarrow y \\ y \rightarrow x}} \frac{1}{N_c C_F} \tilde{U}_z^{ab} \text{tr} (t^a U_x t^b U_y^\dagger) = 1, \quad (7.29)$$

which shows that



$$(7.30)$$

is the correct normalisation factor for the 3-point correlator. Coincidence limits of this kind are trivial when the objects of interest are simple 2- and 3-point correlators. They become useful when more complicated parametric equations need to be checked, such as those encountered for the 4- and 6-point correlators.

7.2.3 Evolution equation for \mathcal{G}_{xy}

The parametric equations for the 2- and 3-point correlators are sufficient to find an evolution equation for the GA 2-point function itself, starting from the Balitsky equation. In Eq. (7.1), we use Eq. (7.15) for the 2-point correlators on the left and right of the equation and Eq. (7.25) for the 3-point correlator. This results in

$$\partial_\eta \mathcal{G}_{xy} = \frac{\alpha_s}{\pi^2} \int_z \mathcal{K}_{xzy} \left(1 - \exp \left\{ -\frac{C_A}{2} (\mathcal{G}_{xz} + \mathcal{G}_{yz} - \mathcal{G}_{xy}) \right\} \right), \quad (7.31)$$

which governs the evolution in rapidity Y (from the Balitsky equation) of \mathcal{G}_{xy} [49]. Although the quark and antiquark were taken to be in the fundamental representation in this equation, in [83] it was shown that Eq. (7.31) is the correct result regardless of representation. In Paper [I], this equation was extended to include the odderon three-point function G_{xyz} , but this discussion is postponed until we introduce an extension of the GA in Chapter 8.

7.3 4-point correlators

We now move on to more complicated correlators. Even at the level of the 4-point correlators, finding the correct parametrisation equations becomes significantly more complicated than what was done in the previous section. This is because there is now more than one way to form a multiplet state from four Wilson lines – a problem that was not encountered with the 2- and 3-point correlators. Consequently, Eq. (7.6) becomes a matrix differential equation that results in a system of coupled equations. Fortunately, the matrices involved are symmetric by construction. The 4-point correlators consisting of two fundamental and two antifundamental Wilson lines were calculated in [49]. We give a brief overview of that calculation, since it is helpful in understanding the calculation for the 6-point correlators.

In [102], 4-point correlators were used to calculate correlations in azimuthal angle in DIS. Another motivation for studying higher-point correlators of this kind is that they provide information about other related correlators. Consider, for example, the 3-point operator from Section 7.2.2. Mathematically, the same operator can be

obtained by taking the relevant coincidence limits in a particular 4-point operator:

$$\frac{1}{d_A/4} \text{tr} \left(U_{\mathbf{y}'} t^a U_{\mathbf{x}'}^\dagger t^b \right) \text{tr} \left(U_{\mathbf{x}} t^a U_{\mathbf{y}}^\dagger t^b \right) = \frac{1}{d_A/4} \text{Diagram} \quad (7.32)$$

$$\xrightarrow{\mathbf{y}' \rightarrow \mathbf{x}'} \frac{1}{N_c C_F} \tilde{U}_{\mathbf{x}'}^{ab} \text{tr} \left(t^a U_{\mathbf{x}} t^b U_{\mathbf{y}}^\dagger \right) = \frac{1}{N_c C_F} \text{Diagram} \quad (7.33)$$

Studying higher-point correlators in local limits therefore allows us to simultaneously study processes concerning gluons interacting with the target field.

7.3.1 Matrix equation

In order to form the space of all 4-point correlators, we start with a product of two quarks and two antiquarks

$$U_{\mathbf{x}} \otimes U_{\mathbf{y}}^\dagger \otimes U_{\mathbf{x}'} \otimes U_{\mathbf{y}'}^\dagger = \text{Diagram} \quad (7.34)$$

The target line at the bottom of the diagrams is omitted henceforth for clarity in diagrams with more than two projectiles. The notation \otimes is used to emphasize that this is a matrix product with suppressed open indices

$$\begin{array}{c} j \text{---} \text{---} i \\ k \text{---} \text{---} l \\ j' \text{---} \text{---} i' \\ k' \text{---} \text{---} l' \end{array} \quad (7.35)$$

There are two multiplets that can be formed, which are drawn in the notation of [103]. One choice for an orthonormal basis consists of the normalised singlet–singlet and octet states

$$\mathbf{B} := \left(\begin{array}{c} \text{Diagram} \\ \frac{1}{N_c} \\ \text{Diagram} \end{array}, \begin{array}{c} \text{Diagram} \\ \frac{1}{\sqrt{d_A/4}} \\ \text{Diagram} \end{array} \right), \quad (7.36)$$

as used in [49]. Each solid line corresponds to a Dirac delta and each vertex corresponds to a generator such that

$$\begin{array}{c} \text{Diagram} \\ \text{Diagram} \end{array} = \delta_{i_1, l_1} \delta_{i_2, l_2}, \quad \text{and} \quad \begin{array}{c} \text{Diagram} \\ \text{Diagram} \end{array} = t_{i_1, l_1}^a t_{i_2, l_2}^a. \quad (7.37)$$

In order to write the second one of these in terms of Dirac deltas, we can use the Fierz identity given in Eq. (4.49), which can be written as

$$2t_{i_1, l_1}^a t_{i_2, l_2}^a = \delta_{i_1, l_1} \delta_{i_2, l_2} - \frac{1}{N_c} \delta_{i_1, l_2} \delta_{i_2, l_1}, \quad (7.38)$$

$$2 \begin{array}{c} \leftarrow \\ \bullet \\ \leftarrow \\ \bullet \\ \leftarrow \end{array} = \begin{array}{c} \curvearrowright \\ \bullet \\ \curvearrowleft \end{array} - \frac{1}{N_c} \begin{array}{c} \leftarrow \\ \bullet \\ \rightarrow \end{array}. \quad (7.39)$$

It is also possible to choose a different basis, such as

$$\left(\begin{array}{c} \curvearrowright \\ \bullet \\ \curvearrowright \end{array}, \begin{array}{c} \curvearrowright \\ \bullet \\ \curvearrowleft \end{array} \right). \quad (7.40)$$

This is equivalent to \mathbf{B} and results in the same parametric equations for the 4-point correlators. Any multiplets can be used for the calculation, provided they form an orthonormal basis.

The 2×1 structure of \mathbf{B} means that Eq. (7.6) is now a 2×2 matrix equation. On the left side is a matrix of operators

$$\begin{aligned} \mathcal{A}(\eta) &:= \begin{pmatrix} \frac{1}{N_c^2} \begin{array}{c} \bullet \\ \bullet \\ \bullet \\ \bullet \end{array} & \frac{1}{N_c \sqrt{d_{\Lambda/4}}} \begin{array}{c} \bullet \\ \bullet \\ \bullet \\ \bullet \end{array} \\ \frac{1}{N_c \sqrt{d_{\Lambda/4}}} \begin{array}{c} \bullet \\ \bullet \\ \bullet \\ \bullet \end{array} & \frac{1}{d_{\Lambda/4}} \begin{array}{c} \bullet \\ \bullet \\ \bullet \\ \bullet \end{array} \end{pmatrix} \quad (7.41) \\ &= \begin{pmatrix} \frac{1}{N_c^2} \text{tr} \left(U_{\mathbf{y}'} U_{\mathbf{x}'}^\dagger \right) \text{tr} \left(U_{\mathbf{x}} U_{\mathbf{y}}^\dagger \right) & \frac{1}{N_c \sqrt{d_{\Lambda/4}}} \text{tr} \left(U_{\mathbf{y}'} t^a U_{\mathbf{x}'}^\dagger \right) \text{tr} \left(U_{\mathbf{x}} t^a U_{\mathbf{y}}^\dagger \right) \\ \frac{1}{N_c \sqrt{d_{\Lambda/4}}} \text{tr} \left(U_{\mathbf{y}'} U_{\mathbf{x}'}^\dagger t^b \right) \text{tr} \left(U_{\mathbf{x}} U_{\mathbf{y}}^\dagger t^b \right) & \frac{1}{d_{\Lambda/4}} \text{tr} \left(U_{\mathbf{y}'} t^a U_{\mathbf{x}'}^\dagger t^b \right) \text{tr} \left(U_{\mathbf{x}} t^a U_{\mathbf{y}}^\dagger t^b \right) \end{pmatrix}. \quad (7.42) \end{aligned}$$

This is formed by wedging the product of Wilson lines in Eq. (7.34) between the basis vectors, i.e. by calculating $\mathbf{B}^\top \left(U_{\mathbf{x}} \otimes U_{\mathbf{y}}^\dagger \otimes U_{\mathbf{x}'} \otimes U_{\mathbf{y}'}^\dagger \right) \mathbf{B}$, where

$$\mathbf{B}^\top = \begin{pmatrix} \begin{array}{c} \curvearrowright \\ \bullet \\ \curvearrowright \end{array} \\ \begin{array}{c} \curvearrowright \\ \bullet \\ \curvearrowleft \end{array} \\ \frac{1}{\sqrt{d_{\Lambda/4}}} \begin{array}{c} \bullet \\ \bullet \\ \bullet \\ \bullet \end{array} \end{pmatrix} = \begin{pmatrix} \frac{1}{N_c} \delta_{j_1, k_1} \delta_{j_2, k_2} \\ \frac{1}{\sqrt{d_{\Lambda/4}}} t_{j_1, k_1}^b t_{j_2, k_2}^b \end{pmatrix}. \quad (7.43)$$

To read the mathematical expressions from the diagrams, one traces each loop along the direction of the arrows and denotes it by a trace, then multiplies all loops

contributing to a particular diagram. For the bottom right element in Eq. (7.41), for example, we get

$$\begin{aligned}
 B_2^\top \left(U_{\mathbf{x}} \otimes U_{\mathbf{y}}^\dagger \otimes U_{\mathbf{x}'} \otimes U_{\mathbf{y}'}^\dagger \right) B_2 &= \frac{1}{\sqrt{d_A/4}} \text{diagram} \times \text{diagram} \times \frac{1}{\sqrt{d_A/4}} \text{diagram} \quad (7.44) \\
 &= \frac{1}{\sqrt{d_A/4}} t_{j_1, k_1}^a t_{j_2, k_2}^a \left(U_{\mathbf{x}} \otimes U_{\mathbf{y}}^\dagger \otimes U_{\mathbf{x}'} \otimes U_{\mathbf{y}'}^\dagger \right). \quad (7.45)
 \end{aligned}$$

It is also possible to set up the calculation such that one considers two separate 2×1 column vectors, as is done in [96], for example. We choose to keep the matrix structure following [49] as a matter of convenience for calculating the transition matrix. Eq. (7.6) is now written as

$$\partial_\eta \langle \mathcal{A}(\eta) \rangle = - \langle \mathcal{M} \mathcal{A}(\eta) \rangle, \quad (7.46)$$

where \mathcal{M} is the transition matrix that is still to be calculated.

7.3.2 Transition matrix

Before solving Eq. (7.46), the transition matrix must be calculated. The right side of Eq. (7.46) is given by

$$-\mathcal{M} \mathcal{A}(\eta) := - \begin{pmatrix} \mathcal{M}^{(1,1)} & \mathcal{M}^{(1,2)} \\ \mathcal{M}^{(2,1)} & \mathcal{M}^{(2,2)} \end{pmatrix} \begin{pmatrix} \frac{1}{N_c^2} \text{diagram} & \frac{1}{N_c \sqrt{d_A/4}} \text{diagram} \\ \frac{1}{N_c \sqrt{d_A/4}} \text{diagram} & \frac{1}{d_A/4} \text{diagram} \end{pmatrix} \quad (7.47)$$

$$= - \begin{pmatrix} \frac{1}{N_c^2} \text{diagram} & \frac{1}{N_c \sqrt{d_A/4}} \text{diagram} \\ \frac{1}{N_c \sqrt{d_A/4}} \text{diagram} & \frac{1}{d_A/4} \text{diagram} \end{pmatrix}. \quad (7.48)$$

These are the diagrams that contain the relevant \mathcal{G} content that need to be calculated in order to extract \mathcal{M} .

As an example of how this setup works, consider the top left element of the

matrix in Eq. (7.48):

$$[\mathcal{M}\mathcal{A}(\eta)]_{11} = \frac{1}{N_c^2} \text{diagram} \quad (7.49)$$

$$= \mathcal{M}^{(1,1)} \frac{1}{N_c^2} \text{diagram} + \mathcal{M}^{(1,2)} \frac{1}{N_c \sqrt{d_A/4}} \text{diagram}. \quad (7.50)$$

From the right side of Eq. (7.6), it follows that Eq. (7.50) is the same as

$$-\frac{1}{2} \int_{uv} G_{uv} L_u^a L_v^a \mathcal{A}^{(1,1)}(\eta) = -\frac{1}{2} \int_{uv} G_{uv} L_u^a L_v^a \frac{1}{N_c^2} \text{diagram} = \frac{1}{N_c^2} \text{diagram}. \quad (7.51)$$

The \mathcal{G} content of the rightmost diagram can be separated from the target interaction by inserting a complete set of states:

$$\frac{1}{N_c^2} \text{diagram} = \frac{1}{N_c^2} \text{diagram} \left(\sum_n |n\rangle \langle n| \right) \text{diagram} \quad (7.52)$$

$$= \frac{1}{N_c^2} \text{diagram} \left(\frac{1}{N_c^2} \text{diagram} + \frac{1}{d_A/4} \text{diagram} \right) \text{diagram} \quad (7.53)$$

$$= \frac{1}{N_c^4} \text{diagram} \text{diagram} + \frac{1}{N_c^2 d_A/4} \text{diagram} \text{diagram}. \quad (7.54)$$

Then, direct comparison with Eq. (7.50) gives the two transition matrix elements

$$\mathcal{M}^{(1,1)} = -\frac{1}{N_c^2} \text{diagram} \quad \text{and} \quad \mathcal{M}^{(1,2)} = -\frac{1}{N_c \sqrt{d_A/4}} \text{diagram}. \quad (7.55)$$

Similarly, by calculating the other three elements of the matrix in Eq. (7.48), we get the full transition matrix

$$\mathcal{M} = - \begin{pmatrix} \frac{1}{N_c^2} \text{diagram} & \frac{1}{N_c \sqrt{d_A/4}} \text{diagram} \\ \frac{1}{N_c \sqrt{d_A/4}} \text{diagram} & \frac{1}{d_A/4} \text{diagram} \end{pmatrix}, \quad (7.56)$$

where [49]

$$\mathcal{M}^{(1,1)} = C_F (\mathcal{G}'_{xy} + \mathcal{G}'_{x'y'}), \quad (7.57)$$

$$\mathcal{M}^{(1,2)} = \frac{\sqrt{d_A/4}}{C_A} (\mathcal{G}'_{x'x} + \mathcal{G}'_{y'y} - \mathcal{G}'_{x'y} - \mathcal{G}'_{y'x}), \quad (7.58)$$

$$\begin{aligned} \mathcal{M}^{(2,2)} = & \left(C_F - \frac{C_A}{2} \right) (\mathcal{G}'_{xy} + \mathcal{G}'_{x'y'}) + \frac{C_d + C_A}{4} (\mathcal{G}'_{x'x} + \mathcal{G}'_{y'y}) \\ & - \frac{C_d - C_A}{4} (\mathcal{G}'_{x'y} + \mathcal{G}'_{y'x}). \end{aligned} \quad (7.59)$$

Now we have a completed differential equation to solve in the form of Eq. (7.46).

7.3.3 Differential equation solution

It is straightforward to solve Eq. (7.46) by exponentiating the right side, giving

$$\langle \mathcal{A}(\eta) \rangle = \left\langle P_\eta \exp \left\{ - \int_{\eta_0}^{\eta} d\bar{\eta} \mathcal{M} \right\} \mathcal{A}(\eta_0) \right\rangle, \quad (7.60)$$

where P_η denotes path ordering in rapidity η and the normalisation factor $\mathcal{A}(\eta_0)$ is set by the initial condition. The part of $\langle \mathcal{A}(\eta) \rangle$ that is of interest for the study of the 6-point correlators presented in Paper[III] is the so-called *rigid exponential*. This is found by assuming that the transition matrices at different parametrisation rapidities commute. Consequently, the path ordering in η can be neglected and what remains is

$$\langle \mathcal{A}^{\text{rigid}}(\eta) \rangle := \left\langle \exp \left\{ - \int^{\eta} d\bar{\eta} \mathcal{M} \right\} \right\rangle. \quad (7.61)$$

The explicit rigid exponential solution for the 4-point correlators is provided in [49].

7.3.4 Local limits

The final task regarding the 4-point correlators is the check of coincidence limits to ensure that the expressions provided in Eqs. (7.57), (7.58) and (7.59) are consistent with the 2- and 3-point correlators from Section 7.2. These checks are shown explicitly here, since the same method is applied in the case of the 6-point correlators in the next section, where they are lengthy and therefore omitted. First, we consider the case of putting one of the quarks and one of the antiquarks at the same coordinate.

Taking the limit $\mathbf{x} \rightarrow \mathbf{y}$ for each element of \mathcal{M} gives

$$\lim_{\mathbf{x} \rightarrow \mathbf{y}} \mathcal{M}^{(1,1)} = C_F \mathcal{G}'_{\mathbf{x}'\mathbf{y}'}, \quad (7.62)$$

$$\lim_{\mathbf{x} \rightarrow \mathbf{y}} \mathcal{M}^{(1,2)} = 0, \quad (7.63)$$

$$\lim_{\mathbf{x} \rightarrow \mathbf{y}} \mathcal{M}^{(2,2)} = \left(C_F - \frac{C_A}{2} \right) \mathcal{G}'_{\mathbf{x}'\mathbf{y}'} + \frac{C_A}{2} (\mathcal{G}'_{\mathbf{x}'\mathbf{y}} + \mathcal{G}'_{\mathbf{y}'\mathbf{y}}). \quad (7.64)$$

The off-diagonal elements of $\mathcal{A}(\eta)$ are expected to vanish in this limit because of the unitarity of the Wilson lines – this is consistent with Eq. (7.63). The matrix equation given in Eq. (7.46) therefore decouples into two separate equations. The equation for $\mathcal{A}^{(1,1)}(\eta)$, together with Eq. (7.62), reproduces the 2-point correlator parametrisation given in Eq. (7.15). The equation for $\mathcal{A}^{(2,2)}(\eta)$, together with Eq. (7.64), reproduces the 3-point correlator parametrisation given in Eq. (7.25). Any other limit besides $\mathbf{x} \rightarrow \mathbf{y}$ which puts one of the quarks and one of the antiquarks at the same coordinate gives the same results.

In addition to the first limit, we can also put the remaining quark and antiquark at the same coordinate. Then

$$\lim_{\substack{\mathbf{x} \rightarrow \mathbf{y} \\ \mathbf{x}' \rightarrow \mathbf{y}'}} \mathcal{M}^{(1,1)} = 0, \quad (7.65)$$

$$\lim_{\substack{\mathbf{x} \rightarrow \mathbf{y} \\ \mathbf{x}' \rightarrow \mathbf{y}'}} \mathcal{M}^{(2,2)} = C_A \mathcal{G}'_{\mathbf{y}'\mathbf{y}}. \quad (7.66)$$

The first line vanishes as expected. The second line is consistent with the dipole parametrisation Eq. (7.15) in the adjoint representation. These limits therefore show that the parametric equations for the 4-point correlators are consistent with those of the 2- and 3-point correlators.

The last set of limits that can be considered is $\mathbf{x} \rightarrow \mathbf{x}'$ and $\mathbf{y} \rightarrow \mathbf{y}'$, corresponding to the two quarks at one coordinate and the two antiquarks at another coordinate. To make sense of this, it is necessary to change from the basis in Eq. (7.36) to a third equivalent set

$$\left(\frac{1}{\sqrt{N_c(N_c+1)/2}} \begin{array}{c} \text{---} \text{---} \\ \text{---} \text{---} \\ \text{---} \text{---} \end{array} \begin{array}{c} \text{---} \text{---} \\ \text{---} \text{---} \\ \text{---} \text{---} \end{array} \begin{array}{c} \text{---} \text{---} \\ \text{---} \text{---} \\ \text{---} \text{---} \end{array} \begin{array}{c} \text{---} \text{---} \\ \text{---} \text{---} \\ \text{---} \text{---} \end{array} \right)^\top. \quad (7.67)$$

We have used

$$\begin{array}{c} \text{---} \text{---} \\ \text{---} \text{---} \end{array} \begin{array}{c} \text{---} \text{---} \\ \text{---} \text{---} \end{array} = \frac{1}{2} \left(\begin{array}{c} \text{---} \text{---} \\ \text{---} \text{---} \end{array} + \begin{array}{c} \text{---} \text{---} \\ \text{---} \text{---} \end{array} \right), \quad (7.68)$$

$$\begin{array}{c} \text{---} \text{---} \\ \text{---} \text{---} \end{array} \begin{array}{c} \text{---} \text{---} \\ \text{---} \text{---} \end{array} = \frac{1}{2} \left(\begin{array}{c} \text{---} \text{---} \\ \text{---} \text{---} \end{array} - \begin{array}{c} \text{---} \text{---} \\ \text{---} \text{---} \end{array} \right), \quad (7.69)$$

for symmetry and antisymmetry operators, respectively, following the notation of [104]. A more detailed discussion of this particular basis is given in [49].

7.4 6-point correlators

Next, we extend the method used to calculate the 4-point correlators to calculate the 6-point correlator consisting of three fundamental and three antifundamental Wilson lines. Two of these correlators, namely

$$\left\langle S_{xz}^{(2)} S_{zz'}^{(2)} S_{z'y}^{(2)} \right\rangle = \left\langle \frac{1}{N_c^3} \text{tr} \left(U_x U_z^\dagger \right) \text{tr} \left(U_z U_{z'}^\dagger \right) \text{tr} \left(U_{z'} U_y^\dagger \right) \right\rangle \quad (7.70)$$

and

$$\left\langle S_{xzz'yz'}^{(6)} \right\rangle = \left\langle \frac{1}{N_c} \text{tr} \left(U_x U_z^\dagger U_{z'} U_y^\dagger U_z U_{z'}^\dagger \right) \right\rangle, \quad (7.71)$$

appear in the NLO BK equation discussed in Section 3.3.3 and are therefore of particular interest. The full calculation of these correlators in the GA is provided in Paper [III], where they are also compared numerically to their counterparts in the large- N_c limit.

7.4.1 Matrix equation

In order to form the space of all 6-point correlators, the product of Wilson lines in Eq. (7.34) is extended to

$$U_x \otimes U_y^\dagger \otimes U_{x'} \otimes U_{y'}^\dagger \otimes U_{x''} \otimes U_{y''}^\dagger = \begin{array}{c} \text{---} \\ \text{---} \\ \text{---} \\ \text{---} \\ \text{---} \\ \text{---} \end{array} \begin{array}{c} \blacktriangleleft \\ \blacktriangleleft \\ \blacktriangleleft \\ \blacktriangleleft \\ \blacktriangleleft \\ \blacktriangleleft \end{array} \begin{array}{c} x \\ y \\ x' \\ y' \\ x'' \\ y'' \end{array}, \quad (7.72)$$

with open indices

$$\begin{array}{c} j \text{---} \\ k \text{---} \\ j' \text{---} \\ k' \text{---} \\ j'' \text{---} \\ k'' \text{---} \end{array} \begin{array}{c} \blacktriangleleft \\ \blacktriangleleft \\ \blacktriangleleft \\ \blacktriangleleft \\ \blacktriangleleft \\ \blacktriangleleft \end{array} \begin{array}{c} i \\ l \\ i' \\ l' \\ i'' \\ l'' \end{array}. \quad (7.73)$$

There are now six ways to join the endpoints on either side in a consistent way with the arrow directions to form multipliants. On the right side, for example, we can use one of the simple elements of the (not orthogonal) set

$$\mathbf{B}^{\text{sim}} := \left(\frac{1}{\sqrt{N_c^3}} \begin{array}{c} \curvearrowright \\ \curvearrowright \\ \curvearrowright \end{array}, \frac{1}{\sqrt{N_c^3}} \begin{array}{c} \curvearrowright \\ \curvearrowright \\ \curvearrowright \end{array}, \frac{1}{\sqrt{N_c^3}} \begin{array}{c} \curvearrowright \\ \curvearrowright \\ \curvearrowright \end{array}, \frac{1}{\sqrt{N_c^3}} \begin{array}{c} \curvearrowright \\ \curvearrowright \\ \curvearrowright \end{array}, \frac{1}{\sqrt{N_c^3}} \begin{array}{c} \curvearrowright \\ \curvearrowright \\ \curvearrowright \end{array}, \frac{1}{\sqrt{N_c^3}} \begin{array}{c} \curvearrowright \\ \curvearrowright \\ \curvearrowright \end{array} \right). \quad (7.74)$$

The two required operators from Eqs. (7.70) and (7.71) can be formed using B_1^{sim} and B_5^{sim} and then taking the appropriate coincidence limits, i.e.

$$S_{xy}^{(2)} S_{yx''}^{(2)} S_{x''y''}^{(2)} = (B_1^{\text{sim}})^\top \left[\lim_{\substack{x' \rightarrow y \\ y' \rightarrow x''}} \left(U_x \otimes U_y^\dagger \otimes U_{x'} \otimes U_{y'}^\dagger \otimes U_{x''} \otimes U_{y''}^\dagger \right) \right] B_1^{\text{sim}} \quad (7.75)$$

$$= \lim_{\substack{x' \rightarrow y \\ y' \rightarrow x''}} \frac{1}{N_c^3} \begin{array}{c} \curvearrowleft \\ \curvearrowleft \\ \curvearrowleft \end{array} \times \begin{array}{c} \color{blue}{\curvearrowright} \\ \color{green}{\curvearrowright} \\ \color{red}{\curvearrowright} \\ \color{blue}{\curvearrowright} \\ \color{green}{\curvearrowright} \\ \color{red}{\curvearrowright} \end{array} \times \begin{array}{c} \curvearrowright \\ \curvearrowright \\ \curvearrowright \end{array}, \quad (7.76)$$

and

$$S_{xzx'yzz'}^{(6)} = (B_1^{\text{sim}})^\top \left[\lim_{\substack{x' \rightarrow y \\ y' \rightarrow x''}} \left(U_x \otimes U_y^\dagger \otimes U_{x'} \otimes U_{y'}^\dagger \otimes U_{x''} \otimes U_{y''}^\dagger \right) \right] B_5^{\text{sim}} \quad (7.77)$$

$$= \lim_{\substack{x' \rightarrow y \\ y' \rightarrow x''}} \frac{1}{N_c} \begin{array}{c} \curvearrowleft \\ \curvearrowleft \\ \curvearrowleft \end{array} \times \begin{array}{c} \color{blue}{\curvearrowright} \\ \color{green}{\curvearrowright} \\ \color{red}{\curvearrowright} \\ \color{blue}{\curvearrowright} \\ \color{green}{\curvearrowright} \\ \color{red}{\curvearrowright} \end{array} \times \begin{array}{c} \curvearrowright \\ \curvearrowright \\ \curvearrowright \end{array}. \quad (7.78)$$

The exact transverse coordinate labels are different from those that appear in the 6-point correlators of the NLO BK equation. They have been relabelled here to be consistent with the labels from Section 7.3.

Natural basis

The natural extension of the orthonormal basis \mathbf{B} defined in Eq. (7.36) for the 4-point correlators is then

$$\mathbf{B}^{\text{nat}} := \left(\frac{1}{\sqrt{N_c^3}} \begin{array}{c} \curvearrowright \\ \curvearrowright \\ \curvearrowright \end{array}, \sqrt{\frac{1}{N_c d_\Lambda/4}} \begin{array}{c} \color{blue}{\curvearrowright} \\ \color{blue}{\curvearrowright} \\ \color{blue}{\curvearrowright} \end{array}, \sqrt{\frac{1}{N_c d_\Lambda/4}} \begin{array}{c} \color{blue}{\curvearrowright} \\ \color{blue}{\curvearrowright} \\ \color{blue}{\curvearrowright} \end{array}, \sqrt{\frac{1}{N_c d_\Lambda/4}} \begin{array}{c} \color{blue}{\curvearrowright} \\ \color{blue}{\curvearrowright} \\ \color{blue}{\curvearrowright} \end{array}, \sqrt{\frac{1}{-N_c d_\Lambda/8}} \begin{array}{c} \color{blue}{\curvearrowright} \\ \color{blue}{\curvearrowright} \\ \color{blue}{\curvearrowright} \end{array}, \sqrt{\frac{1}{C_d d_\Lambda/8}} \begin{array}{c} \color{blue}{\curvearrowright} \\ \color{blue}{\curvearrowright} \\ \color{blue}{\curvearrowright} \end{array} \right). \quad (7.79)$$

The black and white dots in the last two elements denote the antisymmetric and symmetric structure constants, $f^{abc} = -2i\text{tr}([t^a, t^b], t^c)$ and $d^{abc} = 2\text{tr}(\{t^a, t^b\}, t^c)$, respectively, so that

$$\begin{array}{c} \text{---} \\ \text{---} \\ \text{---} \end{array} \begin{array}{c} \text{---} \\ \bullet \\ \text{---} \end{array} = f^{abc} t_{i_1, l_1}^a t_{i_2, l_2}^b t_{i_3, l_3}^c \quad \text{and} \quad \begin{array}{c} \text{---} \\ \text{---} \\ \text{---} \end{array} \begin{array}{c} \text{---} \\ \circ \\ \text{---} \end{array} = d^{abc} t_{i_1, l_1}^a t_{i_2, l_2}^b t_{i_3, l_3}^c. \quad (7.80)$$

Using the Fierz identity given in Eq. (7.39), it is possible to write any of the elements in \mathbf{B}^{nat} solely in terms of the elements in \mathbf{B}^{sim} . Then the appropriate linear combinations of the elements of \mathbf{B}^{nat} can be used in place of B_1^{sim} and B_5^{sim} in Eqs. (7.70) and (7.71).

Similarly to the calculation of the 4-point correlators, Eq. (7.6) must now be used in the form

$$\partial_\eta \mathcal{A}(\eta) = -\mathcal{M} \mathcal{A}(\eta), \quad (7.81)$$

(cf. Eq. (7.46)) to calculate the parametric equations for each 6-point correlator. Since the basis is six-dimensional, Eq. (7.81) is a 6×6 matrix differential equation. If we proceed to solve it in the same way as the 4-point correlators in Section 7.3.3, we would need to exponentiate a 6×6 matrix. This is not feasible analytically, so we proceed in a different way.

Improved basis

The ultimate goal of the 6-point correlator calculation is to study those that appear in the NLO BK equation. We can therefore choose specific transverse coordinates that give the desired correlators in the end. From the analysis in Section 7.3.4 of the 4-point correlators in certain coincidence limits, we know that the parametric equations for the 6-point correlators must reduce consistently to the equations for the lower-point correlators already calculated. Since the particular 6-point correlators in the NLO BK equation already contain some redundancy in the transverse coordinates, this can be exploited using our knowledge of the lower-point correlators.

We begin with the assumption that, in the limits $\mathbf{x}' \rightarrow \mathbf{y}$ and $\mathbf{y}' \rightarrow \mathbf{x}''$, a basis \mathbf{B}^{imp} can be found such that one part of Eq. (7.81) reproduces the 2-point correlator equation and another independent part reproduces the 4-point correlator. This means that the transition matrix in Eq. (7.81) takes the block-diagonal form

$$\lim_{\substack{\mathbf{x}' \rightarrow \mathbf{y} \\ \mathbf{y}' \rightarrow \mathbf{x}''}} \mathcal{M} = \begin{pmatrix} \mathcal{M}_3^{(3 \times 3)} & 0 & 0 \\ 0 & \mathcal{M}_2^{(2 \times 2)} & 0 \\ 0 & 0 & \mathcal{M}_1^{(1 \times 1)} \end{pmatrix} \quad (7.82)$$

in this basis, where the dimensionality of each block is given as the superscript ($n \times n$). The resulting differential equation splits into three parts,

$$\partial_\eta \langle \mathcal{A}_3^{(3 \times 3)}(\eta) \rangle = - \langle \mathcal{M}_3^{(3 \times 3)} \mathcal{A}_3^{(3 \times 3)}(\eta) \rangle, \quad (7.83)$$

$$\partial_\eta \langle \mathcal{A}_2^{(2 \times 2)}(\eta) \rangle = - \langle \mathcal{M}_2^{(2 \times 2)} \mathcal{A}_2^{(2 \times 2)}(\eta) \rangle, \quad (7.84)$$

$$\partial_\eta \langle \mathcal{A}_1^{(1 \times 1)}(\eta) \rangle = - \langle \mathcal{M}_1^{(1 \times 1)} \mathcal{A}_1^{(1 \times 1)}(\eta) \rangle, \quad (7.85)$$

where each of the operator matrices can be formed from the basis \mathbf{B}^{imp} as

$$\mathcal{A}_3^{(3 \times 3)}(\eta) = (B_1^{\text{imp}}, B_2^{\text{imp}}, B_3^{\text{imp}})^\top \left[\lim_{\substack{x' \rightarrow y \\ y' \rightarrow x''}} (U_x \otimes U_y^\dagger \otimes U_{x'} \otimes U_{y'}^\dagger \otimes U_{x''} \otimes U_{y''}^\dagger) \right] \times (B_1^{\text{imp}}, B_2^{\text{imp}}, B_3^{\text{imp}}), \quad (7.86)$$

$$\mathcal{A}_2^{(2 \times 2)}(\eta) = (B_4^{\text{imp}}, B_5^{\text{imp}})^\top \left[\lim_{\substack{x' \rightarrow y \\ y' \rightarrow x''}} (U_x \otimes U_y^\dagger \otimes U_{x'} \otimes U_{y'}^\dagger \otimes U_{x''} \otimes U_{y''}^\dagger) \right] \times (B_4^{\text{imp}}, B_5^{\text{imp}}), \quad (7.87)$$

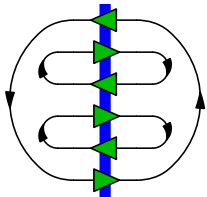
$$\mathcal{A}_1^{(1 \times 1)}(\eta) = (B_6^{\text{imp}})^\top \left[\lim_{\substack{x' \rightarrow y \\ y' \rightarrow x''}} (U_x \otimes U_y^\dagger \otimes U_{x'} \otimes U_{y'}^\dagger \otimes U_{x''} \otimes U_{y''}^\dagger) \right] B_6^{\text{imp}}. \quad (7.88)$$

The claim is that Eq. (7.88) reproduces the 2-point correlator parametrisation given in Eq. (7.15) and that Eq. (7.87) reproduces one of the 4-point correlator parametrisations given by Eq. (7.61) (with the transition matrix elements from Eqs. (7.57), (7.58) and (7.59)).

A systematic way to try to find the proposed basis \mathbf{B}^{imp} is to calculate each of the correlators

$$(B_i^{\text{sim}})^\top \left[\lim_{\substack{x' \rightarrow y \\ y' \rightarrow x''}} (U_x \otimes U_y^\dagger \otimes U_{x'} \otimes U_{y'}^\dagger \otimes U_{x''} \otimes U_{y''}^\dagger) \right] B_j^{\text{sim}} \quad (7.89)$$

for $1 \leq i, j \leq 6$, and see which of these reproduces the required lower-point correlator equations. Doing so gives

$$\lim_{\substack{x' \rightarrow y \\ y' \rightarrow x''}} \frac{1}{N_c^3} \left(\text{Diagram} \right) = \frac{1}{N_c} \text{tr} (U_x U_y^\dagger), \quad (7.90)$$


7. The Gaussian Approximation

for $i = j = 6$, which is just the 2-point correlator. So $B_6^{\text{imp}} := B_6^{\text{sim}}$. Next, we find two basis elements that are linearly independent of B_6^{sim} and that reproduce one of the 4-point correlator equations. These elements are found to be

$$B_4^{\text{imp}} := \frac{1}{\sqrt{2N_c d_A}} (-B_2^{\text{sim}} + B_3^{\text{sim}}), \quad (7.91)$$

$$B_5^{\text{imp}} := \frac{1}{\sqrt{2N_c d_A}} \left(-B_2^{\text{sim}} - B_3^{\text{sim}} + \frac{2}{N_c} B_6^{\text{sim}} \right). \quad (7.92)$$

The corresponding expression to Eq. (7.90) is a lengthy combination of various 6-point operators; how the 4-point correlator parametrisations emerge is shown in the next subsection. Finally, the last three elements of the improved basis can be chosen in any way such that they are orthonormal to B_4^{imp} , B_5^{imp} and B_6^{imp} . We choose

$$B_1^{\text{imp}} := \frac{1}{\sqrt{N_c^2 d_A C_d/2}} \left(\frac{N_c}{2} B_1^{\text{sim}} - B_2^{\text{sim}} - B_3^{\text{sim}} - B_4^{\text{sim}} + \frac{N_c}{2} B_5^{\text{sim}} + \frac{2}{N_c} B_6^{\text{sim}} \right), \quad (7.93)$$

$$B_2^{\text{imp}} := \frac{1}{\sqrt{2N_c d_A}} (-B_1^{\text{sim}} + B_5^{\text{sim}}), \quad (7.94)$$

$$B_3^{\text{imp}} := \frac{1}{\sqrt{N_c d_A}} \left(-B_4^{\text{sim}} + \frac{1}{N_c} B_6^{\text{sim}} \right). \quad (7.95)$$

The final basis choice is therefore

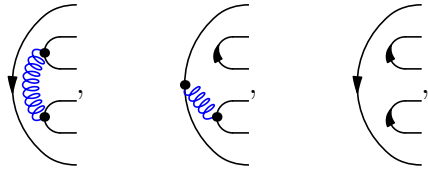
$$(\mathbf{B}^{\text{imp}})^{\top} := \begin{pmatrix} \frac{1}{\sqrt{N_c^2 d_A C_d/2}} \left[\frac{N_c}{2} \begin{matrix} \text{C} \\ \text{C} \end{matrix} - \begin{matrix} \text{C} \\ \text{C} \end{matrix} - \begin{matrix} \text{C} \\ \text{C} \end{matrix} - \begin{matrix} \text{C} \\ \text{C} \end{matrix} + \frac{N_c}{2} \begin{matrix} \text{C} \\ \text{C} \end{matrix} + \frac{2}{N_c} \begin{matrix} \text{C} \\ \text{C} \end{matrix} \right] \\ \frac{1}{\sqrt{2N_c d_A}} \begin{bmatrix} \text{C} \\ -\text{C} + \begin{matrix} \text{C} \\ \text{C} \end{matrix} \end{bmatrix} \\ \frac{1}{\sqrt{N_c d_A}} \begin{bmatrix} \text{C} \\ -\begin{matrix} \text{C} \\ \text{C} \end{matrix} + \frac{1}{N_c} \begin{matrix} \text{C} \\ \text{C} \end{matrix} \end{bmatrix} \\ \frac{1}{\sqrt{2N_c d_A}} \begin{bmatrix} \text{C} \\ -\begin{matrix} \text{C} \\ \text{C} \end{matrix} + \begin{matrix} \text{C} \\ \text{C} \end{matrix} \end{bmatrix} \\ \frac{1}{\sqrt{2N_c d_A}} \begin{bmatrix} \text{C} \\ -\begin{matrix} \text{C} \\ \text{C} \end{matrix} - \begin{matrix} \text{C} \\ \text{C} \end{matrix} + \frac{2}{N_c} \begin{matrix} \text{C} \\ \text{C} \end{matrix} \end{bmatrix} \\ \frac{1}{\sqrt{N_c^3}} \begin{matrix} \text{C} \\ \text{C} \end{matrix} \end{pmatrix}. \quad (7.96)$$

It is easier to see why this basis choice works to block-diagonalise the transition

matrix in the appropriate limits if the Fierz identity in Eq. (7.39) is used to write

$$(\mathbf{B}^{\text{imp}})^\top = \begin{pmatrix} \frac{1}{\sqrt{N_c^2 d_A C_d/2}} \left[N_c \begin{array}{c} \text{C} \\ \text{C} \end{array} + N_c \begin{array}{c} \text{C} \\ \text{C} \end{array} - 2 \begin{array}{c} \text{C} \\ \text{C} \end{array} - 2 \begin{array}{c} \text{C} \\ \text{C} \end{array} \right] \\ \frac{1}{\sqrt{2N_c d_A}} \left[2 \begin{array}{c} \text{C} \\ \text{C} \end{array} - 2 \begin{array}{c} \text{C} \\ \text{C} \end{array} \right] \\ \frac{1}{\sqrt{N_c d_A}} \left[-2 \begin{array}{c} \text{C} \\ \text{C} \end{array} \right] \\ \frac{1}{\sqrt{2N_c d_A}} \left[2 \begin{array}{c} \text{C} \\ \text{C} \end{array} + \begin{array}{c} \text{C} \\ \text{C} \end{array} \right] \\ \frac{1}{\sqrt{2N_c d_A}} \left[-2 \begin{array}{c} \text{C} \\ \text{C} \end{array} - 2 \begin{array}{c} \text{C} \\ \text{C} \end{array} \right] \\ \frac{1}{\sqrt{N_c^3}} \begin{array}{c} \text{C} \\ \text{C} \end{array} \end{pmatrix}. \quad (7.97)$$

In particular, notice that the bottom three elements contain the diagrams



$$\begin{array}{c} \text{Diagram 1} \\ \text{Diagram 2} \\ \text{Diagram 3} \end{array}, \quad (7.98)$$

which all reduce to basis elements from the 2- and 4-point correlator calculations in the limits $\mathbf{x}' \rightarrow \mathbf{y}, \mathbf{y}' \rightarrow \mathbf{x}''$. This is why \mathbf{B}^{imp} results in a block-diagonalised transition matrix in these limits.

7.4.2 Transition matrix

Using \mathbf{B}^{imp} as a basis to calculate Eq. (7.81) in the same way as for the 4-point correlators results in a transition matrix of the form given in Eq. (7.82):

$$\lim_{\substack{\mathbf{x}' \rightarrow \mathbf{y} \\ \mathbf{y}' \rightarrow \mathbf{x}''}} \mathcal{M} = \begin{pmatrix} \mathcal{M}_3^{(3 \times 3)} & 0 & 0 \\ 0 & \mathcal{M}_2^{(2 \times 2)} & 0 \\ 0 & 0 & \mathcal{M}_1^{(1 \times 1)} \end{pmatrix}, \quad (7.99)$$

where

$$\mathcal{M}_1 = C_F \mathcal{G}'_{\mathbf{x}, \mathbf{y}} \quad (7.100)$$

and

$$\mathcal{M}_2 = \frac{N_c}{4} \begin{pmatrix} \mathcal{M}_2^{(1,1)} & \mathcal{M}_2^{(1,2)} \\ \mathcal{M}_2^{(1,2)} & \mathcal{M}_2^{(2,2)} \end{pmatrix}, \quad (7.101)$$

with

$$\mathcal{M}_2^{(1,1)} = \mathcal{M}_2^{(2,2)} = \mathcal{G}'_{x,z} + \mathcal{G}'_{y,z} - \frac{2}{N_c^2} \mathcal{G}'_{x,y} + \mathcal{G}'_{x,z'} + \mathcal{G}'_{y,z'}, \quad (7.102)$$

$$\mathcal{M}_2^{(1,2)} = \mathcal{G}'_{x,z} + \mathcal{G}'_{y,z} - \mathcal{G}'_{x,z'} - \mathcal{G}'_{y,z'}. \quad (7.103)$$

These can be shown to agree with the transition matrices for the 2- and 4-point correlators, respectively. For the 3×3 transition sub-matrix in Eq. (7.99), we get

$$\mathcal{M}_3 = \begin{pmatrix} \frac{N_c}{4} \Gamma'_1 & \frac{\sqrt{N_c C_d}}{4} \Gamma'_2 & 0 \\ \frac{\sqrt{N_c C_d}}{4} \Gamma'_2 & \frac{N_c}{4} \Gamma'_1 & -\frac{1}{\sqrt{2}} \Gamma'_2 \\ 0 & -\frac{1}{\sqrt{2}} \Gamma'_2 & \Gamma'_0 \end{pmatrix}, \quad (7.104)$$

where

$$\Gamma_0 := C_F \mathcal{G}_{x,y} + N_c \mathcal{G}_{z,z'}, \quad (7.105)$$

$$\Gamma_1 := \mathcal{G}_{x,z} + \mathcal{G}_{y,z} - \frac{2}{N_c^2} \mathcal{G}_{x,y} + \mathcal{G}_{x,z'} + \mathcal{G}_{y,z'} + 2\mathcal{G}_{z,z'}, \quad (7.106)$$

$$\Gamma_2 := \mathcal{G}_{x,z} - \mathcal{G}_{y,z} - \mathcal{G}_{x,z'} + \mathcal{G}_{y,z'}, \quad (7.107)$$

and $\Gamma'_i := \partial_\eta \Gamma_i$ for $i = 0, 1, 2$. This is needed to find the 6-point correlators for the NLO BK equation.

7.4.3 Differential equation solutions

With the transition matrix in block-diagonal form, Eq. (7.81) separates into Eqs. (7.83), (7.84) and (7.85). These can be solved independently from one another following the procedure from Section 7.3.3.

1×1 equation

First, we solve the simple one-dimensional equation by using Eq. (7.100) in Eq. (7.85) to get

$$\partial_\eta \langle \mathcal{A}_1(\eta) \rangle = - \langle C_F \mathcal{G}'_{x,y} \mathcal{A}_1(\eta) \rangle. \quad (7.108)$$

Using Eq. (7.88) gives

$$\mathcal{A}_1(\eta) = \lim_{\substack{\mathbf{x}' \rightarrow \mathbf{y} \\ \mathbf{y}' \rightarrow \mathbf{x}''}} \frac{1}{N_c^3} \left(\text{Diagram} \right) = \frac{1}{N_c} \text{tr} (U_{\mathbf{x}} U_{\mathbf{y}}^\dagger), \quad (7.109)$$

as already seen in Eq. (7.90). This leads to the solution

$$\left\langle \frac{1}{N_c} \text{tr} (U_{\mathbf{x}} U_{\mathbf{y}}^\dagger) \right\rangle = \exp \{-C_F \mathcal{G}_{\mathbf{x}\mathbf{y}}(\eta)\}, \quad (7.110)$$

which is exactly the 2-point correlator parametrisation in Eq. (7.15).

2 × 2 equation

Next, we solve the 2 × 2 matrix equation by using Eq. (7.101) in Eq. (7.84) to get

$$\partial_\eta \langle \mathcal{A}_2(\eta) \rangle = - \left\langle \frac{N_c}{4} \begin{pmatrix} \mathcal{M}_2^{(1,1)} & \mathcal{M}_2^{(1,2)} \\ \mathcal{M}_2^{(1,2)} & \mathcal{M}_2^{(2,2)} \end{pmatrix} \mathcal{A}_2(\eta) \right\rangle. \quad (7.111)$$

The explicit elements of the correlator matrix $\langle \mathcal{A}_2(\eta) \rangle$ contain cumbersome linear combinations of various six-point operators. They are provided in diagrammatic form in the appendix of Paper [III]. After some simplification, they may be written as

$$\begin{aligned} \mathcal{A}_2^{(1,1)}(\eta) &= \mathcal{A}_2^{(2,2)}(\eta) \\ &= \frac{1}{2d_A} \left[\text{tr} (U_{\mathbf{y}} U_{\mathbf{y}''}^\dagger) \text{tr} (U_{\mathbf{x}} U_{\mathbf{y}}^\dagger) - \frac{2}{N_c} \text{tr} (U_{\mathbf{y}''}^\dagger U_{\mathbf{x}}) + \text{tr} (U_{\mathbf{x}''} U_{\mathbf{y}''}^\dagger) \text{tr} (U_{\mathbf{x}} U_{\mathbf{x}''}^\dagger) \right], \end{aligned} \quad (7.112)$$

$$\begin{aligned} \mathcal{A}_2^{(1,2)}(\eta) &= \mathcal{A}_2^{(2,1)}(\eta) \\ &= \frac{1}{2d_A} \left[\text{tr} (U_{\mathbf{y}} U_{\mathbf{y}''}^\dagger) \text{tr} (U_{\mathbf{x}} U_{\mathbf{y}}^\dagger) - \text{tr} (U_{\mathbf{x}''} U_{\mathbf{y}''}^\dagger) \text{tr} (U_{\mathbf{x}} U_{\mathbf{x}''}^\dagger) \right]. \end{aligned} \quad (7.113)$$

For the single trace term in Eq. (7.112), the parametrisation of the dipole correlator given in Eq. (7.15) can be used to rewrite the trace as an exponential of \mathcal{G} . Using the rigid exponentiation method, the solution of Eq. (7.111) is found to be

$$\begin{aligned} \mathcal{A}_2(\eta) &= \frac{1}{2} e^{\frac{1}{2N_c} \mathcal{G}_{\mathbf{x}\mathbf{y}''}} \\ &\times \begin{pmatrix} e^{-\frac{N_c}{2} (\mathcal{G}_{\mathbf{x}\mathbf{x}''} + \mathcal{G}_{\mathbf{x}''\mathbf{y}''})} + e^{-\frac{N_c}{2} (\mathcal{G}_{\mathbf{x}\mathbf{y}} + \mathcal{G}_{\mathbf{y}\mathbf{y}''})} & -e^{-\frac{N_c}{2} (\mathcal{G}_{\mathbf{x}\mathbf{x}''} + \mathcal{G}_{\mathbf{x}''\mathbf{y}''})} + e^{-\frac{N_c}{2} (\mathcal{G}_{\mathbf{x}\mathbf{y}} + \mathcal{G}_{\mathbf{y}\mathbf{y}''})} \\ -e^{-\frac{N_c}{2} (\mathcal{G}_{\mathbf{x}\mathbf{x}''} + \mathcal{G}_{\mathbf{x}''\mathbf{y}''})} + e^{-\frac{N_c}{2} (\mathcal{G}_{\mathbf{x}\mathbf{y}} + \mathcal{G}_{\mathbf{y}\mathbf{y}''})} & e^{-\frac{N_c}{2} (\mathcal{G}_{\mathbf{x}\mathbf{x}''} + \mathcal{G}_{\mathbf{x}''\mathbf{y}''})} + e^{-\frac{N_c}{2} (\mathcal{G}_{\mathbf{x}\mathbf{y}} + \mathcal{G}_{\mathbf{y}\mathbf{y}''})} \end{pmatrix}. \end{aligned} \quad (7.114)$$

7. The Gaussian Approximation

In order to reconcile this with the 4-point correlator expressions from Section 7.3, the particular elements in the operator matrix

$$\begin{pmatrix} \frac{1}{N_c^2} \text{diagram} & \frac{1}{N_c \sqrt{d_A/4}} \text{diagram} \\ \frac{1}{N_c \sqrt{d_A/4}} \text{diagram} & \frac{1}{d_A/4} \text{diagram} \end{pmatrix} \quad (7.115)$$

given in Eq. (7.41) need to be extracted from $\mathcal{A}_2(\eta)$. This can be achieved by taking the sum of $\mathcal{A}_2^{(1,1)}(\eta)$ and $\mathcal{A}_2^{(1,2)}(\eta)$ to get

$$\begin{aligned} \left\langle \frac{1}{N_c^2} \text{diagram} \right\rangle_{\substack{x'=y \\ y'=y''}} &= \left\langle \frac{1}{N_c^2} \text{tr} (U_{\mathbf{y}} U_{\mathbf{y}''}^\dagger) \text{tr} (U_{\mathbf{x}} U_{\mathbf{y}}^\dagger) \right\rangle \\ &= \frac{2C_F}{N_c} \exp \left\{ \frac{1}{2N_c} \mathcal{G}_{\mathbf{x}\mathbf{y}''} \right\} \exp \left\{ -\frac{N_c}{2} (\mathcal{G}_{\mathbf{x}\mathbf{y}} + \mathcal{G}_{\mathbf{y}\mathbf{y}''}) \right\} + \frac{1}{N_c^2} \exp \{-C_F \mathcal{G}_{\mathbf{x}\mathbf{y}''}\}. \end{aligned} \quad (7.116)$$

This is the same as the explicit solution for the top left element of Eq. (7.115) that is provided in [49], which means that our calculation of \mathcal{A}_2 is consistent with the 4-point correlator parametrisations. The other expression that follows from Eq. (7.114) comes from the difference of $\mathcal{A}_2^{(1,1)}(\eta)$ and $\mathcal{A}_2^{(1,2)}(\eta)$ and leads to the same expression shown in Eq. (7.116).

3 × 3 equation

Finally, the last matrix differential equation is found by using Eq. (7.103) in Eq. (7.83) to get

$$\partial_\eta \langle \mathcal{A}_3(\eta) \rangle = - \left\langle \left(\begin{pmatrix} \frac{N_c}{4} \Gamma'_1 & \frac{\sqrt{N_c C_d}}{4} \Gamma'_2 & 0 \\ \frac{\sqrt{N_c C_d}}{4} \Gamma'_2 & \frac{N_c}{4} \Gamma'_1 & -\frac{1}{\sqrt{2}} \Gamma'_2 \\ 0 & -\frac{1}{\sqrt{2}} \Gamma'_2 & \Gamma'_0 \end{pmatrix} \mathcal{A}_3(\eta) \right) \right\rangle. \quad (7.117)$$

Since the solution is the matrix exponentiation of a 3×3 matrix, it can be found analytically. Recall that this is only possible due to our choice of basis \mathbf{B}^{imp} , which allowed us to block-diagonalise the full 6×6 transition matrix and separate the full matrix equation into three independent pieces.

The exponentiation of the 3×3 transition matrix \mathcal{M}_3 is straightforward and the result is provided in Section III.D of Paper [III]. Despite the lengthy expressions contained there, notice that there are only simple functions of \mathcal{G} . This means that, even though the parametric equations may be tedious to extract, the procedure is

straightforward algebraically. In a similar way that Eq. (7.116) was found from the solution of the 2×2 matrix differential equation, the relevant correlators

$$\left\langle S_{\mathbf{x}\mathbf{y}}^{(2)} S_{\mathbf{y}\mathbf{x}''}^{(2)} S_{\mathbf{x}''\mathbf{y}''}^{(2)} \right\rangle = \lim_{\substack{\mathbf{x}' \rightarrow \mathbf{y} \\ \mathbf{y}' \rightarrow \mathbf{x}''}} \left\langle \frac{1}{N_c^3} \left[\text{Diagram} \right] \right\rangle, \quad (7.118)$$

$$\left\langle S_{\mathbf{x}\mathbf{z}\mathbf{x}'\mathbf{y}\mathbf{z}\mathbf{z}'}^{(6)} \right\rangle = \lim_{\substack{\mathbf{x}' \rightarrow \mathbf{y} \\ \mathbf{y}' \rightarrow \mathbf{x}''}} \left\langle \frac{1}{N_c} \left[\text{Diagram} \right] \right\rangle \quad (7.119)$$

can be extracted from the solution of the 3×3 matrix equation. This procedure is explained in Section III.E of Paper [III]. Once these expressions are found, the dipole parametrisation may be used to write

$$\mathcal{G}_{\mathbf{x}\mathbf{y}} = -\frac{1}{C_F} \ln \left\langle \frac{1}{N_c} \text{tr} (U_{\mathbf{x}} U_{\mathbf{y}}^\dagger) \right\rangle. \quad (7.120)$$

This can be substituted into the parametric equation for any other correlator that is written in terms of \mathcal{G} , thereby relating higher-order correlators to the dipole.

The 6-point correlator calculation has been verified in all possible coincidence limits, in the same way that the 4-point correlator calculation was checked in Section 7.3.4. Particular coordinate configurations have also been used to study the final parametric equations, in order to get an idea of the behaviour of the 6-point correlators in the NLO BK equation. These results, as well as the numerical implementation of the analytical calculation in the NLO BK equation, are shown in Section IV of Paper [III].

Chapter summary

In this chapter, we have used the GA to truncate the evolution equations for Wilson line correlators. We have demonstrated how this is used to calculate simple correlators, such as the 2- and 3-point correlators. We have also discussed the calculation of the 4-point correlators from [49], since the same method was used to study the 6-point correlators. In the latter case, the ability to find a particular multiplet basis when there are only four distinct transverse coordinates, allowed us to simplify the calculation substantially. This led to explicit analytical expressions for the 6-point correlators, particularly those found in the NLO BK equation.

8

Beyond the Gaussian Approximation

In Chapter 7, the GA was used to calculate several Wilson line correlators. In this chapter, we introduce an extension to the GA and use it to study the 2-, 3- and 4-point correlators of Chapter 7. Ultimately, the goal is to obtain the odderon equation studied in Paper [I]. The odderon, as first suggested in [105], is the charge-parity-odd (C-odd) counterpart to the pomeron. This defining characteristic of the odderon is necessary, for example, to account for the production of colourless C-even states such as the neutral pion in exclusive DIS. Since the calculational details of the odderon evolution equation are not discussed in the paper, we provide them here. For the numerical implementation, the reader is referred in particular to Sections VI and VII of Paper [I].

We begin this chapter by introducing the extended Gaussian approximation (eGA) and then studying its properties in Section 8.1. In Section 8.2, the eGA is used to calculate 4-point correlators. In Section 8.3, we discuss the emergence of the odderon as a consequence of the extension of the GA and its effect on the parametrisations of the 2- and 3-point correlators.

8.1 The extended GA operator

Recall Eq. (7.6),

$$\partial_\eta \langle \mathcal{O}[U] \rangle (\eta) = \left\langle -\frac{1}{2} \int_{uv} G_{uv}(\bar{\eta}) L_u^a L_v^a \mathcal{O}[U] \right\rangle (\eta), \quad (8.1)$$

which was used to calculate various correlators in the previous chapter. For the dipole correlator of Section 7.2.1, for example, we solved the differential equation

$$\partial_\eta \left\langle \frac{1}{N_c} \left[\text{Diagram: Wilson line with a loop} \right] \right\rangle = \left\langle -\frac{1}{2} \frac{1}{N_c} \left[\text{Diagram: Wilson line with a loop and a ghost line} \right] \times \int_{uv} G_{uv}(\bar{\eta}) L_u^a L_v^a \times \left[\text{Diagram: Wilson line with a loop} \right] \right\rangle \quad (8.2)$$

$$\sim \left\langle \left[\text{Diagram: Wilson line with a loop and a ghost line} \right] \right\rangle, \quad (8.3)$$

to obtain the dipole parametrisation. The so-called transition matrix was calculated by operating with the GA operator

$$G_{uv}(\bar{\eta}) L_u^a L_v^a \sim \left[\text{Diagram: Wilson line with a loop and a ghost line} \right]. \quad (8.4)$$

The simplest extension to this operator would be the inclusion of other products of two Lie derivatives. The inclusion of an $R_u^a R_v^a$ term is trivial, since the operation of L_u^a and R_u^a on the same Wilson line is effectively the same, up to a sign. Instead of Eq. (8.1), we would have

$$\partial_\eta \langle \mathcal{O}[U] \rangle (\eta) = \left\langle -\frac{1}{2} \int_{uv} G_{uv}(\bar{\eta}) \frac{1}{2} (L_u^a L_v^a + R_u^a R_v^a) \mathcal{O}[U] \right\rangle (\eta) \quad (8.5)$$

and the physics discussions of the previous chapter do not change significantly. On the other hand, the inclusion of mixed terms $L_u^a R_v^a$ and $R_u^a L_v^a$ is more complicated, since this introduces a gluon interaction with the target. Since there is little experimental motivation to consider such an addition to the GA, we do not proceed in this direction.

Instead, we introduce a 3-point function to the right side of Eq. (8.1). For the dipole correlator, for example, this would add contributions of the type

$$\left[\text{Diagram: Wilson line with a loop and a ghost line, black dot} \right] \quad \text{and} \quad \left[\text{Diagram: Wilson line with a loop and a ghost line, white dot} \right] \quad (8.6)$$

to Eq. (8.4). These diagrams contain an antisymmetric structure constant f^{abc} at each three-gluon vertex, denoted by a large black dot. Symmetric contributions

$$\left[\text{Diagram: Wilson line with a loop and a ghost line, white dot} \right] \quad \text{and} \quad \left[\text{Diagram: Wilson line with a loop and a ghost line, black dot} \right] \quad (8.7)$$

also need to be considered, where the three-gluon vertex now has a large white dot for each factor d^{abc} . Contributions of these types may be included in the definition of the parametrisation according to

$$\begin{aligned} \partial_\eta \langle \mathcal{O}[U] \rangle (\eta) = & \left\langle - \left[\frac{1}{2} \int_{\mathbf{uv}} G_{\mathbf{uv}}(\bar{\eta}) L_{\mathbf{u}}^a L_{\mathbf{v}}^a \right. \right. \\ & \left. \left. + \int_{\mathbf{uvw}} [f^{abc} G_{\mathbf{uvw}}^f(\bar{\eta}) + d^{abc} G_{\mathbf{uvw}}^d(\bar{\eta})] L_{\mathbf{u}}^a L_{\mathbf{v}}^b L_{\mathbf{w}}^c \right] \mathcal{O}[U] \right\rangle (\eta). \end{aligned} \quad (8.8)$$

The various terms are referred to henceforth as the

- GA operator $G_{\mathbf{uv}}(\bar{\eta}) L_{\mathbf{u}}^a L_{\mathbf{v}}^a$
- antisymmetric eGA operator $f^{abc} G_{\mathbf{uvw}}^f(\bar{\eta}) L_{\mathbf{u}}^a L_{\mathbf{v}}^b L_{\mathbf{w}}^c$
- symmetric eGA operator $d^{abc} G_{\mathbf{uvw}}^d(\bar{\eta}) L_{\mathbf{u}}^a L_{\mathbf{v}}^b L_{\mathbf{w}}^c$.

As with the 2-point function, the explicit rapidity dependence of the 3-point functions are suppressed henceforth for clarity.

At this stage, the symmetry properties of the 3-point functions G^f and G^d in Eq. (8.8) are not known. They can be found by first writing G^f and G^d as linear combinations of all possible permutations of the transverse coordinates:

$$\begin{aligned} G_{\mathbf{uvw}}^f L_{\mathbf{u}}^a L_{\mathbf{v}}^b L_{\mathbf{w}}^c \longrightarrow & \frac{1}{6} \left[G_{\mathbf{uvw}}^f L_{\mathbf{u}}^a L_{\mathbf{v}}^b L_{\mathbf{w}}^c + G_{\mathbf{vuw}}^f L_{\mathbf{v}}^a L_{\mathbf{w}}^b L_{\mathbf{u}}^c + G_{\mathbf{wuv}}^f L_{\mathbf{w}}^a L_{\mathbf{u}}^b L_{\mathbf{v}}^c \right. \\ & \left. + G_{\mathbf{uvw}}^f L_{\mathbf{u}}^a L_{\mathbf{w}}^b L_{\mathbf{v}}^c + G_{\mathbf{vuw}}^f L_{\mathbf{v}}^a L_{\mathbf{u}}^b L_{\mathbf{w}}^c + G_{\mathbf{wvu}}^f L_{\mathbf{w}}^a L_{\mathbf{v}}^b L_{\mathbf{u}}^c \right], \end{aligned} \quad (8.9)$$

$$\begin{aligned} G_{\mathbf{uvw}}^d L_{\mathbf{u}}^a L_{\mathbf{v}}^b L_{\mathbf{w}}^c \longrightarrow & \frac{1}{6} \left[G_{\mathbf{uvw}}^d L_{\mathbf{u}}^a L_{\mathbf{v}}^b L_{\mathbf{w}}^c + G_{\mathbf{vuw}}^d L_{\mathbf{v}}^a L_{\mathbf{w}}^b L_{\mathbf{u}}^c + G_{\mathbf{wuv}}^d L_{\mathbf{w}}^a L_{\mathbf{u}}^b L_{\mathbf{v}}^c \right. \\ & \left. + G_{\mathbf{uvw}}^d L_{\mathbf{u}}^a L_{\mathbf{w}}^b L_{\mathbf{v}}^c + G_{\mathbf{vuw}}^d L_{\mathbf{v}}^a L_{\mathbf{u}}^b L_{\mathbf{w}}^c + G_{\mathbf{wvu}}^d L_{\mathbf{w}}^a L_{\mathbf{v}}^b L_{\mathbf{u}}^c \right]. \end{aligned} \quad (8.10)$$

The positions of the coordinate indices on the G 's in these expressions should now be taken literally. In order to make these expressions more manageable, all coordinate and colour indices are ordered so that an overall $L_{\mathbf{u}}^a L_{\mathbf{v}}^b L_{\mathbf{w}}^c$ can be factored out.

8.1.1 Ordering transverse coordinates

To order the transverse coordinates $\mathbf{u}, \mathbf{v}, \mathbf{w}$, we make use of the commutator written as

$$[L_{\mathbf{u}}^a, L_{\mathbf{v}}^b] = i f^{abd} \delta_{\mathbf{uv}} L_{\mathbf{u}}^d = \frac{1}{2} i f^{abd} \delta_{\mathbf{uv}} (L_{\mathbf{u}}^d + L_{\mathbf{v}}^d), \quad (8.11)$$

As an example, the fifth term in Eq. (8.9) becomes

$$G_{vuw}^f L_v^a L_u^b L_w^c = G_{vuw}^f (L_u^b L_v^a + [L_v^a, L_u^b]) L_w^c \quad (8.12)$$

$$= G_{vuw}^f \left(L_u^b L_v^a + \frac{1}{2} i f^{abd} \delta_{uv} (L_u^d + L_v^d) \right) L_w^c \quad (8.13)$$

$$= G_{vuw}^f L_u^b L_v^a L_w^c + \frac{1}{2} i f^{abd} (G_{uuw}^f L_u^d L_w^c + G_{vvw}^f L_v^d L_w^c). \quad (8.14)$$

Notice that for each use of the commutator, two new terms are introduced, both of which contain only two coordinate indices. We write

$$f^{abc} G_{uvw}^f L_u^a L_v^b L_w^c \longrightarrow (\hat{G}^{f2} + \hat{G}^{f3}), \quad (8.15)$$

where \hat{G}^{f2} contains terms with two Lie derivatives and \hat{G}^{f3} contains terms with three Lie derivatives. Explicitly, the resulting expressions from Eq. (8.9) are

$$\begin{aligned} \hat{G}^{f2} := & \frac{1}{12} i f^{abc} [f^{acd} (G_{uuu}^f L_u^d L_w^b + G_{vvv}^f L_v^d L_w^b) \\ & + f^{bcd} (G_{vuu}^f L_v^a L_u^d + G_{vww}^f L_v^a L_w^d) + f^{abd} (G_{uuu}^f L_u^d L_v^c + G_{www}^f L_w^d L_v^c) \\ & + f^{acd} (G_{vvv}^f L_u^b L_v^d + G_{wuu}^f L_u^b L_w^d) + f^{bcd} (G_{uvv}^f L_u^a L_v^d + G_{uww}^f L_u^a L_w^d) \\ & + f^{abd} (G_{uuu}^f L_u^d L_w^c + G_{vvv}^f L_v^d L_w^c) + f^{bcd} (G_{wuu}^f L_w^a L_u^d + G_{wvv}^f L_w^a L_v^d) \\ & + f^{acd} (G_{vvv}^f L_u^d L_v^b + G_{wvv}^f L_w^d L_v^b) + f^{abd} (G_{vuu}^f L_u^c L_v^d + G_{wuu}^f L_u^c L_w^d)] \quad (8.16) \end{aligned}$$

and

$$\begin{aligned} \hat{G}^{f3} := & \frac{1}{6} f^{abc} [G_{uvw}^f L_u^a L_v^b L_w^c + G_{vuw}^f L_u^c L_v^a L_w^b + G_{wuv}^f L_u^b L_v^c L_w^a \\ & + G_{uvw}^f L_u^a L_v^c L_w^b + G_{vuw}^f L_u^b L_v^a L_w^c + G_{wuv}^f L_u^c L_v^b L_w^a]. \quad (8.17) \end{aligned}$$

For Eq. (8.10), the result is simpler because each time the commutator is used to reorder coordinates, terms with a factor f^{abc} cancel with the overall factor d^{abc} . Therefore, only terms with three distinct coordinates can survive:

$$\begin{aligned} d^{abc} G_{uvw}^d L_u^a L_v^b L_w^c \longrightarrow \hat{G}^d := & \frac{1}{6} d^{abc} [G_{uvw}^d L_u^a L_v^b L_w^c + G_{wuv}^d L_u^b L_v^c L_w^a \\ & + G_{vuw}^d L_u^c L_v^a L_w^b + G_{uuv}^d L_u^a L_v^c L_w^b + G_{vuu}^d L_u^b L_v^a L_w^c + G_{wvu}^d L_u^c L_v^b L_w^a]. \quad (8.18) \end{aligned}$$

8.1.2 Ordering colour indices

The reshuffling of coordinate indices in \hat{G}^{f2} , \hat{G}^{f3} and \hat{G}^d results in colour indices becoming disordered. This can be fixed using the antisymmetry and symmetry of

the structure constants f^{abc} and d^{abc} , respectively. For the operator \hat{G}^{f2} , every term in Eq. (8.16) has only two coordinates, which can be relabelled as follows. In terms containing \mathbf{u} and \mathbf{w} , we replace $\mathbf{w} \rightarrow \mathbf{v}$; in terms containing \mathbf{v} and \mathbf{w} , we replace $\mathbf{w} \rightarrow \mathbf{u}$. Then Eq. (8.16) becomes

$$\begin{aligned} \hat{G}^{f2} = & \frac{1}{12} i f^{abc} [f^{acd} (2G_{uvu}^f L_u^d L_v^b + G_{uvu}^f L_u^d L_v^b + 2G_{vuv}^f L_u^b L_v^d + G_{vuv}^f L_v^d L_u^b) \\ & + 3f^{bcd} (G_{uvv}^f L_u^a L_v^d + G_{vuu}^f L_v^a L_u^d) + f^{abd} (3G_{uuv}^f L_u^d L_v^c + 2G_{vuv}^f L_u^c L_v^d \\ & + G_{vuv}^f L_v^d L_u^c)]. \end{aligned} \quad (8.19)$$

Each f^{abc} can be written as a difference of traces as $f^{abc} = -2i [\text{tr}(t^a t^b t^c) - \text{tr}(t^a t^c t^b)]$. Using the Fierz identity from Eq. (7.39) and simplifying each trace gives

$$\begin{aligned} \hat{G}^{f2} = & \frac{iN_c}{6} [-2G_{uvu}^f L_u^b L_v^b - G_{uvu}^f L_u^b L_v^b - 2G_{vuv}^f L_u^b L_v^b - G_{vuv}^f L_v^b L_u^b \\ & + 3G_{uvv}^f L_u^a L_v^a + 3G_{vuu}^f L_v^a L_u^a + 3G_{uuv}^f L_u^c L_v^c + 2G_{vuv}^f L_u^c L_v^c + G_{vuv}^f L_v^c L_u^c]. \end{aligned} \quad (8.20)$$

Since $[L_u^a, L_v^a] = 0$, the product of Lie derivatives can be written in terms of the anticommutator $\frac{1}{2}\{L_u^a, L_v^a\} = L_u^a L_v^a$ in order to highlight the symmetry of the term. Then

$$\hat{G}^{f2} = \frac{iN_c}{4} G_{uv}^{(2)} \{L_u^a, L_v^a\}, \quad (8.21)$$

where

$$G_{uv}^{(2)} := G_{uuv}^f - G_{uvu}^f + G_{vuu}^f + (\mathbf{u} \leftrightarrow \mathbf{v}). \quad (8.22)$$

In the expressions for \hat{G}^{f3} and \hat{G}^d , all colour indices are contracted within each term, so these can be relabelled and the colour indices in the Lie derivatives can be reordered. This results in

$$\hat{G}^{f3} = \frac{1}{6} f^{abc} (G_{uvw}^f + G_{vuw}^f + G_{wuv}^f - G_{uuv}^f - G_{vuv}^f - G_{wvu}^f) L_u^a L_v^b L_w^c, \quad (8.23)$$

$$\hat{G}^d = \frac{1}{6} d^{abc} (G_{uvw}^f + G_{vuw}^f + G_{wuv}^f + G_{uuv}^f + G_{vuv}^f + G_{wvu}^f) L_u^a L_v^b L_w^c. \quad (8.24)$$

8.1.3 Symmetry properties of the final eGA operator

So far, we have simple explicit expressions for \hat{G}^{f2} , \hat{G}^{f3} and \hat{G}^d , as given by Eqs. (8.21), (8.23) and (8.24), respectively. The next step is to determine the

symmetry properties of these three objects. Such information is very useful when lengthy expressions in the calculation of correlators need to be simplified.

Recall the symmetry and antisymmetry operators

$$\begin{array}{|} \hline \hline \hline \hline \\ \hline \end{array} = \frac{1}{2} \left(\begin{array}{|} \hline \hline \hline \hline \\ \hline \end{array} + \begin{array}{|} \hline \hline \hline \hline \\ \hline \end{array} \right), \quad (8.25)$$

$$\begin{array}{|} \hline \hline \hline \hline \\ \hline \end{array} = \frac{1}{2} \left(\begin{array}{|} \hline \hline \hline \hline \\ \hline \end{array} - \begin{array}{|} \hline \hline \hline \hline \\ \hline \end{array} \right), \quad (8.26)$$

from Eqs. (7.68) and (7.69), respectively. These can be extended to any number of objects. For example,

$$\begin{array}{|} \hline \hline \hline \hline \\ \hline \end{array} \quad \text{and} \quad \begin{array}{|} \hline \hline \hline \hline \\ \hline \end{array} \quad (8.27)$$

are the symmetric and antisymmetric linear combinations of three objects. With these, it can be shown [104] that any set of three objects can be written as

$$\begin{array}{|} \hline \hline \hline \hline \\ \hline \end{array} = \begin{array}{|} \hline \hline \hline \hline \\ \hline \end{array} + \frac{4}{3} \begin{array}{|} \hline \hline \hline \hline \\ \hline \end{array} + \frac{4}{3} \begin{array}{|} \hline \hline \hline \hline \\ \hline \end{array} + \begin{array}{|} \hline \hline \hline \hline \\ \hline \end{array}. \quad (8.28)$$

(This can be verified by expanding each of the symmetric and antisymmetric operators in all four terms on the right side).

We now apply Eq. (8.28) to the indices $\mathbf{u}, \mathbf{v}, \mathbf{w}$. In Eqs. (8.9) and (8.10), we introduce auxiliary factors m_i , where $i = 1, \dots, 4$ corresponding to

$$\begin{array}{|} \hline \hline \hline \hline \\ \hline \end{array} \longrightarrow m_1, \quad (8.29)$$

$$\begin{array}{|} \hline \hline \hline \hline \\ \hline \end{array} \longrightarrow m_2, \quad (8.30)$$

$$\begin{array}{|} \hline \hline \hline \hline \\ \hline \end{array} \longrightarrow m_3, \quad (8.31)$$

$$\begin{array}{|} \hline \hline \hline \hline \\ \hline \end{array} \longrightarrow m_4. \quad (8.32)$$

By wrapping each contribution within these auxiliary factors, it is possible to keep the G 's corresponding to each of the four terms in Eq. (8.28) distinct from one other. At the end of the calculation, all m_i 's are set to 1 – they are merely a bookkeeping device.

For the operator \hat{G}^{f2} , separating terms in this way results in

$$\begin{aligned} \hat{G}^{f2} = \frac{iN_c}{18} & \left[m_1 (2 (G_{\mathbf{u}\mathbf{v}\mathbf{v}}^f + 2G_{\mathbf{u}\mathbf{v}\mathbf{u}}^f + G_{\mathbf{v}\mathbf{u}\mathbf{u}}^f) + G_{\mathbf{v}\mathbf{v}\mathbf{u}}^f + G_{\mathbf{v}\mathbf{u}\mathbf{v}}^f + G_{\mathbf{u}\mathbf{v}\mathbf{v}}^f) \right. \\ & + m_2 (2 (2G_{\mathbf{u}\mathbf{v}\mathbf{v}}^f - G_{\mathbf{u}\mathbf{v}\mathbf{u}}^f - G_{\mathbf{v}\mathbf{u}\mathbf{u}}^f + G_{\mathbf{v}\mathbf{v}\mathbf{u}}^f) - G_{\mathbf{v}\mathbf{v}\mathbf{v}}^f - G_{\mathbf{u}\mathbf{v}\mathbf{v}}^f) \\ & \left. + 3m_3 (-2G_{\mathbf{u}\mathbf{v}\mathbf{u}}^f + 2G_{\mathbf{v}\mathbf{u}\mathbf{u}}^f - G_{\mathbf{v}\mathbf{v}\mathbf{v}}^f + G_{\mathbf{u}\mathbf{v}\mathbf{v}}^f) \right] \{L_{\mathbf{u}}^a, L_{\mathbf{v}}^a\}. \end{aligned} \quad (8.33)$$

Since the mixed symmetry terms m_1 and m_2 survive, we can conclude that \hat{G}^{f2} has both symmetric and antisymmetric contributions. For the operator \hat{G}^{f3} , only the antisymmetric m_4 term survives. Instead of expressing Eq. (8.23) as a sum of six terms, it can be written as

$$\frac{1}{6} (G_{\mathbf{u}\mathbf{v}\mathbf{v}}^f + G_{\mathbf{v}\mathbf{u}\mathbf{u}}^f + G_{\mathbf{u}\mathbf{v}\mathbf{u}}^f - G_{\mathbf{u}\mathbf{v}\mathbf{v}}^f - G_{\mathbf{v}\mathbf{u}\mathbf{u}}^f - G_{\mathbf{u}\mathbf{v}\mathbf{u}}^f) = G_{\mathbf{u}\mathbf{v}\mathbf{v}}^f, \quad (8.34)$$

so that

$$\hat{G}^{f3} = f^{abc} G_{\mathbf{u}\mathbf{v}\mathbf{w}}^f L_{\mathbf{u}}^a L_{\mathbf{v}}^b L_{\mathbf{w}}^c, \quad (8.35)$$

where $G_{\mathbf{u}\mathbf{v}\mathbf{w}}^f$ is understood henceforth to be *totally antisymmetric*. For the operator \hat{G}^d , only the symmetric m_1 term survives. This means that \hat{G}^d can be written as

$$\hat{G}^d = d^{abc} G_{\mathbf{u}\mathbf{v}\mathbf{w}}^d L_{\mathbf{u}}^a L_{\mathbf{v}}^b L_{\mathbf{w}}^c, \quad (8.36)$$

where $G_{\mathbf{u}\mathbf{v}\mathbf{w}}^d$ is understood henceforth to be *totally symmetric*.

Putting all three operators of the eGA together, the final form of the parametrisation equation becomes

$$\begin{aligned} \partial_\eta \langle \mathcal{O}[U] \rangle (\eta) = \left\langle - \left[\frac{1}{2} \int_{\mathbf{u}\mathbf{v}} (G_{\mathbf{u}\mathbf{v}} + iN_c G_{\mathbf{u}\mathbf{v}}^{(2)}) L_{\mathbf{u}}^a L_{\mathbf{v}}^a \right. \right. \\ \left. \left. + \int_{\mathbf{u}\mathbf{v}\mathbf{w}} (f^{abc} G_{\mathbf{u}\mathbf{v}\mathbf{w}}^f + d^{abc} G_{\mathbf{u}\mathbf{v}\mathbf{w}}^d) L_{\mathbf{u}}^a L_{\mathbf{v}}^b L_{\mathbf{w}}^c \right] \mathcal{O}[U] \right\rangle (\eta), \end{aligned} \quad (8.37)$$

with $G_{\mathbf{u}\mathbf{v}\mathbf{w}}^f$ and $G_{\mathbf{u}\mathbf{v}\mathbf{w}}^d$ understood to be antisymmetric and symmetric, respectively. The $G_{\mathbf{u}\mathbf{v}}^{(2)}$ term that contributes to the original GA 2-point function $G_{\mathbf{u}\mathbf{v}}$ contains both symmetric and antisymmetric contributions. The symmetric part of the original term $f^{abc} G_{\mathbf{u}\mathbf{v}\mathbf{w}}^f L_{\mathbf{u}}^a L_{\mathbf{v}}^b L_{\mathbf{w}}^c$ as introduced in Eq. (8.8) has now been extracted and is contained wholly in $G_{\mathbf{u}\mathbf{v}\mathbf{w}}^{(2)}$. This is why the $G_{\mathbf{u}\mathbf{v}\mathbf{w}}^f$ term in Eq. (8.37) is now totally antisymmetric.

8.2 The 4-point correlator beyond the GA

Now that we have established the symmetry properties of the eGA operators, we use them to see how the parametric equations for the 4-point correlators discussed

in Section 7.3 are modified. Since the terms in Eq. (8.37) are additive, we consider each to act individually on the correlator matrix $\langle \mathcal{A}(\eta) \rangle$. The three contributions are resummed in the end.

The procedure followed here is similar to that of Section 7. By analogy with the transition matrix \mathcal{M} in Eq. (7.46), the following three new transition matrices are defined, corresponding to the three terms in Eq. (8.37):

$$\mathcal{M}_{(2)} := \begin{pmatrix} \mathcal{M}_{(2)}^{(1,1)} & \mathcal{M}_{(2)}^{(1,2)} \\ \mathcal{M}_{(2)}^{(2,1)} & \mathcal{M}_{(2)}^{(2,2)} \end{pmatrix}, \quad (8.38)$$

corresponding to the 2-point operator $G_{uv} + iN_c G_{uv}^{(2)} L_u^a L_v^a$,

$$\mathcal{M}_f := \begin{pmatrix} \mathcal{M}_f^{(1,1)} & \mathcal{M}_f^{(1,2)} \\ \mathcal{M}_f^{(2,1)} & \mathcal{M}_f^{(2,2)} \end{pmatrix}, \quad (8.39)$$

corresponding to the antisymmetric eGA operator $f^{abc} G_{uvw}^f L_u^a L_v^b L_w^c$, and

$$\mathcal{M}_d := \begin{pmatrix} \mathcal{M}_d^{(1,1)} & \mathcal{M}_d^{(1,2)} \\ \mathcal{M}_d^{(2,1)} & \mathcal{M}_d^{(2,2)} \end{pmatrix}, \quad (8.40)$$

corresponding to the symmetric eGA operator $d^{abc} G_{uvw}^d L_u^a L_v^b L_w^c$. Each of these can be calculated following the method of Section 7.3.2 – their results are given below. We also discuss the coincidence limits of each case in order to verify that our results are self-consistent with the expressions from Chapter 7.

8.2.1 Transition matrix from the 2-point eGA operator

In order to calculate the elements of $\mathcal{M}_{(2)}$ defined in Eq. (8.38), we act with the second term in Eq. (8.37) on a product of two fundamental and two antifundamental Wilson lines:

$$\partial_\eta \left\langle \begin{array}{c} \text{---} \text{---} \text{---} \text{---} \\ \text{---} \text{---} \text{---} \text{---} \\ \text{---} \text{---} \text{---} \text{---} \\ \text{---} \text{---} \text{---} \text{---} \end{array} \right\rangle = \left\langle -\frac{iN_c}{2} \int_{uv} G_{uv}^{(2)} L_u^a L_v^a \begin{array}{c} \text{---} \text{---} \text{---} \text{---} \\ \text{---} \text{---} \text{---} \text{---} \\ \text{---} \text{---} \text{---} \text{---} \\ \text{---} \text{---} \text{---} \text{---} \end{array} \right\rangle. \quad (8.41)$$

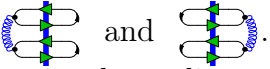
This gives

$$\mathcal{M}_{(2)}^{(1,1)} = \frac{iN_c^3}{2} \left(-G_{\mathbf{x}\mathbf{y}}^{(2)} - G_{\mathbf{x}'\mathbf{y}'}^{(2)} + G_{\mathbf{x}\mathbf{x}\mathbf{x}}^f + G_{\mathbf{y}\mathbf{y}\mathbf{y}}^f + G_{\mathbf{x}'\mathbf{x}'\mathbf{x}'}^f + G_{\mathbf{y}'\mathbf{y}'\mathbf{y}'}^f \right), \quad (8.42)$$

$$\mathcal{M}_{(2)}^{(1,2)} = \frac{iN_c^3 \sqrt{d_A}}{8} \left(G_{\mathbf{x}\mathbf{x}'}^{(2)} - G_{\mathbf{x}\mathbf{y}'}^{(2)} - G_{\mathbf{y}\mathbf{x}'}^{(2)} + G_{\mathbf{y}\mathbf{y}'}^{(2)} \right), \quad (8.43)$$

$$\begin{aligned} \mathcal{M}_{(2)}^{(2,2)} = \frac{iN_c d_A}{32} & \left(G_{\mathbf{x}\mathbf{y}}^{(2)} + G_{\mathbf{x}'\mathbf{y}'}^{(2)} - 2 \left[G_{\mathbf{x}\mathbf{x}'}^{(2)} + G_{\mathbf{y}\mathbf{y}'}^{(2)} \right] + (1 - d_A) \left[G_{\mathbf{x}\mathbf{y}'}^{(2)} + G_{\mathbf{y}\mathbf{x}'}^{(2)} \right] \right. \\ & \left. + d_A \left[G_{\mathbf{x}\mathbf{x}\mathbf{x}}^f + G_{\mathbf{y}\mathbf{y}\mathbf{y}}^f + G_{\mathbf{x}'\mathbf{x}'\mathbf{x}'}^f + G_{\mathbf{y}'\mathbf{y}'\mathbf{y}'}^f \right] \right). \end{aligned} \quad (8.44)$$

Notice the following from these expressions:

- The G^f 's in $\mathcal{M}_{(2)}^{(1,1)}$ do not mix the Wilson lines at \mathbf{x} and \mathbf{y} with those at \mathbf{x}' and \mathbf{y}' . Cross-terms, i.e. terms with both primed and unprimed coordinates, do not appear because this would mean that colour gets carried between the two dipoles. Since the dipoles are in singlet states in this case (this is the (1, 1) element of $\mathcal{M}_{(2)}$ specifically), this is not possible.
- Element $\mathcal{M}_{(2)}^{(1,2)}$ contains all the terms that $\mathcal{M}_{(2)}^{(1,1)}(\eta)$ does not. The two corresponding off-diagonal operator matrix elements are . Since colour is now exchanged between the primed and unprimed coordinate Wilson lines via the octet state on one side, only terms with one-gluon exchange between the two top and two bottom Wilson lines are allowed.
- Element $\mathcal{M}_{(2)}^{(2,2)}$ contains all possible G^f 's with two indices. Cross-terms are allowed because any colour transfer can be compensated for by the octet states on either side.

In keeping with the analysis made in Section 7.3.4 for the transition matrix in various coincidence limits, we consider the effects on $\mathcal{M}_{(2)}$. In the limit $\mathbf{x} \rightarrow \mathbf{y}$, in which upper quark and antiquark are placed at the same coordinate, the elements of $\mathcal{M}_{(2)}$ become

$$\lim_{\mathbf{x} \rightarrow \mathbf{y}} \mathcal{M}_{(2)}^{(1,1)} = \frac{iN_c^3}{2} \left(-G_{\mathbf{x}'\mathbf{y}'}^{(2)} + G_{\mathbf{x}'\mathbf{x}'\mathbf{x}'}^f + G_{\mathbf{y}'\mathbf{y}'\mathbf{y}'}^f \right), \quad (8.45)$$

$$\lim_{\mathbf{x} \rightarrow \mathbf{y}} \mathcal{M}_{(2)}^{(1,2)} = 0, \quad (8.46)$$

$$\begin{aligned} \lim_{\mathbf{x} \rightarrow \mathbf{y}} \mathcal{M}_{(2)}^{(2,2)} = \frac{iN_c d_A}{32} & \left(-N_c^2 \left[G_{\mathbf{y}\mathbf{y}'}^{(2)} + G_{\mathbf{y}\mathbf{y}}^{(2)} \right] + G_{\mathbf{x}'\mathbf{y}'}^{(2)} + 2N_c^2 G_{\mathbf{y}\mathbf{y}\mathbf{y}}^f \right. \\ & \left. + d_A \left[G_{\mathbf{x}'\mathbf{x}'\mathbf{x}'}^f + G_{\mathbf{y}'\mathbf{y}'\mathbf{y}'}^f \right] \right). \end{aligned} \quad (8.47)$$

As expected, all traces over the upper two Wilson lines vanish in $\mathcal{M}_{(2)}^{(1,1)}$ because there is no way for them to connect to the bottom dipole that is in a singlet state. $\mathcal{M}_{(2)}^{(1,2)}$ becomes zero as all terms cancel pairwise. In fact, by writing \hat{G}^{f^2} in the expansion of Eq. (8.33) shows that each auxiliary factor m_i goes to zero independently in the limit $\mathbf{x} \rightarrow \mathbf{y}$.

In addition, we can impose a second limit $\mathbf{x}' \rightarrow \mathbf{y}'$, giving

$$\lim_{\substack{\mathbf{x} \rightarrow \mathbf{y} \\ \mathbf{x}' \rightarrow \mathbf{y}'}} \mathcal{M}_{(2)}^{(1,1)} = 0, \quad (8.48)$$

$$\lim_{\substack{\mathbf{x} \rightarrow \mathbf{y} \\ \mathbf{x}' \rightarrow \mathbf{y}'}} \mathcal{M}_{(2)}^{(2,2)} = \frac{iN_c^3 d_A}{16} \left(-G_{\mathbf{y}\mathbf{y}'}^{(2)} + G_{\mathbf{y}\mathbf{y}\mathbf{y}}^f + G_{\mathbf{y}'\mathbf{y}'\mathbf{y}'}^f \right). \quad (8.49)$$

Now $\mathcal{M}_{(2)}^{(1,1)}$ vanishes by the same logic that all terms with single dipoles vanish in the first limit $\mathbf{x} \rightarrow \mathbf{y}$.

The other limit that can be studied is $\mathbf{x} \rightarrow \mathbf{y}'$. This gives

$$\lim_{\mathbf{x} \rightarrow \mathbf{y}'} \mathcal{M}_{(2)}^{(1,1)} = \frac{iN_c^3}{2} \left(-G_{\mathbf{y}\mathbf{y}'}^{(2)} - G_{\mathbf{x}'\mathbf{y}'}^{(2)} + G_{\mathbf{y}\mathbf{y}\mathbf{y}}^f + G_{\mathbf{x}'\mathbf{x}'\mathbf{x}'}^f + G_{\mathbf{y}'\mathbf{y}'\mathbf{y}'}^f \right), \quad (8.50)$$

$$\lim_{\mathbf{x} \rightarrow \mathbf{y}'} \mathcal{M}_{(2)}^{(1,2)} = \frac{iN_c^3 \sqrt{d_A}}{8} \left(-G_{\mathbf{y}\mathbf{x}'}^{(2)} + G_{\mathbf{y}\mathbf{y}'}^{(2)} + G_{\mathbf{x}'\mathbf{y}'}^{(2)} - 2G_{\mathbf{y}'\mathbf{y}'\mathbf{y}'}^f \right), \quad (8.51)$$

$$\lim_{\mathbf{x} \rightarrow \mathbf{y}'} \mathcal{M}_{(2)}^{(2,2)} = \frac{iN_c d_A}{32} \left((1 - d_A)G_{\mathbf{y}\mathbf{x}'}^{(2)} + d_A G_{\mathbf{y}\mathbf{y}\mathbf{y}}^f + d_A G_{\mathbf{x}'\mathbf{x}'\mathbf{x}'}^f + 2G_{\mathbf{y}'\mathbf{y}'\mathbf{y}'}^f \right). \quad (8.52)$$

The terms in $\mathcal{M}_{(2)}^{(1,1)}$ that vanished in the limit $\mathbf{x} \rightarrow \mathbf{y}$ no longer vanish because the limit $\mathbf{x} \rightarrow \mathbf{y}'$ now connects the two dipoles to each other. $\mathcal{M}_{(2)}^{(1,2)}$ also survives because there is no longer a pairwise cancellation of terms. Taking a second limit $\mathbf{x}' \rightarrow \mathbf{y}'$ in these results gives

$$\lim_{\substack{\mathbf{x} \rightarrow \mathbf{y}' \\ \mathbf{x}' \rightarrow \mathbf{y}'}} \mathcal{M}_{(2)}^{(1,1)} = iN_c^3 \left(-G_{\mathbf{y}\mathbf{y}'}^{(2)} + G_{\mathbf{y}\mathbf{y}\mathbf{y}}^f + G_{\mathbf{y}'\mathbf{y}'\mathbf{y}'}^f \right), \quad (8.53)$$

$$\lim_{\substack{\mathbf{x} \rightarrow \mathbf{y}' \\ \mathbf{x}' \rightarrow \mathbf{y}'}} \mathcal{M}_{(2)}^{(2,2)} = \frac{iN_c d_A}{16} \left(-G_{\mathbf{y}\mathbf{y}'}^{(2)} + G_{\mathbf{y}\mathbf{y}\mathbf{y}}^f + G_{\mathbf{y}'\mathbf{y}'\mathbf{y}'}^f \right), \quad (8.54)$$

$$\lim_{\substack{\mathbf{x} \rightarrow \mathbf{y}' \\ \mathbf{x}' \rightarrow \mathbf{y}'}} \mathcal{M}_{(2)}^{(1,2)} = -\frac{iN_c^3 \sqrt{d_A}}{4} \left(-G_{\mathbf{y}\mathbf{y}'}^{(2)} + G_{\mathbf{y}\mathbf{y}\mathbf{y}}^f + G_{\mathbf{y}'\mathbf{y}'\mathbf{y}'}^f \right). \quad (8.55)$$

In this case, all the elements have the same G content but different prefactors.

As in the GA, it is possible to study other limits, such as $\mathbf{x} \rightarrow \mathbf{x}'$ by making a change of basis as described in Section 7.3.4. From the limits considered so far, we can conclude that our transition matrix $\mathcal{M}_{(2)}^{(1,1)}$ has been calculated correctly.

8.2.2 Transition matrix from the antisymmetric 3-point eGA operator

Next, we calculate the contribution of the second term in Eq. (8.37) by considering

$$\partial_\eta \left\langle \begin{array}{c} \text{---} \text{---} \text{---} \text{---} \\ \text{---} \text{---} \text{---} \text{---} \\ \text{---} \text{---} \text{---} \text{---} \\ \text{---} \text{---} \text{---} \text{---} \end{array} \begin{array}{c} \text{---} \text{---} \text{---} \text{---} \\ \text{---} \text{---} \text{---} \text{---} \\ \text{---} \text{---} \text{---} \text{---} \\ \text{---} \text{---} \text{---} \text{---} \end{array} \begin{array}{c} x \\ y \\ x' \\ y' \end{array} \right\rangle = \left\langle - \int_{uvw} f^{abc} G_{uvw}^f L_u^a L_v^b L_w^c \begin{array}{c} \text{---} \text{---} \text{---} \text{---} \\ \text{---} \text{---} \text{---} \text{---} \\ \text{---} \text{---} \text{---} \text{---} \\ \text{---} \text{---} \text{---} \text{---} \end{array} \begin{array}{c} x \\ y \\ x' \\ y' \end{array} \right\rangle. \quad (8.56)$$

Since the eGA 3-point function G_{uvw}^f is totally antisymmetric, only G^f 's with three different indices can appear in \mathcal{M}_f . This means that $\mathcal{M}_f^{(1,1)}$ must be zero, which works out in practise due to all terms containing $\text{tr}(t^a) = 0$. The final transition matrix elements are

$$\mathcal{M}_f^{(1,1)} = 0, \quad (8.57)$$

$$\mathcal{M}_f^{(1,2)} = \frac{3iN_c^2 \sqrt{d_A}}{2} \left(G_{xyx'}^f - G_{xyy'}^f + G_{xx'y'}^f - G_{yyx'y'}^f \right), \quad (8.58)$$

$$\mathcal{M}_f^{(2,2)} = 0. \quad (8.59)$$

The vanishing of $\mathcal{M}_f^{(2,2)}$ is somewhat unexpected, but can be explained by expanding each octet state using the Fierz identity. Then the octet–octet operator becomes four terms

$$\begin{array}{c} \text{---} \text{---} \text{---} \text{---} \\ \text{---} \text{---} \text{---} \text{---} \\ \text{---} \text{---} \text{---} \text{---} \\ \text{---} \text{---} \text{---} \text{---} \end{array} = \frac{1}{4} \left(\begin{array}{c} \text{---} \text{---} \text{---} \text{---} \\ \text{---} \text{---} \text{---} \text{---} \\ \text{---} \text{---} \text{---} \text{---} \\ \text{---} \text{---} \text{---} \text{---} \end{array} - \frac{1}{N_c} \begin{array}{c} \text{---} \text{---} \text{---} \text{---} \\ \text{---} \text{---} \text{---} \text{---} \\ \text{---} \text{---} \text{---} \text{---} \\ \text{---} \text{---} \text{---} \text{---} \end{array} - \frac{1}{N_c} \begin{array}{c} \text{---} \text{---} \text{---} \text{---} \\ \text{---} \text{---} \text{---} \text{---} \\ \text{---} \text{---} \text{---} \text{---} \\ \text{---} \text{---} \text{---} \text{---} \end{array} + \frac{1}{N_c^2} \begin{array}{c} \text{---} \text{---} \text{---} \text{---} \\ \text{---} \text{---} \text{---} \text{---} \\ \text{---} \text{---} \text{---} \text{---} \\ \text{---} \text{---} \text{---} \text{---} \end{array} \right). \quad (8.60)$$

By the same reasoning that $\mathcal{M}_f^{(1,1)}$ is zero, so too are the first and last terms in this sum. The remaining two terms are traces in opposite directions that cancel each other. Element $\mathcal{M}_f^{(1,2)}$, on the other hand, makes no colour flow transgressions and so all possible antisymmetric G^f 's are present. The relative signs among the terms in $\mathcal{M}_f^{(1,2)}(\eta)$ are due to the sign difference between the differential operator L acting on a quark or antiquark.

The coincidence limits are straightforward to evaluate for $\mathcal{M}_{(2)}^{(1,2)}$. They are

$$\lim_{x \rightarrow y} \mathcal{M}_f^{(1,2)} = \frac{3iN_c^2 \sqrt{d_A}}{2} \left(G_{yyx'}^f - G_{yyy'}^f \right), \quad (8.61)$$

$$\lim_{x \rightarrow y'} \mathcal{M}_f^{(1,2)} = \frac{3iN_c^2 \sqrt{d_A}}{2} \left(G_{yy'y'}^f - G_{x'y'y'}^f \right), \quad (8.62)$$

$$\lim_{\substack{x \rightarrow y' \\ x' \rightarrow y}} \mathcal{M}_f^{(1,2)} = \lim_{\substack{x \rightarrow y \\ x' \rightarrow y'}} \mathcal{M}_f^{(1,2)} = 0. \quad (8.63)$$

These are consistent with what is expected based on the corresponding physical scenarios, as already discussed in detail for $\mathcal{M}_{(2)}$.

8.2.3 Transition matrix from the symmetric 3-point eGA operator

Finally, we consider the totally symmetric term in Eq. (8.37) by calculating

$$\partial_\eta \left\langle \begin{array}{c} \text{---} \text{---} \text{---} \text{---} \\ \text{---} \text{---} \text{---} \text{---} \\ \text{---} \text{---} \text{---} \text{---} \\ \text{---} \text{---} \text{---} \text{---} \end{array} \begin{array}{c} \color{blue}{\leftarrow} \\ \color{blue}{\leftarrow} \\ \color{blue}{\leftarrow} \\ \color{blue}{\leftarrow} \end{array} \begin{array}{c} x \\ y \\ x' \\ y' \end{array} \right\rangle = \left\langle - \int_{uvw} d^{abc} G_{uvw}^d L_u^a L_v^b L_w^c \begin{array}{c} \text{---} \text{---} \text{---} \text{---} \\ \text{---} \text{---} \text{---} \text{---} \\ \text{---} \text{---} \text{---} \text{---} \\ \text{---} \text{---} \text{---} \text{---} \end{array} \begin{array}{c} \color{blue}{\leftarrow} \\ \color{blue}{\leftarrow} \\ \color{blue}{\leftarrow} \\ \color{blue}{\leftarrow} \end{array} \begin{array}{c} x \\ y \\ x' \\ y' \end{array} \right\rangle. \quad (8.64)$$

We can expect the transition matrix \mathcal{M}_d to be more complicated in structure than \mathcal{M}_f because the antisymmetry of G^f that lead to several terms cancelling in the calculation of \mathcal{M}_f is no longer applicable. We get

$$\mathcal{M}_d^{(1,1)} = -\frac{3iC_d C_F}{2} \left(-G_{xy}^{\mathcal{O}} - G_{x'y'}^{\mathcal{O}} + \frac{1}{3} [G_{xxx}^d - G_{yyy}^d + G_{x'x'x'}^d - G_{y'y'y'}^d] \right), \quad (8.65)$$

$$\mathcal{M}_d^{(1,2)} = -\frac{3iN_c C_d \sqrt{d_A}}{4} \left(G_{xy'}^{\mathcal{O}} + G_{x'y}^{\mathcal{O}} + G_{xx'x'}^d - G_{yyy'}^d + G_{x'x'x}^d - G_{y'y'y}^d - 2 [G_{xyx'}^d - G_{xyy'}^d + G_{x'y'x}^d - G_{x'y'y}^d] \right), \quad (8.66)$$

$$\mathcal{M}_d^{(2,2)} = -\frac{3iC_d}{4N_c} \left(G_{xy}^{\mathcal{O}} + G_{x'y'}^{\mathcal{O}} + (1 - d_A) [G_{xy'}^{\mathcal{O}} - G_{y'x'}^{\mathcal{O}}] + \frac{d_A}{3} [G_{xxx}^d - G_{yyy}^d + G_{x'x'x'}^d - G_{y'y'y'}^d] - 2 [G_{xx'x'}^d - G_{yyy'}^d + G_{x'x'x}^d - G_{y'y'y}^d] + 4 [G_{xyx'}^d - G_{xyy'}^d + G_{x'x'y'}^d - G_{y'x'y'}^d] \right), \quad (8.67)$$

where $G_{xy}^{\mathcal{O}} := G_{xxy}^d - G_{yyx}^d$. As in the $\mathcal{M}_{(2)}^{(1,1)}$ case, $\mathcal{M}_d^{(1,1)}$ does not contain any cross-terms between the two dipoles. The 1/3 that appears both here and in $\mathcal{M}_d^{(2,2)}$ is a symmetry factor. All possible permutations of coordinate indices are present in $\mathcal{M}_d^{(2,2)}$. In $\mathcal{M}_d^{(1,2)}$, however, only G^d 's that link the two dipoles appear. This is necessary to compensate for the colour transfer by the octet state on one side.

\mathcal{M}_d simplifies significantly in the limit $\mathbf{x} \rightarrow \mathbf{y}$:

$$\lim_{\mathbf{x} \rightarrow \mathbf{y}} \mathcal{M}_d^{(1,1)} = -\frac{3iC_d C_F}{2} \left(G_{x'y'}^{\mathcal{O}} + \frac{1}{3} [G_{x'x'x'}^d - G_{y'y'y'}^d] \right), \quad (8.68)$$

$$\lim_{\mathbf{x} \rightarrow \mathbf{y}} \mathcal{M}_d^{(1,2)} = 0, \quad (8.69)$$

$$\lim_{\mathbf{x} \rightarrow \mathbf{y}} \mathcal{M}_d^{(2,2)} = -\frac{3iC_d}{4N_c} \left(N_c^2 [G_{yx'}^{\mathcal{O}} - G_{yy'}^{\mathcal{O}}] + G_{x'y'}^{\mathcal{O}} + \frac{d_A}{3} [G_{x'x'x'}^d - G_{y'y'y'}^d] \right). \quad (8.70)$$

Additionally, imposing a second limit $\mathbf{x}' \rightarrow \mathbf{y}'$ gives

$$\lim_{\substack{\mathbf{x} \rightarrow \mathbf{y} \\ \mathbf{x}' \rightarrow \mathbf{y}'}} \mathcal{M}_d^{(1,1)}(\eta) = \lim_{\substack{\mathbf{x} \rightarrow \mathbf{y} \\ \mathbf{x}' \rightarrow \mathbf{y}'}} \mathcal{M}_d^{(2,2)}(\eta) = 0 \quad (8.71)$$

as it should.

In the limit $\mathbf{x} \rightarrow \mathbf{y}'$, we get

$$\lim_{\mathbf{x} \rightarrow \mathbf{y}'} \mathcal{M}_d^{(1,1)} = -\frac{3iC_d C_F}{2} \left(G_{\mathbf{y}\mathbf{y}'}^{\mathcal{O}} - G_{\mathbf{x}'\mathbf{y}'}^{\mathcal{O}} - \frac{1}{3} [G_{\mathbf{y}\mathbf{y}\mathbf{y}}^d - G_{\mathbf{x}'\mathbf{x}'\mathbf{x}'}^d] \right), \quad (8.72)$$

$$\lim_{\mathbf{x} \rightarrow \mathbf{y}'} \mathcal{M}_d^{(1,2)} = -\frac{3iN_c C_d \sqrt{d_A}}{4} (G_{\mathbf{y}\mathbf{x}'}^{\mathcal{O}} - G_{\mathbf{y}\mathbf{y}'}^{\mathcal{O}} + G_{\mathbf{x}'\mathbf{y}'}^{\mathcal{O}}), \quad (8.73)$$

$$\lim_{\mathbf{x} \rightarrow \mathbf{y}'} \mathcal{M}_d^{(2,2)} = -\frac{3i}{4N_c} \left(G_{\mathbf{y}\mathbf{y}'}^{\mathcal{O}} - G_{\mathbf{x}'\mathbf{y}'}^{\mathcal{O}} + (d_A - 1)G_{\mathbf{y}\mathbf{x}'}^{\mathcal{O}} + \frac{d_A}{3} [G_{\mathbf{y}\mathbf{y}\mathbf{y}}^d + G_{\mathbf{x}'\mathbf{x}'\mathbf{x}'}^d] \right). \quad (8.74)$$

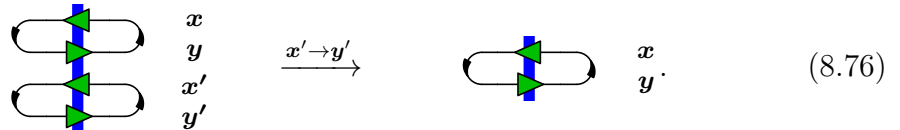
Taking a second limit $\mathbf{x}' \rightarrow \mathbf{y}$ gives zero in all cases:

$$\lim_{\substack{\mathbf{x} \rightarrow \mathbf{y}' \\ \mathbf{x}' \rightarrow \mathbf{y}}} \mathcal{M}_d^{(1,1)} = \lim_{\substack{\mathbf{x} \rightarrow \mathbf{y}' \\ \mathbf{x}' \rightarrow \mathbf{y}}} \mathcal{M}_d^{(2,2)} = \lim_{\substack{\mathbf{x} \rightarrow \mathbf{y}' \\ \mathbf{x}' \rightarrow \mathbf{y}}} \mathcal{M}_d^{(1,2)} = 0. \quad (8.75)$$

With these results, we may conclude that our expression for \mathcal{M}_d is consistent with all our previously calculated parametric equations.

8.3 The odderon contribution to simple correlators

We have thus far completely calculated the transition matrix \mathcal{M} in the extended GA parametrisation scheme for the 4-point correlators. This can be used to find the modifications to the 2- and 3-point correlator parametrisations discussed in Section 7.2. For the 2-point correlator, only the singlet–singlet elements in the limit $\mathbf{x}' \rightarrow \mathbf{y}'$ need to be considered, since this becomes



$$\begin{array}{ccc} \begin{array}{c} \text{---} \text{---} \text{---} \text{---} \\ \text{---} \text{---} \text{---} \text{---} \\ \text{---} \text{---} \text{---} \text{---} \\ \text{---} \text{---} \text{---} \text{---} \end{array} & \begin{array}{c} x \\ y \\ x' \\ y' \end{array} & \xrightarrow{x' \rightarrow y'} & \begin{array}{c} \text{---} \text{---} \text{---} \\ \text{---} \text{---} \text{---} \end{array} & \begin{array}{c} x \\ y \end{array} \end{array} \quad (8.76)$$

The transition elements and the octet–octet terms necessarily vanish because there is no second dipole to which the octet states can connect. Similarly, the only relevant matrix elements for the 3-point correlator are the octet–octet terms in the limit

$x' \rightarrow y'$:

The diagram shows two Feynman diagrams connected by an arrow labeled $x' \rightarrow y'$. The left diagram has two external lines labeled x and y on the right, and two internal lines labeled x' and y' on the left. A vertical blue bar is in the center, with two green arrows pointing right. Blue wavy lines connect the top and bottom external lines to the bar. The right diagram is similar but the external lines are labeled x and y on the left, and the internal lines are labeled x and y on the right. The blue wavy lines now connect the top and bottom internal lines to the bar.

Since the singlet–singlet and octet–octet elements of \mathcal{M}_f are zero, the only new information that can be added to the GA parametrisations for the 2- and 3-point correlators comes from \mathcal{M}_d . This addition is called the *odderon*, a symmetric three-gluon state in the t-channel.

The contribution from G^d to the 2-point correlator is obtained from the transition matrix element $\mathcal{M}_d^{(1,1)}$. By translational invariance (equivalent here to conservation of the identity matrix under rapidity evolution), it can be shown that $G_{xxx}^d = 0$. Then Eq. (8.65) gives

$$\lim_{x' \rightarrow y'} \mathcal{M}_d^{(1,1)} = \frac{3iC_d C_F}{2} G_{xy}^{\mathcal{O}}, \quad (8.78)$$

which is the only new term to be included in the parametrisation of the 2-point correlator. The new differential equation is

$$\partial_\eta \left\langle \frac{\text{tr}(U_x U_y^\dagger)}{N_c} \right\rangle = - \left(C_F \mathcal{G}'_{xy} + \frac{3iC_d C_F}{2} G_{xy}^{\mathcal{O}} \right) \left\langle \frac{\text{tr}(U_x U_y^\dagger)}{N_c} \right\rangle, \quad (8.79)$$

which has the solution

$$\left\langle \frac{\text{tr}(U_x U_y^\dagger)}{N_c} \right\rangle = \exp \left\{ -C_F \mathcal{G}_{xy} - \frac{3iC_d C_F}{2} G_{xy}^{\mathcal{O}} \right\}. \quad (8.80)$$

Once again using $G_{xxx}^d = 0$, the octet–octet element from Eq. (8.67) required for the 3-point correlator becomes

$$\lim_{x' \rightarrow y' = z} \mathcal{M}_d^{(2,2)} = -\frac{3iC_d}{4N_c} (G_{xy}^{\mathcal{O}} + N_c^2 G_{zx}^{\mathcal{O}} + N_c^2 G_{yz}^{\mathcal{O}}). \quad (8.81)$$

The new differential equation is

$$\begin{aligned} \partial_\eta \left\langle \frac{\tilde{U}_z^{ab} \text{tr}(t^a U_x t^b U_y^\dagger)}{N_c C_F} \right\rangle = & - \left[\frac{C_A}{2} (\mathcal{G}'_{xz} + \mathcal{G}'_{yz} - \mathcal{G}'_{xy}) + C_F \mathcal{G}'_{xy} \right. \\ & \left. - \frac{3iC_d}{4N_c} (G_{xy}^{\mathcal{O}} + N_c^2 G_{zx}^{\mathcal{O}} + N_c^2 G_{yz}^{\mathcal{O}}) \right] \left\langle \frac{\tilde{U}_z^{ab} \text{tr}(t^a U_x t^b U_y^\dagger)}{N_c C_F} \right\rangle, \quad (8.82) \end{aligned}$$

which has the solution

$$\begin{aligned} & \left\langle \frac{\tilde{U}_{\mathbf{z}}^{ab} \text{tr} (t^a U_{\mathbf{x}} t^b U_{\mathbf{y}}^\dagger)}{N_c C_F} \right\rangle \\ &= \exp \left\{ -\frac{C_A}{2} (\mathcal{G}_{\mathbf{xz}} + \mathcal{G}_{\mathbf{yz}} - \mathcal{G}_{\mathbf{xy}}) - C_F \mathcal{G}_{\mathbf{xy}} + \frac{3iC_d}{4N_c} (G_{\mathbf{xy}}^{\mathcal{O}} + N_c^2 G_{\mathbf{zx}}^{\mathcal{O}} + N_c^2 G_{\mathbf{yz}}^{\mathcal{O}}) \right\}. \end{aligned} \quad (8.83)$$

Eqs. (8.80) and (8.83) are our final parametric equations including the odderon contribution for the 2- and 3-point correlators, respectively. One possible consistency check to perform is to take the limit $\mathbf{z} \rightarrow \mathbf{x}$ in Eq. (8.83). This should reduce the 3-point correlator expression to the 2-point correlator expression, and does indeed reproduce Eq. (8.80).

8.3.1 Evolution equation for G^d

In Section 7.2.3, the parametric equations for the 2- and 3-point correlators were used in the Balitsky equation to derive a rapidity evolution equation for the GA 2-point function $\mathcal{G}_{\mathbf{xy}}$. The calculation from there can be repeated using the new expressions, Eqs. (8.80) and (8.83). After some algebra, it follows that

$$\partial_\eta \langle \tilde{G}_{\mathbf{xy}}^{\mathcal{O}} \rangle = \left\langle \frac{\alpha_s}{\pi^2} \int_{\mathbf{z}} \tilde{\mathcal{K}}_{\mathbf{xzy}} \left(1 - \exp \left\{ -\frac{N_c}{2} (\tilde{G}_{\mathbf{xz}}^{\mathcal{O}} + \tilde{G}_{\mathbf{zy}}^{\mathcal{O}} - \tilde{G}_{\mathbf{xy}}^{\mathcal{O}}) \right\} \right) \right\rangle, \quad (8.84)$$

where $\tilde{G}_{\mathbf{xy}}^{\mathcal{O}} := \mathcal{G}_{\mathbf{xy}} + \frac{3}{2}iC_d G_{\mathbf{xy}}^{\mathcal{O}}$ has been defined to emphasize the fact that the GA $\mathcal{G}_{\mathbf{xy}}$ and the odderon $G_{\mathbf{xy}}^{\mathcal{O}}$ appear in similar ways in this expression. That is, up to an overall colour factor, the linear combination of terms that appear on the right side of Eq. (8.84) are the same.

Eq. 8.84 is the final evolution equation for G^d (contained implicitly in the definition of $G^{\mathcal{O}}$) that was studied in Paper [I]. The LO BK equation was used to numerically implement the evolution of the odderon. The ultimate conclusion from our analysis was that the odderon is difficult to observe experimentally, (due to its relatively small contribution in comparison to the pomeron) to the dipole amplitude and its fast decay with increasing rapidity. Details of the numerical work are provided in Sections VII and VIII of Paper [I].

Chapter summary

In this chapter, we have extended the GA from Chapter 7 by including two new 3-point functions in the definition of the approximation parametrisation. The first task was to study the symmetry properties of these new functions. This resulted in a 2-point function $G^{(2)}$ with mixed symmetry, a totally antisymmetric 3-point function G^f and a totally symmetric 3-point function G^d . We have used the eGA to study 4-point correlators. These have been checked in various coincidence limits to ensure their consistency with the results from Section 7.3. Finally, we have investigated the so-called odderon by using the eGA to calculate the 2- and 3-point correlators. This gave a final evolution equation for the odderon function, which we have studied further in Paper [I].

9

Conclusion and Outlook

In this thesis, we have discussed the evolution of Wilson line correlators in the CGC effective field theory. These are important to understand and predict the cross sections of various processes within an ultrarelativistic collision. In particular, we have used the BK and JIMWLK equations to study the nonlinear evolution of correlators as a function of rapidity. The JIMWLK equation, which is typically formulated as a Fokker–Planck equation, has been studied in detail as a Langevin equation. We have also discussed how to use the Langevin formalism to study correlators of Wilson lines separated by a large rapidity. By going to the dilute limit, we have seen how BFKL dynamics emerge from the stochastic picture of evolution. Given this new insight into the Langevin framework of JIMWLK, the next step would be to numerically implement the bilocal Langevin equations studied in Paper [II]. There is much phenomenological work to be done in this direction, by applying such an implementation to various physical processes, particularly those that will be seen at the future EIC. Some predictions for observing saturation at the EIC have been made in [106].

A significant fraction of this thesis has been dedicated to the GA and its extensions. We have discussed the calculational details behind the parametric equations of the 6-point correlators that appear in the NLO BK equation. The somewhat surprising results from the numerical implementation of these equations requires further work. In Paper [III], the comparison of our finite- N_c expressions to their large- N_c counterparts showed an order 1% agreement between the two. It is not yet understood why exactly this occurs. A useful next step would be to look more closely at the 6-point correlators in various regions of coordinate space to see where their dominant contributions lie. By considering our parametric equations for the 6-point correlators in coincidence limits, it may be possible to understand the surprising agreement between the large- and finite- N_c versions. Such a study may

also be helpful if it can be extended to other correlators or even generalised.

Finally, the last chapter of this thesis discussed a natural extension of the GA by including a 3-point function to the approximation definition. We have calculated the 4-point correlators using this extension and verified the results by taking coincidence limits. An important consequence of the eGA is that an evolution equation for the odderon can be derived. This has been implemented numerically in Paper [I] and is of great interest at the moment due to the experimental observation of the odderon at the LHC [107]. It may be interesting to include the contributions from the eGA to correlators from other physical processes to see if the odderon has a significant contribution to their cross sections. The work covered in this thesis is only a small fraction of what needs to be done in order to understand the internal structure of nuclear matter from the perspective of the CGC formalism. With the increasing ability of modern collider experiments to access higher energies, saturation physics becomes increasingly important to understand theoretically.

Bibliography

- [I] T. Lappi, A. Ramnath, K. Rummukainen and H. Weigert, *JIMWLK evolution of the odderon*, *Phys. Rev. D* **94** (2016) no. 5 054014 [[arXiv:1606.00551](#) [hep-ph]].
- [II] T. Lappi and A. Ramnath, *Unequal rapidity correlators in the dilute limit of the JIMWLK evolution*, *Phys. Rev. D* **100** (2019) no. 5 054003 [[arXiv:1904.00782](#) [hep-ph]].
- [III] T. Lappi, H. Mäntysaari and A. Ramnath, *Next-to-leading order Balitsky-Kovchegov equation beyond large N_c* , *Phys. Rev. D* **102** (2020) no. 7 074027 [[arXiv:2007.00751](#) [hep-ph]].
- [4] T. Regge, *Introduction to complex orbital momenta*, *Nuovo Cim.* **14** (1959) 951.
- [5] G. Chew and S. C. Frautschi, *Principle of Equivalence for All Strongly Interacting Particles Within the S Matrix Framework*, *Phys. Rev. Lett.* **7** (1961) 394.
- [6] V. Gribov, *Partial waves with complex orbital angular momenta and the asymptotic behavior of the scattering amplitude*, *Sov. Phys. JETP* **14** (1962) 1395.
- [7] E. Iancu, A. Leonidov and L. D. McLerran, *Nonlinear gluon evolution in the color glass condensate. 1.*, *Nucl. Phys. A* **692** (2001) 583 [[arXiv:hep-ph/0011241](#)].
- [8] E. Iancu, A. Leonidov and L. D. McLerran, *The Renormalization group equation for the color glass condensate*, *Phys. Lett. B* **510** (2001) 133 [[arXiv:hep-ph/0102009](#)].
- [9] V. Gribov and L. Lipatov, *Deep inelastic $e p$ scattering in perturbation theory*, *Sov. J. Nucl. Phys.* **15** (1972) 438.

- [10] V. Gribov and L. Lipatov, *e+ e- pair annihilation and deep inelastic e p scattering in perturbation theory*, *Sov. J. Nucl. Phys.* **15** (1972) 675.
- [11] G. Altarelli and G. Parisi, *Asymptotic Freedom in Parton Language*, *Nucl. Phys. B* **126** (1977) 298.
- [12] Y. L. Dokshitzer, *Calculation of the Structure Functions for Deep Inelastic Scattering and e+ e- Annihilation by Perturbation Theory in Quantum Chromodynamics.*, *Sov. Phys. JETP* **46** (1977) 641.
- [13] L. Lipatov, *Reggeization of the Vector Meson and the Vacuum Singularity in Nonabelian Gauge Theories*, *Sov. J. Nucl. Phys.* **23** (1976) 338.
- [14] E. A. Kuraev, L. N. Lipatov and V. S. Fadin, *Multi - Reggeon Processes in the Yang-Mills Theory*, *Sov. Phys. JETP* **44** (1976) 443.
- [15] E. Kuraev, L. Lipatov and V. S. Fadin, *The Pomeron Singularity in Nonabelian Gauge Theories*, *Sov. Phys. JETP* **45** (1977) 199.
- [16] I. Balitsky and L. Lipatov, *The Pomeron Singularity in Quantum Chromodynamics*, *Sov. J. Nucl. Phys.* **28** (1978) 822.
- [17] L. Lipatov, *The Bare Pomeron in Quantum Chromodynamics*, *Sov. Phys. JETP* **63** (1986) 904.
- [18] Y. V. Kovchegov, *Small x F(2) structure function of a nucleus including multiple pomeron exchanges*, *Phys. Rev. D* **60** (1999) 034008 [[arXiv:hep-ph/9901281](https://arxiv.org/abs/hep-ph/9901281)].
- [19] I. Balitsky, *Operator expansion for high-energy scattering*, *Nucl. Phys. B* **463** (1996) 99 [[arXiv:hep-ph/9509348](https://arxiv.org/abs/hep-ph/9509348)].
- [20] J. Jalilian-Marian, A. Kovner, A. Leonidov and H. Weigert, *The Wilson renormalization group for low x physics: Towards the high density regime*, *Phys. Rev. D* **59** (1998) 014014 [[arXiv:hep-ph/9706377](https://arxiv.org/abs/hep-ph/9706377)].
- [21] J. Jalilian-Marian, A. Kovner, A. Leonidov and H. Weigert, *Unitarization of gluon distribution in the doubly logarithmic regime at high density*, *Phys. Rev. D* **59** (1999) 034007 [[arXiv:hep-ph/9807462](https://arxiv.org/abs/hep-ph/9807462)]. [Erratum: *Phys.Rev.D* 59, 099903 (1999)].
- [22] J. Jalilian-Marian, A. Kovner and H. Weigert, *The Wilson renormalization group for low x physics: Gluon evolution at finite parton density*, *Phys. Rev. D* **59** (1998) 014015 [[arXiv:hep-ph/9709432](https://arxiv.org/abs/hep-ph/9709432)].

-
- [23] E. Ferreiro, E. Iancu, A. Leonidov and L. McLerran, *Nonlinear gluon evolution in the color glass condensate. 2.*, *Nucl. Phys. A* **703** (2002) 489 [[arXiv:hep-ph/0109115](#)].
- [24] N. N. Nikolaev and B. Zakharov, *Color transparency and scaling properties of nuclear shadowing in deep inelastic scattering*, *Z. Phys. C* **49** (1991) 607.
- [25] N. Nikolaev and B. G. Zakharov, *Pomeron structure function and diffraction dissociation of virtual photons in perturbative QCD*, *Z. Phys. C* **53** (1992) 331.
- [26] N. N. Nikolaev and B. Zakharov, *The Triple pomeron regime and the structure function of the pomeron in the diffractive deep inelastic scattering at very small x* , *Z. Phys. C* **64** (1994) 631 [[arXiv:hep-ph/9306230](#)].
- [27] A. H. Mueller, *Soft gluons in the infinite momentum wave function and the BFKL pomeron*, *Nucl. Phys. B* **415** (1994) 373.
- [28] A. H. Mueller, *Unitarity and the BFKL pomeron*, *Nucl. Phys. B* **437** (1995) 107 [[arXiv:hep-ph/9408245](#)].
- [29] Y. V. Kovchegov and E. Levin, *Quantum chromodynamics at high energy*, vol. 33. Cambridge University Press, 8, 2012.
- [30] H. Weigert, *Evolution at small $x(bj)$: The Color glass condensate*, *Prog. Part. Nucl. Phys.* **55** (2005) 461 [[arXiv:hep-ph/0501087](#)].
- [31] F. Gelis and B. Schenke, *Initial State Quantum Fluctuations in the Little Bang*, *Ann. Rev. Nucl. Part. Sci.* **66** (2016) 73 [[arXiv:1604.00335](#) [[hep-ph](#)]].
- [32] E. Iancu and R. Venugopalan, *The Color glass condensate and high-energy scattering in QCD*. 3, 2003. [arXiv:hep-ph/0303204](#).
- [33] F. Gelis, E. Iancu, J. Jalilian-Marian and R. Venugopalan, *The Color Glass Condensate*, *Ann. Rev. Nucl. Part. Sci.* **60** (2010) 463 [[arXiv:1002.0333](#) [[hep-ph](#)]].
- [34] J. L. Albacete and C. Marquet, *Gluon saturation and initial conditions for relativistic heavy ion collisions*, *Prog. Part. Nucl. Phys.* **76** (2014) 1 [[arXiv:1401.4866](#) [[hep-ph](#)]].
- [35] E. Levin and M. Ryskin, *The Hadron - Nucleus Interaction in $\{QCD\}$ at High-energy*, *Nucl. Phys. B* **304** (1988) 805.
- [36] A. H. Mueller, *Small x Behavior and Parton Saturation: A QCD Model*, *Nucl. Phys. B* **335** (1990) 115.

- [37] M. E. Peskin and D. V. Schroeder, *An introduction to quantum field theory*. Westview, Boulder, CO, 1995. Includes exercises.
- [38] F. Halzen and A. D. Martin, *Quarks and leptons: an introductory course in modern particle physics*. Wiley, New York, NY, 1984.
- [39] G. F. Sterman, *An Introduction to Quantum Field Theory*. Cambridge Univ. Press, Cambridge, 1993.
- [40] J. Callan, Curtis G. and D. J. Gross, *High-energy electroproduction and the constitution of the electric current*, *Phys. Rev. Lett.* **22** (1969) 156.
- [41] **ZEUS** collaboration, S. Chekanov *et. al.*, *Measurement of the neutral current cross-section and $F(2)$ structure function for deep inelastic $e + p$ scattering at HERA*, *Eur. Phys. J. C* **21** (2001) 443 [[arXiv:hep-ex/0105090](#)].
- [42] **ALICE** collaboration, S. Acharya *et. al.*, *Measurement of prompt D^0 , D^+ , D^{*+} , and D_S^+ production in p - Pb collisions at $\sqrt{s_{NN}} = 5.02$ TeV*, *JHEP* **12** (2019) 092 [[arXiv:1906.03425](#) [[nucl-ex](#)]].
- [43] M. Hentschinski and K. Kutak, *Signs for the onset of gluon saturation in exclusive photo-production of vector mesons*, *PoS LHCP2019* (2019) 039 [[arXiv:1908.03494](#) [[hep-ph](#)]].
- [44] G. Giacalone and C. Marquet, *Signature of gluon saturation in forward di-hadron correlations at the Large Hadron Collider*, *Nucl. Phys. A* **982** (2019) 291 [[arXiv:1807.06388](#) [[hep-ph](#)]].
- [45] L. D. McLerran and R. Venugopalan, *Gluon distribution functions for very large nuclei at small transverse momentum*, *Phys. Rev. D* **49** (1994) 3352 [[arXiv:hep-ph/9311205](#)].
- [46] L. D. McLerran and R. Venugopalan, *Computing quark and gluon distribution functions for very large nuclei*, *Phys. Rev. D* **49** (1994) 2233 [[arXiv:hep-ph/9309289](#)].
- [47] L. D. McLerran and R. Venugopalan, *Green's functions in the color field of a large nucleus*, *Phys. Rev. D* **50** (1994) 2225 [[arXiv:hep-ph/9402335](#)].
- [48] A. Ayala, J. Jalilian-Marian, L. D. McLerran and R. Venugopalan, *The Gluon propagator in nonAbelian Weizsacker-Williams fields*, *Phys. Rev. D* **52** (1995) 2935 [[arXiv:hep-ph/9501324](#)].
- [49] C. Marquet and H. Weigert, *New observables to test the Color Glass Condensate beyond the large- N_c limit*, *Nucl. Phys. A* **843** (2010) 68 [[arXiv:1003.0813](#) [[hep-ph](#)]].

-
- [50] H. Weigert, *Unitarity at small Bjorken x* , *Nucl. Phys. A* **703** (2002) 823 [[arXiv:hep-ph/0004044](#)].
- [51] G. Beuf, *Dipole factorization for DIS at NLO: Loop correction to the $\gamma_{T,L}^* \rightarrow q\bar{q}$ light-front wave functions*, *Phys. Rev. D* **94** (2016) no. 5 054016 [[arXiv:1606.00777](#) [hep-ph]].
- [52] G. Beuf, *Dipole factorization for DIS at NLO: Combining the $q\bar{q}$ and $q\bar{q}g$ contributions*, *Phys. Rev. D* **96** (2017) no. 7 074033 [[arXiv:1708.06557](#) [hep-ph]].
- [53] H. Hänninen, T. Lappi and R. Paatelainen, *One-loop corrections to light cone wave functions: the dipole picture DIS cross section*, *Annals Phys.* **393** (2018) 358 [[arXiv:1711.08207](#) [hep-ph]].
- [54] J. Jalilian-Marian, A. Kovner, A. Leonidov and H. Weigert, *The BFKL equation from the Wilson renormalization group*, *Nucl. Phys. B* **504** (1997) 415 [[arXiv:hep-ph/9701284](#)].
- [55] R. Ellis, W. Stirling and B. Webber, *QCD and collider physics*, vol. 8. Cambridge University Press, 2, 2011.
- [56] S. Weinberg, *The quantum theory of fields. Vol. 2: Modern applications*. Cambridge University Press, 8, 2013.
- [57] J. Gao, M. Guzzi, J. Huston, H.-L. Lai, Z. Li, P. Nadolsky, J. Pumplin, D. Stump and C. P. Yuan, *CT10 next-to-next-to-leading order global analysis of QCD*, *Phys. Rev. D* **89** (2014) no. 3 033009 [[arXiv:1302.6246](#) [hep-ph]].
- [58] J. R. Forshaw and D. Ross, *Quantum chromodynamics and the pomeron*, vol. 9. Cambridge University Press, 1, 2011.
- [59] V. Barone and E. Predazzi, *High-Energy Particle Diffraction*, vol. v.565 of *Texts and Monographs in Physics*. Springer-Verlag, Berlin Heidelberg, 2002.
- [60] F. Low, *A Model of the Bare Pomeron*, *Phys. Rev. D* **12** (1975) 163.
- [61] S. Nussinov, *Colored Quark Version of Some Hadronic Puzzles*, *Phys. Rev. Lett.* **34** (1975) 1286.
- [62] S. Nussinov, *A Perturbative Recipe for Quark Gluon Theories and Some of Its Applications*, *Phys. Rev. D* **14** (1976) 246.
- [63] T. Regge, *Bound states, shadow states and Mandelstam representation*, *Nuovo Cim.* **18** (1960) 947.

- [64] V. S. Fadin, E. A. Kuraev and L. N. Lipatov, *On the Pomeron singularity in Asymptotically Free Theories*, *Phys. Lett. B* **60** (1975) 50.
- [65] M. Froissart, *Asymptotic behavior and subtractions in the Mandelstam representation*, *Phys. Rev.* **123** (1961) 1053.
- [66] A. Martin, *Unitarity and high-energy behavior of scattering amplitudes*, *Phys. Rev.* **129** (1963) 1432.
- [67] R. J. Glauber, *Cross-sections in deuterium at high-energies*, *Phys. Rev.* **100** (1955) 242.
- [68] V. Franco and R. J. Glauber, *High-energy deuteron cross-sections*, *Phys. Rev.* **142** (1966) 1195.
- [69] V. N. Gribov, *Glauber corrections and the interaction between high-energy hadrons and nuclei*, *Sov. Phys. JETP* **29** (1969) 483.
- [70] R. J. Glauber and G. Matthiae, *High-energy scattering of protons by nuclei*, *Nucl. Phys. B* **21** (1970) 135.
- [71] V. N. Gribov, *Interaction of gamma quanta and electrons with nuclei at high-energies*, *Sov. Phys. JETP* **30** (1970) 709.
- [72] R. D. Woods and D. S. Saxon, *Diffuse Surface Optical Model for Nucleon-Nuclei Scattering*, *Phys. Rev.* **95** (1954) 577.
- [73] A. H. Mueller and B. Patel, *Single and double BFKL pomeron exchange and a dipole picture of high-energy hard processes*, *Nucl. Phys. B* **425** (1994) 471 [[arXiv:hep-ph/9403256](#)].
- [74] N. N. Nikolaev, B. G. Zakharov and V. R. Zoller, *The s channel approach to Lipatov's pomeron and hadronic cross-sections*, *JETP Lett.* **59** (1994) 6 [[arXiv:hep-ph/9312268](#)].
- [75] N. N. Nikolaev, B. G. Zakharov and V. R. Zoller, *The Spectrum and solutions of the generalized BFKL equation for total cross-section*, *Phys. Lett. B* **328** (1994) 486 [[arXiv:hep-th/9401052](#)].
- [76] I. Balitsky and G. A. Chirilli, *Next-to-leading order evolution of color dipoles*, *Phys. Rev. D* **77** (2008) 014019 [[arXiv:0710.4330](#) [[hep-ph](#)]].
- [77] E. Iancu and Y. Mulian, *Forward dijets in proton-nucleus collisions at next-to-leading order: the real corrections*, *JHEP* **03** (2021) 005 [[arXiv:2009.11930](#) [[hep-ph](#)]].

-
- [78] Y. Hatta and E. Iancu, *Collinearly improved JIMWLK evolution in Langevin form*, *JHEP* **08** (2016) 083 [[arXiv:1606.03269](#) [[hep-ph](#)]].
- [79] K. Rummukainen and H. Weigert, *Universal features of JIMWLK and BK evolution at small x* , *Nucl. Phys. A* **739** (2004) 183 [[arXiv:hep-ph/0309306](#)].
- [80] A. H. Mueller, *A Simple derivation of the JIMWLK equation*, *Phys. Lett. B* **523** (2001) 243 [[arXiv:hep-ph/0110169](#)].
- [81] J.-P. Blaizot, E. Iancu and H. Weigert, *Nonlinear gluon evolution in path integral form*, *Nucl. Phys. A* **713** (2003) 441 [[arXiv:hep-ph/0206279](#)].
- [82] A. Kovner, J. G. Milhano and H. Weigert, *Relating different approaches to nonlinear QCD evolution at finite gluon density*, *Phys. Rev. D* **62** (2000) 114005 [[arXiv:hep-ph/0004014](#)].
- [83] Y. V. Kovchegov, J. Kuokkanen, K. Rummukainen and H. Weigert, *Subleading- $N(c)$ corrections in non-linear small- x evolution*, *Nucl. Phys. A* **823** (2009) 47 [[arXiv:0812.3238](#) [[hep-ph](#)]].
- [84] T. Lappi, *Gluon spectrum in the glasma from JIMWLK evolution*, *Phys. Lett. B* **703** (2011) 325 [[arXiv:1105.5511](#) [[hep-ph](#)]].
- [85] A. Dumitru, J. Jalilian-Marian, T. Lappi, B. Schenke and R. Venugopalan, *Renormalization group evolution of multi-gluon correlators in high energy QCD*, *Phys. Lett. B* **706** (2011) 219 [[arXiv:1108.4764](#) [[hep-ph](#)]].
- [86] T. Lappi and H. Mäntysaari, *On the running coupling in the JIMWLK equation*, *Eur. Phys. J. C* **73** (2013) no. 2 2307 [[arXiv:1212.4825](#) [[hep-ph](#)]].
- [87] T. Altinoluk and A. Kovner, *Particle Production at High Energy and Large Transverse Momentum - 'The Hybrid Formalism' Revisited*, *Phys. Rev. D* **83** (2011) 105004 [[arXiv:1102.5327](#) [[hep-ph](#)]].
- [88] G. A. Chirilli, B.-W. Xiao and F. Yuan, *Inclusive Hadron Productions in pA Collisions*, *Phys. Rev. D* **86** (2012) 054005 [[arXiv:1203.6139](#) [[hep-ph](#)]].
- [89] M. Hentschinski, H. Weigert and A. Schafer, *Extension of the color glass condensate approach to diffractive reactions*, *Phys. Rev. D* **73** (2006) 051501 [[arXiv:hep-ph/0509272](#)].
- [90] A. Kovner, M. Lublinsky and H. Weigert, *Treading on the cut: Semi inclusive observables at high energy*, *Phys. Rev. D* **74** (2006) 114023 [[arXiv:hep-ph/0608258](#)].

- [91] A. Kovner and M. Lublinsky, *One gluon, two gluon: Multigluon production via high energy evolution*, *JHEP* **11** (2006) 083 [[arXiv:hep-ph/0609227](#)].
- [92] E. Iancu and J. Laidet, *Gluon splitting in a shockwave*, *Nucl. Phys. A* **916** (2013) 48 [[arXiv:1305.5926](#) [[hep-ph](#)]].
- [93] E. Iancu and D. N. Triantafyllopoulos, *JIMWLK evolution for multi-particle production in Langevin form*, *JHEP* **11** (2013) 067 [[arXiv:1307.1559](#) [[hep-ph](#)]].
- [94] F. Gelis, T. Lappi and R. Venugopalan, *High energy factorization in nucleus-nucleus collisions. 3. Long range rapidity correlations*, *Phys. Rev. D* **79** (2009) 094017 [[arXiv:0810.4829](#) [[hep-ph](#)]].
- [95] S. Caron-Huot, *When does the gluon reggeize?*, *JHEP* **05** (2015) 093 [[arXiv:1309.6521](#) [[hep-th](#)]].
- [96] J. P. Blaizot, F. Gelis and R. Venugopalan, *High-energy pA collisions in the color glass condensate approach. 2. Quark production*, *Nucl. Phys. A* **743** (2004) 57 [[arXiv:hep-ph/0402257](#)].
- [97] F. Dominguez, C. Marquet, B.-W. Xiao and F. Yuan, *Universality of Unintegrated Gluon Distributions at small x*, *Phys. Rev. D* **83** (2011) 105005 [[arXiv:1101.0715](#) [[hep-ph](#)]].
- [98] E. Iancu, K. Itakura and L. McLerran, *A Gaussian effective theory for gluon saturation*, *Nucl. Phys. A* **724** (2003) 181 [[arXiv:hep-ph/0212123](#)].
- [99] E. Iancu and D. N. Triantafyllopoulos, *Higher-point correlations from the JIMWLK evolution*, *JHEP* **11** (2011) 105 [[arXiv:1109.0302](#) [[hep-ph](#)]].
- [100] E. Iancu and D. N. Triantafyllopoulos, *JIMWLK evolution in the Gaussian approximation*, *JHEP* **04** (2012) 025 [[arXiv:1112.1104](#) [[hep-ph](#)]].
- [101] M. Alvioli, G. Soyez and D. N. Triantafyllopoulos, *Testing the Gaussian Approximation to the JIMWLK Equation*, *Phys. Rev. D* **87** (2013) no. 1 014016 [[arXiv:1212.1656](#) [[hep-ph](#)]].
- [102] A. Dumitru and V. Skokov, *$\cos(4\varphi)$ azimuthal anisotropy in small-x DIS dijet production beyond the leading power TMD limit*, *Phys. Rev. D* **94** (2016) no. 1 014030 [[arXiv:1605.02739](#) [[hep-ph](#)]].
- [103] J. P. Blaizot, F. Gelis and R. Venugopalan, *High-energy pA collisions in the color glass condensate approach. 1. Gluon production and the Cronin effect*, *Nucl. Phys. A* **743** (2004) 13 [[arXiv:hep-ph/0402256](#)].

- [104] P. Cvitanovic, *Group theory: Birdtracks, Lie's and exceptional groups*. Princeton University Press, 2020.
- [105] L. Lukaszuk and B. Nicolescu, *A Possible interpretation of $p p$ rising total cross-sections*, *Lett. Nuovo Cim.* **8** (1973) 405.
- [106] H. Mäntysaari, N. Mueller, F. Salazar and B. Schenke, *Multigluon Correlations and Evidence of Saturation from Dijet Measurements at an Electron-Ion Collider*, *Phys. Rev. Lett.* **124** (2020) no. 11 112301 [[arXiv:1912.05586](#) [nucl-th]].
- [107] **DO, TOTEM** collaboration, V. M. Abazov *et. al.*, *Comparison of pp and $p\bar{p}$ differential elastic cross sections and observation of the exchange of a colorless C -odd gluonic compound*, [arXiv:2012.03981](#) [hep-ex].



ORIGINAL PAPERS

I

JIMWLK EVOLUTION OF THE ODDERON

by

Lappi, T., Ramnath, A., Rummukainen, K., & Weigert, H. 2016

Physical Review D, 94(5), Article 054014

<https://doi.org/10.1103/PhysRevD.94.054014>

Reproduced with kind permission by American Physical Society.

JIMWLK evolution of the odderonT. Lappi^{*}*Department of Physics, University of Jyväskylä, P.O. Box 35, Jyväskylä 40014, Finland
and Helsinki Institute of Physics, University of Helsinki, P.O. Box 64,
Helsinki 00014, Finland*A. Ramnath[†]*Department of Physics, University of Jyväskylä, P.O. Box 35, Jyväskylä 40014, Finland*K. Rummukainen[‡]*Department of Physics and Helsinki Institute of Physics, University of Helsinki, Helsinki 00014, Finland*H. Weigert[§]*Department of Physics, University of Cape Town, Private Bag X3, Rondebosch 7701, South Africa*

(Received 21 June 2016; published 14 September 2016)

We study the effects of a parity-odd “odderon” correlation in Jalilian-Marian–Iancu–McLerran–Weigert–Leonidov–Kovner renormalization group evolution at high energy. Firstly we show that in the eikonal picture where the scattering is described by Wilson lines, one obtains a strict mathematical upper limit for the magnitude of the odderon amplitude compared to the parity-even Pomeron one. This limit increases with N_c , approaching infinity in the infinite N_c limit. We use a systematic extension of the Gaussian approximation including both two- and three-point correlations which enables us to close the system of equations even at finite N_c . In the large- N_c limit we recover an evolution equation derived earlier. By solving this equation numerically we confirm that the odderon amplitude decreases faster in the nonlinear case than in the linear Balitsky-Fadin-Kuraev-Lipatov limit. We also point out that, in the three-point truncation at finite N_c , the presence of an odderon component introduces azimuthal angular correlations $\sim \cos(n\varphi)$ at all n in the target color field. These correlations could potentially have an effect on future studies of multiparticle angular correlations.

DOI: 10.1103/PhysRevD.94.054014

I. INTRODUCTION

High energy hadronic collisions at modern collider energies involve a dense system of gluons. At high enough energy the typical phase space density becomes nonperturbatively large, i.e. of the order of the inverse QCD coupling constant $1/\alpha_s$. In this limit it is better to describe these gluonic degrees of freedom as a classical color field than as a collection of individual particles, in what is known as the color glass condensate (CGC) picture [1,2]. In practice, the important degree of freedom here is the Wilson line, a path-ordered exponential in the color field. It gives the scattering amplitude of a colored high energy particle passing through the CGC target. Increasing the collision energy opens up phase space for the emission of even more gluons, which in this case are treated as quantum fluctuations on top of the classical field. These fluctuations can be systematically integrated out and included in the classical field. This procedure leads to renormalization

group equations that describe the evolution of the Wilson lines as a function of collision energy.

The complete system of evolution equations is known as the Jalilian-Marian–Iancu–McLerran–Weigert–Leonidov–Kovner (JIMWLK) equation [3–13] or equivalently as the Balitsky hierarchy [14–17]. It describes the evolution of the whole probability distribution of Wilson lines. While this equation can be solved, at least at leading order, numerically [18–21], most phenomenological applications rely on simpler approximations. This is typically done by an evolution equation for an expectation value of Wilson lines that can be derived, in some approximation, from the equation for the full probability distribution. The usual approximation here is to use the large- N_c limit, which allows one to truncate the Balitsky hierarchy and obtain an evolution equation for the two-point function of Wilson lines known as the Balitsky-Kovchegov (BK) [14,22] equation. A related approximation, which has an identical dynamical content but can be used to construct the Wilson line expectation values at finite N_c , is provided by the Gaussian approximation.

The Gaussian approximation relates all Wilson line correlators to a single two-point correlator. The purpose

^{*}tuomas.v.v.lappi@jyu.fi[†]anramnat@student.jyu.fi[‡]kari.rummukainen@helsinki.fi[§]heribert.weigert@uct.ac.za

of this paper is to take the first step beyond the Gaussian approximation and introduce an intrinsic three-point correlation function of color charges using a method that can be extended to include all n -point functions up to any fixed finite number of points m in what we refer to as an (exponential) m -point truncation. When this is used to evaluate the evolution equation for the two-point function of Wilson lines (the dipole operator), it turns out that the new three-point function only appears in a specific coordinate limit. It can, in fact, be rewritten as an imaginary part of the earlier two-point function. Physically this new degree of freedom corresponds to the odderon: an interaction by the exchange of a parity-odd particle. Similar modifications to the Gaussian average have been considered before in the context of the McLerran-Venugopalan (MV) [23–25] model (see e.g. [26–28]). Here, we will go beyond the work in these papers and derive evolution equations in rapidity for the odderon amplitude in the exponential three-point approximation, extending earlier large- N_c results [29,30] to finite N_c . We will then numerically solve these evolution equations in a truncation in the harmonic number in the azimuthal direction. To determine the consistency of truncated JIMWLK evolution we complement our discussion with a numerical simulation of parity-even correlations using full untruncated JIMWLK evolution in the Langevin framework, reproducing the same qualitative behavior.

This paper is structured in the following way. First, in Sec. II, we motivate this study by an example of a phenomenological context in which the odderon amplitude appears directly. Then, in Sec. III, we point out that the origin of the dipole amplitude as a correlation function of Wilson lines that live on the SU(3) group manifold places stringent mathematical bounds on the size of the odderon. We then quantify these bounds for specific parametric forms of the initial conditions in Sec. IV. On the same basis we argue that, in the JIMWLK context, the odderon cannot affect observables that do not break rotational symmetry in the transverse plane. Section V presents the derivation of the evolution equations for the odderon component from an exponential n -point truncation. We solve these truncated equations in Sec. VI with a further approximation to the lowest nontrivial $\cos n\theta$ azimuthal harmonic. Then in Sec. VII we construct initial conditions for the JIMWLK equation that include an odderon component and study its evolution in a full (fixed coupling) JIMWLK simulation.

II. OBSERVABLES AND CROSS SECTIONS

The simplest application of JIMWLK evolution is calculating the total cross section in experiments like deep inelastic scattering (DIS), where a spacelike virtual photon is scattered on a nuclear target. At small x and leading order in perturbation theory, the cross section is dominated by the $q\bar{q}$ component of the photon wave function, which interacts eikonally with the target. That is to say that the interaction is driven by an average of the dipole operator

$$\hat{D}_{x,y} = \frac{1}{N_c} \text{tr}(U_x U_y^\dagger). \quad (1)$$

Using the diagrammatic notation introduced in [31] (see Fig. 1), the total cross section can be cast as

$$\left[\begin{array}{c} \text{---} \text{---} \text{---} \\ \text{---} \text{---} \text{---} \end{array} \right] \left[\begin{array}{c} \text{---} \text{---} \text{---} \\ \text{---} \text{---} \text{---} \end{array} \right] \\ = 2 \begin{array}{c} \text{---} \text{---} \text{---} \\ \text{---} \text{---} \text{---} \end{array} - \begin{array}{c} \text{---} \text{---} \text{---} \\ \text{---} \text{---} \text{---} \end{array} - \begin{array}{c} \text{---} \text{---} \text{---} \\ \text{---} \text{---} \text{---} \end{array} \quad (2)$$

and allows access only to the real part of the dipole correlator contained in the last two terms of Eq. (2), since

$$\langle \text{tr}(U_x U_y^\dagger) \rangle(Y) + \langle \text{tr}(U_x^\dagger U_y) \rangle(Y) = 2 \langle \text{Re tr}(U_x U_y^\dagger) \rangle(Y). \quad (3)$$

As indicated, the average will depend on $Y = (\ln 1/x)$ with the Y dependence governed by JIMWLK evolution.

The dipole operator *does* give rise to imaginary parts in a *generic* average $\langle \hat{D}_{x,y} \rangle(Y)$, i.e. over an ensemble not explicitly tailored to have a vanishing imaginary part, but one needs more detailed experiments to access this information. (We will argue in Sec. III that this is in fact an absolute statement, at least within the JIMWLK context.) The single transverse spin asymmetry (STSA) is such an

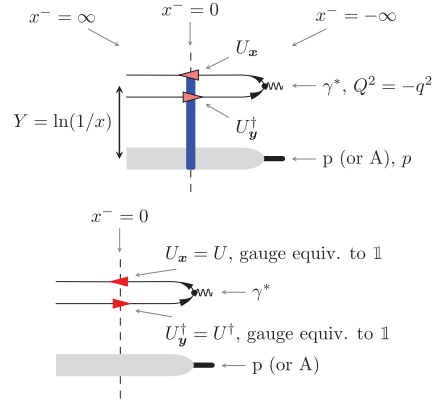


FIG. 1. Diagrammatic representation of the amplitude for γ^*A scattering at small x at momentum transfer $Q^2 = -q^2$ as introduced in [31]. Light cone “time” x^- runs from right to left. The interacting “out state” (top diagram) contains nontrivial interactions between projectile and target. The interaction region is indicated by a vertical bar at $x^- = 0$ with superimposed explicit markers for the Wilson lines picked up by each projectile constituent. An arrow to the left indicates a U , an arrow to the right a U^{-1} . Arrows on gluon lines stand for Wilson lines in the adjoint representation. The noninteracting “in state” (bottom diagram) instead has no interactions and correspondingly constant Wilson line factors at $x^- = 0$ which are gauge equivalent to the unit element.

observable. Kovchegov and Sievert [32] have in fact suggested a new mechanism to generate a contribution to STSA at small x that is triggered by this imaginary part. The contribution suggested by Kovchegov and Sievert takes the diagrammatic form

$$\begin{aligned}
 & \left[\text{Diagram 1} + \text{Diagram 2} \right] \left[\text{Diagram 3} + \text{Diagram 4} \right] \\
 &= \text{Diagram 5} + \text{Diagram 6} \\
 &+ \text{Diagram 7} + \text{Diagram 8}
 \end{aligned} \quad (4)$$

where the incoming quark is taken (probabilistically) from the incoming projectile.

In Eq. (4) the momentum and spin of the quark in the final state are tagged and the color in the initial state is summed over. Tagging the quark momentum leads to different coordinates on the corresponding Wilson lines in amplitude and complex conjugate amplitude. The gluon momentum is integrated over so that the gluon Wilson line in the last term cancels between the two sides of the cut. The color correlators from the right-hand side of Eq. (4) result in the following terms:

$$\begin{aligned}
 \mathcal{I}^{(q)} = & \left\langle \frac{\text{tr}(U_z U_y^\dagger)}{N_c} - \frac{1}{d_A} \tilde{U}_x^{ab} 2\text{tr}(t^a U_z t^b U_w^\dagger) \right. \\
 & \left. - \frac{1}{d_A} \tilde{U}_x^{ab} 2\text{tr}(t^a U_u t^b U_y^\dagger) + \frac{\text{tr}(U_u U_w^\dagger)}{N_c} \right\rangle. \quad (5)
 \end{aligned}$$

The STSA is driven by the contributions that are anti-symmetric under exchange of the quark and antiquark coordinates $z \leftrightarrow y$ and thus the imaginary part of, for example, the first term.

III. GROUP THEORY CONSTRAINTS ON THE REAL AND IMAGINARY PARTS OF $q\bar{q}$ CORRELATORS

Most readers familiar with JIMWLK and BK simulations will be prepared to accept that the $q\bar{q}$ and $q\bar{q}g$ correlators in Eq. (5), with normalization factors included, are *real* and interpolate between 1 at distances much smaller than the inverse saturation scale and 0 at pairwise separations much larger than the inverse saturation scale. This behavior is indeed respected by JIMWLK evolution in all its forms, provided it is satisfied by the initial condition.

This situation changes if one allows imaginary parts to arise. We will illustrate the situation with a discussion of the $q\bar{q}$ dipole correlator and its underlying configurations that appear explicitly in a Langevin simulation of JIMWLK evolution. To this end, note that these configurations appear

as explicit $SU(N_c)$ matrices U_x .¹ This remains true for the products entering the $q\bar{q}$ correlators: $U_x U_y^\dagger \in SU(N_c)$ is unitary and therefore has N_c eigenvalues of the form $e^{i\phi_i(x,y)}$, $i = 1, \dots, N_c \in \mathbb{N}$. All of them are functions of both coordinates and live on the unit circle. The determinant condition $\det(U_x U_y^\dagger) = 1$ then enforces that the phases of the eigenvalues sum to an integer multiple of 2π . Suppressing the coordinate dependence on the $\phi_i(x,y)$ we have, for each pair of points

$$1 = \det(U_x U_y^\dagger) = e^{i \sum_{i=1}^{N_c} \phi_i} \Leftrightarrow \sum_{i=1}^{N_c} \phi_i = 2\pi n; \quad n \in \mathbb{Z}. \quad (6)$$

The trace of the dipole operator is therefore fully determined by $N_c - 1$ phases $\phi_i \in [0, 2\pi[$.

Using the constraint (6) to remove ϕ_{N_c} , one finds an expression for the trace of our group element $U_x U_y^\dagger$ that reads

$$\frac{1}{N_c} \text{tr}(U_x U_y^\dagger) = \frac{1}{N_c} \left(\sum_{i=1}^{N_c-1} e^{i\phi_i} + e^{-i \sum_{i=1}^{N_c-1} \phi_i} \right). \quad (7)$$

This trace falls into a simply connected closed subset of the complex plane, bounded by the curve

$$h_{N_c}(\theta) = \frac{1}{N_c} \left((N_c - 1)e^{i\theta} + e^{-i(N_c-1)\theta} \right), \quad (8)$$

where $\theta \in [0, 2\pi[$. (See [33] for a recent discussion of these textbook results.) Equation (8) has a very simple geometric interpretation: The center of a small circle (represented by the second term) is traveling along the perimeter of a large circle (represented by the first term).² While the large circle is traversed once in a counterclockwise direction, the small traveling circle is traversed clockwise N_c times. The line traced out by $h_{N_c}(\theta)$ in this manner is called a hypocycloid. The curve is fully contained in the unit circle and, for fixed N_c , has cusps at the N_c th roots of unity—these are the only points where the curve touches the unit circle. These points correspond to specific group elements that form the center of the group $\{e^{i2\pi n/N_c} \mid n \in \mathbb{Z}/N_c\}$. In Fig. 2 both the geometric origin and the cusp structure are illustrated for a few values of N_c . For $N_c \rightarrow \infty$, the hypocycloid will approximate the unit circle. The value $N_c = 2$ does not allow for an imaginary part at all—the underlying reason is

¹All arguments here assume that the coupling to the target is described fully through Wilson lines, i.e. the absence of sub-eikonal corrections, as is the case for all JIMWLK evolution.

²This description is adapted from the formula—alternatively, one might describe the boundary as the curve traced by a point on a circle of radius $1/N_c$ that rolls on the inside of the unit circle, starting with both circles touching at 1.

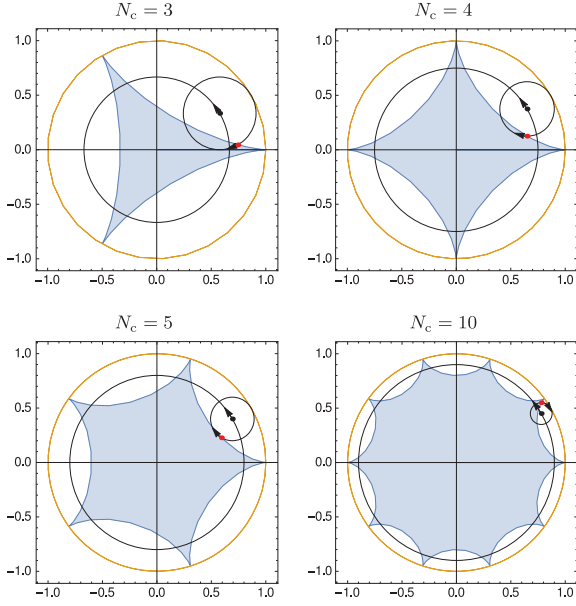


FIG. 2. Geometric origin and shape of the hypocycloids traced out by $h_{N_c}(\theta)$. The shaded region corresponds to allowed values of $\text{tr}(U_x U_y^\dagger)/N_c$, i.e. the set of points in the complex plane reached by Eq. (7).

that the group is pseudoreal, i.e. $U^\dagger = \epsilon U \epsilon$ ($\epsilon = [e^{ij}]$) is isomorphic to U . In this vein, $N_c = 3$ is the first case that allows an imaginary part and has, at the same time, the strongest limitations on its size from the group structure alone.

The dipole correlator appears as an average over such configurations and can be parametrized in terms of two real degrees of freedom

$$\begin{aligned} S_{xy}(Y) &:= \langle \text{tr}(U_x U_y^\dagger) \rangle(Y)/N_c \\ &= 1 - P_{xy}(Y) + iO_{xy}(Y) \\ &= e^{-C_F(P_{xy} + iO_{xy})(Y)}, \end{aligned} \quad (9)$$

i.e. either directly through real and imaginary parts ($1 - P_{xy}$ and O_{xy} , respectively) or exponentially via a logarithmic modulus and phase (P_{xy} and O_{xy} , respectively). Noting that complex conjugation simply swaps the coordinates on S , $S_{xy}^* = S_{yx}$ implies that P and \mathcal{P} are symmetric, while O and \mathcal{O} are antisymmetric under the exchange of x and y . This symmetry property links them to the Pomeron and odderon, respectively.

One striking observation is that nothing inherently prevents the real part, the Pomeron contribution, from taking negative values—the hypocycloids allow negative real parts. In fact the Wilson line dipole correlators of Eq. (9) are averages of configurations falling into the interior of the hypocycloid $h_{N_c}(\theta)$ and thus are even

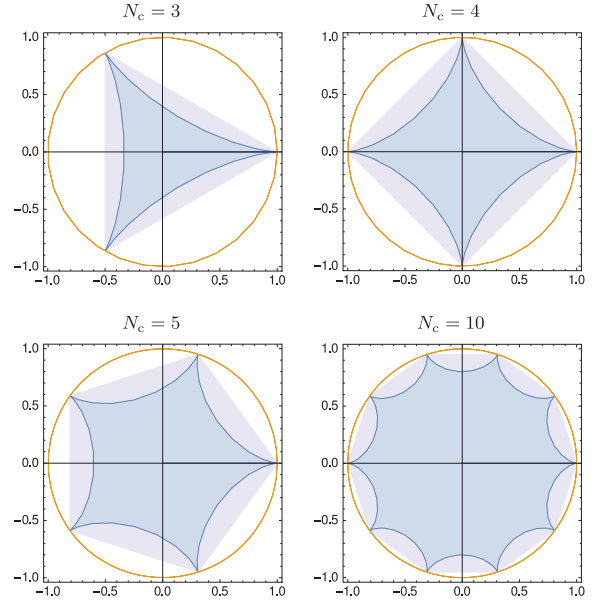


FIG. 3. Average group element traces must fall within a polygon connecting the N_c th roots of unity. For $N_c \rightarrow \infty$ the polygon will approximate the unit circle.

slightly less constrained: Such an average may fall outside the hypocycloid but must remain inside a polygon connecting the cusps, as illustrated for a few values of N_c in Fig. 3. For $N_c \in \mathbb{Z} \geq 2$, where there is a well-defined interior, the bounding polygon can be parametrized by

$$p_{N_c}(\theta) = \frac{\cos(\frac{\pi}{N_c})}{\cos(\text{mod}(\theta, \frac{2\pi}{N_c}) - \frac{\pi}{N_c})} e^{i\theta}, \quad (10)$$

again with $\theta \in [0, 2\pi[$.

Let us emphasize that this is not in contradiction with the bounds observed for real correlators in earlier simulations. In fact, consistent, real-valued initial conditions for the $q\bar{q}$ and $q\bar{q}g$ correlators of Eq. (5) during evolution lie between the fixed points at 1 and 0 and the evolution equation does not develop an imaginary part starting from a real initial condition respecting these bounds.

This behavior is in fact a generic requirement on a consistent evolution equation for Wilson line dipole correlators. To expose the physics content of this statement, parametrize a point inside the hypocycloid or inside its bounding polygon by a real factor $\rho \in [0, 1]$ and a point on the boundary $b_{N_c}(\theta)$ [with $b_{N_c}(\theta)$ either given by $h_{N_c}(\theta)$ or $p_{N_c}(\theta)$], so that the Wilson line correlator (the average) takes the form

$$\langle \text{tr}(U_x U_y^\dagger) \rangle(Y)/N_c = \rho_{xy}(Y) b_{N_c}(\theta_{xy}(Y)). \quad (11)$$

Like for the ingredients of Eq. (9) there are clear symmetry requirements on ρ and θ in Eq. (11): They must be

symmetric and antisymmetric, respectively, under exchange of \mathbf{x} and \mathbf{y} . If the measurement is both translationally and rotationally symmetric in the transverse plane [i.e. in the absence of an additional transverse vector $\hat{\mathbf{s}}$ to furnish the sign change via a factor $\hat{\mathbf{s}} \cdot (\mathbf{x} - \mathbf{y})$], the contribution of any antisymmetric function such as θ_{xy} must vanish. In that case Eq. (11) can be reduced to $S_{xy}(Y) = \rho_{xy}(Y) \in [0, 1]$; i.e. the solutions are restricted to the intersection of the hypocycloid with the *positive* real axis. (See also Sec. VII where this mechanism is demonstrated for JIMWLK ensembles.)

The need for additional directional information is a physics requirement: To be able to see an odderon contribution in an experiment one needs to break rotational symmetry in the transverse plane such as is done by measuring a spin asymmetry in STSA. The total cross section, by contrast, averages over all directions $\hat{\mathbf{s}}$ (in the average that forms the correlator) and thus forces $b_{N_c} \rightarrow 1$. In this case there is no scope for an average odderon contribution to couple to the real part visible in Eq. (3); it is zero throughout.

As a mathematical constraint, one needs an imaginary part in the initial condition for the *average* to allow it to move away from the interval $[0, 1]$ and, in particular, for the real part to turn negative. (Note that this does not imply that individual configurations may not fall onto the negative real axis; see again Sec. VII for explicit examples.)

To conclude this section, we note that the perturbative limit $r \rightarrow 0$ takes $\langle \text{tr}(U_x U_y^\dagger) \rangle(Y)/N_c \rightarrow 1$ and thus is associated with strong correlations and the trivial center element $U_x U_x^\dagger = 1$. The origin on the other hand corresponds to $\langle \text{tr}(U_x U_y^\dagger) \rangle(Y)/N_c \rightarrow 0$ and thus the long distance limit where the Wilson lines are uncorrelated. The remaining center elements (at least for $N_c = 3$) correspond to maximally anticorrelated configurations.

If such configurations are not present with considerable weight, the averages will not have any chance of being pulled outside the hypocycloid into the remainder of then enveloping polygon. The perturbatively motivated initial conditions discussed in Sec. IV below do not lead to such behavior despite the presence of noticeable anticorrelation in one of the examples.

IV. CONSTRAINTS ON THE INITIAL CONDITIONS

The physics expectations for the total cross section in the absence of an imaginary part severely restrict the form of the initial condition. The simplest assumption, based on exponentiating the r^2 behavior of leading-order light cone perturbation theory, leads to the well-known Golec-Biernat–Wüsthoff (GBW) [34] ansatz $S_{xy} = e^{-(\mathbf{x}-\mathbf{y})^2 Q_s^2/4}$, where Q_s is the GBW saturation scale. The MV model modifies this with a logarithmic correction in the exponent, and evolution at leading order will carry any of these into a

scaling form entirely imposed by the nonlinear form of the evolution equation. For our discussion here, all of these forms are suitable since at leading order (see, however [35–38]) evolution will quickly readjust these to take on the features of the scaling form.

If we allow for a nonzero odderon admixture, the choice of a physically meaningful initial condition for the pair of \mathcal{P} and \mathcal{O} needs some thought. At short distance, light cone perturbation theory leads to $\mathcal{P}_{xy} \propto |\mathbf{x} - \mathbf{y}|^2$ and $\mathcal{O}_{xy} \propto |\mathbf{x} - \mathbf{y}|^3$ [29], but the symmetry properties imposed by complex conjugation require the presence of an additional transverse vector $\hat{\mathbf{s}}$ as discussed in Sec. III. We thus expect a short distance $r \ll 1/Q_s$ behavior of the form

$$\mathcal{P}_{xy} \propto r^2, \quad \mathcal{O}_{xy} \propto \kappa r^2 \mathbf{r} \cdot \hat{\mathbf{s}} = \kappa r^3 \hat{\mathbf{r}} \cdot \hat{\mathbf{s}}, \quad (12)$$

where $\mathbf{r} = \mathbf{x} - \mathbf{y}$ and $\hat{\mathbf{r}} = \mathbf{r}/r$. If we measure both contributions in (12) in the same units, κ serves to parametrize the normalization of the odderon relative to the Pomeron amplitude. We will see in the following that it is constrained by the group theory limits on the scattering amplitude in the dilute limit $r \rightarrow 0$.

As discussed in Sec. III, we can impose the group theory constraints on the amplitude at two levels of rigor. Physically we would expect that the average amplitude itself is within the group manifold. In principle, it is also possible that the average amplitude is within the polygon region defined by linear combinations of amplitudes in the group.

In the first, more physical case, this leads in the $r \rightarrow 0$ limit to the constraint

$$\mathcal{O}_r \leq \frac{\sqrt{2}}{3} \frac{N_c - 2}{\sqrt{N_c - 1}} (\mathcal{P}_r)^{3/2}. \quad (13)$$

Assuming that the Pomeron has the perturbative behavior

$$\mathcal{P}_r \approx r^2 Q_s^2/4 \quad (14)$$

and parametrizing the odderon with a general power law as

$$\mathcal{O}_r \approx \kappa (r Q_s/2)^\alpha, \quad (15)$$

this leads to the constraint $\alpha \geq 3$. Thus, the result $\mathcal{O}_r \sim r^3$ of Ref. [29] indeed corresponds to the mildest r dependence allowed by the group theory constraint. Assuming now the power $\alpha = 3$ we get the limit

$$\kappa \leq \frac{\sqrt{2}}{3} \frac{N_c - 2}{\sqrt{N_c - 1}} \Big|_{N_c=3} = \frac{1}{3}. \quad (16)$$

We want to stress the remarkable nature of this result. With linear Balitsky-Fadin-Kuraev-Lipatov (BFKL) evolution the magnitudes of the Pomeron and odderon amplitudes are only limited by phenomenology. The interpretation of

the scattering amplitude in terms of the Wilson line immediately places a nonperturbative mathematical upper limit on the odderon amplitude.

Strictly speaking the averages of $SU(N_c)$ matrices need not be inside the group. Thus, in principle the upper limit for the odderon follows from restricting the expectation value of the amplitude to lie inside the N_c -sided polygon with corners at the N_c roots of unity. This leads in the limit $r \rightarrow 0$ to

$$\mathcal{O}_r \leq \frac{\sin \frac{2\pi}{N_c}}{1 - \cos \frac{2\pi}{N_c}} \mathcal{P}_r. \quad (17)$$

For amplitudes parametrized as in (14) and (15), this leads to the less stringent limit $\alpha \geq 2$. For the limiting power $\alpha = 2$ the odderon amplitude is constrained to $\kappa(\alpha = 2) \leq \frac{\sin \frac{2\pi}{N_c}}{1 - \cos \frac{2\pi}{N_c}}$. For the value $\alpha = 3$, any value of κ satisfies this more lax version of the group theory constraint sufficiently close to $r = 0$. From larger dipole sizes one does obtain an upper limit on κ , but this limit is universal in the same way; i.e. it depends on the functional form at larger r .

As practical initial conditions for evolution including the odderon, we suggest two possible extensions of the GBW parametrization:

$$\langle \text{tr}(U_x U_y^\dagger) \rangle(Y_0)/N_c = e^{-r^2 Q_0^2/4 + i\kappa r^3 Q_0^3/8\hat{r} \cdot \hat{s}} \quad (18)$$

or

$$\langle \text{tr}(U_x U_y^\dagger) \rangle(Y_0)/N_c = e^{-r^2 Q_0^2/4 (1 + i\kappa r^3 Q_0^3/8\hat{r} \cdot \hat{s})}. \quad (19)$$

Exponentiating the real part ensures that both the short- and long-distance behavior are qualitatively correct: The $\mathbf{x} - \mathbf{y} \rightarrow \mathbf{0}$ limit produces 1 and the limit $\mathbf{x} - \mathbf{y} \rightarrow \infty$ produces 0. We have no similar bias for or against exponentiating the imaginary contribution, but the two choices have very different consequences: Ansatz (18) leads to anticorrelations in the real part while (19) does not—see Figs. 4 and 5. This is qualitatively different, but neither option can be excluded on purely theoretical grounds.

The initial conditions (18) and (19) are visualized in Fig. 6. As discussed above, in order for the average amplitude to stay within the group manifold, we must have $\kappa \leq 1/3$. For the functional form of Eq. (19) the parametrization stays within the triangle allowed for linear combinations of $SU(N_c = 3)$ Wilson lines for

$$\kappa \leq \frac{2\sqrt{\frac{2}{3}}(e^{W(-3e^{-3/2}/2)} + 3/2)}{(3 + 2W(-3e^{-3/2}/2))^{3/2}} \approx 0.9867, \quad (20)$$

where W is the Lambert function, defined as the solution of $z = W(z)e^{W(z)}$. We see that for the other parametrization

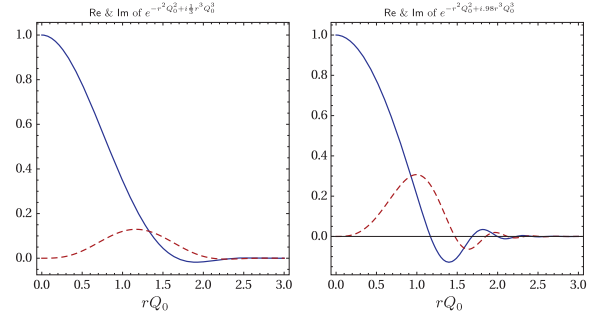


FIG. 4. Perturbatively motivated initial conditions for both real and imaginary parts (solid blue and red dashed curve, respectively) of $\langle \text{tr}(U_x U_y^\dagger) \rangle(Y_0)/N_c = e^{-r^2 Q_0^2 + i\kappa r^3 Q_0^3 \hat{r} \cdot \hat{s}}$ at $\hat{r} \cdot \hat{s} = 1$ assuming no extreme anticorrelations to drive the correlator outside the hypocycloid (left) and relaxing this condition (right). In both cases, real and imaginary parts show modulation only near $Q_s(Y_0)$.

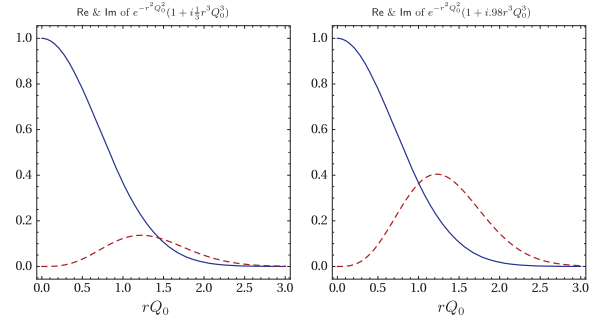


FIG. 5. Perturbatively motivated initial conditions for both real and imaginary parts (solid blue and red dashed curve, respectively) of $\langle \text{tr}(U_x U_y^\dagger) \rangle(Y_0)/N_c = e^{-r^2 Q_0^2 + i\kappa r^3 Q_0^3 \hat{r} \cdot \hat{s}}$ at $\hat{r} \cdot \hat{s} = 1$ assuming no extreme anticorrelations to drive the correlator outside the hypocycloid (left) and relaxing this condition (right). In both cases real and imaginary parts show modulation only near $Q_s(Y_0)$.

(18), the amplitude stays within the triangular region for the same values κ .

In both cases, $\kappa \lesssim 1$ so that real and imaginary parts show modulation only near $Q_s(Y_0)$ and thus provide perturbatively consistent starting points for evolution in a calculation where $Q_s(Y_0)$ is assumed to be in the perturbative domain. Note that the size of the odderon peak (the maximum of imaginary parts shown in red in Figs. 4 and 5) is severely limited by the bounds on κ .

V. GAUSSIAN AND HIGHER-ORDER EXPONENTIAL TRUNCATIONS

The dependence of the Wilson lines on the factorization rapidity that separates the small- and large- x degrees of freedom in the CGC formalism is given by the JIMWLK equation [3–13] or equivalently by the Balitsky hierarchy

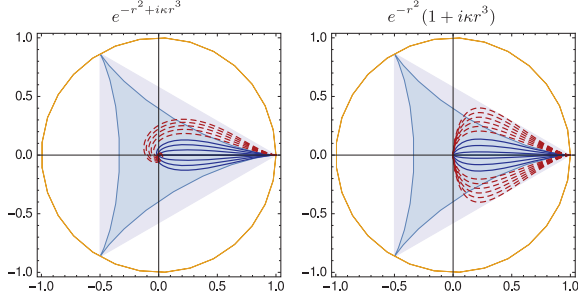


FIG. 6. Perturbatively motivated initial conditions for Pomeron + odderon configuration averages. Lowest-order perturbative calculations yield r^2 and r^3 behavior for small $r = |\mathbf{x} - \mathbf{y}|$ in the Pomeron and odderon channel, respectively. The plots show how different initial conditions seeded with this behavior at small r traverse the complex plane. In the parametrizations shown κ parametrizes the ratio of characteristic scales in the Pomeron and odderon sector. To fall into the allowed region $|\kappa|$ must be small ($|\kappa| \leq \frac{1}{3}$, blue; $\kappa \leq .98$, dashed red and blue lines), which limits the possible size of the Pomeron contribution in the initial condition; see Figs. 4 and 5.

[14–17]. The Balitsky hierarchy is a coupled set of integro-differential equations for operators made from products of Wilson lines. The first equation of the hierarchy is

$$\frac{d}{dY} \langle \text{tr}(U_x U_y^\dagger) \rangle = \frac{\alpha_s}{\pi^2} \int d^2z \tilde{\mathcal{K}}_{xzy} \times \langle \tilde{U}_z^{ab} \text{tr}(t^a U_x t^b U_y^\dagger) - C_F \text{tr}(U_x U_y^\dagger) \rangle, \quad (21)$$

where $\tilde{\mathcal{K}}_{xzy} = \frac{(x-y)^2}{(x-z)^2(z-y)^2}$. It relates the rapidity dependence of the dipole operator to a combination of dipole and three-point operators. The equation is derived by considering the emission of one soft gluon from the dipole; it is therefore not surprising that the three-point function involved is the same as in the STSA cross section (5). Using the Fierz identity, Eq. (21) becomes

$$\frac{d}{dY} \left\langle \frac{\text{tr}(U_x U_y^\dagger)}{N_c} \right\rangle = \frac{\alpha_s}{\pi^2} \frac{N_c}{2} \int d^2z \tilde{\mathcal{K}}_{xzy} \times \left\langle \frac{\text{tr}(U_x U_y^\dagger) \text{tr}(U_x U_y^\dagger)}{N_c} - \frac{\text{tr}(U_x U_y^\dagger)}{N_c} \right\rangle. \quad (22)$$

This form is often used to truncate the hierarchy by factorizing

$$\left\langle \frac{\text{tr}(U_x U_y^\dagger) \text{tr}(U_x U_y^\dagger)}{N_c} \right\rangle \xrightarrow{\text{fact}} \left\langle \frac{\text{tr}(U_x U_y^\dagger)}{N_c} \right\rangle \left\langle \frac{\text{tr}(U_x U_y^\dagger)}{N_c} \right\rangle \quad (23)$$

in the spirit of an independent scattering approximation for dipoles. The resulting closed mean-field equation

$$\frac{d}{dY} \left\langle \frac{\text{tr}(U_x U_y^\dagger)}{N_c} \right\rangle = \frac{\alpha_s}{\pi^2} \frac{N_c}{2} \int d^2z \tilde{\mathcal{K}}_{xzy} \times \left[\left\langle \frac{\text{tr}(U_x U_y^\dagger)}{N_c} \right\rangle \left\langle \frac{\text{tr}(U_x U_y^\dagger)}{N_c} \right\rangle - \left\langle \frac{\text{tr}(U_x U_y^\dagger)}{N_c} \right\rangle \right] \quad (24)$$

is the Balitsky-Kovchegov equation [14,22] and is a crucial tool in practical phenomenological applications of the CGC formalism.

To develop a better understanding of the possible physics content of the correlators in Eq. (5) and their JIMWLK evolution, we now turn to a set of systematically extendable truncations of the Balitsky hierarchy associated with the dipole operator, the simplest of which is known as the Gaussian truncation.

The motivation and prototype of this truncation is a procedure applied to the calculation of the gluon density in the MV model already in Ref. [3] and heavily reused since [31,39–43]. The method relies on the fact that Wilson lines are given as path-ordered exponentials in the gauge field as

$$U_x = P \exp \left\{ ig \int dx^- A_{x,x^-}^{a,+} t^a \right\} \quad (25)$$

and the assumption—intrinsic to the MV model—that the correlators of the A field in the exponent obey Gaussian statistics with only a local correlation in the longitudinal coordinate

$$g^2 \langle A_{x,x^-}^{a,+} A_{y,y^-}^{b,+} \rangle = \delta(x^- - y^-) \delta^{ab} G_{x^- , y^-}. \quad (26)$$

The MV model further assumes a specific form of the correlation function

$$\partial_x^2 \partial_y^2 G_{x^- , y^-} = g^2 \mu^2(x^-) \delta_{xy}, \quad (27)$$

but the latter is not a necessary ingredient for the truncations and will not be assumed in the following.

One advantage of such a procedure is that all possible correlators with any number of Wilson lines automatically obey all group theoretical relations imposed in any possible coincidence limit, such as the relationships listed in Fig. 7. More generally, we can achieve this feature by parametrizing Wilson line correlators in a Gaussian manner via

$$\langle \dots \rangle(\eta) = \langle P_\eta e^{\int_{\eta_0}^\eta d\eta' [\frac{1}{2} \int_{uv} G_{uv}(\eta') i \nabla_u^a i \nabla_v^a] \dots} \rangle(\eta_0), \quad (28)$$

where we have replaced x^- by a general coordinate space longitudinal (rapidity) variable $\eta \sim \ln x^-$. Practically, Eq. (28) allows one to find a parametrization for any set of correlators with consistent coincidence limits (such as listed in Fig. 7) by solving the functional differential equation

$$\frac{d}{d\eta} \langle F[U] \rangle(\eta) = \frac{1}{2} \int_{u,v} \langle G_{uv}(X) i \nabla_u^a i \nabla_v^a F[U] \rangle(\eta) \quad (29)$$

$$\begin{array}{c}
\begin{array}{ccc}
& z \mapsto x \text{ or } y & \rightarrow C_F \text{tr}(U_x U_y^\dagger) \\
\text{tr}(U_z t^a U_z^\dagger U_x t^a U_y^\dagger) = \tilde{U}^{ab} \text{tr}(t^a U_x t^b U_y^\dagger) & & \xrightarrow{y \mapsto x} N_c C_F \\
& & \xrightarrow{z \mapsto x} \\
& & \uparrow \\
& & \frac{1}{2} \tilde{\text{tr}}(\tilde{U}_z \tilde{U}_x^\dagger) \\
& & \uparrow \\
& & \frac{1}{2} (\text{tr}(U_x U_z^\dagger))^2 - 1 \\
& & \uparrow \\
& & \frac{1}{2} \text{tr}(U_x U_z^\dagger) \text{tr}(U_z U_y^\dagger) - \frac{1}{2N_c} \text{tr}(U_x U_y^\dagger) \\
& & \xrightarrow{y \mapsto x} \\
& & \uparrow \\
& & \text{Fierz} \\
& & \downarrow \\
& & \frac{1}{2} \text{tr}(U_x U_z^\dagger) \text{tr}(U_z U_y^\dagger) - \frac{1}{2N_c} \text{tr}(U_x U_y^\dagger)
\end{array}
\end{array}$$

FIG. 7. Correlator relations between $q\bar{q}g$, $q\bar{q}$ and gg .

to parametrize some *singlet* observable $\langle F[U] \rangle$ in terms of the two-point correlator G_{uv} . The simplest example is the $q\bar{q}$ correlator with $F[U] \rightarrow \text{tr}(U_x U_y^\dagger)/N_c$ for which this functional equation indeed turns into a closed differential equation. For more complicated operators such as $q^2 \bar{q}^2$, the functional equation turns into a set of coupled differential equations that need to be solved simultaneously. The expectation values of several different Wilson line operators with a Gaussian weight have been calculated in the literature, e.g. in Refs. [3,31,40–45].

The simplest generalization of the Gaussian truncation is what we will call the three-point exponential truncation. It includes the two-point contribution from the Gaussian truncation but adds all mathematically independent three-point functions to the exponential. This can be summarized by

$$\begin{aligned}
\langle \dots \rangle(\eta) = & \left\langle P_\eta \exp \left\{ \int_{\eta_0}^\eta d\eta' \left[\frac{1}{2} \int_{uv} G_{uv}(\eta') i \nabla_u^a i \nabla_v^a \frac{1}{3!} \int_{uvw} G_{uvw}^d(\eta') d^{abc} i \nabla_u^a i \nabla_v^b i \nabla_w^c \right. \right. \right. \\
& \left. \left. \left. \times \frac{1}{3!} \int_{uvw} G_{uvw}^f(\eta') f^{abc} i \nabla_u^a i \nabla_v^b i \nabla_w^c + 4 \text{ pts} \right] \right\} \dots(\eta_0) \right\rangle. \quad (30)
\end{aligned}$$

As indicated there is, in principle, no obstruction to higher n -point functions to this parametrization functional.

Note that in Eq. (30) both G and G^d are fully symmetrical under exchange of any pair of transverse coordinates, while G^f has slightly more complicated features but will not enter any of the correlators in Eqs. (3) and (5) so that we have no need to discuss it in any more detail.

We choose $G_{uu} = 0$ and $G_{uuu} = 0$ as this simplifies some of the expressions below from the outset. The correlators in Eq. (21) then take the form

$$S_{xy} = \frac{\langle \text{tr}(U_x U_y^\dagger) \rangle}{N_c} = e^{-C_F \mathcal{G}_{xy}} \quad (31a)$$

and

$$\frac{\langle U_z^{ab} \text{tr}(t^a U_x t^b U_y^\dagger) \rangle}{2N_c C_F} = e^{-\frac{N_c}{2}(\mathcal{G}_{xz} + \mathcal{G}_{zy} - \mathcal{G}_{xy}) - C_F \mathcal{G}_{xy}} \quad (31b)$$

where

$$\mathcal{G}_{xy}(\eta) = (\mathcal{P} + i\mathcal{O})_{xy} \quad (31c)$$

whose real and imaginary parts are literally the \mathcal{P} and \mathcal{O} introduced as parametrization functions of the complex number $\langle \text{tr}(U_x U_y^\dagger) \rangle(Y)/N_c$. The truncation procedure asserts that they also consistently parametrize the $q\bar{q}g$ correlator and provides an explicit expression of \mathcal{G} in terms

of G and G^d and their respective initial conditions at η_0 :

$$\mathcal{P}_{xy}(\eta) := \int_{\eta_0}^\eta d\eta' G_{xy} + \mathcal{P}_{xy}(\eta_0) = \mathcal{P}_{yx}(\eta), \quad (32a)$$

$$\begin{aligned}
i\mathcal{O}_{xy}(\eta) &:= \frac{C_d}{4} \int_{\eta_0}^\eta d\eta' (G_{yxx}^d - G_{yyx}^d) + i\mathcal{O}_{xy}(\eta_0) \\
&= -i\mathcal{O}_{yx}(\eta). \quad (32b)
\end{aligned}$$

Strikingly, the observables considered here do *not* allow access to G_{uvw} with all three coordinates independent despite the fact that the $q\bar{q}g$ correlator features three distinct coordinates. For G_{uvw} to occur with its full coordinate dependence one needs for example a protonlike state which remains outside the scope of this paper.

In the literature one often uses the same notation for the factorization rapidity Y and the longitudinal coordinate in the path-ordered exponential η (or $\ln x^-$). With the physical interpretation given above these are, however, not the same quantity. The coordinate x^- that gives the interpretation of the Wilson line as a path-ordered exponential in the color field is a spatial coordinate along the trajectory of the path-ordered exponential. The local structure of the correlation function in the longitudinal coordinate essentially imposes the Gaussian property on the distribution of Wilson lines, since these are made up of independent infinitesimal increments. The coordinate x^- is, however, not directly

related to an experimental observable, but cross sections always depend on Wilson lines integrated over x^- .

The rapidity Y , on the other hand, is a longitudinal *momentum* scale separating large- and small- x degrees of freedom in the CGC formalism. The scale Y is a factorization scale in the renormalization group evolution and should be chosen according to the typical longitudinal momentum scale in the studied scattering process. A loose uncertainty principle argument states that for a momentum space scale Y , the fields in the target are localized in a coordinate space interval $\Delta x^- \sim \exp\{Y\}$. Thus, identifying η and Y is indeed justified at the leading logarithmic level (but not at higher orders in perturbation theory). This identification is not needed or used anywhere in the present calculation and we will keep the separate notation for these two variables.

It is important to realize that Eq. (29) is a parametrization equation that expresses singlet Wilson line correlators in terms of a two-point function whose Y dependence needs to be derived *separately* or is *known a priori*. Thus, the solutions of the parametrization equation, e.g. Eqs. (31a) and (31b), have an unknown dependence on the factorization rapidity Y that will need to be derived from the actual QCD dynamics.

One way to derive an equation for the dependence of the two-point function \mathcal{G} on the factorization rapidity Y is to take the *solutions* of Eq. (29) and insert them into the appropriate equations from the Balitsky hierarchy. Every equation of the hierarchy leads to a different equation for \mathcal{G} . Choosing this equation to be the equation (21) for the expectation value of $\text{tr}(U_x U_y^\dagger)/N_c$ dipole leads to a Gaussian truncation of the JIMWLK hierarchy.

It is also possible to rewrite the parametrization equation (30) in terms of a more abstract longitudinal

coordinate, which can then be chosen to be equal to the evolution rapidity. This procedure can be used to simplify the coupled evolution equations for more complicated higher-point operators of Wilson lines [31], at the expense of losing the physical interpretation of the longitudinal coordinate. Here we will concentrate on the evolution equation for just the dipole operator and can easily remain with the physical interpretation of η as being related to x^- and distinct from the momentum rapidity Y .

As indicated in Eq. (32), the effective two-point functions *do* show the required symmetry properties of $\langle \text{tr}(U_x U_y^\dagger) \rangle / N_c$ under complex conjugation; one obtains a consistent *gauge-invariant* truncation of the associated Balitsky hierarchy with the evolution equation

$$\frac{d}{dY} \mathcal{G}_{xy} = \frac{\alpha_s}{\pi^2} \int d^2z \mathcal{K}_{xzy} (1 - e^{-\frac{N_c}{2}[\mathcal{G}_{xz} + \mathcal{G}_{zy} - \mathcal{G}_{xy}]}), \quad (33)$$

which obviously couples real and imaginary parts. Equation (33) generalizes the large- N_c results of [29,30] to finite N_c .

The solutions to the parametrization equations (31) and thus the evolution equation (33) differ from their BK counterpart for the total cross section in the Gaussian truncation only through a nonvanishing imaginary part $i\mathcal{O} \neq 0$ appearing in \mathcal{G} . Indeed $i\mathcal{O} = 0$ and $\mathcal{P} \in [0, \infty]$ is a consistent solution to this equation which leads to a successful phenomenology for HERA data at small x [46]: If the initial condition for \mathcal{G} is real, the equation never generates an imaginary part. This can be seen from the coupled equations for the real and imaginary parts explicitly:

$$\frac{d}{dY} \mathcal{P}_{xy}(Y) = \frac{\alpha_s}{\pi^2} \int d^2z \mathcal{K}_{xzy} \left[1 - e^{-\frac{N_c}{2}[\mathcal{P}_{xz} + \mathcal{P}_{zy} - \mathcal{P}_{xy}](Y)} \cos \left(\frac{N_c}{2} [\mathcal{O}_{xz} + \mathcal{O}_{zy} - \mathcal{O}_{xy}](Y) \right) \right], \quad (34a)$$

$$\frac{d}{dY} \mathcal{O}_{xy}(Y) = \frac{\alpha_s}{\pi^2} \int d^2z \mathcal{K}_{xzy} \left[e^{-\frac{N_c}{2}[\mathcal{P}_{xz} + \mathcal{P}_{zy} - \mathcal{P}_{xy}](Y)} \sin \left(\frac{N_c}{2} [\mathcal{O}_{xz} + \mathcal{O}_{zy} - \mathcal{O}_{xy}](Y) \right) \right]. \quad (34b)$$

VI. EVOLUTION IN THE THREE-POINT EXPONENTIAL TRUNCATION

There are many different ways to rewrite the equation before implementing it numerically. The most prominent among these is the possibility to map (33) into the BK equation, as noted in [1]. Let us briefly recapitulate how this is done. Inserting the Gaussian correlator parametrizations of the three-point exponential truncation (31) into the first equation of the Balitsky hierarchy (21) and canceling an overall factor of N_c , we get

$$\begin{aligned} \frac{d}{dY} e^{-C_F \mathcal{G}_{xy}} &= \frac{\alpha_s C_F}{\pi^2} \int d^2z \tilde{\mathcal{K}}_{xzy} \\ &\times (e^{-\frac{N_c}{2}[\mathcal{G}_{xz} + \mathcal{G}_{zy} - \mathcal{G}_{xy}] - C_F \mathcal{G}_{xy}} - e^{-C_F \mathcal{G}_{xy}}). \end{aligned} \quad (35)$$

From here it is straightforward to arrive at Eq. (33) after canceling an overall factor $e^{-C_F \mathcal{G}_{xy}}$ common to both sides.

To derive the relation between the BK equation and the Gaussian truncation one starts by multiplying both sides of Eq. (33) with $- \frac{N_c}{2} e^{-\frac{N_c}{2} \mathcal{G}_{xy}}$, leading to the alternative form

$$\frac{d}{dY} e^{-\frac{N_c}{2} \mathcal{G}_{xy}} = \frac{\alpha_s N_c}{\pi^2} \frac{1}{2} \int d^2z \mathcal{K}_{xzy} \times (e^{-\frac{N_c}{2} [\mathcal{G}_{xz} + \mathcal{G}_{zy}]} - e^{-\frac{N_c}{2} \mathcal{G}_{xy}}) \quad (36)$$

for this evolution equation. Now, after identifying

$$S_{xy}^{\text{BK}} := e^{-\frac{N_c}{2} \mathcal{G}_{xy}}, \quad (37)$$

it is manifest that Eq. (36) is equivalent to the BK equation

$$\frac{d}{dY} S_{xy}^{\text{BK}} = \frac{\alpha_s N_c}{\pi^2} \frac{1}{2} \int d^2z \tilde{\mathcal{K}}_{xzy} (S_{xz}^{\text{BK}} S_{zy}^{\text{BK}} - S_{xy}^{\text{BK}}). \quad (38)$$

Equations (33), (35), (36), and (38) are all equivalent: They all determine the evolution for the same function \mathcal{G} and will lead to the same Y dependence provided we set the same initial condition on \mathcal{G} . The difference between the Gaussian truncation and the large- N_c BK equation (in the sense the term is commonly used) is in the relation between the physical scattering amplitude and the solution of the evolution equation. In the large- N_c limit the solution of the BK equation S^{BK} is assumed to be the physical scattering amplitude. In the finite- N_c Gaussian truncation the physical scattering amplitude is related to the fundamental two-point correlator \mathcal{G} by (33) and to the solution of the BK equation by (36). Thus the physical scattering amplitude is obtained from the solution of the BK equation as

$$S_{xy} = \left\langle \frac{\text{tr}(U_x U_y^\dagger)}{N_c} \right\rangle = (S_{xy}^{\text{BK}})^{\frac{2C_F}{N_c}}. \quad (39)$$

Thus the real and imaginary parts of the physical dipole operator in the Gaussian truncation S_{xy} , expressed in terms of the real and imaginary parts of the BK-evolved dipole, read

$$\text{Re} S_{xy} = |S_{xy}^{\text{BK}}|^{\frac{2C_F}{N_c}} \cos \left\{ \frac{2C_F}{N_c} \arctan \frac{\text{Im} S_{xy}^{\text{BK}}}{\text{Re} S_{xy}^{\text{BK}}} \right\}, \quad (40)$$

$$\text{Im} S_{xy} = |S_{xy}^{\text{BK}}|^{\frac{2C_F}{N_c}} \sin \left\{ \frac{2C_F}{N_c} \arctan \frac{\text{Im} S_{xy}^{\text{BK}}}{\text{Re} S_{xy}^{\text{BK}}} \right\}. \quad (41)$$

Note that a purely real solution of the BK equation still gives a purely real dipole expectation value, but the presence of an imaginary part in the BK equation affects both the real and imaginary parts of the physical dipole.

Separating the identity from the BK-equation dipole operator S^{BK} , one gets the scattering amplitude $N_r^{\text{BK}} = 1 - S_r^{\text{BK}}$, where $\mathbf{r} = \mathbf{x} - \mathbf{y}$. In line with our earlier conventions in Eq. (9) we denote its real and imaginary parts as $P_r^{\text{BK}} := \text{Re}(N_r^{\text{BK}})$, the BK *Pomeron* and $O_r^{\text{BK}} := \text{Im}(N_r^{\text{BK}})$, the BK *odderon*. In terms of these, the evolution equation (38) now becomes a set of two real integro-differential equations

$$\frac{dP_r^{\text{BK}}}{dY} = \frac{\alpha_s N_c}{2\pi^2} \int d^2r' \frac{r^2}{r'^2 r'^2} (P_{r'}^{\text{BK}} + P_{r''}^{\text{BK}} - P_r^{\text{BK}} - P_r^{\text{BK}} P_{r'}^{\text{BK}} + O_r^{\text{BK}} O_{r'}^{\text{BK}}), \quad (42)$$

$$\frac{dO_r^{\text{BK}}}{dY} = \frac{\alpha_s N_c}{2\pi^2} \int d^2r' \frac{r^2}{r'^2 r'^2} (O_{r'}^{\text{BK}} + O_{r''}^{\text{BK}} - O_r^{\text{BK}} - P_{r'}^{\text{BK}} O_{r''}^{\text{BK}} - O_r^{\text{BK}} P_{r'}^{\text{BK}}), \quad (43)$$

where $\mathbf{r}'' \equiv \mathbf{r} - \mathbf{r}'$. These equations are identical to those derived in Refs. [29,30] in the large- N_c limit. As discussed above, what changes at finite N_c in the Gaussian truncation is the relation between the solution of these equations and the physical scattering amplitude, which is now given by Eqs. (40) and (41).

Recall that from the definition of S_r it follows that $S_r^* = S_{-r}$. This in turn imposes separate symmetry properties on the real and imaginary parts of $\mathcal{G} = \mathcal{P} + i\mathcal{O}$ which are correctly reproduced by our truncation in Eq. (32). Via (37) they directly imply that $S_r^{\text{BK}*} = S_{-r}^{\text{BK}}$. Thus the real and imaginary parts of the amplitude are odd or even under reflections:

$$P_{-r}^{\text{BK}} = P_r^{\text{BK}}, \quad (44)$$

$$O_{-r}^{\text{BK}} = -O_r^{\text{BK}}. \quad (45)$$

For the linear BFKL part of the equation it is particularly convenient to decompose the solution to the evolution equation in terms of eigenfunctions of the kernel, both in $|\mathbf{r}|$ and in azimuthal angle. For the nonlinear case it is more convenient to continue working in r space, but we can still perform a Fourier series expansion in the azimuthal angle. The symmetry (44) and (45) dictates that the Pomeron and odderon can only have even or odd harmonics, respectively:

$$P_r^{\text{BK}} = \sum_{n=0}^{\infty} P_{2n}^{\text{BK}}(r) \cos(2n\varphi_r), \quad (46)$$

$$O_r^{\text{BK}} = \sum_{n=0}^{\infty} O_{2n+1}^{\text{BK}}(r) \cos((2n+1)\varphi_r), \quad (47)$$

where φ_r is the angle of the vector \mathbf{r} with respect to an (arbitrary) reaction plane. Based on the known BFKL dynamics in the linear regime, we expect the small azimuthal harmonics to dominate in the high energy regime. Our working hypothesis here is that the same is true also in the nonlinear case. This allows us to efficiently study the equations by truncating the series and only keeping the lowest harmonics. We can control the error made in this approximation *ex post* by calculating the rapidity dependence of the first neglected term in the series from the ones that are kept.

A quick examination of Eqs. (42) and (43) reveals that the usual azimuthal $P_0^{\text{BK}}(r)$ is a fixed point of the equation. Including the lowest odderon harmonic $O_1^{\text{BK}}(r)$ will generate a second Pomeron $P_2^{\text{BK}}(r)$ through the $(O^{\text{BK}}(r))^2$ term in (42), which again will generate a higher $O_3^{\text{BK}}(r)$ harmonic through the nonlinear $P^{\text{BK}}O^{\text{BK}}$ coupling in (43). In this way, including an odderon will automatically generate an infinite tower of higher harmonics in both the odderon and the Pomeron amplitudes. In principle, it could thus be possible that, through this coupling, an odderon component would have an observable signal in

a P -even observable such as dijet correlations at an electron-ion collider [47].

For this first numerical study we have truncated the series to the smallest harmonics of both the Pomeron and odderon, i.e. $P_0^{\text{BK}}(r)$ and $O_1^{\text{BK}}(r)$, by dropping the $O_r^{\text{BK}}O_{r'}^{\text{BK}}$ term from the Pomeron evolution equation (42). With this truncation, the Pomeron amplitude stays rotationally invariant and the odderon equation (43) can be solved as such with only the lowest harmonic $O_1^{\text{BK}}(r)$. To see this explicitly, note that with only the azimuthally symmetric component in the Pomeron amplitude, we can write the odderon equation as

$$\begin{aligned} \frac{dO_1^{\text{BK}}(r) \cos \theta}{dY} = & \frac{\alpha_s N_c}{2\pi^2} \int d^2r' \frac{r^2}{r'^2 r''^2} \times (O_1^{\text{BK}}(r') \cos \theta' + O_1^{\text{BK}}(r'') \cos \theta'' - O_1^{\text{BK}}(r) \cos \theta \\ & - P_0^{\text{BK}}(r') O_1^{\text{BK}}(r'') \cos \theta'' - O_1^{\text{BK}}(r') P_0^{\text{BK}}(r'') \cos \theta'), \end{aligned} \quad (48)$$

where θ, θ' and θ'' are the angles of r, r' and r'' with respect to the x axis. In practice we can solve Eq. (43) by choosing the vector r to lie on the x axis, with thus $\cos \varphi_r = 1$. To show explicitly that this is the case, we use $(r'')^2 = r^2 + (r')^2 - 2rr' \cos(\theta - \theta')$ and $\cos \theta'' = (r \cos \theta - r' \cos \theta')/r''$ to write this as

$$\begin{aligned} \frac{dO_1^{\text{BK}}(r) \cos \theta}{dY} = & \frac{\alpha_s N_c}{2\pi^2} \int dr' d\theta' r' \frac{r^2}{(r')^2 (r'')^2} \times \left[(1 - P_0^{\text{BK}}(r'')) O^{\text{BK}_1}(r') \cos \theta' \right. \\ & \left. + (1 - P_0^{\text{BK}}(r')) O_1^{\text{BK}}(r'') \frac{r \cos \theta - r' \cos \theta'}{r''} - O_1^{\text{BK}}(r) \cos \theta \right]. \end{aligned} \quad (49)$$

We then take $\phi = \theta' - \theta$ as a new integration variable and use the identity $\cos(\theta') = \cos \phi \cos \theta - \sin \phi \sin \theta$. Now the terms that are proportional to $\sin \theta$ are also proportional to $\sin \phi$ times an even function of ϕ and vanish upon integration over ϕ , leaving every term on the right-hand side of Eq. (49) proportional to $\cos \theta$. Thus, as discussed earlier, with this approximation of a θ -independent Pomeron amplitude the equation for the $\cos \theta$ harmonic of the odderon closes. We can cancel the $\cos \theta$ from Eq. (49), and we are left with the truncated set of equations

$$\frac{dP_0^{\text{BK}}(r)}{dY} = \frac{\alpha_s N_c}{2\pi^2} \int d^2r' \frac{r^2}{r'^2 r''^2} (P_0^{\text{BK}}(r') + P_0^{\text{BK}}(r'') - P_0^{\text{BK}}(r) - P_0^{\text{BK}}(r') P_0^{\text{BK}}(r'')), \quad (50)$$

$$\frac{dO_1^{\text{BK}}(r)}{dY} = \frac{\alpha_s N_c}{2\pi^2} \int dr' d\phi r' \frac{r^2}{(r')^2 (r'')^2} \left[(1 - P_0^{\text{BK}}(r'')) O^{\text{BK}_1}(r') \cos \phi + (1 - P_0^{\text{BK}}(r')) O_1^{\text{BK}}(r'') \frac{r - r' \cos \phi}{r''} - O_1^{\text{BK}}(r) \right], \quad (51)$$

with $(r'')^2 = r^2 + (r')^2 - 2rr' \cos \phi$.

We will now proceed to numerically solve Eqs. (50) and (51). We will parametrize the initial condition as in Eq. (19):

$$P_0^{\text{BK}}(r'')|_{Y=0} = 1 - \exp\left\{-\frac{Q_0^2 r^2}{4}\right\}, \quad (52)$$

$$O_1^{\text{BK}}(r)|_{Y=0} = -\kappa \exp\left\{-\frac{Q_0^2 r^2}{4}\right\} \left(\frac{Q_0^3 r^3}{8}\right), \quad (53)$$

with the maximal value $\kappa = 1/3$. Figure 8 shows the resulting amplitudes. For the Pomeron part one sees the

familiar ‘‘traveling wave’’ solution moving towards smaller dipoles with rapidity. The odderon amplitude, on the other hand, merely decreases in magnitude but its characteristic dipole size scale does not decrease. This behavior is quantified further in Figs. 9 and 10, showing the height of the odderon amplitude peak as a function of rapidity and the ratio of the (BK) odderon to the (BK) Pomeron amplitude.

In the calculations presented above, we have neglected the odderon squared term in the evolution equation. This can be justified by the fact that, since it has not yet been unambiguously observed experimentally, the odderon amplitude can be expected to be small. Also expectations based on the linear evolution equation would lead to an odderon amplitude that

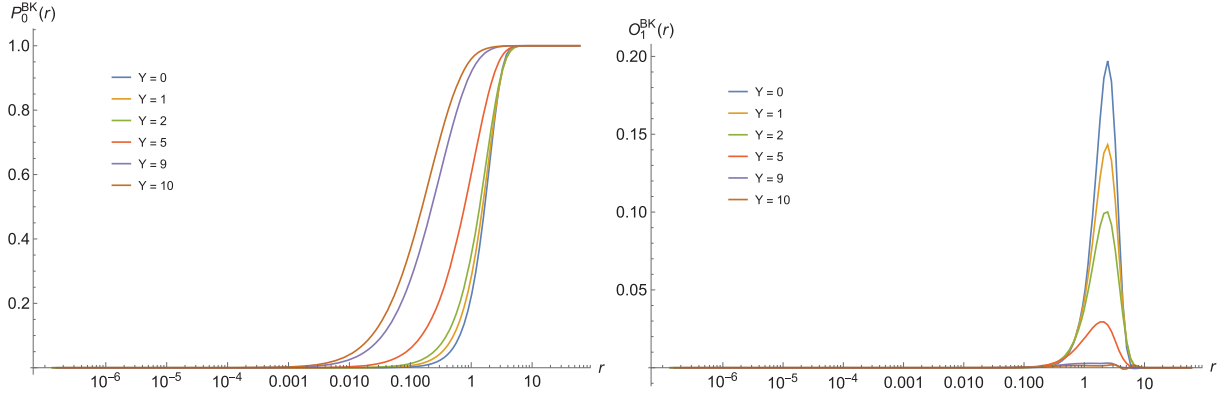


FIG. 8. Evolution of the Pomeron (left) and odderon (right) amplitudes according to Eqs. (50) and (51) with the initial condition (19) with $\kappa = 1/3$.

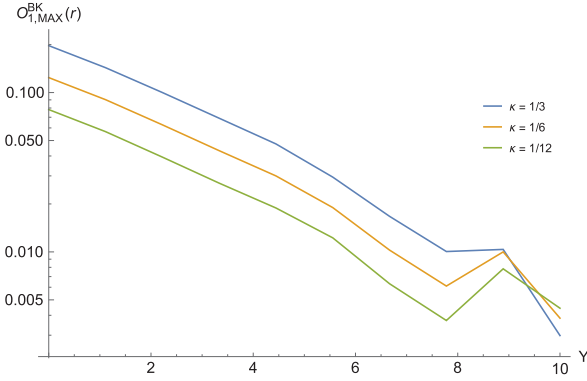


FIG. 9. Plot of the height of the odderon peak (as shown in Fig. 8) as a function of rapidity. Three different values $\kappa = 1/3$, $1/6$ and $1/12$ are shown.

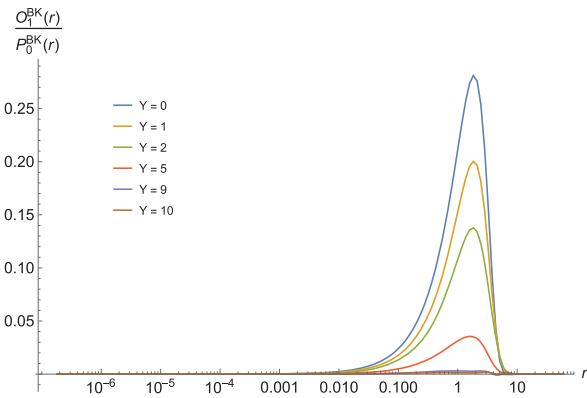


FIG. 10. Ratio of $\mathcal{O}(r)/\mathcal{P}(r)$ for $\kappa = 1/3$ as a function of r at different rapidities.

decreases as a function of rapidity [29,30]. Within the truncation of the harmonic series (46) and (47) one can estimate the size of this approximation by evaluating the contribution of the first neglected term on one time step, i.e. the contribution of the odderon squared term to the evolution equation of the Pomeron. As discussed previously, the square of the odderon term $O_1^{BK}(r) \cos \theta$ gives both a θ -independent and a $\cos 2\theta$ contribution to the evolution equation of the Pomeron. We denote the coefficients of these by a_1 and a_2 ; i.e. we write

$$\frac{dP_r^{BK}}{dY} = [\text{BK}] + a_1(r) + a_2(r) \cos(2\theta_r). \quad (54)$$

We can now compare the odderon terms to the rotationally invariant solution. Figure 11 shows the initial condition for the fairly large value of $\kappa = 1/3$. It can be seen that the odderon squared terms are negligible in the small- r region that drives the evolution. The θ -independent a_1 term is particularly small, while a_2 is slightly larger. We conclude

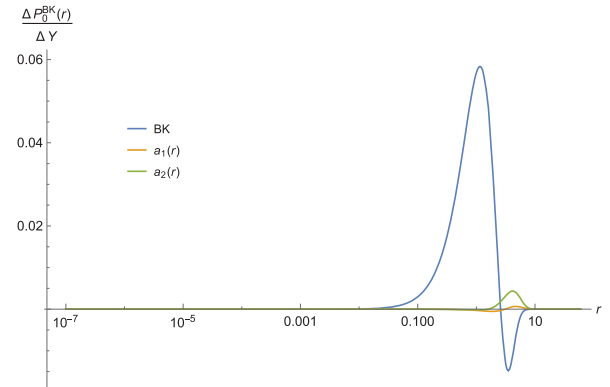


FIG. 11. Contribution to $\Delta\mathcal{P}_r/\Delta Y$ in one step in rapidity from: the BK equation, $a_1(r)$ and $a_2(r)$, with the maximal odderon amplitude $\kappa = 1/3$.

that the main effect of the nonlinear odderon term is not to modify the evolution of the rotationally invariant $P_0^{\text{BK}}(r)$ amplitude but to introduce a small $\cos 2\theta$ term into the Pomeron.

VII. FULL LEADING-ORDER JIMWLK EVOLUTION WITH ODDERON ADMIXTURE

Since the evolution equation (33) or (34) is the result of a truncation of the full functional JIMWLK evolution, one may legitimately ask if the truncation deviates quantitatively or even qualitatively from a full JIMWLK simulation. This can be performed at leading order or at partial next-to-leading order with running coupling corrections included. Since in this paper we are only interested in qualitative behavior we have, for simplicity, chosen the former option.

What is quite remarkable is that the only thing that needs to change to perform a simulation run is the initial condition. The Langevin simulation governing JIMWLK evolution is carried out on a square transverse grid. A simulation for the total cross section starts from an initial condition that treats both of the principal directions of the transverse plane in the same way. To obtain an odderon admixture one must break this lattice remnant of rotational invariance and introduce a bias towards one of the directions into the initial condition—the code used for evolution needs no modification at all.

In this work we investigate the properties of the parity-odd initial states with the following simple setup: We use a lattice of size L^2 with periodic boundary conditions. First we generate an ensemble of standard parity-even initial states with a probability distribution

$$P(\text{Re}tr(U_x U_y^\dagger)) \propto \exp(-(x-y)^2/4R^2), \quad (55)$$

using the methods described in [19]. This generates configurations with saturation scale $Q_s \sim 1/R$. The expectation value of the imaginary part of $\langle \text{tr}(U_x U_y^\dagger) \rangle / N_c$ vanishes and its real part falls into the interval between 0 and 1. Such an ensemble is a suitable starting point for a simulation without an odderon admixture.

To introduce an odderon contribution one needs to generate an imaginary part. A convenient way of doing so is to consider a “potential”

$$V[U](\mathbf{x}) = \alpha \sum_y \text{Im}tr(U_x U_y^\dagger) f(\mathbf{x} - \mathbf{y}), \quad (56)$$

where α is a small real parameter and f is an odd function of \mathbf{r} that breaks the symmetry between the two coordinate directions:

$$f(\mathbf{x}) = x_1 e^{-x^2/4R^2} \frac{(x_1^2 - (L/2)^2)(x_2^2 - (L/2)^2)}{L^4}. \quad (57)$$

The last part of the expression merely ensures that $f(x)$ vanishes at the boundaries $x_i = \pm L/2$ so that no discontinuities arise there.

We use a left derivative to define the force induced by the “potential” V as

$$F_a(x) = -\alpha \sum_y \text{Re}tr(\lambda_a U_x U_y^\dagger) f(\mathbf{x} - \mathbf{y}) \quad (58)$$

and make an update $U_x \rightarrow e^{i\alpha F_a(x)\lambda_a} U_x$. This update is repeated a few times for all sites \mathbf{x} . The magnitude of the parity-odd contribution can be modified by adjusting the constant α and the number of update steps.

In Figs. 12–14 we show the behavior of the real and imaginary parts of $\text{tr}(U_x U_y^\dagger)$ as measured on $L^2 = 128^2$ lattices, using (a) no, (b) mild and (c) very large odderon contributions, respectively. Let us discuss the three cases in turn:

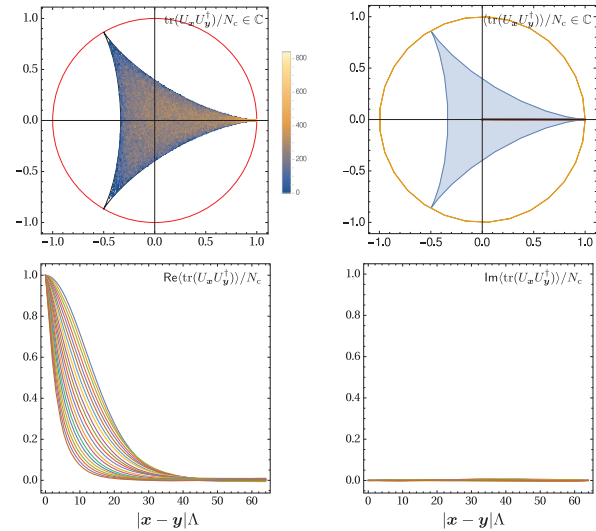


FIG. 12. Leading-order Langevin simulations with curves for different Y values at $N_c = 3$ without an odderon admixture. The top row shows a density histogram of individual trace values (left) and averages (right) for configurations pulled from the ensembles through some Y range. The dipole $\text{tr}(U_x U_y^\dagger)/N_c$ becomes 1 in the short-distance limit. This is why the distribution exhibits a strong maximum there. Note that the configurations cover much of the allowed range with only a small fraction falling near the maximally anticorrelated corners at $e^{\pm i2\pi/3}$. The density distribution is symmetric under reflection about the real axis. The averages fall into the real interval $[0, 1]$, despite the fact that many individual configurations show negative real parts. The bottom row shows real and imaginary parts of the correlator averages for a number of Y values. The real part exhibits the familiar approach to scaling (curves move “left” with increasing Y) and an imaginary part that is zero within good accuracy with only small fluctuations visible.

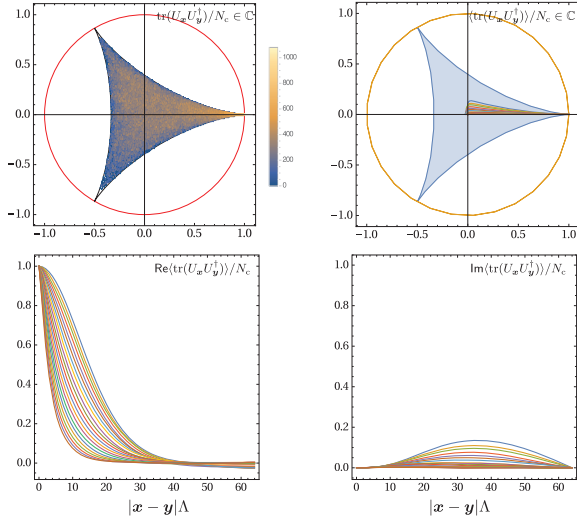


FIG. 13. Leading-order Langevin simulations with curves for different Y values at $N_c = 3$ with a moderate odderon admixture. The top row shows a density histogram of individual trace values (left) and averages (right) for configurations pulled from the ensembles through some Y range. Note that, as in Fig. 12, the configurations cover much of the allowed range with only a small fraction falling near the maximally anticorrelated corners at $e^{\pm i2\pi/3}$. The density distribution now shows a small bias towards positive real parts that leads to a nontrivial imaginary part in the averages. These move towards the real axis as Y increases. The bottom row shows real and imaginary parts of the correlator averages for a number of Y values. The real part now shows a small amount of anticorrelation which is erased quickly. The overall trend is an approach to scaling behavior very similar to that of the odderon-free simulation of Fig. 12. The imaginary part is small and erased in place as Y increases. The two contributions behave in a qualitatively different manner: approach to scaling for the real part (the Pomeron) decay for the imaginary part (the odderon).

- (a) *No odderon in the initial state.*—The ensemble is generated to follow Eq. (42) with no distortion applied so that the average

$$\langle \text{tr}(U_x U_y^\dagger) \rangle(Y)/N_c \in [0, 1] \text{ for all } Y. \quad (59)$$

The imaginary part vanishes in the initial condition and none is generated during evolution. This can likely be traced back to the adjoint nature of the Wilson lines “dressing” the Gaussian noise in the Langevin version of the leading-order JIMWLK equation. Note that this holds despite the fact that individual configurations $\text{tr}(U_x U_y^\dagger)/N_c$ occur anywhere inside the hypocycloid allowed by the constraints discussed in Sec. III. Plots illustrating this simulation are shown in Fig. 12. The top left displays a density histogram of configurations $\text{tr}(U_x U_y^\dagger)/N_c$ which almost fill the whole allowed

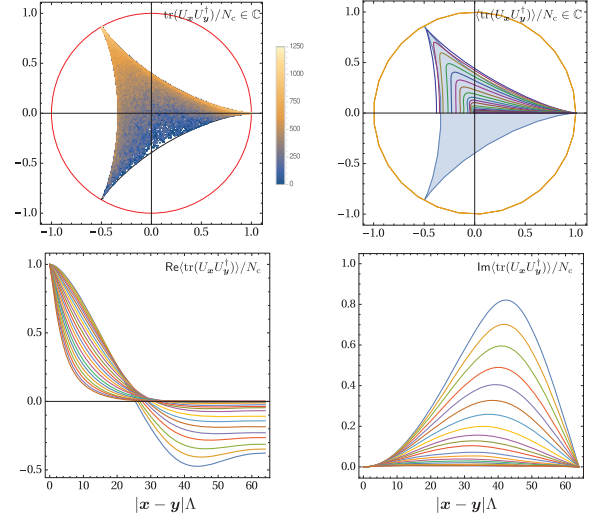


FIG. 14. Leading-order Langevin simulations with curves for different Y values at $N_c = 3$ with a maximized odderon admixture. The layout repeats that of Figs. 12 and 13. The density histogram now shows a second maximum at $e^{i2\pi/3}$, a strong anticorrelating distortion of the initial condition. This manifests itself in averages that (initially) push outside the hypocycloid into the triangle connecting the 3rd roots of unity, as discussed in the text. With this come strong anticorrelations in the real parts in the initial condition. These features that are extreme in the initial conditions nevertheless are erased during evolution which again approaches scaling form. The imaginary parts are maximized in the initial condition beyond what we expect to be physical, but the overall behavior is the same as for a moderate odderon admixture: The odderon contribution is erased in place.

region. Note that the density is lowest at the anticorrelated cusps corresponding to $e^{\pm i2\pi/3}$ and that the distribution is symmetric under a reflection along the real axis. As a consequence, Eq. (59) is satisfied for all Y , as shown top right. The plots in the second row show real and imaginary parts as a function of dipole size.³ The real part shows the familiar decay of the correlation length $R_s(Y)$ and will develop scaling behavior if allowed to evolve far enough.

- (b) *A moderate odderon admixture to the initial state.*—Plots illustrating this simulation are shown in Fig. 13. The density histogram for individual configurations $\text{tr}(U_x U_y^\dagger)/N_c$ shows a bias towards a positive imaginary part, which is confirmed by the averages $\langle \text{tr}(U_x U_y^\dagger) \rangle(Y)/N_c$ shown top right. Along with the appearance of an imaginary part, one observes that the real part shows negative values—anticorrelations appear. This simulation is qualitatively close to what we have discussed in the context of the truncations

³Units can only be assigned after a data fit, which is not the goal of this publication.

with a perturbative boundary condition, although no effort was made to create a literal r^3 behavior for the initial condition.

The striking feature of this is the qualitatively different behavior seen in the Y dependence of real and imaginary parts. While the real part does exhibit a small anticorrelation for $r \gtrsim R_s \equiv 1/Q_s$, the evolution of R_s and the approach to scaling are affected very little by the presence of an imaginary part. The imaginary part is *not* characterized by a moving Y -dependent scale; it shows a single, clearly developed maximum that remains largely at the same distance scale as Y changes. The dominating feature of evolution is that the height of the maximum shrinks—the odderon is erased in place.

- (c) *A maximized odderon admixture in the initial state.*—Plots illustrating this simulation are shown in Fig. 14. The initial condition is maximally distorted and the distribution of trace values has developed a second maximum in the maximally anticorrelated region at $e^{i2\pi/3}$.

This is an extreme case that we have included to illustrate the features of JIMWLK evolution. Due to the extreme initial condition, the dipole averages start to fall outside the hypocycloids and the lattice is too small for the real part to reach zero at large distances. Nevertheless, the behavior of the imaginary part still mirrors that of the realistic odderon admixture: The odderon does not move; it decays in place. We conclude that both the scale shift for the real part and the fixed scale decay for the imaginary part of the dipole correlator are genuine features of JIMWLK evolution, irrespective of the details of the initial condition.

VIII. DISCUSSION

In this paper we have shown how to derive the high energy evolution equations for the odderon amplitude using a consistent three-point truncation of the Balitsky hierarchy. In the large- N_c limit our solution recovers that of [29,30]. Decomposing the amplitudes in terms of Fourier harmonics yields an infinite series of coupled equations. Due to the nonlinear relation between the real and imaginary parts of the physical scattering amplitude, and the solutions of the corresponding BK equation [see Eqs. (40) and (41)], the presence of any odderon component introduces an angular dependence at all harmonics n into the scattering amplitude. This correlation vanishes in the large- N_c limit and would therefore not have been accessible previously. This coupling between the odderon amplitude and higher harmonics could allow for a quantitative experimental access to the odderon component in multiparticle correlations in future precise DIS experiments [48].

By truncating the harmonic series to the first nontrivial terms for both the Pomeron and odderon parts, one gets a closed nonlinear equation for the energy dependence of the

odderon amplitude. We have presented the first numerical solution to this equation available in the literature. We have then completely independently confirmed these results with a numerical lattice solution of the full JIMWLK equation with an initial condition containing an odderon component. Both of these numerical calculations have confirmed the earlier analytical conjectures based on the linear BFKL limit [29,30], showing that the odderon amplitude decreases with increasing collision energy. This observation justifies the truncation of the higher harmonic terms used in the BK-like numerical evaluation (the JIMWLK simulation needs no such truncation).

The odderon appears in full JIMWLK evolution *only* by preparing its initial conditions in a way that breaks rotational invariance in the transverse plane. This mirrors directly what is happening in a measurement process: The ensemble we average over needs to break rotation invariance in both cases. In an experiment this can be achieved by measuring polarizations, as is done in an STSA measurement. The total cross section as an average over a fully symmetric unbiased set of events will not be able to couple to the odderon at all. (Not even through mixing of real and imaginary parts during evolution—there are no average imaginary parts to begin with and none are generated during evolution.) A targeted observable on the other hand, like STSA, can give access to the imaginary parts of Wilson line correlators directly. Once a preselected ensemble of events generates such imaginary parts in the average, they also impact the real parts and may even trigger anticorrelations there. The mechanism for this mixing in full JIMWLK lies in the nonlinear nature of the evolution equation. Judging from the agreement between full JIMWLK evolution and the numerical results in the three-point exponential truncation it would appear that this nonlinear mechanism is well captured in the truncated theory.

The coupling of the odderon component may not have a strong effect on high energy asymptotical behavior even of targeted observables—as we have demonstrated, the odderon still decays with energy even beyond the linear BFKL approximation. At realistic collider energies the question is still open, but only if we consider tailored experiments of sufficient accuracy. If the presence of an odderon contribution comes with anticorrelations in the real parts in its initial condition, this might open new avenues to access them experimentally.

ACKNOWLEDGMENTS

We are grateful to H. Mäntysaari for help with BK numerics. T. L. is supported by the Academy of Finland, Projects No. 267321 and No. 273464. A. R. has been supported by a scholarship from the Center for International Mobility, Finland. K. R. is supported by the Academy of Finland Project No. 267286. H. W. is supported by the National Research Foundation of South Africa (NRF) under CPRR Grant No. 90509.

- [1] H. Weigert, Evolution at small x_{bj} : The color glass condensate, *Prog. Part. Nucl. Phys.* **55**, 461 (2005).
- [2] F. Gelis, E. Iancu, J. Jalilian-Marian, and R. Venugopalan, The color glass condensate, *Annu. Rev. Nucl. Part. Sci.* **60**, 463 (2010).
- [3] J. Jalilian-Marian, A. Kovner, L. D. McLerran, and H. Weigert, The intrinsic glue distribution at very small x , *Phys. Rev. D* **55**, 5414 (1997).
- [4] J. Jalilian-Marian, A. Kovner, A. Leonidov, and H. Weigert, The BFKL equation from the Wilson renormalization group, *Nucl. Phys.* **B504**, 415 (1997).
- [5] J. Jalilian-Marian, A. Kovner, A. Leonidov, and H. Weigert, The Wilson renormalization group for low x physics: Towards the high density regime, *Phys. Rev. D* **59**, 014014 (1998).
- [6] J. Jalilian-Marian, A. Kovner, and H. Weigert, The Wilson renormalization group for low x physics: Gluon evolution at finite parton density, *Phys. Rev. D* **59**, 014015 (1998).
- [7] J. Jalilian-Marian, A. Kovner, A. Leonidov, and H. Weigert, Unitarization of gluon distribution in the doubly logarithmic regime at high density, *Phys. Rev. D* **59**, 034007 (1999); **59**, 099903(E) (1999).
- [8] H. Weigert, Unitarity at small Bjorken x , *Nucl. Phys.* **A703**, 823 (2002).
- [9] E. Iancu, A. Leonidov, and L. D. McLerran, Nonlinear gluon evolution in the color glass condensate. I, *Nucl. Phys.* **A692**, 583 (2001).
- [10] E. Iancu and L. D. McLerran, Saturation and universality in QCD at small x , *Phys. Lett. B* **510**, 145 (2001).
- [11] E. Ferreiro, E. Iancu, A. Leonidov, and L. McLerran, Nonlinear gluon evolution in the color glass condensate. II, *Nucl. Phys.* **A703**, 489 (2002).
- [12] E. Iancu, A. Leonidov, and L. D. McLerran, The renormalization group equation for the color glass condensate, *Phys. Lett. B* **510**, 133 (2001).
- [13] A. H. Mueller, A simple derivation of the JIMWLK equation, *Phys. Lett. B* **523**, 243 (2001).
- [14] I. Balitsky, Operator expansion for high-energy scattering, *Nucl. Phys.* **B463**, 99 (1996).
- [15] I. Balitsky, Factorization for High-Energy Scattering, *Phys. Rev. Lett.* **81**, 2024 (1998).
- [16] I. Balitsky, Factorization and high-energy effective action, *Phys. Rev. D* **60**, 014020 (1999).
- [17] I. Balitsky, Effective field theory for the small- x evolution, *Phys. Lett. B* **518**, 235 (2001).
- [18] J.-P. Blaizot, E. Iancu, and H. Weigert, Nonlinear gluon evolution in path integral form, *Nucl. Phys.* **A713**, 441 (2003).
- [19] K. Rummukainen and H. Weigert, Universal features of JIMWLK and BK evolution at small x , *Nucl. Phys.* **A739**, 183 (2004).
- [20] A. Dumitru, J. Jalilian-Marian, T. Lappi, B. Schenke, and R. Venugopalan, Renormalization group evolution of multi-gluon correlators in high energy QCD, *Phys. Lett. B* **706**, 219 (2011).
- [21] T. Lappi and H. Mäntysaari, On the running coupling in the JIMWLK equation, *Eur. Phys. J. C* **73**, 2307 (2013).
- [22] Y. V. Kovchegov, Small- x F2 structure function of a nucleus including multiple Pomeron exchanges, *Phys. Rev. D* **60**, 034008 (1999).
- [23] L. D. McLerran and R. Venugopalan, Computing quark and gluon distribution functions for very large nuclei, *Phys. Rev. D* **49**, 2233 (1994).
- [24] L. D. McLerran and R. Venugopalan, Gluon distribution functions for very large nuclei at small transverse momentum, *Phys. Rev. D* **49**, 3352 (1994).
- [25] L. D. McLerran and R. Venugopalan, Green's functions in the color field of a large nucleus, *Phys. Rev. D* **50**, 2225 (1994).
- [26] S. Jeon and R. Venugopalan, A classical odderon in QCD at high energies, *Phys. Rev. D* **71**, 125003 (2005).
- [27] A. Dumitru, J. Jalilian-Marian, and E. Petreska, Two-gluon correlations and initial conditions for small- x evolution, *Phys. Rev. D* **84**, 014018 (2011).
- [28] A. Dumitru and E. Petreska, Initial conditions for dipole evolution beyond the McLerran-Venugopalan model, *Nucl. Phys.* **A879**, 59 (2012).
- [29] Y. V. Kovchegov, L. Szymanowski, and S. Wallon, Perturbative odderon in the dipole model, *Phys. Lett. B* **586**, 267 (2004).
- [30] Y. Hatta, E. Iancu, K. Itakura, and L. McLerran, Odderon in the color glass condensate, *Nucl. Phys.* **A760**, 172 (2005).
- [31] C. Marquet and H. Weigert, New observables to test the color glass condensate beyond the large- N_c limit, *Nucl. Phys.* **A843**, 68 (2010).
- [32] Y. V. Kovchegov and M. D. Sievert, Siverson function in the quasiclassical approximation, *Phys. Rev. D* **89**, 054035 (2014).
- [33] N. Kaiser, Mean eigenvalues for simple, simply connected, compact Lie groups, *J. Phys. A* **39**, 15287 (2006).
- [34] K. J. Golec-Biernat and M. Wusthoff, Saturation effects in deep inelastic scattering at low Q^2 and its implications on diffraction, *Phys. Rev. D* **59**, 014017 (1998).
- [35] T. Lappi and H. Mäntysaari, Direct numerical solution of the coordinate space Balitsky-Kovchegov equation at next to leading order, *Phys. Rev. D* **91**, 074016 (2015).
- [36] E. Iancu, J. D. Madrigal, A. H. Mueller, G. Soyez, and D. N. Triantafyllopoulos, Resumming double logarithms in the QCD evolution of color dipoles, *Phys. Lett. B* **744**, 293 (2015).
- [37] E. Iancu, J. D. Madrigal, A. H. Mueller, G. Soyez, and D. N. Triantafyllopoulos, Collinearly-improved BK evolution meets the HERA data, *Phys. Lett. B* **750**, 643 (2015).
- [38] T. Lappi and H. Mäntysaari, Next-to-leading order Balitsky-Kovchegov equation with resummation, *Phys. Rev. D* **93**, 094004 (2016).
- [39] F. Gelis and A. Peshier, Probing colored glass via q anti- q photoproduction, *Nucl. Phys.* **A697**, 879 (2002).
- [40] J. P. Blaizot, F. Gelis, and R. Venugopalan, High energy pA collisions in the color glass condensate approach I: Gluon production and the Cronin effect, *Nucl. Phys.* **A743**, 13 (2004).
- [41] J. P. Blaizot, F. Gelis, and R. Venugopalan, High energy pA collisions in the color glass condensate approach II: Quark production, *Nucl. Phys.* **A743**, 57 (2004).

- [42] F. Dominguez, C. Marquet, B.-W. Xiao, and F. Yuan, Universality of unintegrated gluon distributions at small x , *Phys. Rev. D* **83**, 105005 (2011).
- [43] F. Dominguez, C. Marquet, A. M. Stasto, and B.-W. Xiao, Universality of multiparticle production in QCD at high energies, *Phys. Rev. D* **87**, 034007 (2013).
- [44] F. Dominguez, C. Marquet, and B. Wu, On multiple scatterings of mesons in hot and cold QCD matter, *Nucl. Phys.* **A823**, 99 (2009).
- [45] E. Iancu and D. Triantafyllopoulos, JIMWLK evolution in the Gaussian approximation, *J. High Energy Phys.* 04 (2012) 025.
- [46] J. Kuokkanen, K. Rummukainen, and H. Weigert, HERA-data in the light of small x evolution with state of the art NLO input, *Nucl. Phys.* **A875**, 29 (2012).
- [47] A. Dumitru, T. Lappi, and V. Skokov, The Distribution of Linearly Polarized Gluons and Elliptic Azimuthal Anisotropy in DIS Dijet Production at High Energy, *Phys. Rev. Lett.* **115**, 252301 (2015).
- [48] A. Accardi *et al.*, Electron Ion Collider: The next QCD frontier—Understanding the glue that binds us all, [arXiv: 1212.1701](https://arxiv.org/abs/1212.1701).



II

UNEQUAL RAPIDITY CORRELATORS IN THE DILUTE LIMIT OF THE JIMWLK EVOLUTION

by

Lappi, T., & Ramnath, A. 2019

Physical Review D, 100(5), Article 05400

<https://doi.org/10.1103/PhysRevD.100.054003>

Reproduced with kind permission by American Physical Society.

Unequal rapidity correlators in the dilute limit of the JIMWLK evolution

T. Lappi*

*Department of Physics, P.O. Box 35, 40014 University of Jyväskylä, Finland,
and Helsinki Institute of Physics, P.O. Box 64, 00014 University of Helsinki, Finland*

A. Ramnath†

Department of Physics, P.O. Box 35, 40014 University of Jyväskylä, Finland

(Received 16 May 2019; published 4 September 2019)

We study unequal rapidity correlators in the stochastic Langevin picture of Jalilian-Marian–Iancu–McLerran–Weigert–Leonidov–Kovner (JIMWLK) evolution in the color glass condensate effective field theory. We discuss a diagrammatic interpretation of the long-range correlators. By separately evolving the Wilson lines in the direct and complex conjugate amplitudes, we use the formalism to study two-particle production at large rapidity separations. We show that the evolution between the rapidities of the two produced particles can be expressed as a linear equation, even in the full nonlinear limit. We also show how the Langevin formalism for two-particle correlations reduces to a Balitsky–Fadin–Kuraev–Lipatov (BFKL) picture in the dilute limit and in momentum space, providing an interpretation of BFKL evolution as a stochastic process for color charges.

DOI: 10.1103/PhysRevD.100.054003

I. INTRODUCTION

Multiparticle correlations, in both azimuthal angle and rapidity, are becoming an increasingly important experimental tool to access the properties of QCD in high energy collision systems. There is an intensive debate (see e.g., [1]) on the origin of the structure of azimuthal correlations in small (proton-proton and proton-nucleus) collision systems, where QCD correlations already present in the colliding objects compete with the effects of particle reinteractions (such as hydrodynamical flow or escape bias) in the later stage of the collision. In order to fully sort out the interpretation of the experimental results, it is important to fully understand the QCD dynamics leading to particle correlations. In particular, a characteristic feature of a hydrodynamical-like azimuthal correlation in a hadronic collision is that it extends far in rapidity [2]. Whereas effects at later times, such as resonance decays, have a very short range in rapidity, effects that extend to large rapidity separations must originate early in the collision. This is the case both for hydrodynamical flow, which is sensitive to the coordinate space geometry that is similar at all rapidities, and for correlations between the partons in the colliding

hadrons. Therefore, one needs to understand in QCD how the production of particles in high energy collisions is correlated across large rapidity separations.

The color glass condensate (CGC; see e.g., [3–5]) is an effective theory of QCD for high energy processes. It is based on a separation of scales between “fast” large- x degrees of freedom (d.o.f.) that are integrated out into an effective description and the soft small- x gluons that are the relevant d.o.f. for high energy scattering. The longitudinal momentum cutoff separating these two scales can be varied, and the effect of changing it absorbed into a renormalization of the effective description as a function of the longitudinal momentum (or rapidity) scale. This procedure leads to the JIMWLK¹ evolution equation [6–16], which can be used to resum leading logarithmic (in energy or x) corrections to QCD scattering cross sections. In practical calculations, the convenient d.o.f. for describing high energy QCD scattering is the Wilson line (see e.g., [17]). This is the eikonal scattering amplitude for a partonic probe passing through the target color field. In the CGC picture, the Wilson lines at each point in the transverse plane are stochastic variables drawn from a probability distribution; it is this probability distribution whose dependence on the rapidity $Y = \ln 1/x$ is given by the JIMWLK equation. An equivalent formulation for the evolution of the probability distribution is provided by the Langevin formulation [18], where the Wilson lines themselves depend on rapidity through a stochastic partial

*tuomas.v.v.lappi@jyu.fi

†andrecia.a.ramnath@student.jyu.fi

Published by the American Physical Society under the terms of the Creative Commons Attribution 4.0 International license. Further distribution of this work must maintain attribution to the author(s) and the published article’s title, journal citation, and DOI. Funded by SCOAP³.

¹The acronym stands for Jalilian-Marian–Iancu–McLerran–Weigert–Leonidov–Kovner.

differential equation involving a random noise. In addition to providing a more direct physical picture of the evolution, the Langevin formulation is the basis for numerical solutions of the JIMWLK equation [19–21].

The most common phenomenological applications of the CGC framework involve processes in which one needs only the Wilson lines at one rapidity. This includes deep inelastic scattering (DIS) cross sections [22–30], where the relevant rapidity depends only on the energy of the incident virtual photon, and single inclusive particle production [31–40], where it is determined by the kinematics of the produced particle. This is also true for multiparticle production [41,42], if the produced particles are close to each other in rapidity. The situation becomes more complicated, however, if one is interested in the correlations between particles that are separated by a parametrically large rapidity interval $\Delta Y \gtrsim 1/\alpha_s$.

For the case of two dense projectiles, there is a formalism, developed initially in [43], in which one follows a separate JIMWLK evolution for each of the colliding nuclei (see also [44] for a discussion). While the theoretical status of this formulation is still poorly understood (see e.g., the calculation reported in [45] suggesting that the decorrelation speed in rapidity is not an infrared safe quantity in this framework), it has been used in some phenomenological applications [46]. It has also led, via a k_T -factorized approximation, to the “glasma graph” or related calculations of multiparticle correlations in small collision systems [47–53]. In a perturbative language, the correlation in these calculations originates from two particles being produced from different Balitsky-Fadin-Kuraev-Lipatov (BFKL) ladders. This contribution dominates when both the projectile and the target are parametrically dense, so that there is no suppression for having additional ladders between them. In this sense, these are “dense-dense” calculations, even if done in a k_T -factorized approximation. On the other hand, when both the projectile and the target are dilute, correlated semihard particle production should be dominated by production from a single ladder, or the “jet graphs” in the language of [52,53]. Here, perturbative calculations of azimuthal decorrelations between these (Mueller-Navelet) jets have been performed, even at the next-to-leading-order (NLO) level [54].

For correlations between particles with large rapidity separations, it turns out that the “dilute-dense” case is actually in some sense the most complicated one. In the power counting of [43,55], where the color charge density in the dense target is parametrically large $\rho \sim 1/g$, and in the dilute projectile parametrically small $\rho \sim g$, both the “single ladder” (or jet graph) and “separate ladder” (or glasma graph) contributions are parametrically (in α_s) equally important. Out of these two kinds of contributions, there has been a lot of recent work in understanding the separate ladder contributions beyond the glasma graph approximation [48,49,56–59].

In the case of a dense target, our understanding of how to calculate the single ladder contribution is much less developed. One needs to generalize the fully nonlinear JIMWLK equation to the evolution of not just operators made out of Wilson lines at a single rapidity, but correlations of Wilson lines at different rapidities. For this purpose, a formalism based on the Langevin description of JIMWLK evolution was developed by Iancu and Triantafyllopoulos (IT) in [60] (see also earlier, very similar work in [61,62]). Here, one derives a new Langevin equation for a bilocal quantity that encodes the correlation between Wilson lines at two different rapidities. This formalism has not, however, been fully applied to phenomenology, nor has it been analyzed in more detail.

Our intention in this paper is to do the latter, with the main purpose of elucidating the diagrammatic interpretation of the IT formalism. We do this by starting from the bilocal Langevin description and taking the dilute limit. We show explicitly how this procedure recovers a two-particle correlation originating in particle production from the same BFKL ladder. In the process, we show also that the bilocal Langevin formulation, even in the full nonlinear case, can actually be transformed into a form in which the evolution between the rapidities of the two produced particles is linear. This somewhat surprising, or even counterintuitive, result seems to confirm what has been found earlier in [62,63]. This statement does not mean that the two-particle production process would somehow be fully linear; one still needs to solve the nonlinear evolution equation for the Wilson lines themselves. Rather than explore the full phenomenological consequences of this picture, we will try to elucidate the physics in this formalism and set the stage for such a calculation in future work. For concreteness, we will focus throughout this paper on the two-particle cross section specifically for the production of a quark and a gluon. The incoming projectile is consequently a Wilson line in the fundamental representation; the generalization of this to a gluon probe should be relatively straightforward.

This paper is structured as follows. First, we review the basics of JIMWLK evolution in Sec. II, both in the Fokker-Planck and in the Langevin formulations. We then discuss in Sec. III two-particle production at parametrically similar rapidities, i.e., without evolution between the rapidities of the particles. In Sec. IV, we develop the dilute limit of JIMWLK evolution in terms of color charges or, more accurately, Reggeized gluons, leading to the BFKL equation for the unintegrated gluon distribution. We then move in Sec. V to the IT formalism of Langevin evolution between the rapidities of the two produced particles, slightly rewriting the evolution equation to highlight the linear structure in the evolution between the two rapidities. Finally, in Sec. VI we show how the dilute limit of the IT formalism leads to a factorized structure that one would expect from BFKL dynamics, with a BFKL Green’s function separating the two particles.

II. JIMWLK EVOLUTION

A. The JIMWLK equation in the Fokker-Planck formalism

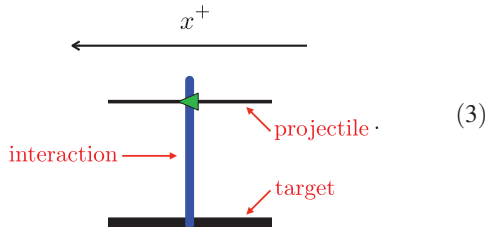
We consider a high energy interaction of a dilute colored probe with the color field of a dense target. In the CGC theory, the expectation value of an observable \hat{O} that is local in rapidity Y is given by

$$\langle \hat{O} \rangle_Y \equiv \int [DU] W_Y[U] \hat{O}. \quad (1)$$

Here $[DU]$ is the functional de Haar measure on $SU(N_c)$, and $W_Y[U]$ is the CGC weight function describing the density distribution at Y of the Wilson lines in the target. These Wilson lines $U = U(x) \equiv U_x$ are unitary, path-ordered exponentials

$$U_x^\dagger \equiv P \exp \left\{ ig \int dx^+ \alpha_x^a(x^+) t^a \right\}, \quad (2)$$

represented diagrammatically following the notation of [20,64,65] as



Here, α_x^a is the color field generated by the target with color index $a = 1, \dots, N_c$ and the t 's are the fundamental generators of $SU(N_c)$. The light-cone time axis x^+ runs from right to left in these diagrams. The Hermitian conjugate Wilson line is then denoted by an arrow facing the opposite way:

$$U_x = \text{---} \overleftarrow{\text{---}} \text{---} \quad (4)$$

An example of a simple observable that is relevant in this context is the quark dipole

$$\hat{S}_{xy} \equiv \frac{\text{tr} \{ U_x^\dagger U_y \}}{N_c} = \frac{1}{N_c} \text{tr} \left\{ \begin{array}{c} \text{---} \overleftarrow{\text{---}} \text{---} \quad x \\ \text{---} \overleftarrow{\text{---}} \text{---} \quad y \end{array} \right\}. \quad (5)$$

The dependence of the target color field on rapidity is described by JIMWLK evolution. Here the CGC weight function evolves from an initial condition Y_{in} to a final Y according to the JIMWLK equation

$$\frac{\partial}{\partial Y} W_Y[U] = H W_Y[U]. \quad (6)$$

Typically, a Gaussian distribution is used for the initial condition $W_{Y_{\text{in}}}$, as in the McLerran-Venugopalan (MV) [66–68] model. The JIMWLK Hamiltonian is

$$H \equiv \frac{1}{8\pi^3} \int_{uvz} \mathcal{K}_{uvz} (L_u^a - \tilde{U}_z^{\dagger ab} R_u^b) (L_v^a - \tilde{U}_z^{\dagger ac} R_v^c), \quad (7)$$

where tildes denote the adjoint representation and two-dimensional coordinate space integrals are denoted with the shorthand $\int_u \equiv \int d^2u$. The JIMWLK kernel is

$$\mathcal{K}_{uvz} \equiv \mathcal{K}_{uz}^i \mathcal{K}_{vz}^i, \quad (8)$$

where

$$\mathcal{K}_{uz}^i = \frac{(\mathbf{u} - \mathbf{z})^i}{(\mathbf{u} - \mathbf{z})^2} \quad (9)$$

is the Weizsäcker-Williams soft gluon emission kernel. The L and R are “left” and “right” Lie derivatives² that act to color rotate the Wilson lines on the left and right sides of the target field, respectively. They are defined as

$$L_u^a \equiv -ig (U_u t^a)_{\alpha\beta} \frac{\delta}{\delta U_{u,\alpha\beta}}, \quad (10)$$

$$R_u^a \equiv -ig (t^a U_u)_{\alpha\beta} \frac{\delta}{\delta U_{u,\alpha\beta}}, \quad (11)$$

where α, β are matrix indices and $\frac{\delta}{\delta U_u}$ acts as an ordinary functional derivative:

$$\frac{\delta}{\delta U_{u,\alpha\beta}} U_{x,\gamma\rho} = \delta_{\alpha\gamma} \delta_{\beta\rho} \delta^{(2)}(\mathbf{u} - \mathbf{x}) \equiv \delta_{\alpha\gamma} \delta_{\beta\rho} \delta_{\mathbf{u}\mathbf{x}}. \quad (12)$$

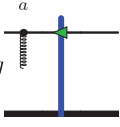
We can represent the action of the Lie derivatives on the Wilson lines as

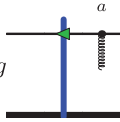
$$R_u^a U_x = -ig \delta_{\mathbf{u}\mathbf{x}} t^a U_x = -ig \begin{array}{c} \text{---} \overleftarrow{\text{---}} \text{---} \\ \text{---} \overleftarrow{\text{---}} \text{---} \end{array} \quad (13)$$

$$L_u^a U_x = -ig \delta_{\mathbf{u}\mathbf{x}} U_x t^a = -ig \begin{array}{c} \text{---} \overleftarrow{\text{---}} \text{---} \\ \text{---} \overleftarrow{\text{---}} \text{---} \end{array} \quad (14)$$

²The naming of the derivatives may seem counterintuitive, but they appear on the opposite side to what is expected due to the light-cone time axis running from right to left in our diagrammatic notation.

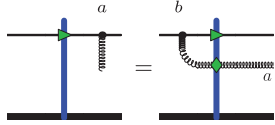
The Hermitian conjugates of these expressions give

$$R_u^a U_x^\dagger = ig \delta_{ux} U_x^\dagger t^a = ig \text{ (diagram) }, \quad (15)$$


$$L_u^a U_x^\dagger = ig \delta_{ux} t^a U_x^\dagger = ig \text{ (diagram) }. \quad (16)$$


The left and right Lie derivatives L and R are related to each other by

$$L_u^a = \tilde{U}_u^{\dagger ab} R_u^b \quad (17)$$

$$\text{(diagram)} = \text{(diagram)} \quad (18)$$


which follows from the identity $\tilde{U}_u^{\dagger ab} t^b = U_u t^a U_u^\dagger$. The Lie derivatives satisfy the commutation relations

$$[L_u^a, L_v^b] = g \delta_{uv} f^{abc} L_u^c, \quad (19)$$

$$[R_u^a, R_v^b] = -g \delta_{uv} f^{abc} R_u^c, \quad (20)$$

$$[L_u^a, R_v^b] = [L_u^a, \tilde{U}_z^{\dagger ab}] = [R_u^a, \tilde{U}_z^{\dagger ab}] = 0. \quad (21)$$

B. The JIMWLK equation in the Langevin formalism

Generically, it can be shown that a Fokker-Planck description of a system's dynamics can be recast in a Langevin description. For the JIMWLK equation, this was done in [18], with a slight simplification introduced in [21] using the form of Eq. (7) with left and right derivatives. Numerical solutions to JIMWLK evolution are more conveniently expressed using the Langevin formulation of the equation, as opposed to the Fokker-Planck formulation discussed in the previous section. This is one reason to explore analytically the Langevin picture. In this formulation, evolution is treated as a random walk in the functional space of Wilson lines. Rapidity acts as a “time” and is discretized as $Y - Y_0 = \epsilon N$ with $\mathbb{Z} \ni N \rightarrow \infty$, $\epsilon \rightarrow 0$, where each evolution step is labeled by $n \in \{0, 1, \dots, N\}$. The averaging over the probability distribution of Wilson lines in Eq. (1) is equivalent to the averaging over a noise term in the stochastic equation. This term can be taken as a localized Gaussian white noise

$$\langle \nu_{x,m}^{i,a} \nu_{y,n}^{j,b} \rangle = \frac{1}{\epsilon} \delta^{ij} \delta^{ab} \delta_{mn} \delta_{xy}, \quad (22)$$

where $\nu_{z,n}^{i,a} \in \mathbb{R}$. The noise is introduced within terms we can call, respectively, “left” and “right” (traceless, Hermitian) color fields

$$\alpha_{x,n}^L \equiv \frac{1}{\sqrt{4\pi^3}} \int_z \mathcal{K}_{xz}^i \nu_{z,n}^i, \quad (23)$$

$$\alpha_{x,n}^R \equiv \frac{1}{\sqrt{4\pi^3}} \int_z \mathcal{K}_{xz}^i U_{z,n} \nu_{z,n}^i U_{z,n}^\dagger, \quad (24)$$

where $\nu_{z,n}^i \equiv \nu_{z,n}^{i,a} t^a$ is an element of the $SU(N_c)$ algebra.

These definitions of α^L and α^R can be interchanged, as long as one is rotated by $\tilde{U}^{\dagger ab}$ with respect to the other; this merely amounts to a redefinition of the noise in Eq. (22) [21]. To be explicit, one defines a rotated noise as

$$\tilde{\nu}_{z,n}^i \equiv \tilde{\nu}_{z,n}^{i,a} t^a \equiv U_{z,n} \nu_{z,n}^i U_{z,n}^\dagger. \quad (25)$$

It is then straightforward to show that this rotated noise is also a Gaussian random variable with

$$\langle \tilde{\nu}_{x,m}^{i,a} \tilde{\nu}_{y,n}^{j,b} \rangle = \frac{1}{\epsilon} \delta^{ij} \delta^{ab} \delta_{mn} \delta_{xy}. \quad (26)$$

With this, one can equally well consider the rotated noise $\tilde{\nu}$ as being independent of the Wilson lines. Thus, the original noise ν and so too α^L are quantities that depend on them. However, the choice of whether to consider ν or $\tilde{\nu}$ has to be made globally for the whole calculation at once, and kept fixed when taking functional derivatives with respect to the Wilson lines. These properties will be crucial later to see how the evolution between the two rapidities becomes independent of the Wilson lines.

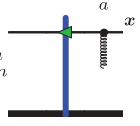
The Langevin equation describing the evolution of a Wilson line from step n to step $n+1$ is written as

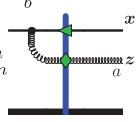
$$U_{x,n+1}^\dagger = e^{ieg\alpha_{x,n}^L} U_{x,n}^\dagger e^{-ieg\alpha_{x,n}^R}. \quad (27)$$

The two matrix exponentials act as infinitesimal color rotations to the left and to the right of the target field, hence the naming of the α 's. If the Wilson line at rapidity step n is represented as

$$U_{x,n}^\dagger \equiv \text{(diagram)}, \quad (28)$$


then we can write

$$\alpha_{x,n}^L U_{x,n}^\dagger = \frac{1}{\sqrt{4\pi^3}} \int_z \mathcal{K}_{xz}^i \nu_{z,n}^{i,a} \quad (29)$$


$$\alpha_{x,n}^R U_{x,n}^\dagger = \frac{1}{\sqrt{4\pi^3}} \int_z \mathcal{K}_{xz}^i \nu_{z,n}^{i,a} \quad (30)$$


Notice that the free color index in these two diagrams contracts with the color index of the noise factor. The Hermiticity of the color fields means that the time step for the complex conjugate Wilson line is simply

$$U_{x,n+1} = e^{ieg\alpha_{x,n}^R} U_{x,n} e^{-ieg\alpha_{x,n}^L} \quad (31)$$

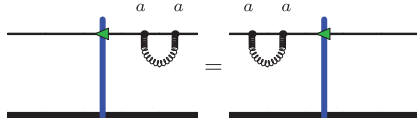
1. Expansion in the time step ϵ

Since ϵ is infinitesimal, we may choose to keep terms only up to order ϵ . The color fields each contain a factor ν , which is of order $\epsilon^{-1/2}$, and always appear multiplied by a factor of ϵ . So $\mathcal{O}(\epsilon\alpha^{L/R}) = \mathcal{O}(\epsilon^{1/2})$, and we can immediately neglect from the expansion powers of $\alpha^{L/R}$ larger than two. Also, since in the end we only need to keep terms of order $(\alpha^{L/R})^2$ multiplied by terms that do not depend on the noise, we can at any stage in the calculation take the expectation value over the noise in such terms.

It is useful to note that Wilson lines appear only in the cross term $\alpha^L \alpha^R$, but not in the squares:

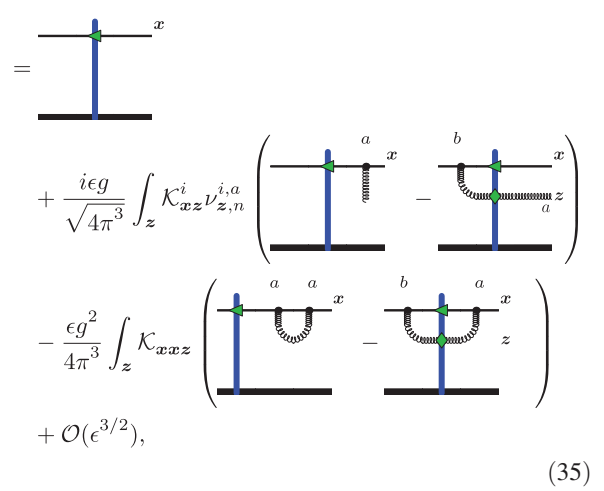
$$\langle (\alpha_{x,n}^L)^2 \rangle = \langle (\alpha_{x,n}^R)^2 \rangle = \frac{C_F}{4\pi^3 \epsilon} \int_z \mathcal{K}_{xxz} \quad (32)$$

In terms of diagrams, this can be expressed as the relation

$$\text{Diagram 1} = \text{Diagram 2} \quad (33)$$


Using these, one step of the Wilson line to the order needed can be written as

$$U_{x,n+1}^\dagger = U_{x,n}^\dagger + \int_z \left(\frac{ieg}{\sqrt{4\pi^3}} \mathcal{K}_{xz}^i \nu_{z,n}^{i,a} - \frac{\epsilon g^2}{4\pi^3} \mathcal{K}_{xxz} t^a \right) \times (t^a U_{x,n}^\dagger - U_{x,n}^\dagger \tilde{U}_{z,n}^{\dagger ab} t^b) + \mathcal{O}(\epsilon^{3/2}) \quad (34)$$

$$= \text{Diagram 1} + \frac{ieg}{\sqrt{4\pi^3}} \int_z \mathcal{K}_{xz}^i \nu_{z,n}^{i,a} \left(\text{Diagram 2} - \text{Diagram 3} \right) - \frac{\epsilon g^2}{4\pi^3} \int_z \mathcal{K}_{xxz} \left(\text{Diagram 4} - \text{Diagram 5} \right) + \mathcal{O}(\epsilon^{3/2}), \quad (35)$$


where the relation (33) can be used to draw the virtual diagram on either side of the target.

By calculating the dipole $\hat{S}_{\tilde{x}\tilde{x},n+1}$ in terms of quantities at the previous step n , we can also derive the first equation of the Balitsky hierarchy:

$$\frac{d}{dY} \frac{\text{tr}\{U_x^\dagger U_y\}}{N_c} = -\frac{N_c \alpha_s}{2 \pi^2} \int_z \tilde{\mathcal{K}}_{xyz} \left(\frac{\text{tr}\{U_{x,n}^\dagger U_{y,n}\}}{N_c} - \frac{\text{tr}\{U_{z,n}^\dagger U_{y,n}\} \text{tr}\{U_{x,n}^\dagger U_{z,n}\}}{N_c^2} \right) + \mathcal{O}(\epsilon^{3/2}). \quad (36)$$

Here, one needs to use the Fierz identity

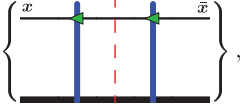
$$2\tilde{U}_z^{ab} \text{tr}\{U_y^\dagger t^a U_x t^b\} = \text{tr}\{U_z^\dagger U_x\} \text{tr}\{U_y^\dagger U_z\} - \frac{1}{N_c} \text{tr}\{U_y^\dagger U_x\} \quad (37)$$

to simplify the color structure and get rid of the adjoint representation matrices. Note that at this order in ϵ (and thus also in the limit $\epsilon \rightarrow 0$), Eq. (36) is exact, even at the level of a single configuration without expectation values. Additionally, taking the expectation value on both sides and using the mean field approximation $\langle \text{tr}\{U_{z,n}^\dagger U_{y,n}\} \text{tr}\{U_{x,n}^\dagger U_{z,n}\} \rangle \approx \langle \text{tr}\{U_{z,n}^\dagger U_{y,n}\} \rangle \langle \text{tr}\{U_{x,n}^\dagger U_{z,n}\} \rangle$ transform Eq. (36) into the Balitsky-Kovchegov (BK) [29,69] equation

$$\frac{d}{dY} \left\langle \frac{\text{tr}\{U_x^\dagger U_y\}}{N_c} \right\rangle = -\frac{N_c \alpha_s}{2 \pi^2} \int_z \tilde{\mathcal{K}}_{xyz} \left(\left\langle \frac{\text{tr}\{U_{x,n}^\dagger U_{y,n}\}}{N_c} \right\rangle - \left\langle \frac{\text{tr}\{U_{z,n}^\dagger U_{y,n}\}}{N_c} \right\rangle \left\langle \frac{\text{tr}\{U_{x,n}^\dagger U_{z,n}\}}{N_c} \right\rangle \right) + \mathcal{O}(\epsilon^{3/2}). \quad (38)$$

III. ONE- AND TWO-PARTICLE PRODUCTION AT EQUAL RAPIDITY

Consider a single quark produced in a proton-nucleus collision. It is described mathematically by a fundamental representation dipole

$$\hat{S}_{x\bar{x}} \equiv \frac{\text{tr} \left\{ U_x^\dagger \bar{U}_{\bar{x}} \right\}}{N_c} = \frac{1}{N_c} \text{tr} \left\{ \left[\begin{array}{c} x \quad \quad \quad \bar{x} \\ \text{---} \text{---} \text{---} \text{---} \text{---} \\ \text{---} \text{---} \text{---} \text{---} \text{---} \\ \text{---} \text{---} \text{---} \text{---} \text{---} \end{array} \right] \right\}, \quad (39)$$


where the dashed line denotes the separation between the direct amplitude (DA) on the left and the complex conjugate amplitude (CCA) on the right. The bars on both the Wilson line and the coordinate in $\bar{U}_{\bar{x}}$ denote that this Wilson line is in the CCA. Henceforth, this bar notation will be used to distinguish between quantities in the DA (unbarred) and the CCA (barred). The cross section for inclusive quark production in a proton-nucleus collision is then

$$\frac{d\sigma_q}{d\eta_p d^2\mathbf{p}} = xq(x) \frac{1}{(2\pi)^2} \int_{x\bar{x}} e^{-ip \cdot (x-\bar{x})} \langle \hat{S}_{x\bar{x}} | \bar{U}=U \rangle_Y. \quad (40)$$

Here, Y is the relative rapidity of the produced quark with respect to the target, x is the longitudinal momentum fraction of the projectile, $xq(x)$ is the quark distribution in the proton, and \mathbf{p} and η_p are the transverse momentum and rapidity, respectively, of the quark. The dipole expectation value can be obtained by averaging the dipole operator over the probability distribution of the Wilson lines according to Eq. (1), except that at this stage, the DA and CCA should still be regarded as independent:

$$\langle \hat{S}_{x\bar{x}} \rangle_Y = \int [DU][D\bar{U}] W_Y[U, \bar{U}] \hat{S}_{x\bar{x}}. \quad (41)$$

For inclusive quark-gluon production (both the quark and the gluon emitted with rapidity Y with respect to the target), the cross section can be written compactly in terms of a “production Hamiltonian” [60–62] operating on the quark cross section:

$$\frac{d\sigma_{qg}}{d\eta_p d^2\mathbf{p} d\eta_\kappa d^2\mathbf{k}} = \frac{1}{(2\pi)^4} \int_{x\bar{x}} e^{-ip \cdot (x-\bar{x})} \langle H_{\text{prod}}(\mathbf{k}) \hat{S}_{x\bar{x}} | \bar{U}=U \rangle_Y. \quad (42)$$

Here, the quark has transverse momentum \mathbf{p} and pseudorapidity η_p , and the gluon has transverse momentum \mathbf{k} and pseudorapidity η_κ . The production Hamiltonian is given by [60]

$$H_{\text{prod}}(\mathbf{k}) = \frac{1}{4\pi^3} \int_{y\bar{y}} e^{-ik \cdot (y-\bar{y})} \int_{u\bar{u}} \mathcal{K}_{yu}^i \mathcal{K}_{\bar{y}\bar{u}}^i \\ \times (L_u^a - \bar{U}_y^{\dagger ab} R_u^b) (\bar{L}_{\bar{u}}^a - \bar{U}_{\bar{y}}^{\dagger ac} \bar{R}_{\bar{u}}^c), \quad (43)$$

which correctly accounts for all possible ways that a second gluon can be produced. Notice that transverse coordinates y and \bar{y} are kept distinct, and the Lie derivatives with respect to the Wilson lines in the DA and CCA are kept separate. In spite of the notational similarity, this makes H_{prod} a somewhat more complicated operator than the JIMWLK Hamiltonian in Eq. (7).

In order to evaluate the cross section, the four terms in

$$(L_u^a - \bar{U}_y^{\dagger ab} R_u^b) (\bar{L}_{\bar{u}}^a - \bar{U}_{\bar{y}}^{\dagger ac} \bar{R}_{\bar{u}}^c) \hat{S}_{x\bar{x}} \quad (44)$$

need to be calculated, where the left and right Lie derivatives can be evaluated using Eqs. (13) and (16). Only once all the functional derivatives have been evaluated can we set $\bar{U} = U$, since there is no more need to distinguish between Wilson lines in the DA and CCA separately. Substituting the results into Eq. (42) gives

$$\frac{d\sigma_{2g}}{d\eta_p d^2\mathbf{p} d\eta_\kappa d^2\mathbf{k}} \\ = \frac{1}{(2\pi)^4} \frac{\alpha_s}{\pi^2} \int_{x\bar{x}y\bar{y}} e^{-ip \cdot (x-\bar{x}) - ik \cdot (y-\bar{y})} \mathcal{K}_{yx}^i \mathcal{K}_{\bar{y}\bar{x}}^i \\ \times \left\langle C_f \frac{\text{tr} \{ U_{\bar{x}} U_x^\dagger \}}{N_c} - (\bar{U}_{\bar{y}}^{\dagger ab} + \bar{U}_y^{\dagger ab}) \frac{\text{tr} \{ t^b U_{\bar{x}} t^a U_x^\dagger \}}{N_c} \right. \\ \left. + (U_{\bar{y}} U_y^\dagger)^{ab} \frac{\text{tr} \{ t^a U_{\bar{x}} U_x^\dagger t^b \}}{N_c} \right\rangle_Y, \quad (45)$$

where the integrals over u and \bar{u} have been evaluated using the delta functions $\delta_{u\bar{x}} \delta_{u\bar{x}}$ from calculating the Lie derivatives, and the overall constant has been rewritten using $\alpha_s = g^2/(4\pi)$. This is the analogue of the result (in the soft gluon limit $z \rightarrow 0$) of two-gluon production at equal rapidity obtained in Ref. [70]. Note that the rapidities of the quark and gluon are not really equal, because in the production Hamiltonian one has taken the limit where the gluon is soft. However, at this point they are also not parametrically large, so that one would need to consider high energy evolution between the two. Thus, the rapidity separation in Eq. (45), ΔY , satisfies $1 \ll \Delta Y \ll 1/\alpha_s$.

IV. DILUTE LIMIT: STOCHASTIC PICTURE OF BFKL EVOLUTION

In order to understand the connection of the Langevin picture of JIMWLK evolution to the physics of the BFKL equation, we must develop the Wilson lines in the limit of a small color field [28,71–73]. To do this, we start with the fundamental representation Wilson line

$$\begin{aligned}
U_{x,n}^\dagger &\equiv P \exp \left\{ ig \int dx^+ \alpha_{x,n}^a(x^+) t^a \right\} \\
&\equiv e^{i\lambda_{x,n}} \\
&= \mathbb{1} + i\lambda_{x,n} - \frac{1}{2} \lambda_{x,n}^2 + \mathcal{O}(\lambda^3), \quad (46)
\end{aligned}$$

where each real matrix λ is an element of the algebra of $SU(N_c)$ and denotes a one-gluon interaction between projectile and target. We can represent this diagrammatically as

$$U_{x,n}^\dagger = \text{---} + i \text{---} - \frac{1}{2} \text{---} + \mathcal{O}(\lambda^3). \quad (47)$$

The Hermitian conjugate is simply

$$U_{x,n} = e^{-i\lambda_{x,n}} = \mathbb{1} - i\lambda_{x,n} - \frac{1}{2} \lambda_{x,n}^2 + \mathcal{O}(\lambda^3), \quad (48)$$

and an adjoint Wilson line is

$$\begin{aligned}
\tilde{U}_{x,n}^{\dagger ab} &= \delta^{ab} + f^{abc} \lambda_{x,n}^c + 2\text{tr}\{t^a \lambda_{x,n} t^b \lambda_{x,n}\} \\
&\quad - \text{tr}\{t^a \{t^b, \lambda_{x,n}^2\}\} + \mathcal{O}(\lambda^3). \quad (49)
\end{aligned}$$

The part of the Langevin step for Wilson lines in Eq. (34) involving an adjoint representation Wilson line corresponds to the interaction of a gluon with the target shock wave. At step $n = 0$ in this linearized limit, we have

$$U_{x,0}^\dagger \tilde{U}_{z,0}^{\dagger ab} t^b = t^a - f^{abc} \lambda_{z,0}^b t^c + i\lambda_{x,0} t^a + \mathcal{O}(\lambda^2), \quad (50)$$

which we can represent as

$$\begin{aligned}
\text{---} &= \text{---} - \text{---} \\
&+ i \text{---} + \mathcal{O}(\lambda^2). \quad (51)
\end{aligned}$$

Using this, we can write the full Langevin step to linear order in the gluon field as

$$\begin{aligned}
\lambda_{x,n+1} &= \lambda_{x,n} + \int_z \left(\frac{ieg}{\sqrt{4\pi^3}} \mathcal{K}_{xz}^i \nu_{z,n}^{j,a} - \frac{eg^2}{4\pi^3} \mathcal{K}_{xxz} \right) \\
&\quad \times if^{abc} t^c (\lambda_{x,n}^b - \lambda_{z,n}^b) + \mathcal{O}(\epsilon^{3/2}, \lambda^2). \quad (52)
\end{aligned}$$

Diagrammatically, we have

$$\begin{aligned}
\lambda_{x,n+1} &= \text{---} \\
&+ \frac{ieg}{\sqrt{4\pi^3}} \int_z \mathcal{K}_{xz}^i \nu_{z,n}^{j,a} i \left(\text{---} - \text{---} \right) \\
&- \frac{eg^2}{4\pi^3} \int_z \mathcal{K}_{xxz} \left(\text{---} - \text{---} \right) \\
&\quad + \mathcal{O}(\epsilon^{3/2}, \lambda^2). \quad (53)
\end{aligned}$$

Note that the three-gluon vertex can also be written as a commutator:

$$if^{abc} t^c \lambda_{x,n}^b = [t^a, \lambda_{x,n}], \quad (54)$$

$$i \text{---} = \text{---} - \text{---}. \quad (55)$$

Equation (52) is simply a linear iterative equation, for which we can write a formal solution. Separating out a time evolution matrix \mathcal{M} as

$$\begin{aligned}
\mathcal{M}_{xw,n}^{ab} &\equiv \delta_{xw} \delta^{ab} + \int_z \left(\frac{ieg}{\sqrt{4\pi^3}} \mathcal{K}_{xz}^i \nu_{z,n}^{j,c} f^{abc} - \frac{eg^2 N_c}{4\pi^3} \mathcal{K}_{xxz} \delta^{ab} \right) \\
&\quad \times (\delta_{xw} - \delta_{zw}), \quad (56)
\end{aligned}$$

we can write

$$\lambda_{x,n+1}^a = \int_w \mathcal{M}_{xw,n}^{ab} \lambda_{w,n}^b + \mathcal{O}(\epsilon^{3/2}, \lambda^2). \quad (57)$$

This recursive relation has the solution

$$\lambda_{x,n+1}^a = \int_{w_n} \mathcal{M}_{xw_n,n}^{ab} \prod_{j=0}^{n-1} \left(\int_{w_j} \mathcal{M}_{w_{j+1}w_j}^{b_j b_j} \right) \lambda_{w_0,0}^{b_0}. \quad (58)$$

The product of \mathcal{M} 's can be simplified further if necessary, by using Eq. (22) and keeping terms up to linear order in ϵ .

A. Reggeization

As a side note, we can now easily see (following [71]) how the gluon field λ “Reggeizes” in this picture. This is done by taking the expectation value of the single gluon field time step Eq. (52), which eliminates terms linear in ν and leads to

$$\frac{1}{\epsilon} \langle \lambda_{x,n+1} - \lambda_{x,n} \rangle = -\frac{N_c g^2}{2 \cdot 4\pi^3} \int_z \mathcal{K}_{xxz} \langle \lambda_{x,n} - \lambda_{z,n} \rangle + \mathcal{O}(\epsilon^2, \lambda^2), \quad (59)$$

which we may write as

$$\left\langle \frac{d}{dY} \lambda_x \right\rangle = \frac{N_c \alpha_s}{2 \pi^2} \int_z \mathcal{K}_{xxz} \langle \lambda_{z,n} - \lambda_{x,n} \rangle + \mathcal{O}(\epsilon^2, \lambda^2). \quad (60)$$

This equation can be Fourier transformed using

$$\lambda^a(\mathbf{p}) = \int_z e^{ipz} \lambda_z^a \quad (61)$$

and written as

$$\left\langle \frac{d}{dY} \lambda^a(\mathbf{p}) \right\rangle = \langle \alpha_g(\mathbf{p}) \lambda_n^a(\mathbf{p}) \rangle + \mathcal{O}(\epsilon^2, \lambda^2). \quad (62)$$

Here,

$$\alpha_g(\mathbf{p}) \equiv \frac{N_c \alpha_s}{2 \pi^2} \int_z \frac{1}{z^2} (e^{ipz} - 1) \quad (63)$$

is the so-called ‘‘Regge trajectory’’ (see [71]). The gluon is said to Reggeize, meaning that the amplitude for the gluon exchange process scales with energy to the power of the trajectory. In the Langevin picture, Reggeization therefore simply refers to the power law growth of the expectation value of the gluon field.

B. The BFKL equation

Let us then obtain the BFKL equation for the unintegrated gluon distribution. This can be done by first expanding the Wilson lines in the dilute limit and looking at the evolution of a quantity that is quadratic in the expansion parameter λ . For this discussion, it is useful to still keep track of the λ 's in the DA and CCA separately. In order to derive such a quadratic equation, we square Eq. (57). Eventually taking the expectation value of the noise on both sides will remove terms linear in ν and simplify terms quadratic in ν according to Eq. (26). As discussed above, we have expanded to the relevant order in the rapidity step ϵ . After some straightforward color algebra, we obtain

$$\begin{aligned} \lambda_{x,n+1}^a \bar{\lambda}_{x,n+1}^a &= \int_{w\bar{w}} \left[\delta_{wx} \delta_{w\bar{x}} - \frac{N_c \epsilon \alpha_s}{2 \pi^2} \int_z (\mathcal{K}_{x\bar{x}z} \delta_{wx} (\delta_{w\bar{x}} - \delta_{wz}) \right. \\ &\quad + \mathcal{K}_{xxz} (\delta_{wx} - \delta_{wz}) \delta_{w\bar{x}} \\ &\quad \left. - 2\mathcal{K}_{x\bar{x}z} (\delta_{wx} - \delta_{wz}) (\delta_{w\bar{x}} - \delta_{wz}) \right] \lambda_{w,n}^a \bar{\lambda}_{w,n}^a \\ &\quad + \mathcal{O}(\epsilon^{3/2}, \lambda^3). \end{aligned} \quad (64)$$

From this basic equation, one can define two different versions of the BFKL equation. The first one comes naturally when one considers a particle production process, in which one wants to keep a nonzero contribution from both the DA and the CCA. To do this, we define the unintegrated gluon distribution

$$\phi_{x\bar{x}}^n \equiv \langle \lambda_{x,n}^a \bar{\lambda}_{x,n}^a \rangle. \quad (65)$$

Then, Eq. (64) yields the evolution equation

$$\begin{aligned} \phi_{x\bar{x}}^{n+1} - \phi_{x\bar{x}}^n &= -\frac{N_c \epsilon \alpha_s}{2 \pi^2} \int_z [\mathcal{K}_{xxz} (\phi_{x\bar{x}}^n - \phi_{z\bar{x}}^n) + \mathcal{K}_{x\bar{x}z} (\phi_{x\bar{x}}^n - \phi_{xz}^n) \\ &\quad - 2\mathcal{K}_{x\bar{x}z} (\phi_{x\bar{x}}^n - \phi_{xz}^n - \phi_{z\bar{x}}^n + \phi_{zz}^n)] \\ &\quad + \mathcal{O}(\epsilon^{3/2}, \phi^{3/2}). \end{aligned} \quad (66)$$

Note that this does not have the customary form of a coordinate space BFKL equation. Equation (66) acquires a more familiar form, however, in momentum space. To see this, we define the Fourier transform

$$\phi_{x\bar{x}} \equiv \int \frac{d^2\mathbf{p}}{(2\pi)^2} e^{-ip \cdot (x - \bar{x})} \phi(\mathbf{p}) \equiv \int_p e^{-ip \cdot (x - \bar{x})} \phi(\mathbf{p}). \quad (67)$$

$\phi_{x\bar{x}}$ is a function of the relative length $x - \bar{x}$, so we need not transform each coordinate separately. Using this and the Fourier transformed kernel

$$\mathcal{K}_{uv}^i = 2\pi i \int_k e^{-ik \cdot (u - v)} \frac{k^i}{k^2}, \quad (68)$$

the BFKL equation (66) becomes

$$\begin{aligned} \phi^{n+1}(\mathbf{q}) &= \phi^n(\mathbf{q}) + 4N_c \epsilon \alpha_s \int_p \frac{1}{(\mathbf{q} - \mathbf{p})^2} \left(\frac{\phi^n(\mathbf{p}) \mathbf{p}^2}{\mathbf{q}^2} - \frac{1 \phi^n(\mathbf{q}) \mathbf{q}^2}{2 \mathbf{p}^2} \right) \\ &\quad + \mathcal{O}(\epsilon^{3/2}, \phi^{3/2}). \end{aligned} \quad (69)$$

This is immediately recognized as the (color singlet, zero momentum transfer) textbook version of the BFKL equation [74].

The other (Mueller's) version of the BFKL equation [75,76] is obtained when we set the Wilson lines to be equal in the DA and CCA. One then looks at the expansion of the dipole operator up to order λ^2 as

$$\frac{\text{tr}\{U_x^\dagger U_y\}}{N_c} = 1 - \frac{1}{4N_c} (\lambda_x^a - \lambda_y^a) (\lambda_x^a - \lambda_y^a) + \mathcal{O}(\lambda^3). \quad (70)$$

The natural definition of the gluon distribution based on the expansion of the dipole operator is then the so-called ‘‘BFKL pomeron’’ [71]

$$\varphi_{xy} \equiv \langle (\lambda_x^a - \lambda_y^a) (\lambda_x^a - \lambda_y^a) \rangle, \quad (71)$$

which we can write in terms of ϕ by setting $\bar{\lambda} = \lambda$:

$$\phi_{xx} + \phi_{yy} - 2\phi_{xy} \stackrel{\bar{\lambda}=\lambda}{=} \phi_{xy}. \quad (72)$$

Using Eq. (66) for each of the three terms in Eq. (72), one arrives at the Mueller version of the BFKL equation:

$$\phi_{xy}^{n+1} - \phi_{xy}^n = -\frac{N_c \epsilon \alpha_s}{2 \pi^2} \int_z \tilde{\mathcal{K}}_{xyz} [\phi_{xy}^n - \phi_{xz}^n - \phi_{zy}^n]. \quad (73)$$

This is the version of the BFKL equation one usually sees written in coordinate space. It can also be obtained by linearizing the BK equation (38).

It is important to emphasize the relatively trivial but important observation that the two equations, (66) and (73), are closely related but not the same. Equation (66) is usually derived and written in momentum space by considering the BFKL ladder diagrams. It appears naturally for a particle production process in which we want to have an explicit product of the DA and the CCA. Such a calculation would begin with the dipole written diagrammatically as

$$\frac{\text{tr} \{ U_x^\dagger \bar{U}_{\bar{x}} \}}{N_c} = \frac{1}{N_c} \text{tr} \left\{ \begin{array}{c} x \quad \bar{x} \\ \text{---} \text{---} \text{---} \\ | \quad | \\ \text{---} \text{---} \end{array} \right\}.$$

On the other hand, the Mueller version of the BFKL equation (73) is satisfied by an object associated with the elastic amplitude for a color neutral dipole. In our notation, this would be expressed as

$$\frac{\text{tr} \{ U_x^\dagger U_y \}}{N_c} = \frac{1}{N_c} \text{tr} \left\{ \begin{array}{c} x \\ \text{---} \text{---} \text{---} \\ | \\ y \\ \text{---} \end{array} \right\},$$

which is not naturally separated into terms associated with the DA and the CCA. While Eq. (73) is usually written in coordinate space, the momentum space version is straightforward to obtain; it is not particularly simple or useful in this context, so we omit it here.

V. UNEQUAL RAPIDITY CORRELATORS IN JIMWLK

A. Two-particle production

Next, we consider the production of two particles produced at parametrically different rapidities. The rapidity Y_A is closer to that of the target; i.e., it is “earlier” on the evolution trajectory of the target. We want to calculate the double inclusive cross section for the simultaneous production of another particle at a later rapidity Y that is much larger than the first one: $\alpha_s(Y - Y_A) \gg 1$. Unlike the case considered in Sec. III, we now have genuine high energy evolution between the two produced particles due to the

rapidity separation. The situation is rendered more complicated than the JIMWLK evolution considered in Sec. II by the fact that the Wilson line trajectories are now *conditional* ones. This is because they are now aware of the fact that a particle with a specific transverse momentum was produced earlier in the evolution. The IT Langevin formalism for this scenario was set up in [60]. The purpose of our discussion here is to elucidate how this formalism in the dilute limit relates to a conventional BFKL picture.

We begin this discussion as formulated in [60]. After the first part of evolution from rapidity Y_{in} to Y_A for the quark dipole, one obtains the Wilson lines $\bar{U}_{\bar{x},A}$ and $U_{x,A}^\dagger$ at the earlier rapidity Y_A . In order to keep track of the gluon that is produced at Y_A , we consider these Wilson lines to be fixed for now. They act as the initial condition for the second part of the evolution from rapidity Y_A to Y . In terms of the discretization $Y - Y_A = N\epsilon$, we have $Y_0 \equiv Y_A$, $U_0 \equiv U_A$, and $\bar{U}_0 \equiv \bar{U}_A$ at $n = 0$. The expectation value of the cross section for producing a quark at some rapidity Y is then calculated as an average over the noise ν at the end of the stochastic process:

$$\langle \hat{\mathcal{S}}_{x\bar{x}} \rangle_{Y-Y_A} = \langle \hat{\mathcal{S}}_{x\bar{x},N} \rangle_\nu. \quad (74)$$

Equation (1) for the expectation value of an operator at the later rapidity Y is now written as

$$\langle \hat{\mathcal{O}} \rangle_{Y-Y_A} \equiv \int [DUD\bar{U}] W_{Y-Y_A}[U, \bar{U}|U_A, \bar{U}_A] \hat{\mathcal{O}}. \quad (75)$$

We need to have a new conditional weight function $W_{Y-Y_A}[U, \bar{U}|U_A, \bar{U}_A]$ [43], which is the probability of observing Wilson lines U and \bar{U} at rapidity Y , with the condition that there are already Wilson lines U_A and \bar{U}_A at the earlier rapidity Y_A . This weight function obeys the differential equation

$$\frac{\partial}{\partial Y} W_{Y-Y_A}[U, \bar{U}|U_A, \bar{U}_A] = H_{\text{evol}} W_{Y-Y_A}[U, \bar{U}|U_A, \bar{U}_A] \quad (76)$$

[cf. Eq. (6)]. The evolution Hamiltonian H_{evol} is just the conventional JIMWLK Hamiltonian, with the exception that one must now keep track of the Wilson lines and Lie derivatives for the DA and the CCA separately. Thus, there are terms operating only on the DA (11), terms operating only on the CCA (22), and a mixed term (12),

$$H_{\text{evol}} \equiv H_{11} + 2H_{12} + H_{22}, \quad (77)$$

where

$$H_{11} \equiv \frac{1}{8\pi^3} \int_{uvz} \mathcal{K}_{uvz}(L_{u,n}^a - \tilde{U}_{z,n}^{\dagger ab} R_{u,n}^b)(L_{v,n}^a - \tilde{U}_{z,n}^{\dagger ac} R_{v,n}^c), \quad (78)$$

$$H_{12} \equiv \frac{1}{8\pi^3} \int_{u\bar{v}\bar{z}} \mathcal{K}_{u\bar{v}\bar{z}}(L_{u,n}^a - \tilde{U}_{z,n}^{\dagger ab} R_{u,n}^b)(\bar{L}_{\bar{v},n}^a - \tilde{U}_{z,n}^{\dagger ac} \bar{R}_{\bar{v},n}^c), \quad (79)$$

$$H_{22} \equiv \frac{1}{8\pi^3} \int_{\bar{u}\bar{v}\bar{z}} \mathcal{K}_{\bar{u}\bar{v}\bar{z}}(\bar{L}_{\bar{u},n}^a - \tilde{U}_{z,n}^{\dagger ab} \bar{R}_{\bar{u},n}^b)(\bar{L}_{\bar{v},n}^a - \tilde{U}_{z,n}^{\dagger ac} \bar{R}_{\bar{v},n}^c) \quad (80)$$

[cf. Eq. (7) or rather (43)]. Here, the Lie derivatives and the adjoint Wilson lines carry a subscript n to emphasize that they pertain to the current (latest) rapidity in the evolution.

The initial condition at Y_A for the conditional weight function sets Wilson lines for both the DA and the CCA:

$$W_{Y_A}[U, \bar{U}|U_A, \bar{U}_A] = \delta[U - U_A]\delta[\bar{U} - \bar{U}_A]. \quad (81)$$

If one sets the DA and the CCA to be the same at the initial condition, this property is preserved throughout the evolution; at some other rapidity Y_B , we then have

$$W_{Y_B}[U, \bar{U}|U_A, \bar{U}_A] = \delta[U - \bar{U}]W_{Y_B}[U|U_A], \quad (82)$$

where $W_{Y_B}[U|U_A]$ is just the conventional conditional probability [e.g., Eq. (6)] with initial condition

$$W_{Y_A}[U|U_A] = \delta[U - U_A]. \quad (83)$$

The cross section for inclusive two-particle production, as provided by Eq. (42), needs to be modified to account for the fact that the emitted particle has a different rapidity to the projectile. For a gluon emitted from a quark projectile at rapidity Y_A , we must now operate with the production Hamiltonian (43) acting on the Wilson lines at Y_A , i.e., on the initial condition for the conditional evolution [60]:

$$\frac{d\sigma_{qg}}{dY d^2\mathbf{p} dY_A d^2\mathbf{k}_A} = \frac{1}{(2\pi)^4} \int_{x\bar{x}} e^{-ip \cdot (x-\bar{x})} \langle H_{\text{prod}}(\mathbf{k}_A) \langle \hat{S}_{x\bar{x}} \rangle_{Y-Y_A} |_{\bar{U}_A=U_A} \rangle_{Y_A}. \quad (84)$$

Note that there are now two separate averages. The dipole operator is evolved from Y_A to Y with the conditional JIMWLK evolution; the average over these Langevin trajectories is denoted by $\langle \rangle_{Y-Y_A}$. One then operates with the production Hamiltonian, which is a functional derivative with respect to the initial conditions U_A and \bar{U}_A . Only then does one set the Wilson lines to be the same in the DA and the CCA. Finally, one does the average over the earlier rapidity distribution $\langle \rangle_{Y_A}$, using a weight function that has been evolved from Y_{in} to Y_A . This double averaging procedure can be written in a more explicit way with the help of delta functions and conditional probabilities:

$$\frac{d\sigma_{qg}}{dY d^2\mathbf{p} dY_A d^2\mathbf{k}_A} = \frac{1}{(2\pi)^4} \int_{x\bar{x}} e^{-ip \cdot (x-\bar{x})} \int [DU_A] W_{Y_A}[U_A] \int [D\bar{U}_A] \delta[\bar{U}_A - U_A] H_{\text{prod}}(\mathbf{k}_A) \times \int [DUD\bar{U}] W_{Y-Y_A}[U, \bar{U}|U_A, \bar{U}_A] \hat{S}_{x\bar{x}}. \quad (85)$$

In order to proceed, we need the result of the production Hamiltonian operating on the dipole; i.e., we need to calculate $H_{\text{prod}} \hat{S}_{x\bar{x}}$. This expression will have several terms, with left or right Lie derivatives operating on the Wilson lines. We also have to maintain the distinction between barred and unbarred contributions. The resulting expressions involve Wilson lines not only at the rapidity $Y_A \equiv Y_0$ but also at later rapidities Y_n , where the n refers to the discrete Langevin process description we are using. Putting everything together, we can write the cross section as

$$\frac{d\sigma_{qg}}{dY d^2\mathbf{p} dY_A d^2\mathbf{k}_A} = \frac{1}{(2\pi)^4} \frac{1}{4\pi^3} \frac{1}{N_c} \int_{x\bar{x}y\bar{y}} e^{-ip \cdot (x-\bar{x})} \times e^{-ik_A \cdot (y-\bar{y})} \int_{uv} \mathcal{K}_{yu}^i \mathcal{K}_{\bar{y}\bar{v}}^i \langle \langle \mathcal{I}_N \rangle \rangle_{Y_A}, \quad (86)$$

where

$$\mathcal{I}_n := \text{tr} \{ \bar{L}_{\bar{u},0}^a \bar{U}_{\bar{x},n} L_{u,0}^a U_{x,n}^\dagger \} - \tilde{U}_{\bar{y},0}^{\dagger ac} \text{tr} \{ \bar{R}_{\bar{u},0}^c \bar{U}_{\bar{x},n} L_{u,0}^a U_{x,n}^\dagger \} - \tilde{U}_{y,0}^{\dagger ab} \text{tr} \{ \bar{L}_{\bar{u},0}^a \bar{U}_{\bar{x},n} R_{u,0}^b U_{x,n}^\dagger \} + \tilde{U}_{y,0}^{\dagger ab} \tilde{U}_{\bar{y},0}^{\dagger ac} \text{tr} \{ \bar{R}_{\bar{u},0}^c \bar{U}_{\bar{x},n} R_{u,0}^b U_{x,n}^\dagger \}. \quad (87)$$

Before moving forward, let us stress some features of Eqs. (86) and (87). In addition to the Wilson lines at rapidity Y_N , they involve Lie derivatives of Wilson lines at Y_N with respect to Wilson lines at Y_A , e.g., $\bar{L}_{\bar{u},0}^a \bar{U}_{\bar{x},N}$, denoted by the subscript 0 in the Lie derivatives. This is contrary to the evolution Hamiltonian in Eqs. (78), (79), and (80) that involved Lie derivatives with respect to the latest rapidity in the evolution. Additionally, the expression contains adjoint representation Wilson lines at the initial rapidity Y_A , again denoted by the subscript 0. These Lie derivatives are new d.o.f., in some sense like Reggeized gluon propagators, that encode information about the

(de)correlation in rapidity of the Wilson lines. The JIMWLK equation also gives the evolution equations for the Lie derivatives themselves. To find the expressions for RU^\dagger , RU , LU^\dagger , and LU , one starts by acting with the Lie derivatives on Eqs. (27) and (31). However, the four equations are not independent of each other. For example, we may start by finding the equation for RU^\dagger . The Hermitian conjugate will give the equation for RU , and the relation $L_{u,0}^a = \tilde{U}_{u,0}^{\dagger ab} R_{u,0}^b$ can be used to get the equations for LU^\dagger and LU .

The initial conditions at Y_0 for these four bilocal Langevin equations are given by Eqs. (13) to (16):

$$R_{u,n}^a U_{x,0}^\dagger = ig\delta_{ux} U_{x,0}^\dagger t^a, \quad (88)$$

$$R_{u,0}^a U_{x,0} = -ig\delta_{ux} t^a U_{x,0}, \quad (89)$$

$$L_{u,0}^a U_{x,0}^\dagger = ig\delta_{ux} t^a U_{x,0}^\dagger, \quad (90)$$

$$L_{u,0}^a U_{x,0} = -ig\delta_{ux} U_{x,0} t^a. \quad (91)$$

We emphasize once more that the adjoint Wilson lines appearing in \mathcal{I}_n are from the production Hamiltonian; they are always at Y_0 and do not evolve to Y_N .

B. Evolution in rapidity

To derive the evolution equations for the Lie derivatives, we begin by acting on Eq. (27) with a right

Lie derivative. After some manipulations described in [60], we arrive at

$$R_{u,0}^a U_{x,n+1}^\dagger = e^{ieg\alpha_{x,n}^L} R_{u,0}^a U_{x,n}^\dagger e^{-ieg\alpha_{x,n}^R} - \frac{ieg}{\sqrt{4\pi^3}} e^{ieg\alpha_{x,n}^L} U_{x,n}^\dagger \times \int_z \mathcal{K}_{xz}^i [U_{z,n} \nu_{z,n}^i U_{z,n}^\dagger, U_{z,n} R_{u,0}^a U_{z,n}^\dagger]. \quad (92)$$

The quantity $R_{u,0}^a U_{x,n}^\dagger$ describes the evolution from the initial rapidity Y_A , initial coordinate \mathbf{u} , and color index a to the final Wilson line at rapidity step n , coordinate \mathbf{z} , and a color that is encoded in the matrix structure of $R_{u,0}^a U_{z,n}^\dagger$.

In order to understand what Eq. (92) does at each iteration, we can look at one step in evolution in diagrams. First, we Taylor expand the exponentials in ϵ . At $n = 0$, we can use the initial condition Eq. (88) to write

$$R_{u,0}^a U_{x,1}^\dagger = ig\delta_{ux} U_{x,0}^\dagger t^a + ig \int_z \left(\frac{ieg}{\sqrt{4\pi^3}} \mathcal{K}_{xz}^i U_{z,0}^{i,b} - \frac{\epsilon g^2}{4\pi^3} \mathcal{K}_{xxz} t^b \right) \times [\delta_{ux} (t^b U_{x,0}^\dagger t^a - U_{x,0}^\dagger t^a \tilde{U}_{z,0}^{\dagger bc} t^c) - \delta_{uz} (U_{x,0}^\dagger \tilde{U}_{z,0}^{\dagger bc} t^c t^a - U_{x,0}^\dagger t^a \tilde{U}_{z,0}^{\dagger bc} t^c)] + \mathcal{O}(\epsilon^{3/2}). \quad (93)$$

In diagrams, this is

$$R_{u,0}^a U_{x,1}^\dagger = ig \left(\text{diagram} \right) + ig \frac{ieg}{\sqrt{4\pi^3}} \int_z \mathcal{K}_{xz}^i \nu_{z,0}^{i,b} \left(\text{diagram 1} - \text{diagram 2} - \text{diagram 3} + \text{diagram 4} \right) - ig \frac{\epsilon g^2}{4\pi^3} \int_z \mathcal{K}_{xxz} \left(\text{diagram 5} - \text{diagram 6} - \text{diagram 7} + \text{diagram 8} \right) + \mathcal{O}(\epsilon^{3/2}). \quad (94)$$

From this, we can see that after one iteration, Eq. (92) contains all possible diagrams with one gluon inserted on the right of the target (corresponding to color index a in the diagrams), and afterwards either none or one more gluon insertion. The second gluon (corresponding to color indices b and c) can be inserted in four different ways: either to the right or to the left of the target, and either at coordinate

x or z . Additionally, it can be either left as a free color index (contracted by the color of the noise) or reabsorbed by the quark. This makes the 2^3 two-gluon diagrams shown in Eq. (94).

The next iteration of the evolution equation will add more gluons to the diagrams present in Eq. (94), in the same way. The number of terms therefore grows very rapidly

with each step. The same analysis can be done for the LU^\dagger evolution. The only difference will be that the gluons appear on the opposite side of the target.

It is more natural to write Eq. (92) such that the color structure is more explicit. The propagator should have two adjoint representation indices at the ends, i.e., R^{ab} , or equivalently, be an explicitly Hermitian traceless matrix with one additional index, i.e., $R^{ab}t^b$. This more symmetric form is achieved by multiplying RU^\dagger by U from the left. Defining $R_{ux,n}^a \equiv U_{x,n}R_{u,0}^aU_{x,n}^\dagger$, which is conveniently a member of the Lie algebra of $SU(N_c)$, we can write the Langevin step compactly as

$$R_{ux,n+1}^a = e^{ieg\alpha_{x,n}^R} R_{ux,n}^a e^{-ieg\alpha_{x,n}^R} - \frac{ieg}{\sqrt{4\pi^3}} e^{ieg\alpha_{x,n}^R} \int_z \mathcal{K}_{xz}^i [\tilde{\nu}_{z,n}^j, R_{uz,n}^a], \quad (95)$$

where we have used $\tilde{\nu}_{z,n}^j = U_{z,n} \nu_{z,n}^j U_{z,n}^\dagger$ as introduced in Eq. (25). Notice that this equation is linear in $R_{ux,n}^a$, although it resums all orders in the background field, incorporated into the Wilson line.

As mentioned above, the three other required equations, RU , LU^\dagger , and LU , can be obtained directly from Eq. (95). In terms of explicitly Hermitian quantities, we obtain for $\bar{R}_{ux,n}^a \equiv (R_{u,0}^a U_{x,n}) U_{x,n}^\dagger$

$$\bar{R}_{ux,n+1}^a = e^{ieg\alpha_{x,n}^R} \bar{R}_{ux,n}^a e^{-ieg\alpha_{x,n}^R} - \frac{ieg}{\sqrt{4\pi^3}} \int_z \mathcal{K}_{xz}^i [\tilde{\nu}_{z,n}^j, \bar{R}_{uz,n}^a] e^{-ieg\alpha_{x,n}^R}. \quad (96)$$

Defining $L_{ux,n}^a \equiv U_{x,n} L_{u,0}^a U_{x,n}^\dagger$, we get the corresponding equations for the left Lie derivative,

$$L_{ux,n+1}^a = e^{ieg\alpha_{x,n}^R} L_{ux,n}^a e^{-ieg\alpha_{x,n}^R} - \frac{ieg}{\sqrt{4\pi^3}} e^{ieg\alpha_{x,n}^R} \int_z \mathcal{K}_{xz}^i [\tilde{\nu}_{z,n}^j, L_{uz,n}^a], \quad (97)$$

and for $\bar{L}_{ux,n}^a \equiv (L_{u,0}^a U_{x,n}) U_{x,n}^\dagger$,

$$\bar{L}_{ux,n+1}^a = e^{ieg\alpha_{x,n}^R} \bar{L}_{ux,n}^a e^{-ieg\alpha_{x,n}^R} - \frac{ieg}{\sqrt{4\pi^3}} \int_z \mathcal{K}_{xz}^i [\tilde{\nu}_{z,n}^j, \bar{L}_{uz,n}^a] e^{-ieg\alpha_{x,n}^R}. \quad (98)$$

The initial conditions for this set of four evolution equations follow directly from Eqs. (88) to (91):

$$R_{ux,0}^a = ig\delta_{ux} t^a, \quad (99)$$

$$\bar{R}_{ux,0}^a = -ig\delta_{ux} t^a, \quad (100)$$

$$L_{ux,0}^a = ig\delta_{ux} \tilde{U}_{x,0}^{\dagger ab} t^b, \quad (101)$$

$$\bar{L}_{ux,0}^a = -ig\delta_{ux} \tilde{U}_{x,0}^{\dagger ab} t^b. \quad (102)$$

A quick inspection of the equations of motion (95) to (98) reveals in all of them two crucial features. First, they only depend on the “rotated noise” $\tilde{\nu}$ [see Eq. (25)], but not the original unrotated noise ν ; note that this is true also for the “right” color field $\alpha_{x,n}^R$, Eq. (24). Second, their dependence on the Wilson line also comes through the rotated noise, but not separately in terms of explicit Wilson lines in the evolution equations. Thus, if we take the rotated noise as the independent variable that one averages over, all the dependence on the Wilson lines disappears. This means that the quantities $R_{ux,n}^a$, $\bar{R}_{ux,n}^a$, $L_{ux,n}^a$, and $\bar{L}_{ux,n}^a$ satisfy evolution equations that are linear and independent of the Wilson lines, and we can therefore express the evolution between the two rapidities in terms of linear BFKL-like dynamics. This can be made even more explicit by developing the equations in ϵ and, as usual, replacing the terms that are quadratic in the noise with their expectation values. Doing this one gets

$$R_{ux,n+1}^a = R_{ux,n}^a + \frac{ieg}{\sqrt{4\pi^3}} \int_z \mathcal{K}_{xz}^i [\tilde{\nu}_{z,n}^j, R_{ux,n}^a - R_{uz,n}^a] - \frac{N_c \epsilon g^2}{2 \cdot 4\pi^3} \int_z \mathcal{K}_{xxz} (R_{ux,n}^a - R_{uz,n}^a) + \mathcal{O}(\epsilon^{3/2}), \quad (103)$$

$$\bar{R}_{ux,n+1}^a = \bar{R}_{ux,n}^a + \frac{ieg}{\sqrt{4\pi^3}} \int_z \mathcal{K}_{xz}^i [\tilde{\nu}_{z,n}^j, \bar{R}_{ux,n}^a - \bar{R}_{uz,n}^a] - \frac{N_c \epsilon g^2}{2 \cdot 4\pi^3} \int_z \mathcal{K}_{xxz} (\bar{R}_{ux,n}^a - \bar{R}_{uz,n}^a) + \mathcal{O}(\epsilon^{3/2}), \quad (104)$$

$$L_{ux,n+1}^a = L_{ux,n}^a + \frac{ieg}{\sqrt{4\pi^3}} \int_z \mathcal{K}_{xz}^i [\tilde{\nu}_{z,n}^j, L_{ux,n}^a - L_{uz,n}^a] - \frac{N_c \epsilon g^2}{2 \cdot 4\pi^3} \int_z \mathcal{K}_{xxz} (L_{ux,n}^a - L_{uz,n}^a) + \mathcal{O}(\epsilon^{3/2}), \quad (105)$$

$$\bar{L}_{ux,n+1}^a = \bar{L}_{ux,n}^a + \frac{ieg}{\sqrt{4\pi^3}} \int_z \mathcal{K}_{xz}^i [\tilde{\nu}_{z,n}^j, \bar{L}_{ux,n}^a - \bar{L}_{uz,n}^a] - \frac{N_c \epsilon g^2}{2 \cdot 4\pi^3} \int_z \mathcal{K}_{xxz} (\bar{L}_{ux,n}^a - \bar{L}_{uz,n}^a) + \mathcal{O}(\epsilon^{3/2}). \quad (106)$$

The whole cross section, however, is not given by a “ k_T -factorized” expression (unlike the dilute case that we discuss in the next section). This is not true even at equal rapidity, as we have seen in Eq. (45). This is due to the appearance of the Wilson lines in two places in the cross section. First, the initial conditions for $R_{ux,n}^a$, $\bar{R}_{ux,n}^a$, $L_{ux,n}^a$, and $\bar{L}_{ux,n}^a$ depend on the Wilson lines at Y_A . Second, the final expression for the cross section (87) written in terms of these quantities is now

$$\begin{aligned}
\mathcal{I}_n = & \text{tr}\{\bar{L}_{v\bar{x},n}^a U_{\bar{x},n} U_{x,n}^\dagger L_{u\bar{x},n}^a\} - \bar{U}_{\bar{y},0}^{\dagger ac} \text{tr}\{\bar{R}_{v\bar{x},n}^c U_{\bar{x},n} U_{x,n}^\dagger L_{u\bar{x},n}^a\} \\
& - \bar{U}_{\bar{y},0}^{\dagger ab} \text{tr}\{\bar{L}_{v\bar{x},n}^a U_{\bar{x},n} U_{x,n}^\dagger R_{u\bar{x},n}^b\} \\
& + \bar{U}_{\bar{y},0}^{\dagger ab} \bar{U}_{\bar{y},0}^{\dagger ac} \text{tr}\{\bar{R}_{v\bar{x},n}^c U_{\bar{x},n} U_{x,n}^\dagger R_{u\bar{x},n}^b\}. \quad (107)
\end{aligned}$$

We see that this expression involves explicit Wilson lines both at the rapidity of the earlier particle (i.e., $n = 0$) and at the rapidity of the later one (i.e., n). Because of the latter, the expression in the full nonlinear case cannot be written in a k_T -factorized form with only an unintegrated gluon distribution at $n = 0$ and a BFKL Green's function between the rapidities, as we will do in the dilute limit in Sec. VI.

Because the evolution equations (95) to (98) do not depend on the Wilson lines, the dynamics of the evolution of the two-particle correlation between these rapidities is linear. This is a remarkable feature that should significantly simplify a future numerical analysis of the two-particle correlation in this framework. This is generically quite difficult in the original formulation due to the bilocal nature of the ‘‘Reggeized gluon propagators’’ $R_{u\bar{x},n}^a$, $\bar{R}_{u\bar{x},n}^a$, $L_{u\bar{x},n}^a$, and $\bar{L}_{u\bar{x},n}^a$ (i.e., the fact that they depend on two separate coordinate arguments). Note, however, that calculating the cross section requires additionally the nonlinear evolution of the Wilson lines themselves according to conventional JIMWLK. This evolution is *correlated* with that of the Reggeized gluon propagators, since the evolution steps of both quantities are expressed in terms of the same noise at the same rapidity step. Since the evolution step of the latter is linear and does not explicitly involve the Wilson lines, it should be simpler to analyze. However, one *cannot* factorize the expectation value of Eq. (107) as a product of expectation values of a Wilson line operator at rapidity n on the one hand and a two-point function of the Reggeized gluon propagators on the other.

Let us make, in passing, a side note concerning the initial conditions (101) and (102). It would be tempting to get rid of the Wilson line in these initial conditions by defining, instead of $L_{u\bar{x},n}^a \equiv U_{x,n} L_{u,0}^a U_{x,n}^\dagger$, a new quantity $(L_{u,0}^a U_{x,n}^\dagger) U_{x,n}$ and set out to solve its equation of motion. Contrary to $L_{u\bar{x},n}^a$, which has an initial condition that depends on the Wilson line but an evolution that can be expressed in a way that does not, this alternative quantity would have a simple initial condition (only a generator matrix t^a) but an evolution equation that depends on both the noise ν and the rotated noise $\tilde{\nu}$. This would make the linear dynamics of the evolution much more difficult to see explicitly.

The statement of linearity in the evolution between the two rapidities is in fact in agreement with the result for one quark and one gluon production in [63], where it is argued that there can be no pomeron mergings between these two particles. However, the situation becomes more complicated when one considers the production of one quark and two gluons. In this case, the result of [63] is that evolution between the produced particles is genuinely nonlinear.

VI. TWO-PARTICLE CORRELATORS IN THE DILUTE LIMIT

We shall now move on to work out what happens in the dilute limit and show explicitly how to recover an expected BFKL result from this formalism. Our aim is to show that the two-particle cross section in the dilute limit can be expressed as a convolution of an unintegrated gluon distribution at the earlier rapidity Y_A and a BFKL Green's function from Y_A to the rapidity of the quark (see e.g., [77] for calculations of two-particle production from the same BFKL ladder). Although the following calculation is done by linearizing the evolution, it is important to note that due to the linearity of the dynamics in the full case discussed above, the nature of decorrelations in rapidity could be expected to be very similar.

The general idea is to see what happens when we start increasing the rapidity separation between the produced quark and gluon. The gluon is produced at rapidity Y_A ; the quark rapidity increases and the cross section changes accordingly, via JIMWLK evolution. It is important here to note that the JIMWLK evolution is that of the Wilson lines in the dipole operator $\hat{S}_{x\bar{x}}$ at rapidity Y_n only. The Wilson lines and Lie derivatives in the production Hamiltonian H_{prod} remain at the initial rapidity Y_A . In this sense, the JIMWLK evolution ‘‘commutes’’ with the production Hamiltonian and only operates on the dipole operator. We also know that the evolution must be linear, and thus in the dilute limit it must correspond to the BFKL equation (69).

The essential part of the cross section (86) is given by \mathcal{I}_n as defined in Eq. (87): the combination of Wilson lines and their derivatives. To understand how this works, we have to understand the operations of the Lie derivatives in the dilute limit, i.e., how the Lie derivatives as defined in Eqs. (10) and (11) act on λ . The result is obtained by changing the differentiation variable from elements of U to λ , and then performing an expansion in powers of λ . Doing so gives

$$\begin{aligned}
L_{u,0}^a &= g \left(\delta^{ac} - \frac{1}{2} f^{abc} \lambda_{u,0}^b + \mathcal{O}(\lambda^2) \right) \frac{\delta}{\delta \lambda_{u,0}^c}, \\
R_{u,0}^a &= g \left(\delta^{ac} + \frac{1}{2} f^{abc} \lambda_{u,0}^b + \mathcal{O}(\lambda^2) \right) \frac{\delta}{\delta \lambda_{u,0}^c} \quad (108)
\end{aligned}$$

(see also [71]). As expected, the Lie derivatives reduce the term they act on by one power of λ ; they are after all derivatives with respect to the Wilson line. Since the evolution equation for λ is linear, this statement will be true at any step n .

The most straightforward way to proceed would be to derive, in the spirit of [60], evolution equations for the Lie derivatives operating on λ . This can be done in two equivalent ways: either by expanding the evolution equations of the bilocal quantities, e.g., Eq. (92), or by acting with the Lie derivative on the time step of λ [Eq. (52)].

In other words, the operations of Lie differentiating and expanding in λ are commutative. Either procedure results in

$$R_{u,0}^a \lambda_{x,n+1} = R_{u,0}^a \lambda_{x,n} + \int_z \left(\frac{i\epsilon g}{\sqrt{4\pi^3}} \mathcal{K}_{xz}^i \nu_{z,n}^{i,d} - \frac{\epsilon g^2}{4\pi^3} \mathcal{K}_{xxz} t^d \right) \times i f^{abc} t^c R_{u,0}^a (\lambda_{x,n}^b - \lambda_{z,n}^b) + \mathcal{O}(\epsilon^{3/2}, \lambda^2). \quad (109)$$

The equation for LU^\dagger is identical, with $R \rightarrow L$. The initial conditions for the bilocal Langevin equations are given in Eqs. (88) to (91). By expanding them as

$$R_{u,0}^a U_{x,0}^\dagger = ig \delta_{ux} \left(1 + i\lambda_{x,0} - \frac{1}{2} \lambda_{x,0}^2 \right) t^a + \mathcal{O}(\lambda^3), \quad (110)$$

$$L_{u,0}^a U_{x,0}^\dagger = ig \delta_{ux} t^a \left(1 + i\lambda_{x,0} - \frac{1}{2} \lambda_{x,0}^2 \right) + \mathcal{O}(\lambda^3), \quad (111)$$

one easily obtains the initial conditions for the Lie derivatives of λ as

$$R_{u,0}^a \lambda_{x,0} = L_{u,0}^a \lambda_{x,0} = gt^a \delta_{ux} + \mathcal{O}(\lambda). \quad (112)$$

In principle, we could go on to solve these equations, and indeed it is straightforward to write down a full formal solution in terms of the time evolution matrix \mathcal{M}_{xy}^{ab} , as defined in Eq. (56). But our main objective is to look at the cross section directly, as well as to derive an evolution equation for its dependence on the later rapidity Y . To do this, we use the expressions (108) to write the Lie derivatives in H_{prod} as

$$\begin{aligned} & (\bar{L}_{u,0}^a - \tilde{U}_{y,0}^{\dagger ac} \bar{R}_{u,0}^c) (L_{u,0}^a - \tilde{U}_{y,0}^{\dagger ab} R_{u,0}^b) \\ &= g^2 [f^{abc} f^{ade} (\bar{\lambda}_{u,0}^e - \bar{\lambda}_{y,0}^e) (\lambda_{u,0}^c - \lambda_{y,0}^c) + \mathcal{O}(\lambda^3)] \\ & \times \frac{\delta}{\delta \bar{\lambda}_{u,0}^d} \frac{\delta}{\delta \lambda_{u,0}^b}. \end{aligned} \quad (113)$$

We emphasize here that one must take care to perform the functional derivatives in the right order. It is essential to operate first with the Lie derivatives in the DA and the CCA separately. Only after doing this is one allowed to set $\bar{\lambda}_0 = \lambda_0$ at the initial rapidity $Y_0 = Y_A$. On the other hand, the noise ν is the same in the DA and the CCA, so we do not need to keep them separated when averaging over the noise. For example, we can take the expectation value that allowed us to write Eq. (64), even if the expression involves both λ and $\bar{\lambda}$ separately.

An important feature of the operator (113) is that it has exactly one derivative operating on the DA and one on the CCA. Also, since the DA and the CCA evolve separately, λ_n depends only on λ_0 and not on $\bar{\lambda}_0$, and vice versa. Thus, from the expansion of the dipole in Eq. (85) as

$$\hat{S}_{x\bar{x}} = 1 - \frac{1}{4N_c} \lambda_x^a \lambda_x^a - \frac{1}{4N_c} \bar{\lambda}_{\bar{x}}^a \bar{\lambda}_{\bar{x}}^a + \frac{1}{2N_c} \lambda_x^a \bar{\lambda}_{\bar{x}}^a + \mathcal{O}(\lambda^3) \quad (114)$$

[cf. Eq. (70)], we need only to retain the cross term $\sim \lambda \bar{\lambda}$ when operating with the production Hamiltonian.

Using the linearized production Hamiltonian (113) and the linearized dipole (114), we have

$$\begin{aligned} \mathcal{I}_n &= \frac{g^2}{2N_c} f^{abc} f^{ade} (\bar{\lambda}_{u,0}^e - \bar{\lambda}_{y,0}^e) (\lambda_{u,0}^c - \lambda_{y,0}^c) \\ & \times \frac{\delta}{\delta \bar{\lambda}_{u,0}^d} \frac{\delta}{\delta \lambda_{u,0}^b} \bar{\lambda}_{x,n}^f \lambda_{x,n}^f + \mathcal{O}(\lambda^3). \end{aligned} \quad (115)$$

Now we can write the explicit λ 's from the production Hamiltonian (113) in terms of the gluon distribution $\phi_{w\bar{w}}^0$ (65) at the initial rapidity Y_A . Then we can use δ^{ce} from the initial condition of ϕ to simplify the color algebra. We now introduce the definition

$$\mathcal{F}_{x\bar{x}u\bar{u}}^n \equiv \frac{\delta}{\delta \bar{\lambda}_{u,0}^a} \frac{\delta}{\delta \lambda_{u,0}^b} \bar{\lambda}_{x,n}^b \lambda_{x,n}^a \quad (116)$$

for the BFKL Green's function. Note that due to the linear evolution of λ , the relation between $\lambda_{x,n}^b$ and $\lambda_{u,0}^a$ is linear [see e.g., Eq. (58)]. Thus Green's function $\mathcal{F}_{x\bar{x}u\bar{u}}^n$ defined by Eq. (116) does not depend on λ . Using this we get

$$\langle \mathcal{I}_N \rangle = \frac{g^2}{2} (\phi_{u\bar{u}}^0 - \phi_{u\bar{y}}^0 - \phi_{y\bar{u}}^0 + \phi_{y\bar{y}}^0) \mathcal{F}_{x\bar{x}u\bar{u}}^N + \mathcal{O}(\phi^{3/2}), \quad (117)$$

which we can put into the equation for the two-particle cross section (85) to obtain a k_T -factorized expression:

$$\begin{aligned} & \frac{d\sigma_{gg}}{dY d^2p dY_A d^2k_A} \\ &= \frac{1}{(2\pi)^4} \frac{1}{2N_c} \frac{\alpha_s}{\pi^2} \int_{x\bar{x}y\bar{y}u\bar{u}} \mathcal{K}_{yu}^i \mathcal{K}_{y\bar{u}}^i e^{-ip \cdot (x-\bar{x}) - ik_A \cdot (y-\bar{y})} \\ & \times (\phi_{u\bar{u}}^0 - \phi_{u\bar{y}}^0 - \phi_{y\bar{u}}^0 + \phi_{y\bar{y}}^0) \mathcal{F}_{x\bar{x}u\bar{u}}^N + \mathcal{O}(\phi^{3/2}). \end{aligned} \quad (118)$$

At this stage all the functional derivatives are already taken, and we can now finally take the color field to be equal in the DA and the CCA, i.e., take $\lambda = \bar{\lambda}$. We can now, in fact, also replace the ϕ 's with the other gluon distribution φ (71), since they appear in the particular combination

$$\phi_{u\bar{u}}^0 - \phi_{u\bar{y}}^0 - \phi_{y\bar{u}}^0 + \phi_{y\bar{y}}^0 = -\frac{1}{2} (\varphi_{u\bar{u}}^0 - \varphi_{u\bar{y}}^0 - \varphi_{y\bar{u}}^0 + \varphi_{y\bar{y}}^0), \quad (119)$$

where the value of the distribution at zero coordinate separation cancels. This means that the cross section can be equally well written in terms of the gluon distribution ϕ

satisfying the usual BFKL equation (66) [more familiarly Eq. (69) in momentum space] or the BFKL pomeron φ satisfying the Mueller version of the equation, Eq. (73). There is a factor of $-1/2$ difference due to our conventions here. The fact that we are taking derivatives with respect to $\bar{\lambda}_{\bar{u},0}$ and $\lambda_{u,0}$ does not in any way interfere with the BFKL evolution of the gluon density $\bar{\lambda}_{\bar{x},n}^b \lambda_{x,n}^b$. So it is clear that $\mathcal{F}_{x,\bar{x},u,\bar{u}}^n$ satisfies the same equation as $\bar{\lambda}_{\bar{x},n}^b \lambda_{x,n}^b$ with respect to the rapidity index n :

$$\begin{aligned} \mathcal{F}_{x,\bar{x},u,\bar{u}}^{n+1} &= \mathcal{F}_{x,\bar{x},u,\bar{u}}^n - \frac{N_c \epsilon \alpha_s}{2 \pi^2} \int_z [\mathcal{K}_{xxz} (\mathcal{F}_{x,\bar{x},u,\bar{u}}^n - \mathcal{F}_{z,\bar{x},u,\bar{u}}^n) \\ &\quad + \mathcal{K}_{\bar{x}\bar{x}z} (\mathcal{F}_{x,\bar{x},u,\bar{u}}^n - \mathcal{F}_{x,z,u,\bar{u}}^n) \\ &\quad - 2\mathcal{K}_{x\bar{x}z} (\mathcal{F}_{x,\bar{x},u,\bar{u}}^n - \mathcal{F}_{x,z,u,\bar{u}}^n - \mathcal{F}_{z,\bar{x},u,\bar{u}}^n + \mathcal{F}_{z,z,u,\bar{u}}^n)] \\ &\quad + \mathcal{O}(\mathcal{F}^{3/2}) \end{aligned} \quad (120)$$

[cf. Eq. (66)].

Now that we have derived the factorized form for the cross section, Eq. (118), it is easy to write it in momentum space. We use the Fourier representations of the gluon emission kernels, given in Eq. (68), to write

$$\begin{aligned} \frac{d\sigma_{gg}}{dY d^2p dY_A d^2k_A} &= \frac{1}{(2\pi)^2} \frac{1}{4N_c} \frac{\alpha_s}{\pi^2} \int_{x\bar{x}y\bar{y}u\bar{u}w\bar{w}} \frac{\mathbf{l} \cdot \bar{\mathbf{l}}}{\bar{l}^2 l^2} \\ &\quad \times e^{-i\bar{l} \cdot (y-u) - i\bar{l} \cdot (\bar{y}-\bar{u})} e^{-i\mathbf{p} \cdot (x-\bar{x}) - ik_A \cdot (y-\bar{y})} \\ &\quad \times (\delta_{wu} - \delta_{w\bar{y}})(\delta_{\bar{w}\bar{u}} - \delta_{\bar{w}\bar{y}}) \varphi_{w\bar{w}}^0 \mathcal{F}_{x,\bar{x},u,\bar{u}}^N \\ &\quad + \mathcal{O}(\varphi^{3/2}). \end{aligned} \quad (121)$$

Introducing a Fourier representation for the BFKL Green's function

$$\begin{aligned} \mathcal{F}^{n+1}(\mathbf{P}, -\mathbf{P}, \mathbf{m}, -\mathbf{m}) &= \mathcal{F}^n(\mathbf{P}, -\mathbf{P}, \mathbf{m}, -\mathbf{m}) + 4N_c \epsilon \alpha_s \int_{\mathbf{K}} \frac{1}{(\mathbf{P} - \mathbf{K})^2} \left(\mathcal{F}^n(\mathbf{K}, -\mathbf{K}, \mathbf{m}, -\mathbf{m}) \frac{\mathbf{K}^2}{\mathbf{P}^2} - \frac{1}{2} \mathcal{F}^n(\mathbf{P}, -\mathbf{P}, \mathbf{m}, -\mathbf{m}) \frac{\mathbf{P}^2}{\mathbf{K}^2} \right) \\ &\quad + \mathcal{O}(\epsilon^{3/2}, \mathcal{F}^{3/2}) \end{aligned} \quad (125)$$

[cf. Eq. (69)]. A diagrammatic interpretation of this as a typical BFKL ladder is given in Fig. 1. Equation (124) is the main result of this section. It shows that the IT Langevin equation formalism reduces, in the dilute limit, to a conventional correlation between two particles produced from the same BFKL ladder.

The initial condition for the evolution can be read off from the definition (116),

$$\mathcal{F}_{x,\bar{x},u,\bar{u}}^0 = (N_c^2 - 1) \delta_{xu} \delta_{\bar{x}\bar{u}}, \quad (126)$$

or in momentum space,

$$\mathcal{F}^0(\mathbf{P}, \bar{\mathbf{P}}, \mathbf{m}, \bar{\mathbf{m}}) = (N_c^2 - 1) \delta^{(2)}(\mathbf{P} + \mathbf{m}) \delta^{(2)}(\bar{\mathbf{P}} + \bar{\mathbf{m}}). \quad (127)$$

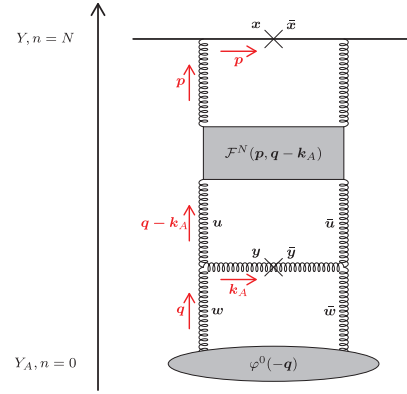


FIG. 1. Coordinate and momentum assignments for the BFKL ladder diagram corresponding to Eq. (125).

$$\mathcal{F}_{x,\bar{x},u,\bar{u}}^n = \int_{\mathbf{P}\bar{\mathbf{P}}\mathbf{m}\bar{\mathbf{m}}} e^{-i(\mathbf{P}\cdot x + \bar{\mathbf{P}}\cdot \bar{x} + \mathbf{m}\cdot u + \bar{\mathbf{m}}\cdot \bar{u})} \mathcal{F}^n(\mathbf{P}, \bar{\mathbf{P}}, \mathbf{m}, \bar{\mathbf{m}}) \quad (122)$$

and

$$\varphi_{xy} \equiv \int_{\mathbf{q}} e^{-i\mathbf{q}\cdot(x-y)} \varphi(\mathbf{q}), \quad (123)$$

we can write

$$\begin{aligned} \frac{d\sigma_{gg}}{dY d^2p dY_A d^2k_A} &= -\frac{\alpha_s}{N_c} \int_{\mathbf{q}} \frac{\mathbf{q}^2}{(\mathbf{q} - \mathbf{k}_A)^2 \mathbf{k}_A^2} \mathcal{F}^N(-\mathbf{p}, \mathbf{p}, \mathbf{q} - \mathbf{k}_A, \\ &\quad -\mathbf{q} + \mathbf{k}_A) \varphi^0(-\mathbf{q}) + \mathcal{O}(\varphi^{3/2}) \end{aligned} \quad (124)$$

with the (zero momentum transfer) BFKL Green's function \mathcal{F} in momentum space satisfying the usual BFKL equation

Using this in the general expression (124) reduces the equal rapidity cross section to a k_T -factorized expression for the two-particle production cross section:

$$\left. \frac{d\sigma_{gg}}{dY d^2p dY_A d^2k_A} \right|_{Y=Y_A} = -\frac{\alpha_s}{(2\pi)^2} \frac{(\mathbf{p} + \mathbf{k}_A)^2}{\mathbf{p}^2 \mathbf{k}_A^2} \varphi^0(\mathbf{p} + \mathbf{k}_A). \quad (128)$$

This expression already has the structure of Fig. 1, with an unintegrated gluon distribution $\mathbf{q}^2 \varphi(\mathbf{q})$ for the gluon taken from the target, and propagators $1/k_A^2$ and $1/p^2$ corresponding to the produced particles. For this case of no evolution in rapidity, the Lipatov vertices for producing the gluon and the

initial condition for the BFKL Green's function combine to produce a simple factor $\delta^{(2)}(\mathbf{q} - \mathbf{k}_A - \mathbf{p})$, which naturally means that in the absence of gluon emission in a ladder, the transverse momentum of the two final-state particles must match that coming from the target.

VII. CONCLUSIONS

In conclusion, we have attempted to clarify here the Langevin formulation [60] of two-particle correlations in JIMWLK evolution, in the case of a dilute probe scattering off a dense color field target. Our first important result is the observation that, although the JIMWLK evolution for the Wilson lines is nonlinear, the evolution of the Lie derivatives encoding the correlation between the two rapidities is in fact not. It can be expressed instead, with a suitable transformation, as a linear equation that is independent of the Wilson lines. This observation seems to confirm the result obtained earlier (in a rather different language) in [63]. This conclusion points toward a much simpler way to calculate the two-particle cross section than a straightforward numerical solution of the bilocal Langevin equations in [60]. Exploring the full phenomenological consequences of this observation is beyond the scope of this paper, but it would be valuable to pursue this in future work.

We have also calculated explicitly the dilute limit of the Langevin formulation, where the decorrelations in azimuthal angle between the two particles are given by a BFKL Green's function between the two rapidities. The physical

picture here is that of color charges, or rather Reggeized gluon fields λ , that change with rapidity in a stochastic process [see e.g., Eqs. (52) and (109)]. The power counting for calculating two-particle correlations in this limit is, however, tricky. This is due to the fact that the two-particle cross section depends on Reggeized gluon fields from the expansion of both the adjoint Wilson lines and the Lie derivatives in the production Hamiltonian. In order to see this connection, it is easier to continue a bit further with the more formal definition in terms of the functional derivatives. The essential feature is that JIMWLK evolution as a function of the quark rapidity Y “commutes” with the production Hamiltonian and only operates on the dipole operator at Y . The evolution of the double inclusive cross section with Y is therefore determined by the evolution of the single inclusive cross section, but with a more complicated initial condition. This feature enabled us to show that in the linearized limit, the result is in fact what one would expect from BFKL dynamics.

ACKNOWLEDGMENTS

We are grateful to R. Boussarie, M. Lublinsky, E. Iancu, and D. Triantafyllopoulos for discussions. T. L. has been supported by the Academy of Finland, Projects No. 267321 and No. 303756. A. R. is supported by the National Research Foundation of South Africa. This work has been supported by the European Research Council, Grant No. ERC-2015-CoG-681707.

-
- [1] S. Schlichting and P. Tribedy, Collectivity in small collision systems: An initial-state perspective, *Adv. High Energy Phys.* **2016**, 8460349 (2016).
 - [2] A. Dumitru, F. Gelis, L. McLerran, and R. Venugopalan, Glasma flux tubes and the near side ridge phenomenon at RHIC, *Nucl. Phys.* **A810**, 91 (2008).
 - [3] E. Iancu and R. Venugopalan, The color glass condensate and high energy scattering in QCD, in *Quark Gluon Plasma*, edited by R. Hwa and X. N. Wang (World Scientific, Singapore, 2003).
 - [4] H. Weigert, Evolution at small x_{bj} : The color glass condensate, *Prog. Part. Nucl. Phys.* **55**, 461 (2005).
 - [5] F. Gelis, E. Iancu, J. Jalilian-Marian, and R. Venugopalan, The color glass condensate, *Annu. Rev. Nucl. Part. Sci.* **60**, 463 (2010).
 - [6] J. Jalilian-Marian, A. Kovner, L. D. McLerran, and H. Weigert, The intrinsic glue distribution at very small x , *Phys. Rev. D* **55**, 5414 (1997).
 - [7] J. Jalilian-Marian, A. Kovner, A. Leonidov, and H. Weigert, The BFKL equation from the Wilson renormalization group, *Nucl. Phys.* **B504**, 415 (1997).
 - [8] J. Jalilian-Marian, A. Kovner, A. Leonidov, and H. Weigert, The Wilson renormalization group for low x physics: Towards the high density regime, *Phys. Rev. D* **59**, 014014 (1998).
 - [9] J. Jalilian-Marian, A. Kovner, and H. Weigert, The Wilson renormalization group for low x physics: Gluon evolution at finite parton density, *Phys. Rev. D* **59**, 014015 (1998).
 - [10] J. Jalilian-Marian, A. Kovner, A. Leonidov, and H. Weigert, Unitarization of gluon distribution in the doubly logarithmic regime at high density, *Phys. Rev. D* **59**, 034007 (1999).
 - [11] H. Weigert, Unitarity at small Bjorken x , *Nucl. Phys.* **A703**, 823 (2002).
 - [12] E. Iancu, A. Leonidov, and L. D. McLerran, Nonlinear gluon evolution in the color glass condensate. I, *Nucl. Phys.* **A692**, 583 (2001).
 - [13] E. Iancu and L. D. McLerran, Saturation and universality in QCD at small x , *Phys. Lett. B* **510**, 145 (2001).
 - [14] E. Ferreira, E. Iancu, A. Leonidov, and L. McLerran, Nonlinear gluon evolution in the color glass condensate. II, *Nucl. Phys.* **A703**, 489 (2002).

- [15] E. Iancu, A. Leonidov, and L. D. McLerran, The renormalization group equation for the color glass condensate, *Phys. Lett. B* **510**, 133 (2001).
- [16] A. H. Mueller, A simple derivation of the JIMWLK equation, *Phys. Lett. B* **523**, 243 (2001).
- [17] W. Buchmüller and A. Hebecker, Semiclassical approach to structure functions at small x , *Nucl. Phys.* **B476**, 203 (1996).
- [18] J.-P. Blaizot, E. Iancu, and H. Weigert, Nonlinear gluon evolution in path integral form, *Nucl. Phys.* **A713**, 441 (2003).
- [19] K. Rummukainen and H. Weigert, Universal features of JIMWLK and BK evolution at small x , *Nucl. Phys.* **A739**, 183 (2004).
- [20] Y. V. Kovchegov, J. Kuokkanen, K. Rummukainen, and H. Weigert, Subleading- N_c corrections in non-linear small- x evolution, *Nucl. Phys.* **A823**, 47 (2009).
- [21] T. Lappi and H. Mäntysaari, On the running coupling in the JIMWLK equation, *Eur. Phys. J. C* **73**, 2307 (2013).
- [22] J. Bjorken, J. B. Kogut, and D. E. Soper, Quantum electrodynamics at infinite momentum: Scattering from an external field, *Phys. Rev. D* **3**, 1382 (1971).
- [23] N. N. Nikolaev and B. G. Zakharov, Colour transparency and scaling properties of nuclear shadowing in deep inelastic scattering, *Z. Phys. C* **49**, 607 (1991).
- [24] N. Nikolaev and B. G. Zakharov, Pomeron structure function and diffraction dissociation of virtual photons in perturbative QCD, *Z. Phys. C* **53**, 331 (1992).
- [25] G. Beuf, Dipole factorization for DIS at NLO: Loop correction to the photon to quark-antiquark light-front wave-functions, *Phys. Rev. D* **94**, 054016 (2016).
- [26] G. Beuf, Dipole factorization for DIS at NLO: Combining the $q\bar{q}$ and $q\bar{q}g$ contributions, *Phys. Rev. D* **96**, 074033 (2017).
- [27] H. Hänninen, T. Lappi, and R. Paatelainen, One-loop corrections to light cone wave functions: The dipole picture DIS cross section, *Ann. Phys. (Amsterdam)* **393**, 358 (2018).
- [28] I. Balitsky and G. A. Chirilli, Photon impact factor and k_T -factorization for DIS in the next-to-leading order, *Phys. Rev. D* **87**, 014013 (2013).
- [29] Y. V. Kovchegov, Small- x F2 structure function of a nucleus including multiple pomeron exchanges, *Phys. Rev. D* **60**, 034008 (1999).
- [30] J. Bartels and A. Kwieciński, NLO corrections to the γ^* impact factor: First numerical results for the real corrections to γ_L^* , *Phys. Rev. D* **70**, 114003 (2004).
- [31] A. Dumitru and J. Jalilian-Marian, Scattering of gluons from the color glass condensate, *Phys. Lett. B* **547**, 15 (2002).
- [32] A. Dumitru and J. Jalilian-Marian, Forward Quark Jets from Protons Shattering the Colored Glass, *Phys. Rev. Lett.* **89**, 022301 (2002).
- [33] A. Dumitru, A. Hayashigaki, and J. Jalilian-Marian, The color glass condensate and hadron production in the forward region, *Nucl. Phys.* **A765**, 464 (2006).
- [34] G. A. Chirilli, B.-W. Xiao, and F. Yuan, One-Loop Factorization for Inclusive Hadron Production in pA Collisions in the Saturation Formalism, *Phys. Rev. Lett.* **108**, 122301 (2012).
- [35] G. A. Chirilli, B.-W. Xiao, and F. Yuan, Inclusive hadron productions in pA collisions, *Phys. Rev. D* **86**, 054005 (2012).
- [36] Z.-B. Kang, I. Vitev, and H. Xing, Next-to-Leading Order Forward Hadron Production in the Small- x Regime: Rapidity Factorization, *Phys. Rev. Lett.* **113**, 062002 (2014).
- [37] B. Ducloué, T. Lappi, and Y. Zhu, Single inclusive forward hadron production at next-to-leading order, *Phys. Rev. D* **93**, 114016 (2016).
- [38] E. Iancu, A. H. Mueller, and D. N. Triantafyllopoulos, CGC factorization for forward particle production in proton-nucleus collisions at next-to-leading order, *J. High Energy Phys.* **12** (2016) 041.
- [39] B. Ducloué, T. Lappi, and Y. Zhu, Implementation of NLO high energy factorization in single inclusive forward hadron production, *Phys. Rev. D* **95**, 114007 (2017).
- [40] B. Ducloué, E. Iancu, T. Lappi, A. H. Mueller, G. Soyez, D. N. Triantafyllopoulos, and Y. Zhu, Use of a running coupling in the NLO calculation of forward hadron production, *Phys. Rev. D* **97**, 054020 (2018).
- [41] C. Marquet, Forward inclusive dijet production and azimuthal correlations in pA collisions, *Nucl. Phys.* **A796**, 41 (2007).
- [42] T. Lappi and H. Mäntysaari, Forward dihadron correlations in deuteron-gold collisions with the Gaussian approximation of JIMWLK, *Nucl. Phys.* **A908**, 51 (2013).
- [43] F. Gelis, T. Lappi, and R. Venugopalan, High energy factorization and long range rapidity correlations in the glasma, *Phys. Rev. D* **79**, 094017 (2009).
- [44] T. Lappi, Initial conditions of heavy ion collisions and high energy factorization, *Acta Phys. Pol. B* **40**, 1997 (2009).
- [45] T. Lappi, Multigluon correlations in JIMWLK, *Nucl. Phys.* **A910-911**, 518 (2013).
- [46] B. Schenke and S. Schlichting, 3D glasma initial state for relativistic heavy ion collisions, *Phys. Rev. C* **94**, 044907 (2016).
- [47] K. Dusling, F. Gelis, T. Lappi, and R. Venugopalan, Long range two-particle rapidity correlations in A + A collisions from high energy QCD evolution, *Nucl. Phys.* **A836**, 159 (2010).
- [48] A. Kovner and M. Lublinsky, Angular correlations in gluon production at high energy, *Phys. Rev. D* **83**, 034017 (2011).
- [49] A. Kovner and M. Lublinsky, On angular correlations and high energy evolution, *Phys. Rev. D* **84**, 094011 (2011).
- [50] A. Dumitru, K. Dusling, F. Gelis, J. Jalilian-Marian, T. Lappi, and R. Venugopalan, The ridge in proton-proton collisions at the LHC, *Phys. Lett. B* **697**, 21 (2011).
- [51] K. Dusling and R. Venugopalan, Azimuthal Collimation of Long Range Rapidity Correlations by Strong Color Fields in High Multiplicity Hadron-Hadron Collisions, *Phys. Rev. Lett.* **108**, 262001 (2012).
- [52] K. Dusling and R. Venugopalan, Evidence for BFKL and saturation dynamics from dihadron spectra at the LHC, *Phys. Rev. D* **87**, 051502 (2013).
- [53] K. Dusling and R. Venugopalan, Explanation of systematics of CMS p + Pb high multiplicity di-hadron data at $\sqrt{s_{NN}} = 5.02$ TeV, *Phys. Rev. D* **87**, 054014 (2013).
- [54] B. Ducloué, L. Szymanowski, and S. Wallon, Confronting Mueller-Navelet jets in NLL BFKL with LHC experiments at 7 TeV, *J. High Energy Phys.* **05** (2013) 096.

- [55] F. Gelis, T. Lappi, and R. Venugopalan, High energy factorization in nucleus-nucleus collisions II—multigluon correlations, *Phys. Rev. D* **78**, 054020 (2008).
- [56] T. Lappi, B. Schenke, S. Schlichting, and R. Venugopalan, Tracing the origin of azimuthal gluon correlations in the color glass condensate, *J. High Energy Phys.* **01** (2016) 061.
- [57] K. Dusling, M. Mace, and R. Venugopalan, Multiparticle Collectivity from Initial State Correlations in High Energy Proton-Nucleus Collisions, *Phys. Rev. Lett.* **120**, 042002 (2018).
- [58] M. Mace, V. V. Skokov, P. Tribedy, and R. Venugopalan, Systematics of azimuthal anisotropy harmonics in proton-nucleus collisions at the LHC from the Color Glass Condensate, *Phys. Lett. B* **788**, 161 (2019).
- [59] Y. V. Kovchegov and D. E. Wertepny, Long-range rapidity correlations in heavy-light ion collisions, *Nucl. Phys.* **A906**, 50 (2013).
- [60] E. Iancu and D. Triantafyllopoulos, JIMWLK evolution for multi-particle production in Langevin form, *J. High Energy Phys.* **11** (2013) 067.
- [61] A. Kovner, M. Lublinsky, and H. Weigert, Treading on the cut: Semi inclusive observables at high energy, *Phys. Rev. D* **74**, 114023 (2006).
- [62] A. Kovner and M. Lublinsky, One gluon, two gluon: Multigluon production via high energy evolution, *J. High Energy Phys.* **11** (2006) 083.
- [63] J. Jalilian-Marian and Y. V. Kovchegov, Inclusive two-gluon and valence quark-gluon production in DIS and pA, *Phys. Rev. D* **70**, 114017 (2004).
- [64] C. Marquet and H. Weigert, New observables to test the color glass condensate beyond the large- N_c limit, *Nucl. Phys.* **A843**, 68 (2010).
- [65] T. Lappi, A. Ramnath, K. Rummukainen, and H. Weigert, JIMWLK evolution of the odderon, *Phys. Rev. D* **94**, 054014 (2016).
- [66] L. D. McLerran and R. Venugopalan, Computing quark and gluon distribution functions for very large nuclei, *Phys. Rev. D* **49**, 2233 (1994).
- [67] L. D. McLerran and R. Venugopalan, Gluon distribution functions for very large nuclei at small transverse momentum, *Phys. Rev. D* **49**, 3352 (1994).
- [68] L. D. McLerran and R. Venugopalan, Green's functions in the color field of a large nucleus, *Phys. Rev. D* **50**, 2225 (1994).
- [69] I. Balitsky, Operator expansion for high-energy scattering, *Nucl. Phys.* **B463**, 99 (1996).
- [70] E. Iancu and J. Laidet, Gluon splitting in a shockwave, *Nucl. Phys.* **A916**, 48 (2013).
- [71] S. Caron-Huot, When does the gluon reggeize, *J. High Energy Phys.* **05** (2015) 093.
- [72] I. I. Balitsky and A. V. Belitsky, Nonlinear evolution in high density QCD, *Nucl. Phys.* **B629**, 290 (2002).
- [73] M. Hentschinski, Color glass condensate formalism, Balitsky-JIMWLK evolution, and Lipatov's high energy effective action, *Phys. Rev. D* **97**, 114027 (2018).
- [74] J. R. Forshaw and D. A. Ross, Quantum chromodynamics and the pomeron, *Cambridge Lect. Notes Phys.* **9**, 1 (1997).
- [75] A. H. Mueller, Soft gluons in the infinite momentum wave function and the BFKL pomeron, *Nucl. Phys.* **B415**, 373 (1994).
- [76] A. H. Mueller and B. Patel, Single and double BFKL pomeron exchange and a dipole picture of high-energy hard processes, *Nucl. Phys.* **B425**, 471 (1994).
- [77] A. Leonidov and D. Ostrovsky, Angular and momentum asymmetry in particle production at high-energies, *Phys. Rev. D* **62**, 094009 (2000).



III

NEXT-TO-LEADING ORDER BALITSKY-KOVCHegov EQUATION BEYOND LARGE NC


by

Lappi, T., Mäntysaari, H., & Ramnath, A. 2020

Physical Review D, 102(7), Article 074027

<https://doi.org/10.1103/physrevd.102.074027>

Reproduced with kind permission by American Physical Society.

Next-to-leading order Balitsky-Kovchegov equation beyond large N_c T. Lappi¹, H. Mäntysaari², and A. Ramnath¹*Department of Physics, University of Jyväskylä, P.O. Box 35, 40014 University of Jyväskylä, Finland and Helsinki Institute of Physics, P.O. Box 64, 00014 University of Helsinki, Finland* (Received 12 July 2020; accepted 2 October 2020; published 29 October 2020)

We calculate finite- N_c corrections to the next-to-leading order (NLO) Balitsky-Kovchegov (BK) equation. We find analytical expressions for the necessary correlators of six Wilson lines in terms of the two-point function using the Gaussian approximation. In a suitable basis, the problem reduces from the diagonalization of a six-by-six matrix to the diagonalization of a three-by-three matrix, which can easily be done analytically. We study numerically the effects of these finite- N_c corrections on the NLO BK equation. In general, we find that the finite- N_c corrections are smaller than the expected $1/N_c^2 \sim 10\%$. The corrections may be large for individual correlators, but have less of an influence on the shape of the amplitude as a function of the dipole size. They have an even smaller effect on the evolution speed as a function of rapidity.

DOI: [10.1103/PhysRevD.102.074027](https://doi.org/10.1103/PhysRevD.102.074027)

I. INTRODUCTION

In hadronic collisions at high energies, large gluon densities are created by the emission of soft gluons carrying a small fraction of the longitudinal momentum of the parent [1]. Nonlinear dynamics of gluons becomes important in such an environment, where parton densities eventually grow to become on the order of the inverse of the QCD coupling α_s . To describe QCD in this region, the color glass condensate (CGC) effective field theory [2] has been developed.

In the CGC framework, cross sections for various scattering processes can be expressed in terms of correlators of Wilson lines. A Wilson line describes the eikonal propagation of a parton in the strong color field of the target. The energy dependence of the target color fields, and thus cross sections, is obtained by solving the so-called Jalilian-Marian–Iancu–McLerran–Weigert–Leonidov–Kovner (JIMWLK) equation [3–6]. This is a perturbative evolution equation that describes the Bjorken- x dependence of a Wilson line. In phenomenological applications, it is usually convenient to work directly in terms of the Wilson line correlators, and to solve instead the Balitsky-Kovchegov (BK) equation [7,8] for the dipole operator (correlator of two Wilson lines), which can be obtained from the JIMWLK equation in the large- N_c limit.

The CGC framework has been used extensively in phenomenological applications at leading order (LO) in

α_s , with the evolution equations resumming contributions $\sim \alpha_s \ln 1/x$ to all orders. Running coupling effects derived in Refs. [9–12] (see also [13]) can also be taken into account. The nonperturbative initial condition for the small- x evolution is obtained by performing fits to the HERA structure function data [1,14], for example in Refs. [15–18] (see also [19,20]). The obtained initial condition can then be used for various calculations, for example particle production in proton-nucleus collisions [17,21–27]. In the future, the nuclear deep inelastic scattering (DIS) experiments at the Electron Ion Collider (EIC) [28,29] in the US, at the LHeC [30] at CERN and at the EicC in China [31] will provide a vast amount of precise data from clean DIS processes. These experiments will be able to probe the nuclear structure where nonlinearities are enhanced by roughly $A^{1/3}$ higher densities compared to the proton. Before the EIC, similar studies limited to the photoproduction region can be performed in ultra-peripheral heavy-ion collisions [32,33].

In order to quantitatively study nonlinear dynamics in high-energy scattering processes (and especially at the future EIC), it is crucial to move beyond LO accuracy. The next-to-leading order (NLO) evolution equations are available: the NLO BK equation was derived in Ref. [34] and the NLO JIMWLK equation was derived in Refs. [35,36]. Similarly, the impact factors are becoming available at NLO for some processes: inclusive DIS [37–41] (in the case of massless quarks), exclusive vector meson production [42,43] (see also [44]) and particle production in proton-nucleus collisions [45]. However, the phenomenological applications of these are still developing [46–51].

The BK equation is usually solved in the large- N_c limit. In the LO case, the large- N_c limit makes it possible to

Published by the American Physical Society under the terms of the Creative Commons Attribution 4.0 International license. Further distribution of this work must maintain attribution to the author(s) and the published article's title, journal citation, and DOI. Funded by SCOAP³.

express the four-point correlator of fundamental representation Wilson lines in terms of the two-point function. In detailed numerical studies, it has been shown that the finite- N_c corrections are smaller than the naive expectation of $\mathcal{O}(1/N_c^2)$ [52,53]. At NLO, the equation involves six-point functions of fundamental Wilson lines that must similarly be expressed in terms of the two-point function in order to close the equation. The purpose of this work is to see if the finite- N_c corrections are similarly small in the case of the NLO equation, where all corrections of the order α_s^2 are taken into account.

In order to numerically solve the BK equation at finite N_c , we use the Gaussian approximation [54–56] to derive analytical parametric equations for the six-point correlators in terms of the two-point correlators. We study numerically the finite- N_c corrections to these correlators, and also their effect on the NLO BK evolution. In addition to the BK equation, higher-point correlators are needed in the calculations of multi-particle correlations in the CGC framework, see eg. Refs. [57–60].

The structure of the paper is as follows. In Sec. II, we introduce the NLO BK equation and provide both the

large- N_c and finite- N_c expressions for the correlators that will be studied. In Sec. III, we introduce the Gaussian approximation, explain the diagrammatic notation used in the rest of the paper and then explain the analytical calculation done for finding the parametric equations for the six-point correlators. Section IV contains the numerical results obtained from using the analytical expressions for the six-point correlators to solve the BK equation. Finally, we end with a few concluding remarks and a summary of our main results.

II. THE BK EQUATION AT NLO

For any product of $n/2$ pairs of fundamental Wilson lines UU^\dagger , we use the notation

$$S_{x_1, x_2, \dots, x_{n-1}, x_n}^{(n)} := \frac{1}{N_c} \text{tr}(U_{x_1} U_{x_2}^\dagger \dots U_{x_{n-1}} U_{x_n}^\dagger). \quad (1)$$

The NLO BK equation in the case of zero active quark flavors ($n_f = 0$) reads [34]

$$\partial_Y \langle S_{xy}^{(2)} \rangle = \frac{\alpha_s N_c}{2\pi^2} K_1^{\text{BC}} \otimes \langle D_1 \rangle + \frac{\alpha_s^2 N_c^2}{16\pi^4} K_{2,1} \otimes \langle D_{2,1} \rangle + \frac{\alpha_s^2 N_c^2}{16\pi^4} K_{2,2} \otimes \langle D_{2,2} \rangle + \mathcal{O}(n_f), \quad (2)$$

where the brackets $\langle \rangle$ refer to the expectation value over target color field configurations. The kernels are

$$K_1^{\text{BC}} = \frac{r^2}{X^2 Y^2} \left[1 + \frac{\alpha_s N_c}{4\pi} \left(\frac{\beta}{N_c} \ln r^2 \mu^2 - \frac{\beta}{N_c} \frac{X^2 - Y^2}{r^2} \ln \frac{X^2}{Y^2} + \frac{67}{9} - \frac{\pi^2}{3} - \frac{10}{9} \frac{n_f}{N_c} - 2 \ln \frac{X^2}{r^2} \ln \frac{Y^2}{r^2} \right) \right], \quad (3)$$

$$K_{2,1} = -\frac{4}{Z^4} + \left\{ 2 \frac{X^2 Y'^2 + X'^2 Y^2 - 4r^2 Z^2}{Z^4 (X^2 Y'^2 - X'^2 Y^2)} + \frac{r^4}{X^2 Y'^2 - X'^2 Y^2} \left[\frac{1}{X^2 Y'^2} + \frac{1}{Y^2 X'^2} \right] + \frac{r^2}{Z^2} \left[\frac{1}{X^2 Y'^2} - \frac{1}{X'^2 Y^2} \right] \right\} \times \ln \frac{X^2 Y'^2}{X'^2 Y^2}, \quad (4)$$

$$K_{2,2} = \left\{ \frac{r^2}{Z^2} \left[\frac{1}{X^2 Y'^2} + \frac{1}{Y^2 X'^2} \right] - \frac{r^4}{X^2 Y'^2 X'^2 Y^2} \right\} \ln \frac{X^2 Y'^2}{X'^2 Y^2}. \quad (5)$$

The convolutions \otimes in Eq. (2) denote integrations over the transverse coordinate z (in K_1^{BC}) or z and z' (in $K_{2,1}$ and $K_{2,2}$). We use the notation $r^2 = (\mathbf{x} - \mathbf{y})^2$, $X^2 = (\mathbf{x} - \mathbf{z})^2$, $X'^2 = (\mathbf{x} - \mathbf{z}')^2$, $Y^2 = (\mathbf{y} - \mathbf{z})^2$, $Y'^2 = (\mathbf{y} - \mathbf{z}')^2$ and $Z^2 = (\mathbf{z} - \mathbf{z}')^2$. We note that the kernel proportional to n_f is also available [34]. Since the purpose of this work is to study the importance of the finite- N_c corrections in the NLO BK equation, we do not include contributions proportional to n_f . The finite- N_c effects could be expected to be similar to the $n_f = 0$ case.

The Wilson line operators appearing in Eq. (2) are

$$\langle D_1 \rangle = \langle S_{xz}^{(2)} S_{zy}^{(2)} \rangle - \langle S_{xy}^{(2)} \rangle, \quad (6)$$

$$\langle D_{2,1} \rangle = \langle S_{xz}^{(2)} S_{z'z'}^{(2)} S_{z'y}^{(2)} \rangle - \frac{1}{N_c^2} \langle S_{x.z.z'.y.z.z'}^{(6)} \rangle - (z' \rightarrow z), \quad (7)$$

$$\langle D_{2,2} \rangle = \langle S_{xz}^{(2)} S_{z'z'}^{(2)} S_{z'y}^{(2)} \rangle - (z' \rightarrow z). \quad (8)$$

Although the original NLO BK equation in the form presented in Ref. [34] does not contain the subtraction $z' \rightarrow z$ in $D_{2,2}$, we have introduced the subtraction to improve numerical stability. This subtraction term has no effect on the final evolution because the integral of $K_{2,2}$ over z' vanishes if the Wilson line operator term does not

depend on z' (see Ref. [34]). We will refer throughout this work to two pieces of the right side of Eq. (2) as the

- (i) $\frac{\alpha_s N_c}{2\pi^2} K_1^{\text{BC}} \otimes \langle D_1 \rangle \sim$ “LO-like” contribution,
- (ii) $\frac{\alpha_s^2 N_c^2}{16\pi^4} K_{2,1} \otimes \langle D_{2,1} \rangle + \frac{\alpha_s^2 N_c^2}{16\pi^4} K_{2,2} \otimes \langle D_{2,2} \rangle \sim$ “NLO-like” contribution.

In other words, we separate the terms in the NLO BK equation by the types of Wilson line correlators, not by the order in α_s . Thus, the LO-like contribution also includes a significant α_s^2 correction.

The interpretation of the NLO BK equation is that one considers all possible ways to emit either one or two gluons, at transverse coordinates z and z' , from the boosted dipole consisting of quarks at transverse coordinates x and y . The effect of the boost is that instead of the original dipole projectile, the original quarks and the emitted gluons scatter off the target color field. As such, the evolution can be seen to describe the evolution of the projectile probing the target structure. On the other hand, the emitted gluons can also be taken to be a part of the target wave function, in which case the boost corresponds to the evolving target color field as probed by the original projectile. For a more detailed discussion on the NLO evolution in the projectile or target wave function, the reader is referred to Ref. [61].

The NLO BK equation is known to be unstable [62] due to the large contributions enhanced by the large double transverse logarithm $\ln X^2/r^2 \ln Y^2/r^2$. We resum these contributions to all orders following the procedure developed in Ref. [63], which was numerically confirmed in Ref. [64] to result in a stable evolution (see also Ref. [65] for an equivalent resummation of the same double logarithms). In addition, we include the running of the QCD coupling by noticing that the terms proportional to the beta function coefficient β in Eq. (3) should be resummed into the running coupling. We implement this resummation by following the Balitsky prescription from Ref. [12]. Both running coupling and double transverse logarithm resummations are included by modifying the kernel K_1^{BC} as

$$\frac{\alpha_s N_c}{2\pi^2} K_1^{\text{BC}} \rightarrow \frac{\alpha_s(r) N_c}{2\pi^2} K_{\text{DLA}} \left[\frac{r^2}{X^2 Y^2} + \frac{1}{X^2} \left(\frac{\alpha_s(X)}{\alpha_s(Y)} - 1 \right) + \frac{1}{Y^2} \left(\frac{\alpha_s(Y)}{\alpha_s(X)} - 1 \right) \right] + K_1^{\text{fin}}. \quad (9)$$

The double log corrections to all orders are taken into account by the factor

$$K_{\text{DLA}} = \frac{J_1(2\sqrt{\bar{\alpha}_s x^2})}{\sqrt{\bar{\alpha}_s x^2}}, \quad (10)$$

where $\bar{\alpha}_s = \alpha_s N_c / \pi$. The double logarithm here is $x = \sqrt{\ln X^2/r^2 \ln Y^2/r^2}$. If $\ln X^2/r^2 \ln Y^2/r^2 < 0$, then an absolute value is used and the Bessel function is changed

from $J_1 \rightarrow I_1$ (see Ref. [63]). The scale of the coupling in K_{DLA} is determined by the smallest dipole $\min\{r^2, X^2, Y^2\}$.

In addition to the double log contributions, one can also resum a set of higher-order contributions enhanced by single transverse logarithms, as shown in Ref. [66]. For the purposes of this paper, this resummation is not necessary and is excluded for simplicity. In this running coupling prescription, we keep the order α_s^2 terms in the kernel K_1^{BC} that are not proportional to the beta function. These are included in the term K_1^{fin} , which reads

$$K_1^{\text{fin}} = \frac{\alpha_s^2(r) N_c^2}{8\pi^3} \frac{r^2}{X^2 Y^2} \left(\frac{67}{9} - \frac{\pi^2}{3} - \frac{10}{9} \frac{n_f}{N_c} \right). \quad (11)$$

The strong coupling constant in the transverse coordinate space is evaluated as

$$\alpha_s(r) = \frac{4\pi}{\beta \ln \left\{ \left[\left(\frac{\mu_0^2}{\Lambda_{\text{QCD}}^2} \right)^c + \left(\frac{4C^2}{r^2 \Lambda_{\text{QCD}}^2} \right)^c \right]^{1/c} \right\}}, \quad (12)$$

where $\beta = (11N_c - 2n_f)/N_c$. We take n_f to be zero in both K_1^{fin} and β . We use $C^2 = 1$ and $\mu_0/\Lambda_{\text{QCD}} = 2.5$ in our numerical calculations, which freezes the coupling at $\alpha_s(r \rightarrow \infty) = 0.762$ in the infrared, and $c = 0.2$ which controls the transition to the infrared region.

The initial condition for the BK equation is taken from the McLerran-Venugopalan (MV) model [67,68]. In the MV model, the color charge density is assumed to be a random Gaussian variable, with a zero expectation value and a variance proportional to the local saturation scale Q_s^2 . The dipole correlator in the MV model is written as

$$\langle S_{x,y}^{(2)} \rangle_{\text{MV}} = \exp \left[-\frac{r^2 Q_{s0}^2}{4} \ln \left(\frac{1}{r \Lambda_{\text{QCD}}} + e \right) \right]. \quad (13)$$

Here, the constant e acts as an infrared regulator. We use $\Lambda_{\text{QCD}} = 0.241 \text{ GeV}$ and $Q_{s0}^2 = 1 \text{ GeV}^2$ in the numerical analysis. In analytical studies of the correlators of Wilson lines in specific “line” coordinate configurations in Sec. IV A, we use the GBW [69] form for the dipole correlator

$$\langle S_{x,y}^{(2)} \rangle_{\text{GBW}} = \exp \left(-\frac{r^2 Q_{s0}^2}{4} \right). \quad (14)$$

In principle, the resummation procedure for the double transverse logs would also change the initial condition, as discussed in Refs. [63,64]. However, since the initial condition is a nonperturbative input for the evolution, we consider Eq. (13) to be the nonperturbative initial condition for the resummed evolution as well. For the

¹A generic estimate [9,13] would be $C^2 = e^{-2\gamma_E} \approx 0.32$. We use a larger value $C^2 = 1$ which results in slightly slower evolution, as the C^2 is usually taken to be a free parameter controlling the coordinate space scale.

the steps for the dipole operator $\langle S_{x,y}^{(2)} \rangle$. A more practical form of Eq. (21) is to write the integral over the parametrization rapidity η in differential form. Then, we have

$$\partial_\eta \langle S_{x,y}^{(2)} \rangle = -\mathcal{M}(\eta) \langle S_{x,y}^{(2)} \rangle, \quad (25)$$

where \mathcal{M} is the so-called transition matrix formed by operating with the argument of the exponential in Eq. (21) on the operator of interest. In this case, there are four contributions from acting with the Lie derivatives on a product of two Wilson lines:

$$L_{u_1}^a L_{u_2}^a (U_x \otimes U_y^\dagger) = L_{u_1}^a L_{u_2}^a \begin{array}{c} \text{---} \\ \text{---} \end{array} \begin{array}{c} \text{---} \\ \text{---} \end{array} \quad (26)$$

$$\begin{aligned} & \sim \begin{array}{c} \text{---} \\ \text{---} \end{array} \begin{array}{c} \text{---} \\ \text{---} \end{array} + \begin{array}{c} \text{---} \\ \text{---} \end{array} \begin{array}{c} \text{---} \\ \text{---} \end{array} \\ & + \begin{array}{c} \text{---} \\ \text{---} \end{array} \begin{array}{c} \text{---} \\ \text{---} \end{array} + \begin{array}{c} \text{---} \\ \text{---} \end{array} \begin{array}{c} \text{---} \\ \text{---} \end{array}. \end{aligned} \quad (27)$$

From this sum, we need to factorize out the original operator $U_x \otimes U_y^\dagger$, so we use the Fierz identity

$$2 \begin{array}{c} \text{---} \\ \text{---} \end{array} = \begin{array}{c} \text{---} \\ \text{---} \end{array} \begin{array}{c} \text{---} \\ \text{---} \end{array} - \frac{1}{N_c} \begin{array}{c} \text{---} \\ \text{---} \end{array}. \quad (28)$$

There is only one way to join the endpoints of the Wilson lines into a singlet operator. This is to trace over them, i.e., wedging them between $\frac{1}{\sqrt{N_c}}$ $\begin{array}{c} \text{---} \\ \text{---} \end{array}$ and $\frac{1}{\sqrt{N_c}}$ $\begin{array}{c} \text{---} \\ \text{---} \end{array}$. Doing so and performing the remaining operations in the exponent of Eq. (21), we get

$$\begin{aligned} \partial_\eta \langle S_{x,y}^{(2)} \rangle &= -C_F \mathcal{G}'_{x,y} \langle S_{x,y}^{(2)} \rangle \\ \Rightarrow \frac{1}{N_c} \begin{array}{c} \text{---} \\ \text{---} \end{array} &= \langle S_{x,y}^{(2)} \rangle = e^{-C_F \mathcal{G}_{x,y}}, \end{aligned} \quad (29)$$

where $C_F = \frac{N_c^2 - 1}{2N_c}$. Since the operators $\begin{array}{c} \text{---} \\ \text{---} \end{array}$ and $\begin{array}{c} \text{---} \\ \text{---} \end{array}$ were normalized, the initial condition at $\eta = 0$ for the differential equation (25) is given by trivial Wilson lines equal to the identity matrix in the absence of a color field. This is the well-known parametric equation for the dipole correlator [55] in the Gaussian approximation.

In the case of n -point correlators larger than the dipole, the operator $\langle \mathcal{O}[U] \rangle$ in Eq. (21) is actually an $n \times n$ matrix of correlators, denoted $\mathcal{A}(\eta)$, and Eq. (25) becomes an $n \times n$ matrix differential equation

$$\partial_\eta \mathcal{A}(\eta) = -\mathcal{M}(\eta) \mathcal{A}(\eta). \quad (30)$$

By construction, \mathcal{M} is a symmetric matrix, so there are at most $\sum_{i=1}^n i = n(n+1)/2$ distinct elements, not $n \times n$.

For example, a product of six Wilson lines is represented in this notation as

$$U_z \otimes U_{z'}^\dagger \otimes U_v \otimes U_y^\dagger \otimes U_x \otimes U_w^\dagger = \begin{array}{c} \text{---} \\ \text{---} \\ \text{---} \\ \text{---} \\ \text{---} \\ \text{---} \end{array} \begin{array}{c} \text{---} \\ \text{---} \\ \text{---} \\ \text{---} \\ \text{---} \\ \text{---} \end{array} \quad (31)$$

(the haphazard assignment of coordinate labels is convenient for the NLO BK equation and will become clear when constructing the transition matrix). The notation here means that this product is actually a matrix with six open indices on the left and another six on the right; we denote them as

$$\begin{array}{c} j_1 \\ k_1 \\ j_2 \\ k_2 \\ j_3 \\ k_3 \end{array} \begin{array}{c} \text{---} \\ \text{---} \\ \text{---} \\ \text{---} \\ \text{---} \\ \text{---} \end{array} \begin{array}{c} i_1 \\ l_1 \\ i_2 \\ l_2 \\ i_3 \\ l_3 \end{array}$$

Since only singlet states are gauge-invariant, the only operators of interest here are singlets. There are six possible ways to join the endpoints of these Wilson lines to form a singlet. Equation (30) is therefore a six-by-six matrix differential equation, as opposed to the much simpler one-dimensional problem illustrated for the dipole correlator.

In analogy to the procedure for the dipole operator, the procedure to use Eq. (30) to find parametric equations for the six-point correlators is as follows:

- (1) Choose a multiplet basis, represented as a column vector \mathbf{B} , of $n = 6$ color structures for the space of all six-point correlators. Each element will have six open color indices, which can contract with the open indices on the left of $U_z \otimes U_{z'}^\dagger \otimes U_v \otimes U_y^\dagger \otimes U_x \otimes U_w^\dagger$. For example, one choice for an element of \mathbf{B} could be

$$\frac{1}{\sqrt{N_c^3}} \begin{array}{c} \text{---} \\ \text{---} \\ \text{---} \\ \text{---} \\ \text{---} \\ \text{---} \end{array} = \frac{1}{\sqrt{N_c^3}} \delta_{j_1, k_1} \delta_{j_2, k_2} \delta_{j_3, k_3} \quad (32)$$

and the corresponding element for the other end of the Wilson line is then

$$\frac{1}{\sqrt{N_c^3}} \begin{matrix} i_1 \\ l_1 \\ i_2 \\ l_2 \\ i_3 \\ l_3 \end{matrix} \begin{matrix} \curvearrowright \\ \curvearrowright \\ \curvearrowright \\ \curvearrowright \\ \curvearrowright \\ \curvearrowright \end{matrix} = \frac{1}{\sqrt{N_c^3}} \delta_{i_1, l_1} \delta_{i_2, l_2} \delta_{i_3, l_3}. \quad (33)$$

The prefactor is a normalization constant found by squaring the basis element.

- (2) Construct the correlator matrix \mathcal{A} by taking $\mathbf{B}(U_z \otimes U_{z'}^\dagger \otimes U_y \otimes U_y^\dagger \otimes U_x \otimes U_w^\dagger)\mathbf{B}^T$. The elements of \mathbf{B} on the left are contracted with the open color indices on the left of the Wilson lines, and the elements of \mathbf{B}^T with the open indices on the right. For example, using the basis element shown above, we have for one of the 36 elements in \mathcal{A} ,

$$\frac{1}{N_c^3} \begin{matrix} j_1 \\ k_1 \\ j_2 \\ k_2 \\ j_3 \\ k_3 \end{matrix} \begin{matrix} \curvearrowright \\ \curvearrowright \\ \curvearrowright \\ \curvearrowright \\ \curvearrowright \\ \curvearrowright \end{matrix} \begin{matrix} i_1 \\ l_1 \\ i_2 \\ l_2 \\ i_3 \\ l_3 \end{matrix} \begin{matrix} \curvearrowright \\ \curvearrowright \\ \curvearrowright \\ \curvearrowright \\ \curvearrowright \\ \curvearrowright \end{matrix} \\ = \frac{1}{N_c^3} \text{tr} \left(U_z U_{z'}^\dagger \right) \text{tr} \left(U_v U_y^\dagger \right) \text{tr} \left(U_x U_w^\dagger \right). \quad (34)$$

- (3) Construct the transition matrix \mathcal{M} by summing (for each element in \mathcal{A}) all possible one-gluon diagrams obtained with the double Lie derivative operator and rewriting the result in terms of elements of \mathcal{A} .
 (4) Solve Eq. (30) by exponentiating \mathcal{M} to find expressions for each element in \mathcal{A} , using as an initial condition the correlator matrix \mathcal{A} corresponding to Wilson lines equal to the identity matrix.

B. Choosing a basis

Starting from a product of six Wilson lines, there are six ways to form multiplets by joining endpoints in all possible ways:

$$\begin{matrix} \curvearrowright & \curvearrowright & \curvearrowright & \curvearrowright & \curvearrowright & \curvearrowright \\ \curvearrowright & \curvearrowright & \curvearrowright & \curvearrowright & \curvearrowright & \curvearrowright \\ \curvearrowright & \curvearrowright & \curvearrowright & \curvearrowright & \curvearrowright & \curvearrowright \end{matrix} \quad (35)$$

The simplest way to construct an orthonormal basis from these would be to use color algebra to choose

$$\mathbf{B} := \begin{pmatrix} \curvearrowright \\ \frac{1}{\sqrt{N_c^3}} \curvearrowright \\ \sqrt{\frac{4}{N_c d_A}} \curvearrowright \\ \sqrt{\frac{4}{N_c d_A}} \curvearrowright \\ \sqrt{\frac{4}{N_c d_A}} \curvearrowright \\ \frac{1}{i} \sqrt{\frac{8}{N_c d_A}} \curvearrowright \\ \sqrt{\frac{8}{C_d d_A}} \curvearrowright \end{pmatrix}. \quad (36)$$

The blue lines denote gluons and the last two elements of \mathbf{B} represent the antisymmetric and symmetric structure constants, respectively, $f_{abc} = -2i\text{tr}([t_a, t_b], t_c)$ and $d_{abc} = 2\text{tr}(\{t_a, t_b\}, t_c)$. The color factors are $d_A = N_c^2 - 1$ and $C_d = \frac{N_c^2 - 4}{N_c}$. The next step would be to use this basis to construct the correlator matrix \mathcal{A} and the transition matrix \mathcal{M} . However, doing so results in a matrix differential equation $\partial_\eta \mathcal{A}(\eta) = -\mathcal{M}(\eta)\mathcal{A}(\eta)$, whose complicated solution is the matrix exponential of a six-by-six matrix \mathcal{M} .

For our case, a better way to proceed is to exploit the structure of the six-point correlators that are actually needed for the NLO BK equation. Since there are only four distinct coordinates in these particular correlators, we make the coordinate assignments

$$\begin{matrix} z \\ z' \\ v \\ y \\ x \\ w \end{matrix} \xrightarrow[\substack{w \rightarrow z \\ v \rightarrow z'}]{} \begin{matrix} z \\ z' \\ z' \\ y \\ x \\ z \end{matrix}. \quad (37)$$

It is easy to see from this that there is one way to join the endpoints such that in the limit $v \rightarrow z', w \rightarrow z$, four Wilson lines cancel (due to unitarity). The result simplifies to a single trace:

$$\frac{1}{\sqrt{N_c^3}} \left(\begin{array}{c} \text{---} \\ \text{---} \\ \text{---} \\ \text{---} \\ \text{---} \\ \text{---} \end{array} \right) \frac{1}{\sqrt{N_c^3}} \xrightarrow[v \rightarrow z']{w \rightarrow z} \frac{1}{N_c^3} N_c^2 \text{tr}(U_x U_y^\dagger). \quad (38)$$

So choosing $\frac{1}{\sqrt{N_c^3}} \left(\begin{array}{c} \text{---} \\ \text{---} \\ \text{---} \end{array} \right)$ as one of our basis elements allows

one dimension of our six-dimensional space of operators to decouple, giving the equation for the dipole correlator. Similarly, the choice of two more particular basis elements results in two correlators that reduce to four-point functions; one due to the limit $v \rightarrow z'$ and the other due to the limit $w \rightarrow z$. Thus, we can expect to choose a further two basis elements such that two more dimensions decouple from the remaining five, corresponding to the equation for the

four-point operators. These two basis elements can be chosen as

$$\frac{1}{\sqrt{2N_c d_A}} \left[- \left(\begin{array}{c} \text{---} \\ \text{---} \\ \text{---} \end{array} \right) + \left(\begin{array}{c} \text{---} \\ \text{---} \\ \text{---} \\ \text{---} \end{array} \right) \right]$$

and

$$\frac{1}{\sqrt{2N_c d_A}} \left[- \left(\begin{array}{c} \text{---} \\ \text{---} \\ \text{---} \end{array} \right) - \left(\begin{array}{c} \text{---} \\ \text{---} \\ \text{---} \\ \text{---} \end{array} \right) + \frac{2}{N_c} \left(\begin{array}{c} \text{---} \\ \text{---} \\ \text{---} \end{array} \right) \right].$$

We will choose the remaining three basis elements such that they are orthonormal to the three already chosen, resulting in the final basis vector

$$\tilde{\mathbf{B}} := \left(\begin{array}{c} \frac{\sqrt{2}}{N_c \sqrt{d_A} C_d} \left[\begin{array}{c} \text{---} \\ \text{---} \\ \text{---} \\ \text{---} \\ \text{---} \\ \text{---} \end{array} \right] \\ \frac{1}{\sqrt{2N_c d_A}} \left[\begin{array}{c} \text{---} \\ \text{---} \\ \text{---} \\ \text{---} \end{array} \right] \\ \frac{1}{\sqrt{N_c d_A}} \left[\begin{array}{c} \text{---} \\ \text{---} \\ \text{---} \\ \text{---} \end{array} \right] \\ \frac{1}{\sqrt{2N_c d_A}} \left[\begin{array}{c} \text{---} \\ \text{---} \\ \text{---} \\ \text{---} \end{array} \right] \\ \frac{1}{\sqrt{2N_c d_A}} \left[\begin{array}{c} \text{---} \\ \text{---} \\ \text{---} \\ \text{---} \end{array} \right] \\ \frac{1}{\sqrt{N_c^3}} \left(\begin{array}{c} \text{---} \\ \text{---} \\ \text{---} \end{array} \right) \end{array} \right). \quad (39)$$

Since this basis is orthonormal, the correlator matrix at the initial condition $\mathcal{A}(\eta = 0)$ will just be the identity matrix.

C. Constructing the correlator matrix and the transition matrix


Due to this choice of basis $\tilde{\mathbf{B}}$, the full matrix differential equation (30) now decouples into three independent equations. This allows us to forego exponentiating a six-by-six matrix; at most we will need to exponentiate a three-by-three matrix, which can be done analytically.

To form the correlator matrix \mathcal{A} , we take the product $\tilde{\mathbf{B}}(U_z \otimes U_z^\dagger \otimes U_v \otimes U_y^\dagger \otimes U_x \otimes U_w^\dagger) \tilde{\mathbf{B}}^T$ and set $w \rightarrow z$

and $v \rightarrow z'$. To form the transition matrix, we act with the argument of the exponential in Eq. (21) on the operator $U_z \otimes U_z^\dagger \otimes U_v \otimes U_y^\dagger \otimes U_x \otimes U_w^\dagger$, then wedge the result between the basis vectors and set $w \rightarrow z$ and $v \rightarrow z'$:

$$\tilde{\mathbf{B}} \left[-\frac{1}{2} \int^\eta d\eta' \int_{u_1, u_2} G_{u_1, u_2}(\eta') L_{u_1}^a L_{u_2}^a \right] \times (U_z \otimes U_z^\dagger \otimes U_v \otimes U_y^\dagger \otimes U_x \otimes U_w^\dagger) \tilde{\mathbf{B}}^T \Big|_{\substack{w \rightarrow z \\ v \rightarrow z'}} \quad (40)$$

Diagrammatically, this is equivalent to summing all possible ways of attaching one gluon line on the

operator , using the Fierz identity to replace the gluon

vertices, and finally closing the Wilson line endpoints on the left and right using the basis vector. For example, the element (6, 6) of the correlator matrix \mathcal{A} is

$$\begin{aligned} \mathcal{A}^{(6,6)}(\eta) &= \tilde{B}_6 \left(U_z \otimes U_{z'}^\dagger \otimes U_v \otimes U_y^\dagger \otimes U_x \otimes U_w^\dagger \right) \tilde{B}_6 \\ &= \frac{1}{N_c^3} \left(\text{Diagram} \right). \end{aligned} \quad (41)$$

We then sum all the diagrams in which a gluon is attached to this diagram so that it joins any two of the six Wilson lines on the right of the target interaction. Using the Fierz identity in Eq. (28), we may write the resulting expression in terms of diagrams with no gluons. After making the substitutions $w \rightarrow z$ and $v \rightarrow z'$, the result will be a linear combination of elements of the operator matrix $\mathcal{A}(\eta)$. From this linear combination, one can read off the elements of column 6 of the transition matrix \mathcal{M} . The explicit expressions for the elements of $\mathcal{A}(\eta)$ in terms of the Wilson line correlators are shown in Appendix.

Performing this procedure for each diagram in $\mathcal{A}(\eta)$, we get the full transition matrix

$$\mathcal{M}(\eta) \Big|_{\substack{w \rightarrow z \\ v \rightarrow z'}} = \begin{pmatrix} \mathcal{M}_3 & 0 & 0 \\ 0 & \mathcal{M}_2 & 0 \\ 0 & 0 & \mathcal{M}_1 \end{pmatrix}(\eta), \quad (42)$$

where the subscripts refer to the dimension of the submatrix.

The first (one-dimensional) transition submatrix is

$$\mathcal{M}_1(\eta) = C_F \mathcal{G}'_{x,y} \quad (43)$$

and upon exponentiation, gives the parametric equation for the dipole correlator as shown in Eq. (29). When inverted, this equation can be used to express the two-point function $\mathcal{G}_{x,y}$ in terms of the dipole correlator. This will be needed to evaluate the higher-point functions in terms of the dipole $\langle \mathcal{S}_{x,y}^{(2)} \rangle$.

The second (two-dimensional) transition submatrix is

$$\mathcal{M}_2(\eta) = \frac{N_c}{4} \begin{pmatrix} \mathcal{M}_2^{(1,1)} & \mathcal{M}_2^{(1,2)} \\ \mathcal{M}_2^{(1,2)} & \mathcal{M}_2^{(1,1)} \end{pmatrix}(\eta), \quad (44)$$

where

$$\mathcal{M}_2^{(1,1)}(\eta) := \mathcal{G}'_{x,z} + \mathcal{G}'_{y,z} - \frac{2}{N_c^2} \mathcal{G}'_{x,y} + \mathcal{G}'_{x,z'} + \mathcal{G}'_{y,z'}, \quad (45)$$

$$\mathcal{M}_2^{(1,2)}(\eta) := \mathcal{G}'_{x,z} + \mathcal{G}'_{y,z} - \mathcal{G}'_{x,z'} - \mathcal{G}'_{y,z'}. \quad (46)$$

The matrix differential equation

$$\partial_\eta \mathcal{A}_2(\eta) = -\mathcal{M}_2(\eta) \mathcal{A}_2(\eta) \quad (47)$$

then gives a coupled system of 2×2 differential equations, out of which 2 are linearly independent, corresponding to the fact that the same transition matrix operates separately on each of the two columns of \mathcal{A}_2 . The exponential solution for this system of equations gives the known parametrization for the four-point correlator with one repeated coordinate [55]

$$\langle \mathcal{S}_{x,z}^{(2)} \mathcal{S}_{z,y}^{(2)} \rangle = \frac{1}{N_c^2} e^{-C_F \mathcal{G}_{x,y}} + \frac{2C_F}{N_c} e^{-C_F \mathcal{G}_{x,y}} e^{-\frac{N_c}{2} (\mathcal{G}_{x,z} + \mathcal{G}_{y,z} - \mathcal{G}_{x,y})}. \quad (48)$$

The third and final (three-dimensional) transition submatrix is

$$\mathcal{M}_3(\eta) = \begin{pmatrix} \frac{N_c}{4} \Gamma'_1 & \frac{\sqrt{N_c C_4}}{4} \Gamma'_2 & 0 \\ \frac{\sqrt{N_c C_4}}{4} \Gamma'_2 & \frac{N_c}{4} \Gamma'_1 & -\frac{1}{\sqrt{2}} \Gamma'_2 \\ 0 & -\frac{1}{\sqrt{2}} \Gamma'_2 & \Gamma'_0 \end{pmatrix}, \quad (49)$$

where

$$\Gamma_0 := C_F \mathcal{G}_{x,y} + N_c \mathcal{G}_{z,z'}, \quad (50)$$

$$\Gamma_1 := \mathcal{G}_{x,z} + \mathcal{G}_{y,z} - \frac{2}{N_c^2} \mathcal{G}_{x,y} + \mathcal{G}_{x,z'} + \mathcal{G}_{y,z'} + 2\mathcal{G}_{z,z'}, \quad (51)$$

$$\Gamma_2 := \mathcal{G}_{x,z} - \mathcal{G}_{y,z} - \mathcal{G}_{x,z'} + \mathcal{G}_{y,z'} \quad (52)$$

and the primes on the Γ 's in Eq. (49) denote derivatives in η . Exponentiating this matrix is the last step required to get expressions for the remaining six-point correlators in \mathcal{A}_3 .

D. Exponentiating the transition matrix \mathcal{M}_3

In order to obtain the six-point functions, it is necessary to solve the differential equation

$$\partial_\eta \mathcal{A}_3(\eta) = -\mathcal{M}_3(\eta) \mathcal{A}_3(\eta). \quad (53)$$

Solving this equation is equivalent to exponentiating the matrix \mathcal{M}_3 , as shown above in the cases of the two- and four-point functions. To exponentiate \mathcal{M}_3 , we consider two different cases: $\Gamma'_2 = 0$ and $\Gamma'_2 \neq 0$. The reason for this will become clear shortly.

When $\Gamma'_2 = 0$, \mathcal{M}_3 in Eq. (49) becomes diagonal and we directly obtain

$$\mathcal{A}_3(\eta) = \begin{pmatrix} e^{-\frac{N_c}{4} \Gamma_1} & 0 & 0 \\ 0 & e^{-\frac{N_c}{4} \Gamma_1} & 0 \\ 0 & 0 & e^{-\Gamma_0} \end{pmatrix}. \quad (54)$$

When $\Gamma'_2 \neq 0$, the matrix elements of \mathcal{A}_3 are calculated by matrix-exponentiating the full \mathcal{M}_3 in Eq. (49), giving

$$\mathcal{A}_3(\eta) = \sum_{i=1}^3 e^{z_i/4} \begin{pmatrix} \frac{a_{11}(z_i)}{d(z_i)} & -\sqrt{C_d N_c} \Gamma_2 \frac{a_{12}(z_i)}{d(z_i)} & -2\sqrt{2C_d N_c} \Gamma_2^2 \frac{a_{13}(z_i)}{d(z_i)} \\ -\sqrt{C_d N_c} \Gamma_2 \frac{a_{12}(z_i)}{d(z_i)} & \frac{m_{22}(z_i)}{d(z_i)} & 2\sqrt{2}\Gamma_2 \frac{a_{23}(z_i)}{d(z_i)} \\ -2\sqrt{2C_d N_c} \Gamma_2^2 \frac{a_{13}(z_i)}{d(z_i)} & 2\sqrt{2}\Gamma_2 \frac{a_{23}(z_i)}{d(z_i)} & \frac{a_{33}(z_i)}{d(z_i)} \end{pmatrix}. \quad (55)$$

Here, z_i are the roots of the cubic polynomial

$$p(z) = z^3 + 2(2\Gamma_0 + N_c \Gamma_1)z^2 + [N_c \Gamma_1(8\Gamma_0 + N_c \Gamma_1) - (N_c^2 + 4)\Gamma_2^2]z + 4[N_c^2 \Gamma_0 \Gamma_1^2 - ((N_c^2 - 4)\Gamma_0 + 2N_c \Gamma_1)\Gamma_2^2]. \quad (56)$$

They are

$$z_1 = \frac{1}{3} \left(-2c_1 + c_3 + \frac{1}{c_3} [(c_1 - 6\Gamma_0)^2 + 3(N_c^2 + 4)\Gamma_2^2] \right), \quad (57)$$

$$z_2 = -\frac{1}{6} \left(16c_1 + c_3(1 - i\sqrt{3}) + \frac{1}{c_3} (1 + i\sqrt{3}) [(c_1 - 6\Gamma_0)^2 + 3(N_c^2 + 4)\Gamma_2^2] \right), \quad (58)$$

$$z_3 = -\frac{1}{6} \left(16c_1 + c_3(1 + i\sqrt{3}) + \frac{1}{c_3} (1 - i\sqrt{3}) [(c_1 - 6\Gamma_0)^2 + 3(N_c^2 + 4)\Gamma_2^2] \right), \quad (59)$$

where

$$c_1 = 2\Gamma_0 + N_c \Gamma_1, \quad (60)$$

$$c_2 = (2c_1 [c_1^2 - 9(N_c^2 - 8)\Gamma_2^2])^2 - 4[c_1^2 + 3(N_c^2 + 4)\Gamma_2^2]^3, \quad (61)$$

$$c_3 = \sqrt[3]{\frac{\sqrt{c_2}}{2} + c_1 [c_1^2 - 9(N_c^2 - 8)\Gamma_2^2]}. \quad (62)$$

The functions of the roots that appear in Eq. (55) are

$$a_{11}(z) = 4N_c \Gamma_0 \Gamma_1 - 8\Gamma_2^2 + (2\Gamma_0 + c_1)z + z^2, \quad (63)$$

$$a_{12}(z) = 4\Gamma_0 + z, \quad (64)$$

$$a_{13}(z) = 1, \quad (65)$$

$$a_{22}(z) = 4N_c \Gamma_0 \Gamma_1 + (2\Gamma_0 + c_1)z + z^2, \quad (66)$$

$$a_{23}(z) = N_c \Gamma_1 + z, \quad (67)$$

$$a_{33}(z) = N_c^2 \Gamma_1^2 - (N_c^2 - 4)\Gamma_2^2 + 2N_c \Gamma_1 z + z^2 \quad (68)$$

$$d(z) = 3z^2 + 4c_1 z + N_c \Gamma_1(8\Gamma_0 + N_c \Gamma_1) - (N_c^2 + 4)\Gamma_2^2. \quad (69)$$

Notice that c_3 may be complex. However, the final expressions for each element in \mathcal{A}_3 are in fact real, as correlators should be. Notice also that c_3 appears in the denominator in the roots. Since $c_3 = 0 \Leftrightarrow \Gamma_2 = 0$ and we have treated the $\Gamma_2 = 0$ case separately, we need not worry about dividing by zero where c_3 appears in the denominator in (57)–(59).

E. Extracting six-point correlators needed for NLO BK

Equation (55) gives the analytical expressions for the correlators formed using basis \tilde{B} , solely in terms of the parameter \mathcal{G} [which can be used to relate these expressions to the dipole via Eq. (29)]. For example,

$$\begin{aligned} \mathcal{A}_3^{(3,3)}(\eta) &= \sum_{i=1}^3 e^{z_i/4} \frac{a_{33}(z_i)}{d(z_i)} \\ &= \frac{1}{N_c d_A} \left\langle \left[-\left(\begin{array}{c} \curvearrowright \\ \curvearrowright \end{array} \right) + \frac{1}{N_c} \left(\begin{array}{c} \curvearrowright \\ \curvearrowright \\ \curvearrowright \end{array} \right) \right] \left[\begin{array}{c} \curvearrowright \\ \curvearrowright \\ \curvearrowright \\ \curvearrowright \end{array} \right] \right\rangle \\ &\quad \times \left[\begin{array}{c} \curvearrowright \\ \curvearrowright \\ \curvearrowright \end{array} \right] + \frac{1}{N_c} \left[\begin{array}{c} \curvearrowright \\ \curvearrowright \end{array} \right] \right\rangle_{\substack{w \rightarrow z \\ v \rightarrow z'}}. \end{aligned} \quad (70)$$

However, the two correlators required in Eqs. (7) and (8) are

$$\langle S_{x,z}^{(2)} S_{z,z'}^{(2)} S_{z',y}^{(2)} \rangle = \frac{1}{N_c^3} \left\langle \left[\begin{array}{c} \curvearrowright \\ \curvearrowright \\ \curvearrowright \end{array} \right] \right\rangle_{\substack{w \rightarrow z \\ v \rightarrow z'}}, \quad (71)$$

$$\langle S_{x,z,z',y,z,z'}^{(6)} \rangle = \frac{1}{N_c} \left\langle \left[\begin{array}{c} \curvearrowright \\ \curvearrowright \\ \curvearrowright \\ \curvearrowright \\ \curvearrowright \\ \curvearrowright \end{array} \right] \right\rangle_{\substack{w \rightarrow z \\ v \rightarrow z'}}. \quad (72)$$

These are not explicitly any of the elements of matrix \mathcal{A}_3 ,

since ζ and $\left(\zeta\right)$ are not basis elements in $\tilde{\mathbf{B}}$. Instead, they are linear combinations of the elements \tilde{B}_i contained in $\tilde{\mathbf{B}}$:

$$\frac{1}{\sqrt{N_c^3}} \zeta = \sqrt{\frac{d_A C_d}{2N_c^3}} \tilde{B}_1 - \frac{1}{N_c} \sqrt{\frac{d_A}{2}} \tilde{B}_2 - \frac{\sqrt{d_A}}{N_c^2} \tilde{B}_3 - \frac{\sqrt{2d_A}}{N_c^2} \tilde{B}_5 + \frac{1}{N_c^2} \tilde{B}_6, \quad (73)$$

$$\frac{1}{\sqrt{N_c^3}} \left(\zeta\right) = \sqrt{\frac{d_A C_d}{2N_c^3}} \tilde{B}_1 + \frac{1}{N_c} \sqrt{\frac{d_A}{2}} \tilde{B}_2 - \frac{\sqrt{d_A}}{N_c^2} \tilde{B}_3 - \frac{\sqrt{2d_A}}{N_c^2} \tilde{B}_5 + \frac{1}{N_c^2} \tilde{B}_6. \quad (74)$$

Using these two expressions, it is simple to get the final equations for the two six-point correlators needed. In terms of the elements of the correlator matrix \mathcal{A}_3 given in Eq. (55) (see Appendix for detailed expressions) they are

$$\langle S_{x,z}^{(2)} S_{z,z'}^{(2)} S_{z',y}^{(2)} \rangle = \frac{1}{N_c^2} \langle S_{x,z,z',y,z,z'}^{(6)} \rangle + \frac{d_A}{N_c^3} (-\sqrt{C_d N_c} \mathcal{A}_3^{(1,2)} + N_c \mathcal{A}_3^{(2,2)} + \sqrt{2} \mathcal{A}_3^{(2,3)}) \quad (75)$$

and

$$\langle S_{x,z,z',y,z,z'}^{(6)} \rangle = -\langle S_{x,y}^{(2)} \rangle + \langle S_{x,z}^{(2)} S_{z,y}^{(2)} \rangle + \langle S_{x,z}^{(2)} S_{z',y}^{(2)} \rangle + \frac{d_A}{N_c} \left(\frac{C_d}{2} \mathcal{A}_3^{(1,1)} - \sqrt{\frac{2C_d}{N_c}} \mathcal{A}_3^{(1,3)} - \frac{N_c}{2} \mathcal{A}_3^{(2,2)} + \frac{1}{N_c} \mathcal{A}_3^{(3,3)} \right). \quad (76)$$

Equations (75) and (76) are the final two expressions needed to solve the NLO BK equation at finite N_c ; they are the main analytical results of this work. It is now possible to express these six-point functions entirely in terms of dipole correlators using Eq. (29). This makes it possible to write the NLO BK equation from Eq. (2) solely in terms of dipole correlators. In such a closed form, it can be solved directly, as was done in the large- N_c case in Refs. [62,64].

To verify the validity of Eqs. (75) and (76), we perform three checks. First, the Gaussian approximation has the built-in property that it should be consistent in color algebra. This means that taking any coincidence limit in which coordinates are made equal in Eqs. (75) and (76), should reduce them to the relevant expressions for the lower-point functions Eqs. (29) and (48). For example, setting $z \rightarrow x$ and $z' \rightarrow y$ in Eq. (75), we reproduce the equation for the dipole (29), as expected.

Secondly, when Eq. (75) is taken in the dilute limit, where the Wilson lines are expanded as

$$U_x = e^{-\lambda_a(\mathbf{x})t^a} \quad (77)$$

$$= 1 - \lambda_a(\mathbf{x})t^a + \mathcal{O}(\lambda^2), \quad \lambda_a(\mathbf{x}) \in \mathbb{R}, \quad (78)$$

Eq. (75) should be the same up to order λ^2 as the parametric equation for the large- N_c counterpart operator. In the case of correlator $\langle S_{x,z}^{(2)} S_{z,z'}^{(2)} S_{z',y}^{(2)} \rangle$, the large- N_c result is just the factorized product of dipole correlators

$$\langle S_{x,z}^{(2)} \rangle \langle S_{z,z'}^{(2)} \rangle \langle S_{z',y}^{(2)} \rangle = e^{-C_F(G_{x,z} + G_{z,z'} + G_{z',y})}. \quad (79)$$

After some algebra, Eq. (75) can be shown to give the same result up to order \mathcal{G} .

Finally, we have confirmed that Eq. (76) reproduces the large- N_c result in the appendix of Ref. [60] in the particular line configuration of coordinates discussed below in Sec. IV A. Since our expression is rather complicated due to the complex roots z_i , we have not been able to analytically take the limit $N_c \rightarrow \infty$ of our expression. Instead we have evaluated our result numerically at very large values of N_c and checked that the result matches that obtained using the expression in Ref. [60].

We note that in Ref. [59], correlators of up to eight Wilson lines have been calculated at finite N_c . The difference between that work and ours is that the authors there are solving the system for a general configuration of coordinates, where it is difficult to find a basis such that the transition matrix would become block diagonal. Consequently, an analytical approach as presented in this paper is not possible. Instead, the authors numerically exponentiate the transition matrix, which is a much more expensive computational procedure than what is needed here.

IV. NUMERICAL RESULTS

We now study numerically the obtained six-point correlators, Eqs. (75) and (76). In particular, we are interested in

the effects of the $1/N_c^2$ suppressed contributions included in these six-point correlators, compared to the large- N_c version in Eq. (16), which was used previously in numerical studies of the NLO BK equation. We will first study these operators in a specific coordinate configuration (with the GBW parametrization for the dipole). We will then integrate the operators over the gluon coordinates z, z' and study the BK evolution starting from an MV model initial condition.

A. Correlators in a line configuration of coordinates

As a baseline for comparison of the six-point correlators in the NLO BK integrand, we consider first the four-point correlator $\langle S_{x,z}^{(2)} S_{z,y}^{(2)} \rangle$ that appears in the LO BK equation. We compare the full finite- N_c result to its large- N_c limit $\langle S_{x,z}^{(2)} \rangle \langle S_{z,y}^{(2)} \rangle$. The finite- N_c correlator is evaluated by applying Eq. (48). For the dipole operator $\langle S^{(2)} \rangle$, we use the GBW form given in Eq. (14). We consider the following, specific but not atypical, configuration of coordinates: x, y and z in a line along the horizontal axis of transverse coordinate space, as shown in Fig. 1. The distance between points y and z is denoted by a , the distance between points x and z is $2a$, and the distance between x and y is $3a$.

We have confirmed that the rough relative magnitude of the finite- N_c effects of the results shown in this subsection are not specific to the actual chosen geometric configuration. To confirm this, we have tested other coordinate configurations, for example the four coordinates placed at the corners of a square. The results of these tests were very similar to the plots shown here for the line configuration. We therefore consider this particular geometry to be representative of the typical magnitude of the finite- N_c corrections.

To show the results as a function of the dimensionless distance scale aQ_s , we define the saturation scale Q_s as

$$\langle S_{x,y}^{(2)} \rangle_{(x-y)^2=2/Q_s^2} = e^{-1/2}. \quad (80)$$

In Fig. 2, the four-point correlator is shown both at finite N_c and at large N_c as a function of the distance aQ_s . Additionally, the magnitude of the finite- N_c correction is shown as a difference between the finite- N_c and large- N_c results, denoted by $\langle S^{(2)} S^{(2)} \rangle - \langle S^{(2)} \rangle \langle S^{(2)} \rangle$. The finite- N_c

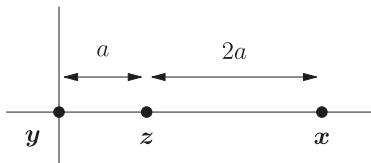


FIG. 1. Coordinates in the LO-like operators of the BK equation placed in a line configuration as a function of some value a .

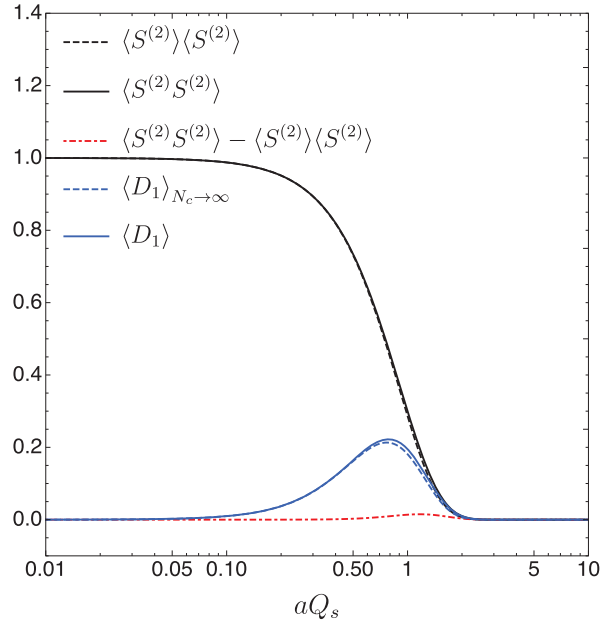


FIG. 2. Correlators in the LO-like piece of the BK equation (2), in the line configuration of coordinates as shown in Fig. 1.

correction to the four-point correlator $\langle S^{(2)} S^{(2)} \rangle$ is found to be negligible. At typical $aQ_s = 1$, the relative finite- N_c correction $(\langle S^{(2)} S^{(2)} \rangle - \langle S^{(2)} \rangle \langle S^{(2)} \rangle) / (\langle S^{(2)} \rangle \langle S^{(2)} \rangle)$ is approximately 5%. The relative correction becomes more important at large aQ_s , in the region which gives only a negligible contribution to the BK evolution. We will return to the discussion of the finite- N_c corrections at $aQ_s \gtrsim 1$ later, when evaluating the six-point functions. Also shown in Fig. 2 is the full LO-like operator factor D_1 (see Eq. (6) from the BK equation, both at large and finite N_c). The difference between the finite- N_c and large- N_c results is the same as the difference for the four-point correlators. The fact that the finite- N_c corrections are smaller than $\sim 1/N_c^2$ is not surprising, as these corrections to the LO BK equation are known to be small [53].

Next, we choose for the four coordinates present in the NLO-like operators in the BK equation a similar line configuration, shown in Fig. 3. In Fig. 4, the behaviour of the operator $\langle S^{(2)} S^{(2)} S^{(2)} \rangle$ and the large- N_c counterpart

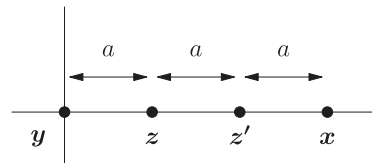


FIG. 3. Coordinates in the NLO-like operators of the BK equation placed in a line configuration as a function of some value a .

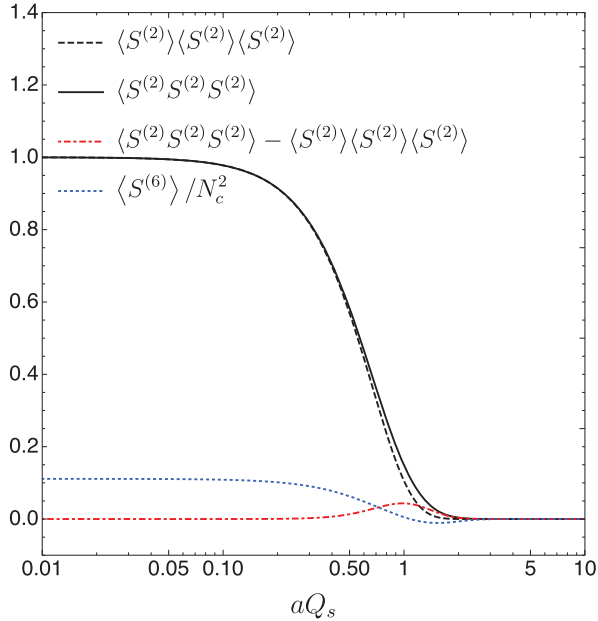


FIG. 4. Six-point correlators present in the NLO BK equation (2), in the line configuration of coordinates as shown in Fig. 3.

$\langle S^{(2)} \rangle \langle S^{(2)} \rangle \langle S^{(2)} \rangle$ are plotted as a function of aQ_s . For the finite- N_c correlator $\langle S^{(2)} S^{(2)} S^{(2)} \rangle$, we use our analytical result Eq. (75). Although the difference between the large- N_c and finite- N_c results (also shown in the figure) is larger here compared to the four-point function shown in Fig. 2, it is still negligible at $aQ_s \ll 1$. On the other hand, the finite- N_c corrections clearly dominate in the region $aQ_s \gtrsim 1$, the relative contribution from $1/N_c^2$ suppressed terms being approximately 40% at $aQ_s = 1$. A similar, although numerically smaller, effect was observed in the four-point function studied above. This can be understood as follows. When $2a \gtrsim 1/Q_s$, the color fields at points \mathbf{x} and \mathbf{z} , as well as at \mathbf{y} and \mathbf{z}' are uncorrelated. However, at finite N_c , the six-point function is also sensitive to the color field correlations between points \mathbf{x} and \mathbf{z}' , as well as between \mathbf{y} and \mathbf{z} that belong to different dipoles and are thus not correlated in the large- N_c limit. When $|\mathbf{x} - \mathbf{z}'| = |\mathbf{y} - \mathbf{z}| \lesssim 1/Q_s$, these correlations do not vanish and actually dominate the full six-point function.

Also shown in Fig. 4 for comparison is the other $1/N_c^2$ suppressed six-point correlator $\frac{1}{N_c^2} \langle S^{(6)} \rangle$ present in the NLO BK integrand at finite- N_c (cf. Eq. (7)). This is plotted using Eq. (76). We can see that the contribution of the six-point function $S^{(6)}/N_c^2$ to $D_{2,2}$ is similar in magnitude as that of the finite- N_c corrections to the dipole cubed operator $S^{(2)} S^{(2)} S^{(2)}$.

In Fig. 5, we use all the above mentioned correlators to plot the NLO-like factors $\langle D_{2,1} \rangle$ and $\langle D_{2,2} \rangle$, as defined by

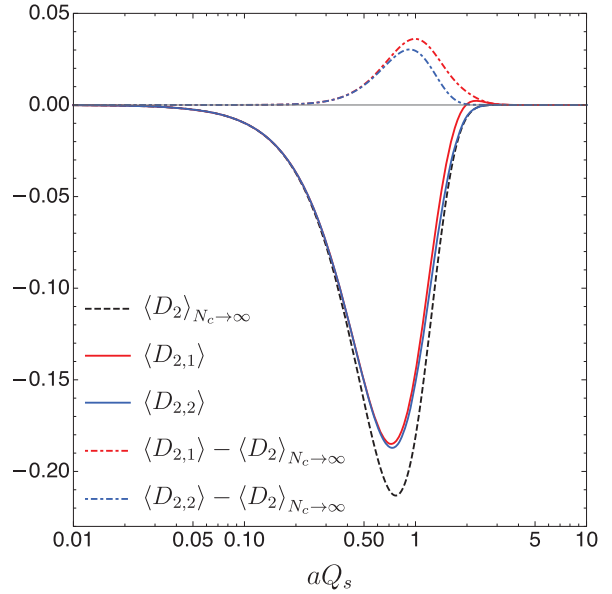


FIG. 5. Correlator factors $\langle D_{2,1} \rangle$ and $\langle D_{2,2} \rangle$ in the NLO-like part of the BK equation (2), in the line configuration of coordinates as shown in Fig. 3. Both factors reduce to the same expression $\langle D_2 \rangle_{\text{Large}N_c}$ in the large- N_c limit, as also shown in the figure.

Eqs. (7) and (8), respectively. Since both quantities reduce to the same expression in the large- N_c limit, only one curve is shown for the large- N_c case. The dashed curves show the differences, i.e., the finite- N_c corrections to $\langle D_{2,1} \rangle$ and $\langle D_{2,2} \rangle$. As already seen when studying the six-point correlators, the finite- N_c corrections are negligible at $aQ_s \ll 1$, but become numerically important when $aQ_s \gtrsim 1$. In comparison to the dashed curves in Fig. 2 for the LO-like case, we see that the finite- N_c corrections in the NLO-like case are larger. At $aQ_s = 1$, the finite- N_c corrections to the operators $\langle D_{2,1} \rangle$ and $\langle D_{2,2} \rangle$ are approximately 20% and 16%, respectively. In comparison, the LO-like operator $\langle D_1 \rangle$ shown in Fig. 2 has a finite- N_c correction of approximately 8%. When considering the full NLO BK evolution, one should keep in mind that the evolution is driven by the dipole sizes $r \lesssim 1/Q_s$. As such, even though the finite- N_c corrections can be large at $r = 1/Q_s$, the actual effect of the $1/N_c^2$ suppressed contributions to the small- x evolution can be smaller. The NLO BK evolution at finite- N_c is studied in the next section.

B. BK evolution at finite N_c

Equipped with the insight gained for the expected behavior of correlators using the line configuration, we move on to studying the full BK equation using the MV model initial condition, shown in Eq. (13), with $Q_{s,0}^2 = 1 \text{ GeV}^2$. Since the finite- N_c corrections to the

individual operators have been found to be small (except at large distances which do not significantly contribute to the BK evolution), we expect the finite- N_c corrections to remain small when performing integrations over gluon coordinates z and z' in Eq. (2).

In Fig. 6, we show the relative evolution speed $\frac{1}{N} \partial_Y N$, where the dipole amplitude $N = N_{x,y}$ is defined as $N_{x,y} = \langle 1 - S_{x,y}^{(2)} \rangle$. This is obtained by integrating the full right side of Eq. (2), first using the large- N_c expressions for the correlators, then again using the finite- N_c expressions. These are shown separately for the LO-like contribution [only the term containing D_1 in the integrand in Eq. (2)] and the NLO-like contribution (only the terms containing $D_{2,1}$ and $D_{2,2}$). As expected from the line configuration studies, we see that the finite- N_c corrections for the NLO-like terms are slightly larger, but of the same order of magnitude as the finite- N_c corrections for the LO-like terms. The finite- N_c corrections vanish when the parent dipole size r is small, and are most important at $rQ_s \sim 1$, as expected from the line configuration analysis presented above.

In Fig. 7, we plot the difference between the large- N_c and finite- N_c cases, separately for the LO-like and NLO-like terms. This shows more clearly that the difference for the

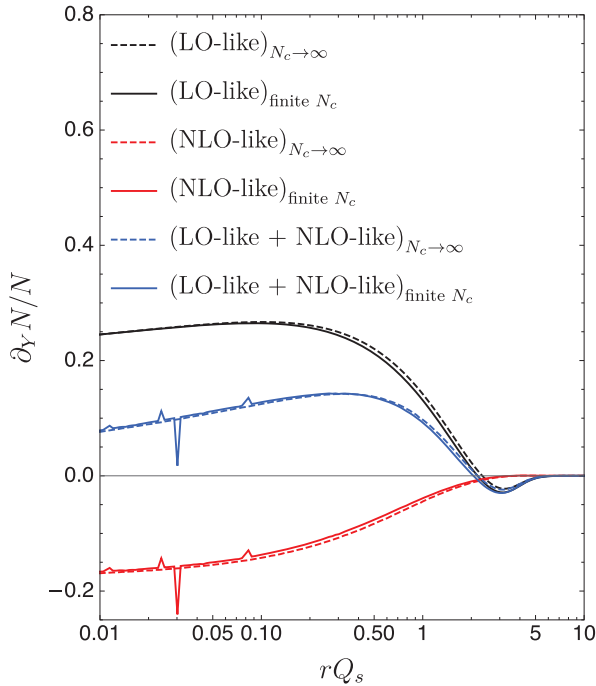


FIG. 6. Evolution speed of the dipole amplitude at the initial condition at large- N_c and at finite- N_c . We show separately the contribution from the LO- and NLO-like terms (note that the LO-like contribution includes the order α_s^2 contribution included in K_1^{fin}).

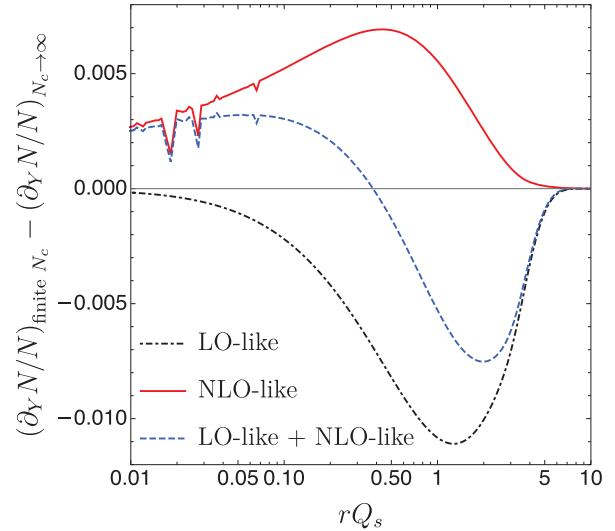


FIG. 7. Difference of the evolution speeds at finite N_c and at large N_c , shown separately for the LO-like, NLO-like and total (LO-like + NLO-like) contributions.

NLO-like terms is of the same order of magnitude as for the LO-like terms. We also note that the difference has the opposite sign in the LO-like and the NLO-like terms. Consequently, a part of the difference cancels in the total evolution speed. At $rQ_s = 1$, the relative finite- N_c correction is approximately 8% in the LO-like contribution and 13% in the NLO-like contribution. The relative magnitude of the total

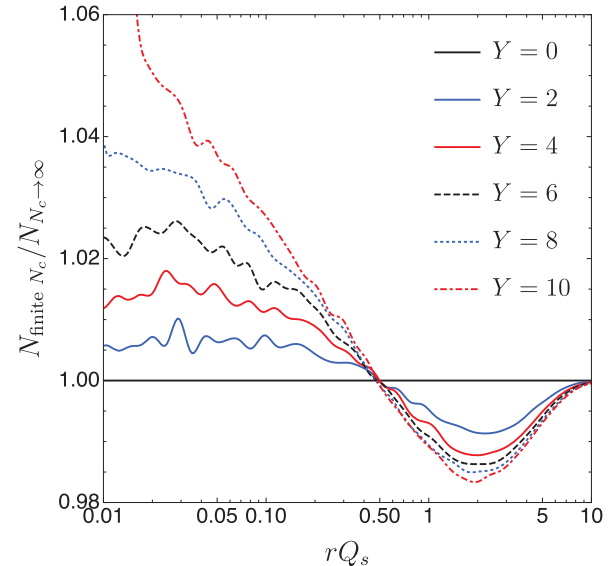


FIG. 8. Evolution for the ratio of the dipole amplitudes obtained by performing the finite- N_c and large- N_c evolutions with the same initial condition.

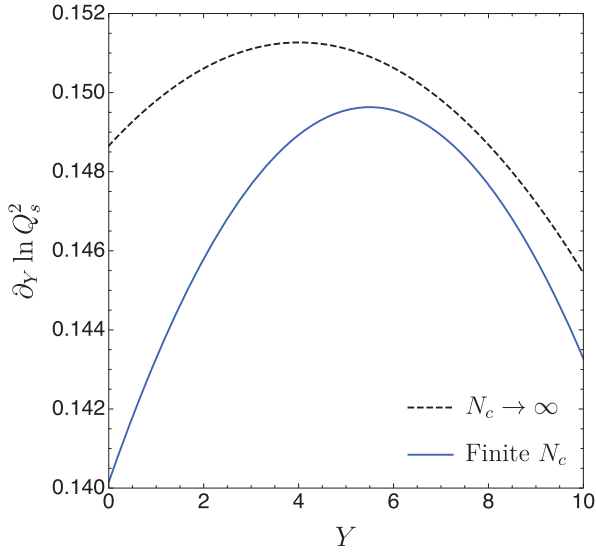


FIG. 9. Evolution speed of the saturation scale Q_s^2 as a function of rapidity at large N_c and at finite N_c .

$1/N_c^2$ suppressed contribution is 5%, which is somewhat smaller than the expected correction of $1/N_c^2 \sim 10\%$.

Finally, the last thing left to study is to move beyond the initial condition and determine how the finite- N_c corrections behave under the NLO BK evolution. In Fig. 8, we show the ratio of the dipole amplitudes N obtained by solving the full NLO BK equation at finite N_c to that at large N_c . At $r \gtrsim 1/Q_s$, when the details of the initial condition are lost and one enters the geometric scaling region, the difference between the large- N_c and finite- N_c cases evolves only very slowly. At small dipoles, the ratio grows approximately linearly in Y . The fact that the total finite- N_c correction is positive at small dipole sizes and negative at large dipoles, as seen in Fig. 7, is found to hold also asymptotically after many units of rapidity evolution.

The evolution speed of the saturation scale, $\partial_Y \ln Q_s^2$, is shown in Fig. 9. Similarly to what is seen in the dipole amplitude plot in Figure 8, we see from this figure that the finite- N_c corrections are more important at the initial condition, slowing down the evolution of Q_s^2 by approximately 5%. Later in the evolution, where the solution approaches the asymptotic shape of the BK evolved dipole, the difference becomes smaller—of the order of 1%. Consequently, even at the initial condition (and especially when the details of the initial condition are lost) the finite- N_c corrections to the evolution speed of Q_s are found to be significantly smaller than the naive expectation of $1/N_c^2$ at NLO.

V. CONCLUSIONS

In this work, we have studied the six-point correlators in the NLO BK equation using the Gaussian approximation.

This allowed us to express these higher-point correlators in terms of the dipole operator. In using our analytical results, we have seen numerically that the overall finite- N_c corrections to the NLO-like part of the BK equation are somewhat smaller than what is naively expected. However, one needs to state the actual quantity being compared in order to quantify this correction.

When correlators are considered between Wilson lines separated by large distances relative to $1/Q_s$, $1/N_c^2$ suppressed corrections may be considerable. Despite these potentially large corrections to individual correlators, these configurations do not contribute much to the right side of the BK equation. Therefore, we find a somewhat smaller, although still significant, effect on the shape of the dipole amplitude as a function of r . The finite- N_c corrections are watered down further when one considers the evolution speed of Q_s as a function of rapidity, especially once the evolution settles toward its asymptotic form away from the initial condition. In general, finite- N_c corrections need to be considered carefully when evaluating the NLO BK equation, since they may have a non-negligible effect at the required accuracy.

ACKNOWLEDGMENTS

This work was supported by the Academy of Finland, projects No. 314764 (H.M.) and No. 321840 (T.L.), and by the National Research Foundation of South Africa (A.R.). A.R. and T.L. are supported by the European Research Council (ERC) under the European Unions Horizon 2020 research and innovation programme (Grant Agreement No. ERC-2015-CoG-681707), and by the EU Horizon 2020 research and innovation programme, STRONG-2020 project (Grant Agreement No. 824093). The content of this article does not reflect the official opinion of the European Union and responsibility for the information and views expressed therein lies entirely with the authors. Computing resources from CSC—IT Center for Science in Espoo, Finland and from the Finnish Grid and Cloud Infrastructure (persistent identifier urn:nbn:fi:research-infras-2016072533) were used in this work.

APPENDIX: CORRELATOR MATRIX $\mathcal{A}(\eta)$

We give here the explicit expressions for the operators contained in the correlator matrix $\mathcal{A}(\eta)$. Since the transition matrix \mathcal{M} block-diagonalizes in basis $\tilde{\mathbf{B}}$, as explained in Sec. III C, we are only interested in the corresponding block-diagonalized matrix

$$\mathcal{A}(\eta) \Big|_{\substack{w \rightarrow z \\ v \rightarrow z}} = \begin{pmatrix} \mathcal{A}_3 & 0 & 0 \\ 0 & \mathcal{A}_2 & 0 \\ 0 & 0 & \mathcal{A}_1 \end{pmatrix} (\eta). \quad (\text{A1})$$

The one-dimensional submatrix is

$$\begin{aligned} \mathcal{A}_1(\eta) &= \left\langle \tilde{B}_6 \right\rangle \\ &= \frac{1}{N_c^3} \left\langle \left(\text{diagram} \right) \right\rangle = \left\langle S_{\mathbf{x},\mathbf{y}}^{(2)} \right\rangle. \end{aligned} \quad (\text{A2})$$

The two-dimensional submatrix is

$$\mathcal{A}_2(\eta) = \left\langle \begin{pmatrix} \tilde{B}_4 \\ \tilde{B}_5 \end{pmatrix} \begin{pmatrix} \tilde{B}_4 & \tilde{B}_5 \end{pmatrix} \right\rangle_{\substack{w \rightarrow z \\ v \rightarrow z'}} = \begin{pmatrix} \mathcal{A}_2^{(1,1)} & \mathcal{A}_2^{(1,2)} \\ \mathcal{A}_2^{(2,1)} & \mathcal{A}_2^{(2,2)} \end{pmatrix}(\eta), \quad (\text{A3})$$

where

$$\mathcal{A}_2^{(1,1)}(\eta) = \frac{1}{2N_c d_A} \left\langle \left(\text{diagram} - 2 \text{diagram} + \text{diagram} \right) \right\rangle_{\substack{w \rightarrow z \\ v \rightarrow z'}}, \quad (\text{A4})$$

$$\mathcal{A}_2^{(1,2)}(\eta) = \frac{1}{2d_A} \left\langle \left(\text{diagram} - \text{diagram} \right) \right\rangle_{\substack{w \rightarrow z \\ v \rightarrow z'}}. \quad (\text{A5})$$

The three-dimensional submatrix is

$$\mathcal{A}_3(\eta) = \left\langle \begin{pmatrix} \tilde{B}_1 \\ \tilde{B}_2 \\ \tilde{B}_3 \end{pmatrix} \begin{pmatrix} \tilde{B}_1 & \tilde{B}_2 & \tilde{B}_3 \end{pmatrix} \right\rangle_{\substack{w \rightarrow z \\ v \rightarrow z'}} = \begin{pmatrix} \mathcal{A}_3^{(1,1)} & \mathcal{A}_3^{(1,2)} & \mathcal{A}_3^{(1,3)} \\ \mathcal{A}_3^{(2,1)} & \mathcal{A}_3^{(2,2)} & \mathcal{A}_3^{(2,3)} \\ \mathcal{A}_3^{(3,1)} & \mathcal{A}_3^{(3,2)} & \mathcal{A}_3^{(3,3)} \end{pmatrix}(\eta), \quad (\text{A6})$$

where

$$\begin{aligned} \mathcal{A}_3^{(1,1)}(\eta) &= \frac{2}{N_c^2 d_A C_d} \left\langle 2N_c S_{\mathbf{x},\mathbf{y}}^{(2)} - N_c^3 S_{\mathbf{x},\mathbf{z}}^{(2)} S_{\mathbf{z},\mathbf{y}}^{(2)} - N_c^3 S_{\mathbf{x},\mathbf{z}'}^{(2)} S_{\mathbf{z}',\mathbf{y}}^{(2)} + \frac{N_c^2}{4} \left(\text{diagram} - N_c \text{diagram} + \frac{N_c^2}{2} \text{diagram} \right) \right. \\ &\quad \left. + \left(\text{diagram} - N_c \text{diagram} + \frac{N_c^2}{4} \text{diagram} \right) \right\rangle_{\substack{w \rightarrow z \\ v \rightarrow z'}}, \end{aligned} \quad (\text{A7})$$

$$\mathcal{A}_3^{(1,2)}(\eta) = \frac{1}{2N_c d_A \sqrt{N_c C_d}} \left\langle -N_c \text{diagram} + 2 \text{diagram} - 2 \text{diagram} + N_c \text{diagram} \right\rangle_{\substack{w \rightarrow z \\ v \rightarrow z'}}, \quad (\text{A8})$$

$$\mathcal{A}_3^{(1,3)}(\eta) = \frac{1}{d_A \sqrt{2C_d N_c}} \left\langle - \text{diagram} + \frac{2}{N_c} \text{diagram} - \text{diagram} \right\rangle_{\substack{w \rightarrow z \\ v \rightarrow z'}}, \quad (\text{A9})$$

$$\mathcal{A}_3^{(2,2)}(\eta) = \frac{1}{2N_c d_A} \left\langle \left(\text{Diagram 1} - 2 \text{Diagram 2} + \text{Diagram 3} \right) \right\rangle_{\substack{w \rightarrow z \\ v \rightarrow z'}} \quad (\text{A10})$$

$$\mathcal{A}_3^{(2,3)}(\eta) = \frac{1}{\sqrt{2}N_c d_A} \left\langle \left(\text{Diagram 4} - \text{Diagram 5} \right) \right\rangle_{\substack{w \rightarrow z \\ v \rightarrow z'}} \quad (\text{A11})$$

$$\mathcal{A}_3^{(3,3)}(\eta) = \frac{1}{N_c d_A} \left\langle -N_c S_{x,y}^{(2)} + \text{Diagram 6} \right\rangle_{\substack{w \rightarrow z \\ v \rightarrow z'}} \quad (\text{A12})$$

-
- [1] H. Abramowicz *et al.* (H1 and ZEUS Collaboration), Combination of measurements of inclusive deep inelastic $e^\pm p$ scattering cross sections and QCD analysis of HERA data, *Eur. Phys. J. C* **75**, 580 (2015).
- [2] F. Gelis, E. Iancu, J. Jalilian-Marian, and R. Venugopalan, The color glass condensate, *Annu. Rev. Nucl. Part. Sci.* **60**, 463 (2010).
- [3] J. Jalilian-Marian, A. Kovner, L. D. McLerran, and H. Weigert, The Intrinsic glue distribution at very small x , *Phys. Rev. D* **55**, 5414 (1997).
- [4] J. Jalilian-Marian, A. Kovner, A. Leonidov, and H. Weigert, The BFKL equation from the Wilson renormalization group, *Nucl. Phys.* **B504**, 415 (1997).
- [5] J. Jalilian-Marian, A. Kovner, A. Leonidov, and H. Weigert, The Wilson renormalization group for low x physics: Towards the high density regime, *Phys. Rev. D* **59**, 014014 (1998).
- [6] E. Iancu and L. D. McLerran, Saturation and universality in QCD at small x , *Phys. Lett. B* **510**, 145 (2001).
- [7] Y. V. Kovchegov, Small x F(2) structure function of a nucleus including multiple pomeron exchanges, *Phys. Rev. D* **60**, 034008 (1999).
- [8] I. Balitsky, Operator expansion for high-energy scattering, *Nucl. Phys.* **B463**, 99 (1996).
- [9] Y. V. Kovchegov and H. Weigert, Triumvirate of running couplings in small- x evolution, *Nucl. Phys.* **A784**, 188 (2007).
- [10] E. Gardi, J. Kuokkanen, K. Rummukainen, and H. Weigert, Running coupling and power corrections in nonlinear evolution at the high-energy limit, *Nucl. Phys.* **A784**, 282 (2007).
- [11] J. L. Albacete and Y. V. Kovchegov, Solving high energy evolution equation including running coupling corrections, *Phys. Rev. D* **75**, 125021 (2007).
- [12] I. Balitsky, Quark contribution to the small- x evolution of color dipole, *Phys. Rev. D* **75**, 014001 (2007).
- [13] T. Lappi and H. Mäntysaari, On the running coupling in the JIMWLK equation, *Eur. Phys. J. C* **73**, 2307 (2013).
- [14] H. Abramowicz *et al.* (H1 and ZEUS Collaborations), Combination and QCD analysis of charm and beauty production cross-section measurements in deep inelastic ep scattering at HERA, *Eur. Phys. J. C* **78**, 473 (2018).
- [15] J. L. Albacete, N. Armesto, J. G. Milhano, P. Quiroga-Arias, and C. A. Salgado, AAMQS: A non-linear QCD analysis of new HERA data at small- x including heavy quarks, *Eur. Phys. J. C* **71**, 1705 (2011).
- [16] J. L. Albacete, J. G. Milhano, P. Quiroga-Arias, and J. Rojo, Linear vs Non-linear QCD evolution: From HERA data to LHC phenomenology, *Eur. Phys. J. C* **72**, 2131 (2012).
- [17] T. Lappi and H. Mäntysaari, Single inclusive particle production at high energy from HERA data to proton-nucleus collisions, *Phys. Rev. D* **88**, 114020 (2013).
- [18] H. Mäntysaari and B. Schenke, Confronting impact parameter dependent JIMWLK evolution with HERA data, *Phys. Rev. D* **98**, 034013 (2018).
- [19] A. H. Rezaeian, M. Siddikov, M. Van de Klundert, and R. Venugopalan, Analysis of combined HERA data in the impact-parameter dependent saturation model, *Phys. Rev. D* **87**, 034002 (2013).

- [20] H. Mäntysaari and P. Zurita, In depth analysis of the combined HERA data in the dipole models with and without saturation, *Phys. Rev. D* **98**, 036002 (2018).
- [21] P. Tribedy and R. Venugopalan, QCD saturation at the LHC: Comparisons of models to p + p and A + A data and predictions for p + Pb collisions, *Phys. Lett. B* **710**, 125 (2012); Erratum, *Phys. Lett. B* **718**, 1154 (2013).
- [22] V. P. Goncalves and M. L. L. da Silva, Probing the Color Glass Condensate in pp collisions at forward rapidities and very low transverse momenta, *Nucl. Phys.* **A906**, 28 (2013).
- [23] B. Ducloué, T. Lappi, and H. Mäntysaari, Forward J/ψ production in proton-nucleus collisions at high energy, *Phys. Rev. D* **91**, 114005 (2015).
- [24] B. Ducloué, T. Lappi, and H. Mäntysaari, Forward J/ψ production at high energy: Centrality dependence and mean transverse momentum, *Phys. Rev. D* **94**, 074031 (2016).
- [25] J. L. Albacete, P. Guerrero Rodríguez, and Y. Nara, Ultra-forward particle production from color glass condensate and Lund fragmentation, *Phys. Rev. D* **94**, 054004 (2016).
- [26] B. Ducloué, T. Lappi, and H. Mäntysaari, Isolated photon production in proton-nucleus collisions at forward rapidity, *Phys. Rev. D* **97**, 054023 (2018).
- [27] H. Mäntysaari and H. Paukkunen, Saturation and forward jets in proton-lead collisions at the LHC, *Phys. Rev. D* **100**, 114029 (2019).
- [28] E. C. Aschenauer, S. Fazio, J. H. Lee, H. Mäntysaari, B. S. Page, B. Schenke, T. Ulrich, R. Venugopalan, and P. Zurita, The electron-ion collider: Assessing the energy dependence of key measurements, *Rep. Prog. Phys.* **82**, 024301 (2019).
- [29] A. Accardi *et al.*, Electron ion collider: The next QCD frontier - understanding the glue that binds us all, *Eur. Phys. J. A* **52**, 268 (2016).
- [30] J. Abelleira Fernandez *et al.* (LHeC Study Group Collaboration), A large hadron electron collider at CERN: Report on the physics and design concepts for machine and detector, *J. Phys. G* **39**, 075001 (2012).
- [31] X. Chen, A plan for electron ion collider in China, *Proc. Sci. DIS2018* (2018) 170 [arXiv:1809.00448].
- [32] C. A. Bertulani, S. R. Klein, and J. Nystrand, Physics of ultra-peripheral nuclear collisions, *Annu. Rev. Nucl. Part. Sci.* **55**, 271 (2005).
- [33] S. R. Klein and H. Mäntysaari, Imaging the nucleus with high-energy photons, *Nat. Rev. Phys.* **1**, 662 (2019).
- [34] I. Balitsky and G. A. Chirilli, Next-to-leading order evolution of color dipoles, *Phys. Rev. D* **77**, 014019 (2008).
- [35] I. Balitsky and G. A. Chirilli, Rapidity evolution of Wilson lines at the next-to-leading order, *Phys. Rev. D* **88**, 111501 (2013).
- [36] A. Kovner, M. Lublinsky, and Y. Mulian, Jalilian-Marian, Iancu, McLerran, Weigert, Leonidov, Kovner evolution at next to leading order, *Phys. Rev. D* **89**, 061704 (2014).
- [37] B. Ducloué, H. Hänninen, T. Lappi, and Y. Zhu, Deep inelastic scattering in the dipole picture at next-to-leading order, *Phys. Rev. D* **96**, 094017 (2017).
- [38] G. Beuf, Dipole factorization for DIS at NLO: Combining the $q\bar{q}$ and $q\bar{q}g$ contributions, *Phys. Rev. D* **96**, 074033 (2017).
- [39] G. Beuf, Dipole factorization for DIS at NLO: Loop correction to the $\gamma_{T,L}^* \rightarrow q\bar{q}$ light-front wave functions, *Phys. Rev. D* **94**, 054016 (2016).
- [40] I. Balitsky and G. A. Chirilli, Photon impact factor in the next-to-leading order, *Phys. Rev. D* **83**, 031502 (2011).
- [41] H. Hänninen, T. Lappi, and R. Paatelainen, One-loop corrections to light cone wave functions: The dipole picture DIS cross section, *Ann. Phys. (Amsterdam)* **393**, 358 (2018).
- [42] R. Boussarie, A. V. Grabovsky, D. Yu. Ivanov, L. Szymanowski, and S. Wallon, Next-to-Leading Order Computation of Exclusive Diffractive Light Vector Meson Production in a Saturation Framework, *Phys. Rev. Lett.* **119**, 072002 (2017).
- [43] M. Escobedo and T. Lappi, Dipole picture and the non-relativistic expansion, *Phys. Rev. D* **101**, 034030 (2020).
- [44] T. Lappi, H. Mäntysaari, and J. Penttala, Relativistic corrections to the vector meson light front wave function, arXiv:2006.02830.
- [45] G. A. Chirilli, B.-W. Xiao, and F. Yuan, Inclusive hadron productions in pA collisions, *Phys. Rev. D* **86**, 054005 (2012).
- [46] B. Ducloué, E. Iancu, T. Lappi, A. H. Mueller, G. Soyez, D. N. Triantafyllopoulos, and Y. Zhu, Use of a running coupling in the NLO calculation of forward hadron production, *Phys. Rev. D* **97**, 054020 (2018).
- [47] B. Ducloué, T. Lappi, and Y. Zhu, Single inclusive forward hadron production at next-to-leading order, *Phys. Rev. D* **93**, 114016 (2016).
- [48] K. Watanabe, B.-W. Xiao, F. Yuan, and D. Zaslavsky, Implementing the exact kinematical constraint in the saturation formalism, *Phys. Rev. D* **92**, 034026 (2015).
- [49] T. Altinoluk, N. Armesto, G. Beuf, A. Kovner, and M. Lublinsky, Single-inclusive particle production in proton-nucleus collisions at next-to-leading order in the hybrid formalism, *Phys. Rev. D* **91**, 094016 (2015).
- [50] A. M. Stasto, B.-W. Xiao, and D. Zaslavsky, Towards the Test of Saturation Physics Beyond Leading Logarithm, *Phys. Rev. Lett.* **112**, 012302 (2014).
- [51] H.-Y. Liu, Y.-Q. Ma, and K.-T. Chao, Improvement for color glass condensate factorization: Single hadron production in pA collisions at next-to-leading order, *Phys. Rev. D* **100**, 071503 (2019).
- [52] K. Rummukainen and H. Weigert, Universal features of JIMWLK and BK evolution at small x, *Nucl. Phys.* **A739**, 183 (2004).
- [53] Y. V. Kovchegov, J. Kuokkanen, K. Rummukainen, and H. Weigert, Subleading-N(c) corrections in non-linear small-x evolution, *Nucl. Phys.* **A823**, 47 (2009).
- [54] H. Fujii, F. Gelis, and R. Venugopalan, Quark pair production in high energy pA collisions: General features, *Nucl. Phys.* **A780**, 146 (2006).
- [55] C. Marquet and H. Weigert, New observables to test the color glass condensate beyond the large- N_c limit, *Nucl. Phys.* **A843**, 68 (2010).
- [56] F. Dominguez, C. Marquet, B.-W. Xiao, and F. Yuan, Universality of unintegrated gluon distributions at small x, *Phys. Rev. D* **83**, 105005 (2011).

- [57] C. Marquet, Forward inclusive dijet production and azimuthal correlations in $p(A)$ collisions, *Nucl. Phys.* **A796**, 41 (2007).
- [58] T. Lappi and H. Mantysaari, Forward dihadron correlations in deuteron-gold collisions with the Gaussian approximation of JIMWLK, *Nucl. Phys.* **A908**, 51 (2013).
- [59] K. Dusling, M. Mace, and R. Venugopalan, Parton model description of multiparticle azimuthal correlations in pA collisions, *Phys. Rev. D* **97**, 016014 (2018).
- [60] F. Dominguez, C. Marquet, A. M. Stasto, and B.-W. Xiao, Universality of multiparticle production in QCD at high energies, *Phys. Rev. D* **87**, 034007 (2013).
- [61] B. Ducloué, E. Iancu, A. H. Mueller, G. Soyez, and D. N. Triantafyllopoulos, Non-linear evolution in QCD at high-energy beyond leading order, *J. High Energy Phys.* **04** (2019) 081.
- [62] T. Lappi and H. Mäntysaari, Direct numerical solution of the coordinate space Balitsky-Kovchegov equation at next to leading order, *Phys. Rev. D* **91**, 074016 (2015).
- [63] E. Iancu, J. D. Madrigal, A. H. Mueller, G. Soyez, and D. N. Triantafyllopoulos, Resumming double logarithms in the QCD evolution of color dipoles, *Phys. Lett. B* **744**, 293 (2015).
- [64] T. Lappi and H. Mäntysaari, Next-to-leading order Balitsky-Kovchegov equation with resummation, *Phys. Rev. D* **93**, 094004 (2016).
- [65] G. Beuf, Improving the kinematics for low- x QCD evolution equations in coordinate space, *Phys. Rev. D* **89**, 074039 (2014).
- [66] E. Iancu, J. D. Madrigal, A. H. Mueller, G. Soyez, and D. N. Triantafyllopoulos, Collinearly-improved BK evolution meets the HERA data, *Phys. Lett. B* **750**, 643 (2015).
- [67] L. D. McLerran and R. Venugopalan, Computing quark and gluon distribution functions for very large nuclei, *Phys. Rev. D* **49**, 2233 (1994).
- [68] L. D. McLerran and R. Venugopalan, Boost covariant gluon distributions in large nuclei, *Phys. Lett. B* **424**, 15 (1998).
- [69] K. J. Golec-Biernat and M. Wusthoff, Saturation effects in deep inelastic scattering at low Q^2 and its implications on diffraction, *Phys. Rev. D* **59**, 014017 (1998).
- [70] A. Dumitru, J. Jalilian-Marian, T. Lappi, B. Schenke, and R. Venugopalan, Renormalization group evolution of multi-gluon correlators in high energy QCD, *Phys. Lett. B* **706**, 219 (2011).
- [71] T. Lappi, B. Schenke, S. Schlichting, and R. Venugopalan, Tracing the origin of azimuthal gluon correlations in the color glass condensate, *J. High Energy Phys.* **01** (2016) 061.
- [72] T. Lappi, A. Ramnath, K. Rummukainen, and H. Weigert, JIMWLK evolution of the odderon, *Phys. Rev. D* **94**, 054014 (2016).
- [73] E. Iancu and D. Triantafyllopoulos, Higher-point correlations from the JIMWLK evolution, *J. High Energy Phys.* **11** (2011) 105.
- [74] J. P. Blaizot, F. Gelis, and R. Venugopalan, High-energy pA collisions in the color glass condensate approach. 1. Gluon production and the Cronin effect, *Nucl. Phys.* **A743**, 13 (2004).
- [75] J. P. Blaizot, F. Gelis, and R. Venugopalan, High-energy pA collisions in the color glass condensate approach. 2. Quark production, *Nucl. Phys.* **A743**, 57 (2004).
- [76] F. Dominguez, C. Marquet, and B. Wu, On multiple scatterings of mesons in hot and cold QCD matter, *Nucl. Phys.* **A823**, 99 (2009).